Edoardo Sanità

Dottorato in Scienze della Terra
PhD Course in Earth Sciences

XXXV Ciclo – *35th Cycle*
2019 – 2022

The complexity of shallow levels tectonics during continental collision: evidence from the boundary between Maritime and Ligurian Alps

Supervisor: Prof. Luca Pandolfi

Co-Supervisor: Prof. Jean Marc Lardeaux

Coordinatore del Corso di Dottorato
Prof. Sandro Moretti

Index

La complessità dei livelli tettonici superficiali durante la collisione continentale: Evidenze dal limite tra le Alpi Marittime and Liguri

Abstract

The boundary between Maritime and Ligurian Alps, southwestern Alps, is classically regarded as formed by a pile of continental- (Briançonnais Units) and oceanic-derived tectonic units (Moglio-Testico Unit and Helminthoid Flysch) stacked toward southwest. The continental units represent the thinned portion of the Europe continental margin, whereas those oceanic are considered as the remnants of the Ligure Piemontese ocean; the latter interposed between the Europe and Adria Plate in the Middle-Late Jurassic. Starting from Late Cretaceous, the convergence between Europe and Adria Plate progressively led to the consumption of the Ligure Piemontese ocean, until to the involvement of the Europe continental margin into the alpine subduction zone during the Eocene time. However, the tectonic units cropping out in this sector of the Alps, are thought to record their deformation patterns under different Pressure (*P*) and Temperature (*T*) conditions related to shallow crustal levels into the Alpine wedge without evidence of deeper-related processes, *i.e.*, subduction-related deformation and/or metamorphism.

In this Thesis, the tectonic units cropping out at the boundary between Maritime and Ligurian Alps were investigated in order to provide a new stratigraphic, structural and metamorphic dataset needed to better constrain their tectonic history. All of the tectonic units are characterized in terms of stratigraphy, structural evolution and metamorphic imprint following a multidisciplinary approach including: fieldwork, stratigraphic analysis, provenance, structural analysis and *P*–*T* estimation.

The collected datasets indicate that, in this sector of the southwestern Alps the tectonic pile is composed by, from the top to the bottom: the Marguareis Unit (Briançonnais Domain); the Moglio-testico Unit (Ligure Piemontese ocean sedimentary cover); the Helminthoid Flsych Unit (Ligurian Domain, ocean-continent transition zone); several continent-derived tectonic slices (Cima del Becco and Chambeuil Slices) with Briançonnais affinity; and the Cabanaira Unit (Briançonnais Domain). The Briançonnais Units succession is coherent with the sedimentary evolution of the Europe continental margin approaching toward the subduction zone as proposed by previous authors; The Moglio-Testico Unit succession shows a transition from pelagic to basin plain deposits reflecting the sedimentary evolution of a portion of the Ligure Piemontese ocean approaching toward the subduction zone; The Helminthoid Flysch Unit sedimentary evolution is coherent with that proposed for the External Ligurian Units cropping out in the Northern Apennine. Structural analysis outlined that each unit recorded a polyphase deformation history dealing with the superposition of pre- syn- and post-coupling tectonic events developed under different *P* and *T* conditions. The pre-Oligocene

pre-coupling structures are represented by superposed folding systems, associated with metamorphic re-crystallization, and confined to each unit. The syn-coupling structures are represented by thrusting and folding cutting the previous structures and developed at shallower crustal levels. These structures are considered as responsible for the coupling of the units and thought to be developed during the late Eocene-early Oligocene. The last deformation history is shared by all of the units and it is represented by flat-lying open folding system with no evidence of metamorphic re-crystallization and high-angles normal to transtensive faulting system which is not able to profoundly modify the previous architecture of the tectonic pile.

Thermobarometric estimation indicates that the tectonic units reached their metamorphic peak conditions spanning from anchizone/epizone to blueschists field, during the pre-coupling events (*i.e.*, before their juxtaposition), and, subsequently, they have been exhumed following different *P–T* paths into the Alpine wedge. The exhumation up to the shallower structural levels is represented by the syn- and post-coupling structures. The whole datasets outlined that the syn-coupling thrusting event played a first order role in the tectonic evolution of this sector of the southwestern Alps.

1. Introduction

1.1 Shallow level tectonics in collisional settings

The reconstruction of the geodynamic evolution of collisional orogens requires the study of processes which took place at different crustal levels during the convergence between different tectonic plates. It is largely accepted that the geodynamic evolution of orogens is the results of different overprinted tectonic processes developed from deep to shallow crustal levels (i.e., Cloos, 1982; Chopin, 1984; Platt, 1987; Handy et al., 2010; Molli and Malavieille, 2011; Rolland et al., 2012; Lardeaux, 2014). These are recorded into the oceanic- and/or continental-derived units progressively involved into the accretionary and/or orogenic wedges (i.e., Chopin, 1984; Malavieille, 1984; Platt, 1987; Storti et al., 2000; Graveleau et al., 2012 and quoted references) experiencing underthrusting, subduction, accretion, off-scraping and exhumation processes. In the 20th century, geologists have focused on the study of deep tectonic processes recorded by high-grade metamorphic units, which are more suitable to record pervasive tectono-metamorphic fabrics. Consequently, a large dataset about the deeper processes-related thermo-mechanical constraints is now available (i.e., Chemenda et al., 1995, 1996; Guillot et al., 2009; Roda et al., 2012; Burov et al., 2014; Schmid et al., 2017; Regorda et al., 2021). By contrast, constraints for the thermo-mechanical evolution of very low- and low-grade units deformed and metamorphosed at shallow crustal levels (*i.e.*, from 4-5 to 30-35 km) are lacking and, therefore, the knowledge of shallow tectonics processes as well as their interaction with the deeper ones (i.e., Culshaw et al., 2006) is far to be clearly understood. This is due to the scarce comprehension of the deformation strain patterns of the units metamorphosed at relative deep crustal levels into the accretionary/orogenic wedges (*i.e.*, under low- to very low-temperature).

For these reasons, the study of shallow levels tectonics is of paramount importance to improve the comprehension of the geodynamic evolution of the collisional orogens. In this frame the interaction and the overprinting between shallow and deep tectonic processes (supra-structures vs infra-structures concept of Culshaw et al., 2006) developed into the accretionary/orogenic wedges must be taken into account. Although it is largely documented that during the geodynamic evolution of orogens the subduction of oceanic lithosphere predates the continental underthrusting and subsequent underplating, a common shallow tectonic history recorded by tectonic units involved at different time and depth into the wedges cannot be excluded. Use this as a filter to discriminate the deeper and the shallower tectonic processes would allow to unravel the tectonic evolution of the units and, consequently, to improve the

comprehension of the geodynamic history of the collisional belt.

1.2 Why study the boundary between the Maritime and Ligurian Alps?

The Western Alpine belt (Figures 1a-b, 2a) is the best example of double-verging collisional orogenic system showing a NE-SW to N-S to

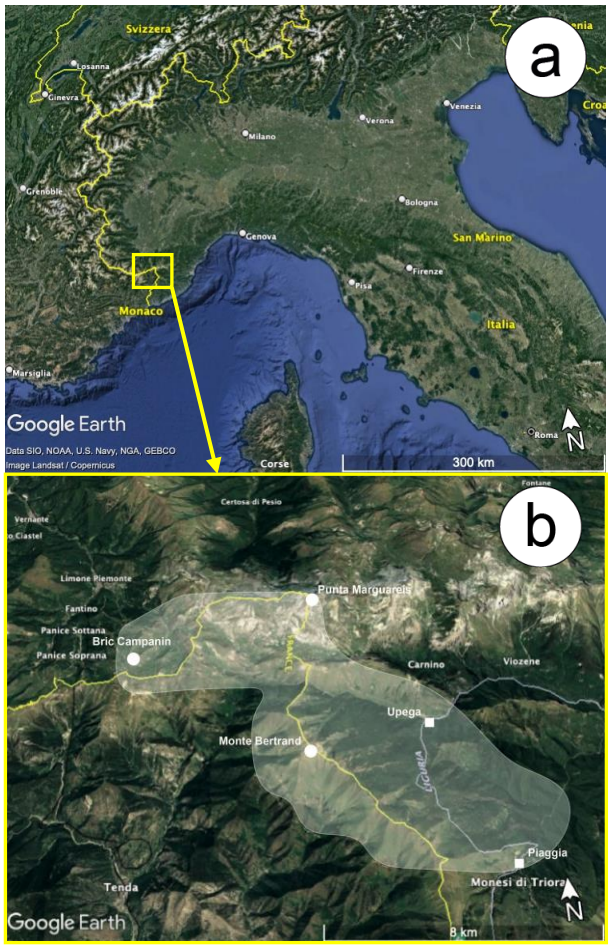

Figure 1. Geographic location of the Western Alps (a) and the investigated area (b).

NW-SW trend and composed by a stack of oceanic and continental tectonic units which experienced deformation and metamorphism at different crustal levels (i.e., Chopin, 1984; Lardeaux and Spalla, 1991; Agard et al., 2001; Lardeaux et al., 2006; Schmid et al., 2004; Handy et al., 2010; Lanari et al., 2012; Strzerzynski et al., 2012; Rebay et al., 2018; Luoni et al., 2021; Hervioue et al., 2022 and many others).

Several authors focused their attention on the study of high-grade units mostly cropping out in the axial domain (*i.e.*, internal zones) of the Alpine belt (Figure 2b). In fact, clear superposition relationships between different generations of tectono-metamorphic fabrics and the radiometric ages, allow a good reconstruction of their tectonic history. Indeed, the low- and very low-grade tectonic units are characterized by penetrative fabrics with local or incomplete (at whole rock-scale) metamorphic re-crystallization, so making the reconstruction of their tectonic history challenging. These units are mostly located toward the westernmost domains (external zones) of the Alpine belt (Figure 2b). This picture can be extended also in the southwestern sector of the Alpine belt where it shows a N-S to NW-SE trend (Figure 2b). From a geological point of view, the southwestern sector of the Alpine belt is characterized by a stack of oceanic- and continental-derived tectonic units characterized by decreasing metamorphic grade toward SW sectors (Vanossi et al., 1984; Vanossi et al., 1986; Bonazzi et al., 1988; Cabella et al., 1988; Capponi and Crispini, 2002; Seno et al., 2003; Seno et al., 2005; Capponi et al., 2009; Molli et al., 2010 and

quoted references; Malatesta et al., 2012; Piana et al., 2014; Piana et al., 2021). The boundary between Maritime and Ligurian Alps (Southwestern Alps, Figures 1b, 2b) is included in this sector and its tectonic evolution has prompted the interest by geologists starting from the second half of the last century since 1960s (i.e., Lanteaume, 1957; 1962; Elter et al., 1961, 1966; Lanteaume, 1968; Vanossi et al., 1986; Brizio et al., 1983; d'Atri et al., 2016; Bertok et al., 2018; Piana et al., 2021). The authors focused their attention on the study of meso- to map-scale evolutionary tectonic models. This area, consisting of a well accessible repeated stack of units, shows huge volumetric outcrop expositions and, therefore, it is a natural laboratory to study orogenic mechanisms affecting tectonic units characterized by tectono-metamorphic evolution developed at different crustal levels. However, does not exist a common interpretation about the structural evolution (i.e., Messiga et al., 1982; Brizio et al., 1983; Vanossi et al., 1984; Bonazzi et al., 1987; Piana et al., 2009; d'Atri et al., 2016; Mueller et al., 2020; Piana et al., 2021) of the units and the interactions between shallow and deep tectonic processes. Consequently, different interpretations led to contrasting evolutionary tectonic model for this sector of the Alpine belt.

In the last twenty years, the authors proposed two constrasting evolutionary tectonic models: (i) thrust tectonic models and (ii) dominant strike-slip tectonic model. Seno et al. (2005) based on the pivotal contributes of Vanossi et al. (1984) and Vanossi et al. (1986) proposed a thrust tectonics model in which the oceanic- and continental-derived units, after their involvement in the Alpine wedge at different depths under low temperature condition, are progressively thrusted toward SW forming the current tectonic stack. Contrary, d'Atri et al. (2016) and Piana et al. (2021) suggested a kinematic model in which high-angles unit-bounding faults played a significant role in the tectonic evolution of this sector of the Alpine belt according with Piana et al. (2009) and (2014).

To verify or question the tectonic evolution of this sector of the belt in which low-grade units are exposed, detailed field mapping combined with structural analysis and modern lab techniques are, therefore, strongly needed.

1.3 Thesis outlines

Currently, the study of orogenic processes developed at shallow crustal levels need of a large range of dataset to constraint the mechanisms of deformation and metamorphism recorded by units during their tectonic trajectories into the accretionary/orogenic wedge. This thesis is aimed to the reconstruction of the tectono-metamorphic evolution of very low- and low-grade units involved in Alpine collision and

cropping out along the boundary between Maritime and Ligurian Alps. The main topics are; (1) the sedimentary evolution of the units; (2) their structural evolution (deep vs shallow tectonic events); (3) *P–T* estimation; (4) and their tectonic evolution in the geodynamic frame of the Western Alps. All these topics will be thus treated and properly discussed in order to provide new constraints to improve the comprehension of the tectonic evolution of the belt during the convergence.

The study area run along the Italian-French boundary (Figures 1b, 2b) in the southwestern sector of the Marguareis Massif to North, and the high Arroscia Valley until the Upega village to South covering an area about 110 km^2 (Figure 1b). Particular attention was paid for the sedimentary and structural evolution of the oceanic and continental-derived units cropping out in the mapped area. Comparison between our structural model with analogue sectors of the Alpine belt is also discussed. Original data were collected by means a multidisciplinary approach including field mapping and lab analysis.

The results of the fieldwork are summarized in detailed geological-structural maps and complemented by stratigraphic logs and *P–T* estimates achieved during the deformation histories recorded by the units (all the methods are showed in the section “methods” while their critical issues are explained in the supplementary materials).

2. Geological setting

2.1 The Western Alpine belt

The western Alpine belt is part of the Alpine-Himalayan collisional system which is composed by Meso-Cenozoic orogens extend for than 1800 km from the Betic Cordillera, in the western Mediterranean area, to the Asian continent. The western Alpine belt shows a NW-SE to NW-SE in its southwestern prolongation represented by the Maritime and Ligurian Alps (Figures 2a-b). Rests of the Alpine belt are largely documented in the northeastern sector of the Corsica Island (*i.e.*, Mattauer *et al.*, 1981; Durand-Delga, 1984; Di Rosa, 2021 and reference therein).

The western Alpine belt consists of a repeated stack of units stemming from different paleogeographic domains (oceanic vs continental). The today geological setting of the belt is the results of a complex geodynamic history started with the Middle Triassic- Early Jurassic pure shear-dominated rifting and subsequent Middle to Late Jurassic simple shear-dominated extension (*i.e.*, Durand-Delga, 1984; Bertotti *et al.*, 1993; Froitzheim and Manatschal, 1996; Marroni *et al.*, 1998; Marroni and Pandolfi, 2007; Manatschal and

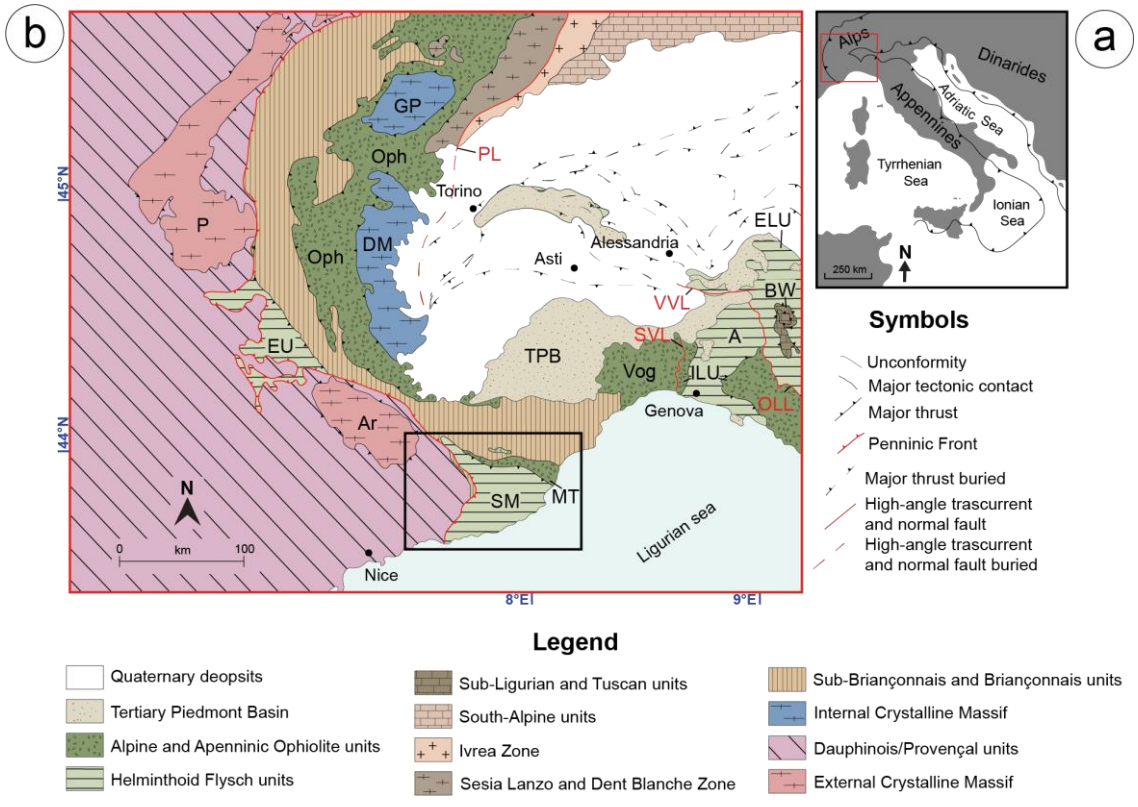

Figure 2. a) Geographic location of the Western Alpine belt. b) Geological setting of the Western Alpine belt re-draw and modified by Molli et al. (2010) and Barbero et al. (2019); the black box indicates the close-up of the Western Ligurian Alps of Figure 2a. TPB: Tertiary Piedmont Basin; GP: Gran Paradiso; DM: Dora Maira; Oph: Ophiolite units; MT: Moglio-Testico Unit; Vog: Voltri group; SM: San Remo-Monte Saccarello Unit; EU: Embrunais-Ubaye; A: Antola Unit; ILU: Internal Ligurian Units; ELU: External Ligurian Units; BW: Bobbio Window; P: Pelvoux; Ar: Argentera; PL: Periadriatic Line; SVL: Sestri-Voltaggio Line; VVL: Villaverna-Varzi Line; OLL: Ottone-Levanto Line.

Müntener, 2009; Spalla *et al.*, 2014). In the Middle-Late Jurassic, the extension led to the continental break-up and subsequent opening of the Ligure Piemontese Ocean that was interposed between European and Adria Plates (*i.e.*, Dewey *et al.*, 1989; Stampfli *et al.*, 2001a; Beltrando *et al.*, 2010a; Handy *et al.*, 2010; Spalla *et al.*, 2014; Schmid *et al.*, 2017; Roda *et al.*, 2019; Agard and Handy, 2021) whose continental margins were characterized by different configurations (*i.e.*, Marroni *et al.*, 1998; 2002; Marroni and Pandolfi, 2007; Manatschal and Müntener, 2009) resulted from the rifting processes. The subsequent NNW-SSE direct convergence between European and Adria Plates produced a SSE-dipping intra-oceanic subduction starting from Late Cretaceous (*i.e.*, Inger *et al.*, 1996; Duchêne *et al.*, 1997; Rubatto *et al.*, 1999; Handy *et al.*, 2010; Thöni *et al.*, 2008; Marroni *et al.*, 2017; Rebay *et al.*, 2018). The subsequent convergence history, about timing and kinematics of the nappe stacking, is well established (*i.e.*, Choukroune *et al.*, 1986; Gidon, 1972; Gratier *et al.*, 1989; Merle and Brun, 1984; Roure *et al.*, 1990; Pfiffner *et al.*, 1997; Schmid and Kissling, 2000; Tricart, 1984; Tricart *et al.*, 2001; Schmid *et al.*, 2017; Dumont *et al.*, 2022). The ongoing NNW-direct motion of the Adria Plate led, before, to the closure of the Ligure Piemontese ocean and then to the involvement of the Europe continental margin in the subduction zone starting from Paleocene-early Eocene (*i.e.*, Elter and Pertusati, 1973; Chopin, 1984; Schmid *et al.*, 1996; Duchene *et al.*, 1997; Rubatto and Hermann, 2001; Michard *et al.* 2002; Michard *et al.*, 2004; Molli, 2008; Handy *et al.*, 2010; Lanari *et al.*, 2012; Sterzinsky *et al.*, 2011). The continental subduction started in the late Paleocene (Schmid *et al.*, 1996), to East, progressively migrating toward West in the middle- to late-Eocene (Michard *et al.*, 2004; Sterzinsky *et al.*, 2011; Lanari *et al.*, 2012). The incoming of the European continental margin in the subduction channel led to the continental collision in late Eocene-early Oligocene (Coward and Dietrich, 1989; Stampfli *et al.*, 2001a; Rosenbaum *et al.*, 2002; Dal Piaz *et al.*, 2003; Simon-Labric *et al.*, 2009; Handy *et al.*, 2010) and, subsequently, the doubly-verging belt started to develop (Coward and Dietrich, 1989; Stampfli *et al.*, 2001; Rosenbaum *et al.*, 2002; Handy *et al.*, 2010; Marroni *et al.*, 2010; Marroni *et al.*, 2017). The involvement of the European continental margin in the subduction channel is marked by the development of the Alpine foreland basins (Sissigh, 2001; Ford and Lickorish, 2004; Ford *et al.*, 2006) toward external zone, and, in the internal one of the belt, by the exhumation up to the surface of oceanic and continental units previously accreted into the alpine wedge at different depths (*i.e.*, Agard *et al.*, 2001; Beltrando *et al.*, 2010; Handy *et al.*, 2010 and quoted references; Gasco *et al.*, 2013). The involvement of the European continental

margin at the subduction zone is associated to the change of convergence direction from NW-SE to WNW-ESE to NE-SW (*i.e.*, Handy *et al.*, 2010; Schmid *et al.*, 2017), with the thrusting of the orogenic Alpine wedge onto the pristine European continental margin located in the western (external) sectors which are gently or not involved in collisional processes (*i.e.*, Bersezio *et al.*, 2002; Corsini *et al.*, 2004; Sanchez *et al.*, 2010, 2011).

The result of this convergence history is a curved and non-cylindric collisional belt, where both continental and oceanic units were involved in subduction, accreted into the Alpine accretionary/orogenic wedge at different depths and rise up to the surface following different exhumation patterns (*i.e.*, Agard *et al.*, 2001, 2002; Tricart *et al.*, 2001; Seno *et al.*, 2003, 2005; Michard *et al.*, 2004; Handy *et al.*, 2010; Sterzinsky *et al.*, 2011; Lanari *et al.*, 2012; Lanari *et al.*, 2014; Ellero and Loprieno, 2017; Rebay *et al.*, 2018; Luoni *et al.*, 2021; Hervioue *et al.*, 2022 and many others).

In the western Alpine belt the oceanic units, classically considered as the remnants of the Ligure-Piemontese Ocean, are represented by basement and cover rocks characterized by different metamorphic imprints ranging from eclogite to blueschists to Very Low-grade conditions (Lemoine and Tricart, 1986; Buroni et al., 2003; Reddy *et al.*, 2003; Bousquet *et al.*, 2004; Bucher and Bousquet, 2007; Pleuger *et al.*, 2007; Schwartz *et al.*, 2007; Agard *et al.*, 2009; Ellero and Loprieno, 2017; Agard *et al.*, 2018; Agard, 2021 and quoted references). Ophiolitic basement with subordinated metasedimemtary covers (i.e., quartzites, marbles and calcschists) are well preserved in the Zermatt-Saas Zone (Bearth, 1967) and in the Monviso Massif (Agard *et al.*, 2001; Schwartz, 2002; Beltrando *et al.*, 2008; Balestro *et al.*, 2015; Balestro *et al.*, 2017). In these zones the units generally show eclogite metamorphic imprint with some meta-ophiolite slices showing ultra-High-Pressure (UHP) metamorphism (Balestro *et al.*, 2015; Balestro *et al.*, 2017; Ellero and Loprieno, 2017; Rebay *et al.*, 2018; Agard *et al.*, 2018; Luoni *et al.*, 2021; Hervioue *et al.*, 2022). Fragments of ophiolitic basement crop out also in the Voltri Massif (central Ligurian Alps, cf. Voltri Group of Chiesa *et al.*, 1975) and in Alpine Corsica (Caron *et al.*, 1979; Marroni *et al.*, 2004; Levi *et al.*, 2007; Vitale Brovarone *et al.*, 2012; Di Rosa *et al.*, 2020). Examples of oceanic cover rocks consisting of calcschist associated with minor bodies of mafic and ultramafic rocks are well exposed in the Combin area (Combin Zone, Bearth, 1967) and in the Queyras area (Schistes Lustres complex, Agard *et al.*, 2009; Agard *et al.*, 2018 and quoted references). These units show a dominant blueschist metamorphic imprint (Ballèvre *et al.*, 1990; Agard *et al.*, 2001; 2009; Schwartz *et al.*, 2013; Lagabrielle *et al.*, 2015; Herviou *et al.*, 2022 and quoted references). However, some ophiolite units of the Western

Alps fall outside of these groups, like the Moglio-Testico Unit (Western Ligurian Alps, Figures 2b, 3a-b), being characterized by both less pervasive deformation and weaker metamorphic imprint (Vanossi et al., 1984).

The oceanic units thrusted toward west onto the Internal Crystalline Massif that together with the Briançonnais Units (Figure 2b, 3a-b)

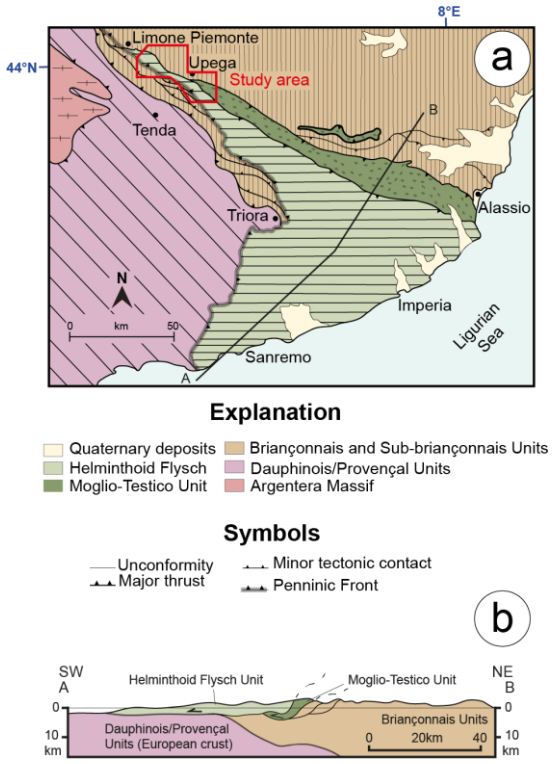

Figure 3. a) Tectonic sketch of the Western Ligurian Alps. The red box indicates the mapped area in this Thesis, and the A-B geological cross-section (b).

are regarded as the fragments of distal Europe continental crusts involved in Alpine continental subduction and affected by High-Pressure-Low-Temperature (*HP–LT*) metamorphic imprint (Chopin, 1984; Paul *et al.*, 2001; Michard *et al.*, 2004; Lardeaux *et al.*, 2006; Béthoux *et al.*, 2007; Schreiber *et al.*, 2010; Handy *et al.*, 2010; Sterzynsky *et al.*, 2011; Lanari *et al.*, 2012; Lanari *et al.*, 2014). However, some authors suggested that the Briançonnais Domain, in the Early Cretaceous time, were a block of continental crust separated by the Europe Plate forming the so-called Briançonnais micro-continent (Frisch, 1979; Stampfli, 1993; Schmid *et al.*, 2004). Wortmann *et al.* (2001) proposed that the Briançonnais Domain was part of the Europe Plate until the end of the Jurassic, whereas Mohn *et al.* (2010) following Lavier and Manatchal (2006) considered the Briançonnais Domain as a portion of continental crust, located in between the European and Adria Plates. The Briançonnais Units, including the Internal Crystalline Massifs and the oceanic units represent the so-called Penninic Units (Dal Piaz *et al.*, 2003; Schmid *et al.*, 2004; Dal Piaz *et al.*, 2010). Toward west, i.e., toward the external sectors, the Penninic Units thrusted by means the so-called Penninic Front, an E-dipping complex thrust zone developed starting from middle to late Eocene age (*i.e.*, Barfety *et al.*, 1996; Ceriani *et al.*, 2001; Lardeaux *et al.*, 2006; Schmid *et al.*, 2017; Cardello *et al.*, 2019), onto the pristine Europe continental margin; the latter is represented by Dauphinois/Helvetic Units whose basement is well-exposed in the External Crystalline Massif (Figures 2b, 3a-b).

2.2 Tectonic setting of the southwest termination of the Alpine belt

Geophysical investigations performed on the western Alpine belt (i.e., Lardeaux *et al*., 2006; Mohn *et al*., 2010; Mosca *et al*., 2010) clearly indicate a doubly-verging crustal-scale architecture. The westernmost (external) edge is represented by a fold-and-thrust belt composed by Dauphinois/Helvetic Units and the External Crystalline Massifs. This is separated by the overlying Penninic Units, here represented by the Briançonnais and oceanic units by means of the southern prolongation of the Penninic front developed starting from early Oligocene age (Barfety *et al*., 1996; Ford *et al*., 1999; Lanteaume, 1962; Lanteaume, 1968; Seno *et al*., 2005; Maino *et al*., 2015 Gosso *et al*., 2019). The Briançonnais Units as well as the Internal Crystalline Massifs are overthrust by the oceanic units representative of the Ligure Piemontese ocean (Paul *et al*., 2001; Lardeaux *et al*., 2006; Schreiber *et al*., 2010).

The Dauphinois/Helvetic Units consist of pre-alpine basement rocks reworked during Alpine collision (Argentera-Mercantour, External Crystalline Massifs) recording Variscan tectonics (Corsini *et al*., 2004; Sanchez *et al*., 2011). These basement rocks are associated with Meso-Cenozoic covers characterized by a polyphase deformation history developed under very low-grade metamorphic conditions (Bersezio *et al*., 2002).

The Briançonnais Units consists of Meso-Cenozoic meta-sedimentary covers, while their pristine pre-Alpine basement is well preserved in the Internal Crystalline Massifs (Compagnoni *et al*., 1974; Malusà *et al*., 2002; Le Bayon and Ballèvre, 2004; Bucher and Bousquet, 2007). Both the Internal Crystalline Massifs and the Briançonnais Units show a polyphase deformation history associated with HP-LT metamorphism (Goffé *et al*., 2004: Bertrand *et al*., 2005; Bousquet *et al*., 2008; Lardeaux, 2014). The oceanic units are here represented by the so-called Moglio-Testico Unit (Figures 3a-b), which is detached from its original oceanic basement and it is characterized by a sedimentary succession of Late Cretaceous-Paleocene(?) age (Haccard, 1961; Lanteaume and Haccard, 1962; Lanteaume, 1962; Galbiati, 1985; Vanossi *et al*., 1986; Marini, 1995). This unit crops out along the western Ligurian Alps segment (Figures 3a-b) and it is characterized by a polyphase deformation history associated with Very Low- to Low-grade metamorphic imprint (Messiga *et al*., 1982; Bonazzi *et al*., 1987).

In the westernmost Ligurian Alps the continental units, i.e., Dauphinois/Helvetic and Briançonnais units and the oceanic-derived Moglio-Testico Unit (Figure 2b, 3a-b) are tectonically overlain by the Late Cretaceous non metamorphic Helminthoid Flysch Unit, cf. San Remo-Monte Saccarello Unit - Sagri, 1984). This unit is detached from its original basement whose paleogeographic nature is still

matter of debate (Kerckhove, 1969; Lanteaume, 1968; Elter *et al*., 1961, Sagri, 1980; Elter, 1997; Mueller *et al*., 2018; Sanità *et al*., 2020). A tectonic pile characterized by a structural architecture like that described above was documented along the Embrunais-Ebaye sector by other authors (Merle, 1982; Merle and Brun, 1984; Michard *et al*., 2004).

2.3 Cenozoic tectonic evolution of the Alps/Apennine junction area

During the Tertiary age, in the junction area between southwestern Alps and the Northern Apennines different interfinger tectonic events took place. In the modern paleotectonic reconstructions (*i.e.*, Elter, 1975; Elter, 1977; Seno et al., 2003, 2005; Molli, 2008; Handy *et al*., 2010; Marroni *et al*. 2016; Marroni *et al*., 2017; Angrand and Monthereau, 2021) it was largely accepted that the oceanic units located along the Ligurian Alps segment (*i.e.*, Capponi and Crispini, 2002; Seno *et al*., 2003; Seno *et al*., 2005; Capponi *et al*., 2009) as well as the oceanic unit cropping out in the Northern Apennine chain (Internal Ligurian Unit, Molli, 2008; Marroni *et al*., 2010; Marroni *et al*., 2017 and quoted references) were involved in the alpine accretionary wedge at different depths during the Paleocene-Early Eocene time. Subsequently, the Briançonnais Units, including the ICM, were involved into the collisional processes, *i.e.*, underthrusting, accretion and subsequent exhumation into the Alpine orogenic wedge. Indeed, the Helminthoid Flysch Unit of the Maritime and Western Ligurian Alps and the Antola Unit (External Ligurian Units, Marroni *et al*., 2002, Marroni *et al*., 2010), the latter currently cropping out at the top of the Northern Apennine stack (Figure 2b, see Marroni *et al*., 2010; 2017 for a detailed discussion about this topic), are thought to be representative of the leading edge and the uppermost units of the Alpine wedge in the middle Eocene (Grandjacquet and Haccard, 1977; Elter, 1997; Seno *et al*., 2005; Molli, 2008; Marroni *et al*., 2010; 2017). During the middle to late Eocene, while subduction continued, continental collision occured and the current tectonic stack, today cropping out in the western Ligurian Alps, started to form (*i.e.*, Vanossi *et al*., 1986; Seno *et al*., 2003, 2005). In the late Eocene-early Oligocene time subduction and exhumation cease in according to the age of the first post-orogenic sediments cropping out in the Tertiary Piedmont Basin (TPB, Lorenz, 1986) visible in the inner (eastward) sector of the Alpine belt (Figure 2b), and in the southern sides of the central Ligurian Alps ("Pietra di Finale", Mosna *et al*., 1990). At the same time of ongoing regional shortening, toward the southern prolongation of the western Alps belt, currently exposed in Corsica Island, the arrival of thicker continental crust leading at the block of the subduction and the presence of still-open oceanic domain east of the Alpine accretionary

wedge allowed subduction flip with the onset of the Apenninic tectonic history (Elter, 1975; Elter, 1977; Molli, 2008; Marroni *et al*., 2010; Marroni *et al*., 2017; Di Rosa, 2021 and quoted references). In the southwest Alpine belt and in Ligurian Units cropping out in the Northern Apennines (*i.e*., the Antola Unit, see Levi *et al*., 2006) this geodynaimc event produced opposite tectonic displacement, the latter superimposed on the older structures, as well as regional-scale back-thrusting and back folding involving all the units cropping out in the Ligurian Alps (*i.e.*, the Briançonnais Units) as suggested by Vanossi *et al*. (1986) and supported by geophysical data (Falletti *et al*., 1995). Especially, the uppermost units (*i.e.*, the Helminthoid Flysch Units) located along the southwest side of the Alpine wedge move westward onto the foreland basin (Merle and Brun, 1984; Seno *et al*., 2005; Perotti *et al*., 2012; Maino *et al*., 2015; Maino and Seno, 2016), while those located on the other side (*i.e.*, toward east) move backward with a E-SE kinematics (Elter, 1975; Daniele and Plesi, 2000; Marroni *et al*., 2002; Levi *et al*., 2006; Molli, 2008; Molli *et al*., 2010 and quoted references).

Toward W and SW-most sectors (*i.e.*, the external sector of the Western Alpine belt) the compressional regime led to the development of thrusts in the Dauphionois/Helvetic Units (Seno *et al*., 2003 and quoted references; Seno *et al*., 2005) and to the emplacement of the Helminthoid Flysch Units onto their early Oligocene topmost deposits (*i.e*., Ventimiglia Flysch, Decarlis *et al*., 2013; Perotti *et al*., 2012; Maino *et al*., 2015). This is in according both with the ages of the youngest turbidite deposits of the Dauphinois/Hellvetic Units in which olistostromes of the upper Helminthoid Flysch Unit were documented, and with the geochronological constraints yielded on thrust surfaces (Maino *et al*., 2015).

Starting from Oligocene onward, the subduction flip associated with the building of the of the Northern Apennine belt implied a regional-scale tectonic shift from compressive to extensive regime which led to the opening of the Ligure-Provençal and Tyrrhenian back-arc Basins and to the rotation of the Corsica-Sardinia Block (Réhault *et al*., 1984; Jolivet *et al*., 1991; Jolivet *et al*., 1998; Doglioni *et al*., 1997; Gueguen *et al*., 1998; Speranza *et al*., 2002; Fellin *et al*., 2005). The latter played a major role in shaping the Alps/Apennines junction and in the fragmentation of the former prolongation of the Alpine belt in the western Mediterranean area (Boccaletti and Guazzone, 1971; Debelmas, 1986; Elter and Pertusati, 1973; Alvarez *et al*., 1974; Laubscher, 1988; Vanossi *et al*., 1994).

Since the ‘70s, some authors proposed that the rotation of the Corsica-Sardinia Block is associated, in the southwestern sectors of the Alps at the boundary between Maritime and Western Ligurian Alps, to an Oligocene E-W-direct sinistral strike-slip shear zone systems (*i.e*., the “Stura Fault” of Laubscher, 1971;

Guillame, 1980). Evidence of this tectonic event were subsequently supported by many authors (Ricou, 1981; Lefebvre, 1983; Ricou and Siddans, 1986; Giglia *et al*., 1996; Bigot-Cormier *et al*., 2006). Strike-slip to transpressive tectonics were invoked also in western Ligurian Alps (Piana *et al*., 2009; D'atri *et al*., 2016; Bertok *et al*., 2018; Piana *et al*., 2021) and though to be responsible of the regional-scale architecture of the northwesternmost sectors of the Ligurian Alps.

3. The boundary between Maritime and Ligurian Alps: The state-of-art

The boundary between Maritime and Ligurian Alps aroused great interest by Alpine geologist in particular during the last twenty years. The investigated area was previously mapped in the Boves Sheet of the 1:100.000 geological map of Italy (Zaccagna *et al.*, 1934) and in the Vieve-Tende Sheet of the 1:50.000 geological map of France (Lanteaume *et al.*, 1990; 1991). However, the lack of a robust stratigraphic database hampered any structural analysis by geologists starting from the '80s (Brizio *et al.*, 1983; Piana *et al.*, 2009; Bertok *et al.*, 2018; Mueller *et al.*, 2020). In his Ph.D. Thesis, Kienast (1963) already invoked intricate tectonic processes to explain the complexes stratigraphic sequences documented in the study area (Cima della Brignola 5-6 km to NE of Punta Marguareis). After that, the pioneering works of Lanteaume (1962) and (1968) outlined this complex tectono-stratigraphic setting describing it along the Maritime and Ligurian Alps segment. In the High Tanaro Valley (western Ligurian Alps), Fierro and Vanossi (1965) emphasized the great difficult to measure the thickness of the sedimentary succession because of the superimposition of different folding system generations.

In the following section, the state-of-art concerning the sedimentary successions and the proposed tectono-metamorphic evolutionary models are summurized.

2.1 Stratigraphic framework of the units

The stratigraphy and sedimentary evolution of the units exposed in the study area have been the main topic of geologists starting with Vanossi (1972), who significantly improved the available chrono- and lithostratigraphic works (Bloch, 1958; Lanteaume, 1962; Guillaume, 1965; Lanteaume, 1968; Campredon, 1977). The same authors described a structural model in which two distinct tectonic units occur: (i) the Marguareis-Nava Unit showing a Meso-Cenozoic succession typical of Briançonnais Domain and mainly composed by Triassic to Late Cretaceous carbonate rocks capped by carbonates and siliciclastic arenites of Tertiary age (cf. *Flysch Noir*, Lanteaume, 1962); (ii) the Late Cretaceous Helminthoid Flysch (cf. *Flysch à Helmintoïdes*, Lanteaume, 1962) characterized by deep-sea siliciclastic turbidite (Bordighera Sandstone, Sagri, 1984) with its basal complex (cf. *basal complexes*, Lanteaume, 1957), the latter made up of manganesiferous shales. The nature of its basement is matter of debated (*i.e.*, Sagri, 1984; Maino and Seno, 2016; Mueller *et al.*, 2018; Sanità *et al.*, 2020). However, authors described deposits showing characteristics similar to what observed for the basal complex, were documented at the base of the Late Cretaceous-Paleogene(?) Moglio-Testico Unit (Haccard, 1961; Lanteaume, 1962; Marini and Terranova, 1985; Galbiati, 1985; Di Giulio,

1992; Marini, 1995). This unit was established for the first time by Lanteaume and Haccard (1962) and it is classically regarded as a sedimentary cover of an oceanic crust (the Ligure-Piemontese Ocean (according with Haccard, 1961; Lanteaume and Haccard, 1962; Galbiati, 1985; Marini, 1995; Galbiati and Cobianchi, 1997) detached from its original basement. The sedimentary sequence is composed by its basal complexes showing chaotic deposits alternated with shales (Moglio Shale, Haccard, 1961) that pass upward to mixed siliciclastic-carbonate deposits characterized by marls alternated to arenites (Testico-Formation, Haccard, 1961). Subsequently, Marini (1995) described two distinct members into the Testico Formation: The older shaly arenaceous, with subordinated marls, Pieve di Teco Member and the younger arenaceous Cesio Member. This unit is tectonically interposed between the Helminthoid Flysch Unit, at the top, and the Briançonnais Units, at the bottom, according with the tectonic frame proposed by Vanossi et al. (1984) and (1986). Based on bio-stratigraphic analogies between the Moglio-Testico and the Helminthoid Flysch Units, many authors (*i.e.*, Sagri, 1984; Vanossi *et al.*, 1984; Galbiati, 1985; Vanossi *et al.*, 1986; Mueller *et al.*, 2018; Manivit and Prud'homme, 1990; Cobianchi *et al.*, 1991; Mueller *et al.*, 2018) proposed a common oceanic origin for these units. Contrary, Elter *et al.* (1961) and subsequently Elter (1997) outlined analogies between the Helminthoid Flysch Units of the Western Alps and the External Ligurian Units cropping out in the Northern Apennine (see Marroni *et al.*, 2002; 2010 for further discussion). The latter are regarded as the sedimentary cover of an ocean-continent transition located close to the Adria Plate (Marroni *et al.*, 1998; Marroni *et al.*, 2002; Marroni *et al.*, 2010; Marroni *et al.*, 2017).

Tectonically located at the base of the Helminthoid Flysch Unit, Lanteaume (1962) and (1968) described different continent-derived tectonic units. (*i.e.*, from European continental margin). This units are documented as tectono-stratigraphic complex (*Lambeaux de Charriage p.p.* Lanteaume, 1962) consisting of siliciclastic turbidite deposits with huge blocks of carbonate rocks with Briançonnais affinity. However, their paleogeographic origin as well as their tectonic meaning are poorly constrained. Similar tectonic frame has been documented in the southernmost sectors (Maino and Seno, 2016). Chaotic rock bodies composed by continental- and Helminthoid Flysch-derived blocks located at the top of the Dauphinois/Helvetic Units occur in the southernmost sectors of the western Ligurian Alps (cf. *Triora Olistostrome Member*, Perotti *et al.*, 2012).

2.2 Tectono-metamorphic and timing constraints

Based on data of Bloch (1958), Lanteaume (1968) and Vanossi (1972), Brizio *et al.* (1983) performed a meso- to map-scale structural analysis on the southwestern sector of the Marguareis Massif. They recognized two tectonic units: The Marguareis Unit (cf. Marguareis-Nava Unit, Vanossi, 1972) showing a typical succession of Briançonnais Domain and the Helminthoid Flysch Unit (cf. San Remo-Monte Saccarello Unit, Sagri, 1979) with its basal complexes (cf. *basal complexes*, Lanteaume, 1957). The authors, in agreement with Lanteaume (1962), documented also a tectono-stratigraphic complex (cf. *Lambeaux de Charriage*, Lanteaume, 1962) tectonically underlying to the Helminthoid Flysch Unit.

Brizio *et al.* (1983) proposed a structural evolution in which the lower part of the basal complex and the Marguareis Unit shared the same polyphase deformation history, the latter characterized by a strain pattern with the superposition of different folding system generations developed from micro-to map-scale. In contrast, the non-metamorphic Helminthoid Flysch Unit and the uppermost part of its basal complexes show a less intricate strain pattern represented by one fold system only. However, the structural relationships between the Helminthoid Flysch and the Briançonnais Units are unclear.

Carminati (2001) suggested that the deformation recorded by the Marguareis Unit developed into a ductile shear zone in an overall southwestward motion of the units during the building of the Alpine wedge at shallow crustal levels.

Subsequently, Piana *et al.* (2009) described a different structural architecture in which high-angle strike-slip to transpressive fault systems mark the boundary between the European-derived continental units (*i.e.*, the Briançonnais and the Dauphinois/Helvetic Units) and the San Remo-Monte Saccarello Unit (cf. Helminthoid Flysch Unit of this work), which previously thrusted onto the continental units. Piana *et al.* (2014) based on illite crystallinity index, highlighted that the fault network separates tectonic units recording different *P–T* conditions ranging from anchizone to lower greenschists facies according with the previous authors (Messiga *et al.*, 1981; Bonazzi *et al.*, 1987). Subsequently, this interpretation was supported by d'Atri *et al.* (2016), Bertok *et al.* (2018) and Piana *et al.* (2021) which proposed that the faulting event played a significant role in the tectonic evolution of the southwestern sectors of the Alps. The same authors proposed that this fault network is part of an E-W direct dextral shear zone active during Alpine collision. Contrary, Mueller *et al.* (2020) according with Maino and Seno (2016), reconstructed a structural frame consisting of a SW-verging tectonic pile where the

Helminthoid Flysch Unit is thrusted onto the European-derived continental units (Dauphinois/Helvetic Units) during late Eocene-early Oligocene age (Maino *et al.*, 2015). Moving from SW toward NE, the Helminthoid Flysch Unit shows overturned tectonic contact with the Briançonnais Units (Ormea Briançonnais Unit, Mueller *et al.*, 2020 - cf. with the Margareis Unit of this work), *i.e.*, the Marguareis Unit tectonically above the Helminhtoid Flysch, both showing contrasted internal deformation patterns as already highlighted by previous authors. Local inverted structural relationships were already outlined by previous authors (Vanossi *et al.*, 1984; Cabella *et al.*, 1987; Di Giulio, 1987; Merizzi and Seno, 1991) which regarded them as the results of local SW-verging later folding event affecting the whole stack of units in this sector the belt.

Geochronological ages about the deformation events are poorly constrained. d'Atri *et al.* (2016) based on the structural and metamorphic data of Piana *et al.* (2009) and (2014) suggested an early Oligocene age for the deformations and the metamorphic imprint recorded by all the tectonic units cropping out in the study area.

Contrary, Michard *et al.* (2004), in according with Moniè (1990), proposed a post-Bartonian age (38 Ma) for the syn-metamorphic deformation phases recorded by the Briançonnais Units cropping out in the Embrunais-Ubaye sector (Western Alps, North of the study area, Figure 2b). This hypothesis was subsequently supported by Strzerzynski *et al.* (2011) and Lanari *et al.* (2014) which estimated 45-37 Ma for the metamorphic peak conditions achieved during the continental subduction of Briançonnais Units in other sectors of the Western Alps.

4. Methodological approaches

4.1 Methods

To reach the goals of this Thesis a multidisciplinary approach has been applied combining fieldwork and lab analyses. Different techniques were considered in order to reconstruct the sedimentary evolution and to constraint the tectono-metamorphic history of the tectonic units cropping out in the investigated area.

- Fieldwork.

The mapped area run along NW-SE direction covering about 110 km^2 from the Bric Campanin-Monte Alpetta ridge, to Northwest, to Piaggia Village to Southeast (Plate 1). The geological survey has been performed using 1:10.000 scale topographic map applying the classic field techniques. Detailed geological and structural maps of the investigated area have been realized. During the fieldwork, samples for different lab analyses have been collected (see Plate 1 for more details).

- Nannofossils and Provenance.

To better constrain the sedimentary evolution of each unit a sampling for the analysis of the calcareous nannofossils content (a profoundly acknowledgement to Dr.sa Catanzariti of the CNR of Pisa for her support to do this analysis) and to characterize the source area of the deposits were collected. The latter was investigated by modal analysis (see S1 supplementary materials for more details about the counting classes) on arenites of the turbiditic deposits in order to estimate the contribution to the sediment of the different rock types of the source area. Point counting (500 to each thin section) has been carried out on medium-to coarse grained arenites by polarizing microscope following the Gazzi-Dickinson technique (Gazzi, 1966; Dickinson, 1970; Zuffa, 1980, 1985), in order to minimize the dependence of arenite composition on grain-size. The sampling criteria in the field have been: (i) the low degree of alteration and (ii) good sorting of the arenites.

- Micro- to map-scale structural analysis.

During fieldwork, the spatial orientation of the main linear and planar structural features (fold axes, stretching and intersection lineations, fault plane-related striae, bedding, axial planes, foliations, thrust planes, shear zones, fault planes) were collected and their mutual relationships are showed in stereographic projections (Schmidt net, lower hemisphere). The systematic collection of the structural features allowed reconstructing the main axial plane traces of folding systems in each unit. In areas where clear meso-scale superposition relationships between different tectonics structures were well evident, samples of meta-pelites were collected to describe the deformations at the micro-scale (nomenclatures and classifications proposed by Ramsay, 1967 and Passchier and Trouw, 2005 were used).

- Pressure and Temperature (*P–T*) estimation. To better constraint the thermomechanical evolution of the tectonic units, the reconstruction of Pressure-Temperature paths (*P–T* paths) is of paramount importance. This is more difficult to do in meta-sedimentary rocks, *i.e.*, meta-pelites, metamorphosed under low temperature conditions where detrital grains remain as relict phases, so impeding to reach chemical equilibrium at whole rock-scale (Frey and Robinson, 1999; Powell *et al*., 2005; Lanari and Engi, 2017). For these reasons, micro-structural observation aimed to attest for costability of a given mineral pair, i.e., chlorite and white micas, allowed me to reasonably assume that condition of local chemical equilibrium (*i.e*., Lanari and Engi, 2017) was attained to calculate the P and T consitions of this equilibrium (see S2 supplementary materials for more details). Thus, calibrated X-ray maps on polished thin section of meta-pelites samples were obtained from Electron MicroProbe Analysis (EPMA) following the suggestions proposed by De Andrade *et al*. (2006) and Lanari *et al*. (2014) (the reader are referred to the S2 supplementary materials for more technical details about the experimental condition during the stage of data acquisition). The composition for each chlorite-phengite pairs is closely linked to micro-structural domains. So, for each chlorite-phengite pair, *P* and *T* estimations were calculate by means XMapTools (Lanari *et al*., 2014) and ChlMicaEqui (Lanari, 2012) programs (the description of the methods is reported on the S2 supplementary materials). Subsequently, the results are compared with the classical geo-thermobarometry available in the literature (Cathelineau, 1998; Masson and Schreyer, 1998; Dubacq *et al*., 2010; Lanari *et al*., 2014; Bourdelle and Cathelineau, 2015).

- Illite Crystallinity (Ill_{IC}) Index and b_0 cell parameter.

Unfortunately, not all of units reached metamorphic conditions (from diagenesis to very low-grade metamorphism) such as to develop (partial or complete) re-crystallization during the deformation events. However, some crystal chemical changes in clay minerals take place producing polytypical and compositional modifications and progressive increase in crystallinity, *i.e*., for the illite mineral, or for the b_0 cell parameter regarded as a function of metamorphic temperature and pressure, under Very Low- to Low-grade metamorphic conditions. Infact, many authors (Weaver, 1961; Kübler, 1967a, b, 1968; Kisch, 1980a, b; Leoni *et al*., 1996; Ellero *et al*., 2001; Ellero et al., 2021) have used the Illite Crystallinity Index (IC index) and the b_0 cell parameter (Sassi and Scolari, 1974; Franceschelli et al., 1989; Ellero *et al*., 2021) in the white potassic micas as a semi-quantitative geothermometer and geobarometer indicators, respectively, to define the transition between diagenesis and metamorphism. This taking in mind that: these

parameters are not related to the metamorphic peak conditions reached by the units; and they are rather sensitive (especially the Ill_{IC}) to temperature and pressure variations recorded by each tectonic unit during the tectono-metamorphic history. The measure of the Ill_{IC} and the b_0 cell parameter was carried out on the white potassic micas in carbonate-free pelites from units in which metamorphic re-crystallization are less developed (see the next sections for more details, the Prof. Marco Lezzerini and Marco Tamponi are profoundly thanked for the technical support during sample preparation and processing). To verify the robustness of the results obtained in this work, a comparison with the data published in literature by different authors in the same tectonic units was performed. Whole-rock and clay fraction were investigated using powder diffractometer (for X-ray Diffraction, technical details about the experimental conditions are reported on the S3 supplementary materials). Each unaltered rock sample was disaggregated using a jaw crusher and then gently grinding to obtain whole-rock powder fraction. This grain-size was further reduced until to obtain a powder <2 µm by separating by the aqueous suspensions from the whole-rock powder following the methods proposed by Leoni *et al*. (1996) by differential settling. The Ill_{IC} was measured on <2 µm grain-size glycolated powder fraction smeared on glass slides (see the S3 supplementary materials for more details). Particular care to the amount of clay materials on all of them (approximately 2mg/cm^3) following Lezzerini *et al*. (1995).

The Ill_{IC} measures the changes in the shape (full width at half maximum, FWHM) of the first basal reflection of illite grains at the X-ray diffraction. The FWHM values expressed in Δ2θ CuKα unit of the illite 10 Ä peaks were expressed in the Crystallinity Index Scale (CIS, Warr and Ferreiro Mählmann, 2015) according to the following linear correlation: CIS=1,4556*FWHM-0,1381, R^2=0,898. In the Illite CIS scale, 0,32 and 0,52 values are the upper and lower limits of the anchizone region and they correspond to the 0,25 and 0,42 Kübler index values (Basel Lab) and Warr and Ferreiro Mählmann (2015) proposed the correlation: (CIS)=1,1523* Kübler values (Basel)+0,0036, R^2=0,986. In the CIS scale, the 0,42 value separates the anchizone region in the upper and lower zone (Warr and Ferreiro Mählmann, 2015). The b_0 cell parameters of potassic white micas was calculated measuring the $d_{060,331}$ spacing using the (211) quartz reflection as internal standard (Sassi and Scolari, 1975; Kisch *et al*., 2006); the positions of mica and quartz reflections were defined on randomly oriented whole-rock powders for each sample (experimental conditions and technical details are reported in the S3 supplementary materials). A detailed list of samples used for all the previous described analysis is reported in the S4 supplementary materials.

5. The tectonic units at the boundary between Maritime and Ligurian Alps: Lithostratigraphy

This work allows me to reconstruct, for the first time in the study area, a structural architecture (Plate 1) where oceanic units are sandwiched between Europe-derived continental units (these results were published on international scientific journals during this Ph.D. project - see Sanità *et al*., 2020; Sanità *et al*., 2021; Sanità *et al*., 2022a). They are, from the structurally highest to the lowest (Plate 1The Marguareis Unit (MU, Brizio *et al*., 1983; cf. Monte Marguareis Unit of Carminati, 2001) that consists of a Meso-Cenozoic sedimentary succession typical of Briançonnais Domain (Vanossi, 1972); The Moglio-Testico Unit (MT, Lanteaume and Haccard, 1962; Marini and Terranova, 1985; Marini, 1995) composed by Late Cretaceous-Paleogene(?) sedimentary succession (Galbiati, 1985) regarded as a fragment of the Ligure Piemontese oceanic cover detached from its original basement (Haccard, 1961; Lanteaume and Haccard, 1962; Vanossi *et al*., 1984 and quoted references); The Helminthoid Flysch Unit (FH, cf. San Remo-Monte Saccarello Unit of Sagri, 1984, and *Flysch a dominant calcaires and Flysch gréseuse* of Lanteaume and Haccard, 1962) stemming from Ligurian Domain; decametric-sized continent-derived tectonic slices here called Cima del Becco (BS) and Chambeuil (CS) Slices (cf. *Lambeaux de Charriage p.p.* of Lanteaume, 1962), and the Cabanaira Unit (CU, cf. *Lambeaux de Charriage p.p.* of Lanteaume, 1962) both showing a sedimentary succession similar to that of the Briançonnais Units. Owing the correlation between the continent-derived slices and the Marguareis Unit (Plate 1), *i.e.*, they are composed by the same lithotypes, their lithostratigraphic features are described together. The stratigraphic features of each tectonic units will be shown starting from the classic orogen-scale structural order (according to Vanossi *et al*., 1984; Seno *et al*., 2003; 2005), *i.e.*, the topmost Helminthoid Flysch Unit, the Moglio-Testico Unit, The Briançonnais units.

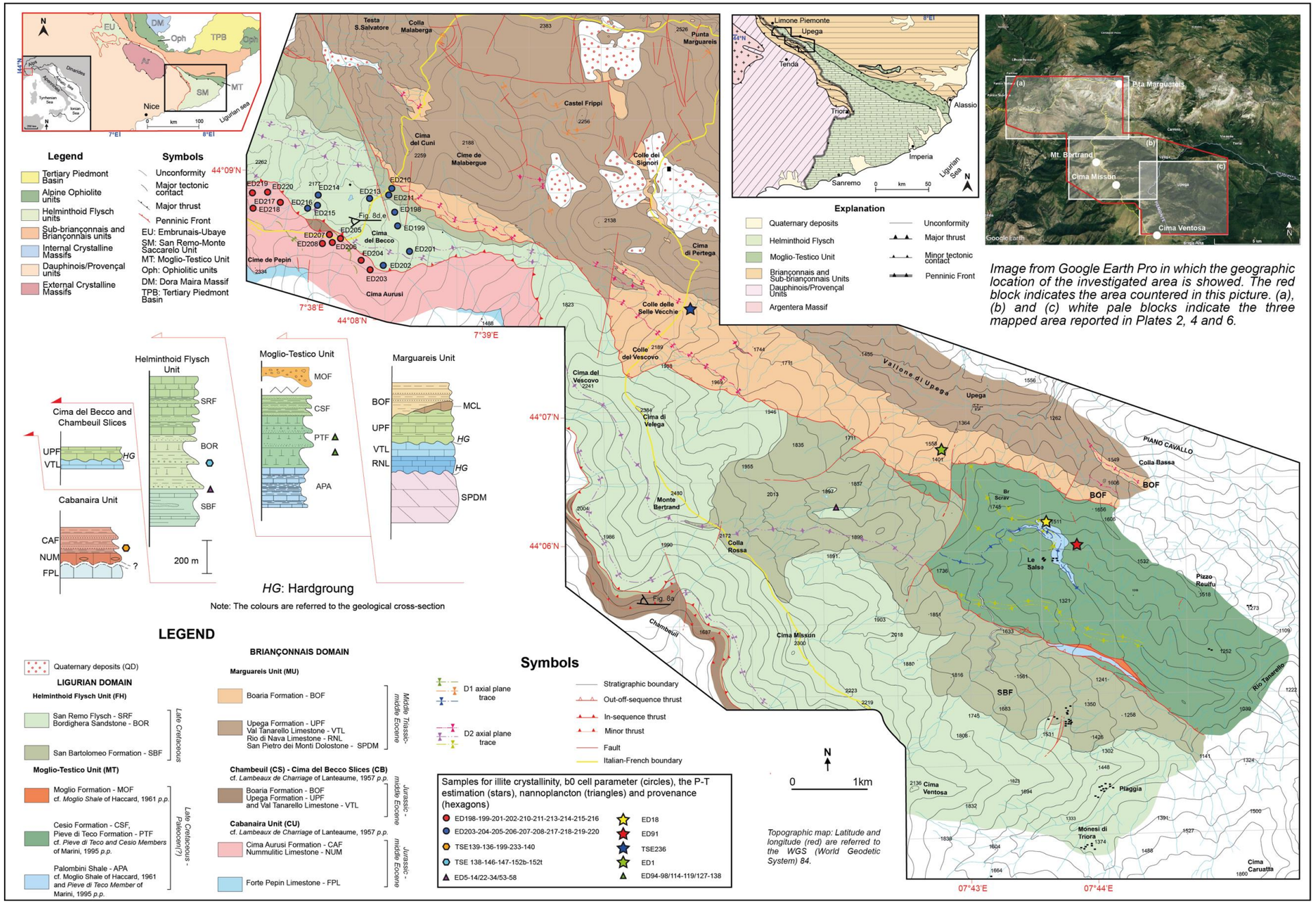

Plate 1. Simplified geological map of the investigated area. The stratigraphic log for each unit is shown. The stratigraphic position and the geographic location of the different samples are reported.

5.1 Lithostratigraphy of the units

- The Helminthoid Flysch Unit

The Helminthoid Flysch Unit shows a NW-SE trend and extends for about 25 km^2 from Bric Campanin to Cima Ventosa (Plate 1) with a thickness of about 750 m. It consists of a non-metamorphic sedimentary succession, showing a fining-upward trend, and detached from its original basement whose nature is unknown. Here, this unit is represented by the San Bartolomeo Formation (Figure 4a, *basal complexes* of Lanteaume, 1957) consisting of varicoloured manganesiferous shales, showing a thickness of 200 m, that upward are intercalated with rare cm-thick beds of fine-grained limestones (Figure 4b) and regarded as deposits sedimented in a basin plain environment, according to Sagri (1984). In their upper part cm-thick lenticular beds of fine-grained quartz-rich arenites showing arkosic composition are also present.

The San Bartolomeo Formation grades upward to the Bordighera Sandstone (Figures 4b-c-d) showing 250-300 m of thickness (Plate 1). This consist of siliciclastic turbidites capped by dm-thick beds of marls and dark shales (Figure 5d) with an arenite/pelite (a/p) ratio >1. The coarse- to medium-grained arenitic beds show high erosive ability testified by up to cm-thick clay-chips (Figure 4c), amalgamation surfaces and erosional base (F5 facies of Mutti, 1992). Stratigraphic features as ripples and plane-parallel lamination are also present. According to Manivit and Prud'Homme (1990) and Cobianchi *et al.* (1991) the depositional environments is related to inner deep-sea fan. The Bordighera Sandstone pass upward to the San Remo Flysch (Plate 1, Figures 4e-f, Lanteaume *et al.*, 1963) represented by calcareous turbidites, (with a thickness of 250 m) characterized plane parallel bedding and coarse-grained bottom, and topped by cm-thick marls and shales (Figure 4f). The relationships between the Bordighera Sandstone and the San Remo Flysch are highlighted by cm-thick beds of arenites alternated with cm-to m-thick beds of calcareous turbidites (Figure 4e). The latter show plane-parallel bedding and coarse-grained bottom. These deposits are related to the deep-sea environments in according with (Lanteaume *et al.*, 1963). 29 samples for the analyses of the calcareous nannofossils content were collected in the whole tectonic unit (see the Plate 1 for the location of the sample and the S4 supplementary materials). Most of samples are barren, while others are characterized by a microfauna assemblage represented only by the more resistant species as *Micula sp., Micula sturophora and Watznaueria* affecting by dissolution, and indicating an age not older than Coniacian. The samples collected at the boundary between the San Bartolomeo Formation and Bordighera Sandstone (ED22-34, the stratigraphic and geographic location of these samples is indicated in Plate 1 and the geographic

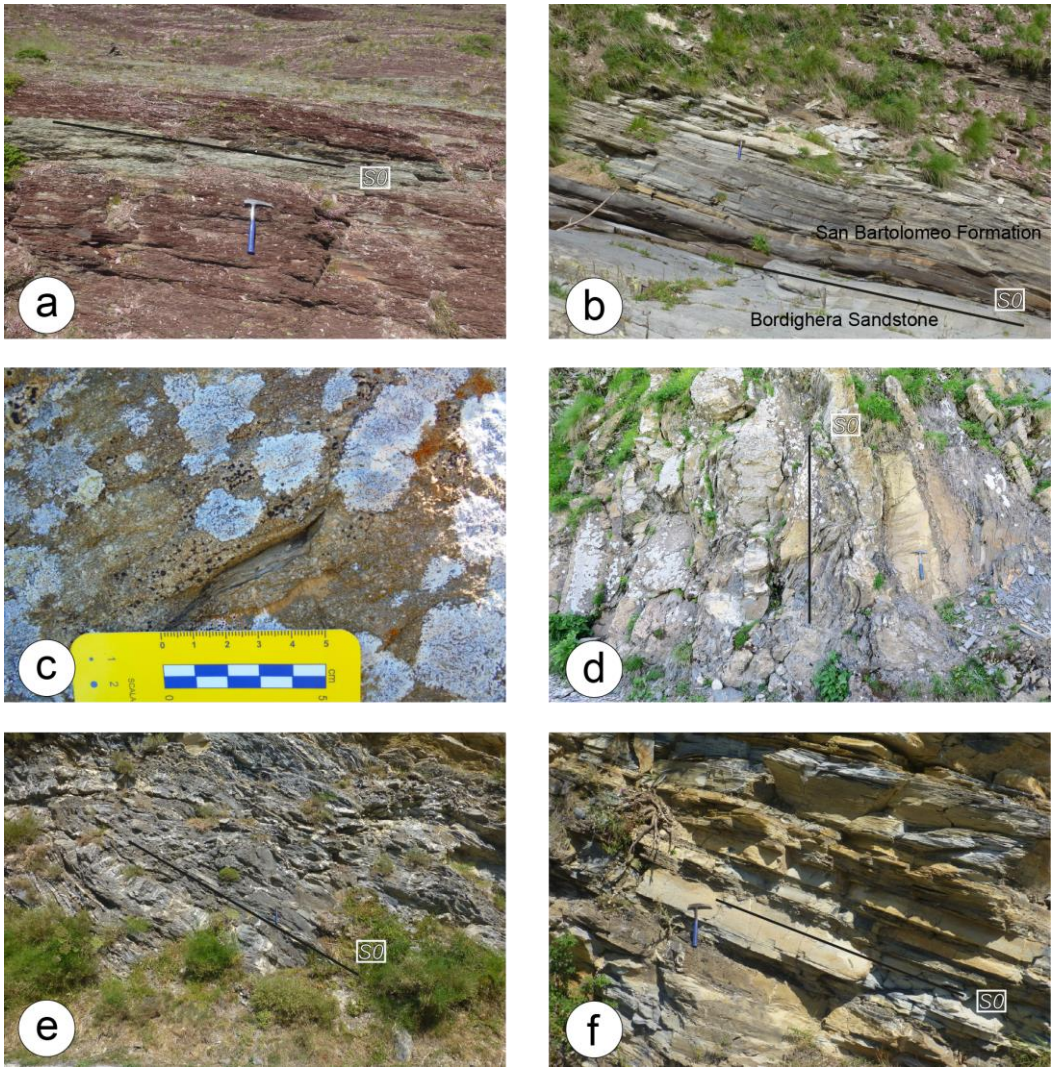

Figure 4. The Helminthoid Flysch Unit formations. a) red to green shales of the San Bartolomeo Formation (Colla Rossa). b) Stratigraphic contact between San Bartolomeo Formation and the Bordighera Sandstone. c) coarse-grained arenites of the Bordighera Sandstone; clay-chips are also present. d) Outcrop of the Bordighera Sandstone with vertical bedding along "Via del Sale". e) Stratigraphic boundary between Bordighera Sandstone and the San Remo Flysch formation, East of Piaggia village. f) Outcrop of San Remo Flysch turbidites near to Piaggia village. S0: bedding.

coordinates are reported in the S4 supplementary materials) show a nannofossils assemblage (*Micula sp. Aspidolithus parcus constrictus, Aspidolithus parcus parcus, Lucianorhabdus sp., Watznaueria*) indicating a Campanian age (Biozone CC18-CC23a, Sissigh, 1977; Biozone NC18-NC20 of Roth, 1978; Biozone UC14-UC16 of Burnett, 1989). This biostratigraphic dataset, according with Manivit and Prud' Homme (1990) and Cobianchi *et al*. (1991), also suggests an older age (Hauterivian?) for the basal complex and a Late Cretaceous age (probably Campanian-Maastrichtian) for the San Remo Flysch deposits.

- The Moglio-Testico Unit

This unit is documented for the first time in the investigated area. It crops out in the southeast sector of the mapped area (Plate 1) covering about 20 km^2 showing a NW-SE trend. It consists of a 700 m thick sedimentary

succession showing a coarsening upward trend (Plate 1). The succession starts with 200-220m-thick of Palombini Shale (APA, cf. Moglio Shale *p.p.* of Haccard, 1961 and

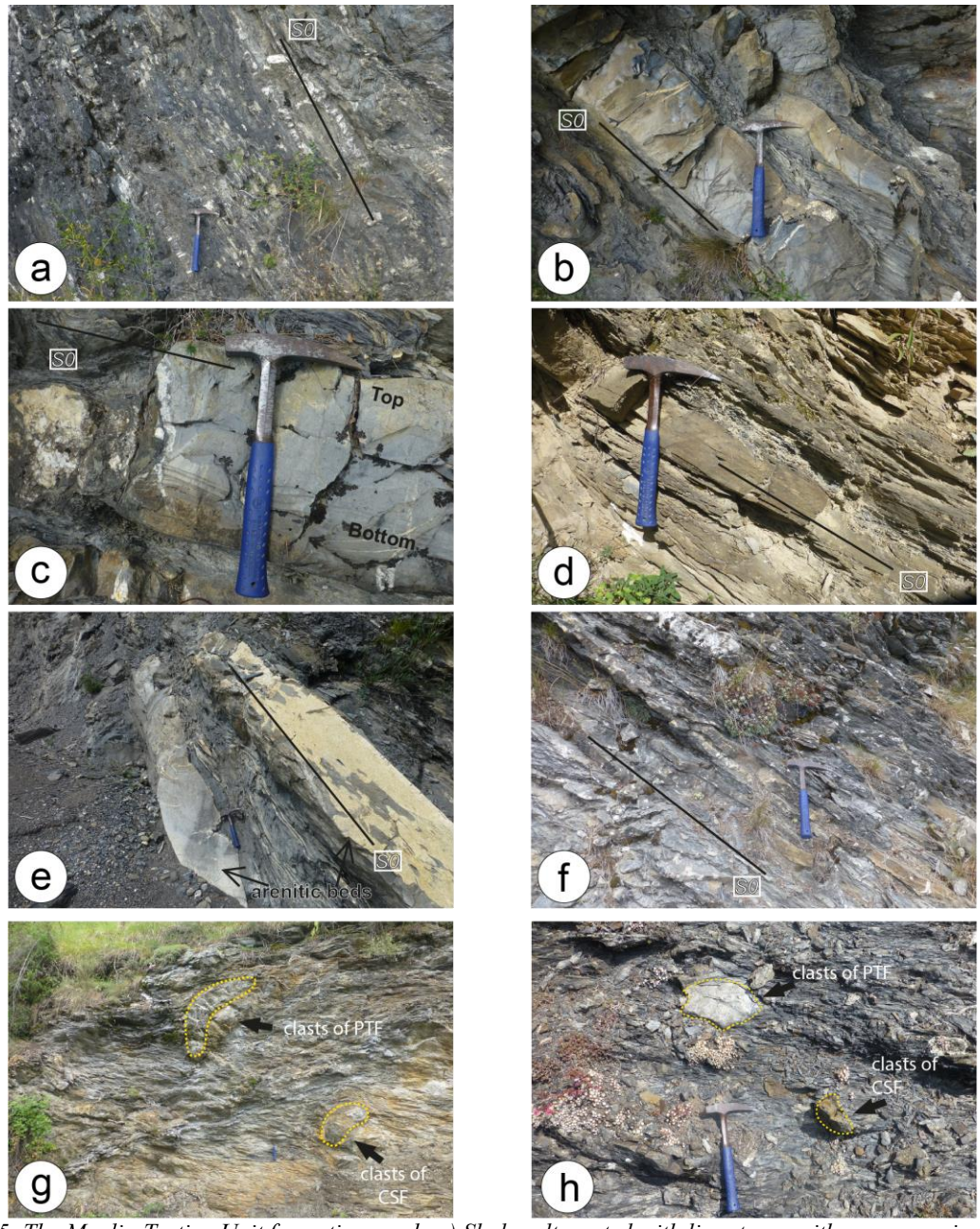

Figure 5. The Moglio-Testico Unit formations. a, b, c) Shales alternated with limestones with coarse-grained base of the Palombini Shale foramtion. d, e) Outcrops of Pieve di Teco Formation along the Val Tanarello stream. f) Outcrop of Caseio Formation near Bric Scravaglion ridge. g, h) Outcrop view of the Moglio Formation chaotic deposits. The orange dashed lines mark the block-matrix boundary. S0: bedding; PTF: Pieve di Teco Formation; CSF: Cesio Formation.

of limestones showing fine-grained arenitic bottom (Figures 5b-c) and plane-parallel bedding. These deposits are related to a pelagic/hemipelagic depositional environment

Pieve di Teco Member *p.p.* of Marini, 1995). These deposits are characterized by cm- to dm-thick beds of black siltstones and shales (Figure 5a) alternated with grey dm-thick beds

(according with Haccard, 1961; Lanteaume and Haccard, 1962). This formation passes upward to the 300 m thick Pieve di Teco Formation (PTF, cf. Pieve di Teco Member

p.p. and Cesio Member *p.p.* of Marini, 1995) showing a plane-parallel bedding consisting of dm-thick beds of marlstones (Figure 5d) alternated with cm- to dm-thick beds of greyish marly-limestones and fine-grained quartz-rich arenitic turbidites showing arkosic or sub-arkosic composition (Figure 5e) topped by cm- to dm- thick beds of shales (F9 facies of Mutti, 1992). The a/p ratio is about ≤1. Normal grading, lamination and ripples are the most recurrent sedimentary features. These deposits were regarded as sedimented in a basin plain environment (according with Boni *et al*., 1971; Marini, 1995). The Pieve di Teco Formation passes upward to the Cesio Formation (CSF, cf. Cesio Member *p.p.* of Marini, 1995) which shows a thickness of about 150 m (Plate 1). These deposits consist of cm-thick beds of medium- to fine-grained quartz-rich arenites, showing arkosic or sub-arkosic composition, alternated with cm-thick beds of black to dark grey shales (Figure 5f) and showing plane-parallel bedding with the a/p ratio is ≤1 (F9 facies of Mutti, 1992). According to Boni et al. (1971) these deposits are related to a basin plain depositional environment. The analysis of the calcareous nannofossils content was performed on 23 samples (the stratigraphic position is indicated in the stratigraphic log of Plate 1 and the geographic coordinates are reported in the S4 supplementary materials). Unfortunately, all of them are barren. Therefore, the Late Cretaceous-Paleocene age range proposed by the previous authors (*i.e.*, Galbiati, 1985; Galbiati and Cobianchi, 1997) for the whole Moglio-Testico Unit is used in this work also. In the mapped area also chaotic deposits (Moglio Formation - MOF, cf. Moglio Shale *p.p.* of Haccard, 1961) have been found as belonging to the succession of the Moglio-Testico Unit (Plate 1). These deposits show a block-in matrix texture with cm- to dm-size fragments of fine to medium grained arenites and carbonates embedded in a shaly matrix (Figures 5g-h). According to their stratigraphic features, these fragments derived from the Palombini Shale, Pieve di Teco and Cesio Fms. It must be underlined that the Moglio Fm. have been recognized in a stack of slices at the base of the Moglio-Testico Unit (Plate 1). This stack includes slices of Palombini Shale, Pieve di Teco Fm. and Moglio Fm. Unfortunately, The Moglio Fm. do not show stratigraphic relationships with the other formations of the Moglio-Testico Unit. To avoid confusion to the reader a synoptic scheme where differences between the classic nomenclature and the

<table>
<tr><th colspan="3">THE MOGLIO-TESTICO UNIT</th></tr>
<tr><td colspan="2" rowspan="2">Stratigraphy from classical geological literature</td><td>Stratigraphy reconstructed in this work</td></tr>
<tr><td>MOGLIO FORMATION (cf. Moglio Shale of Haccard, 1961)</td></tr>
<tr><td rowspan="2">Testico Fm. (Haccard, 1961)</td><td>CESIO MEMBER (Marini, 1995)</td><td>CESIO FORMATION</td></tr>
<tr><td>PIEVE DI TECO MEMBER (Marini, 1995)</td><td>PIEVE DI TECO FORMATION</td></tr>
<tr><td>basal detachment</td><td>MOGLIO SHALE (Haccard, 1961)</td><td>PALOMBINI SHALE</td></tr>
</table>

Figure 6. Synoptic scheme for the Moglio-Testico Unit succession.

new stratigraphic succession reconstructed in this Thesis is shown (Figure 6).

- The Marguareis Unit

It extends for more than 75 km^2 from the Monte Alpetta ridge, to Northwest, until Monte Pian Cavallo, to Southeast, showing a NW-SE trend (Plate 1). It is composed by a Middle Triassic-middle Eocene sedimentary succession (see the stratigraphic log of Plate 1).

The oldest formation is represented by a 200-250 m thick of Middle Triassic peritidal carbonate deposits represented by the San Pietro dei Monti Dolostone (SPDM, Vanossi, 1969). These are characterized by dm-thick beds of white and grey dolostones alternated to dolomitic limestones (Figure 7a). Dasicladaceae are the only fossils recognized in the dolostones, but crinoids were observed in the calcareous levels (Vanossi, 1972). At the top, a Late Triassic and part of Middle Jurassic hiatus occurs (Claudel and Dumont, 1999;

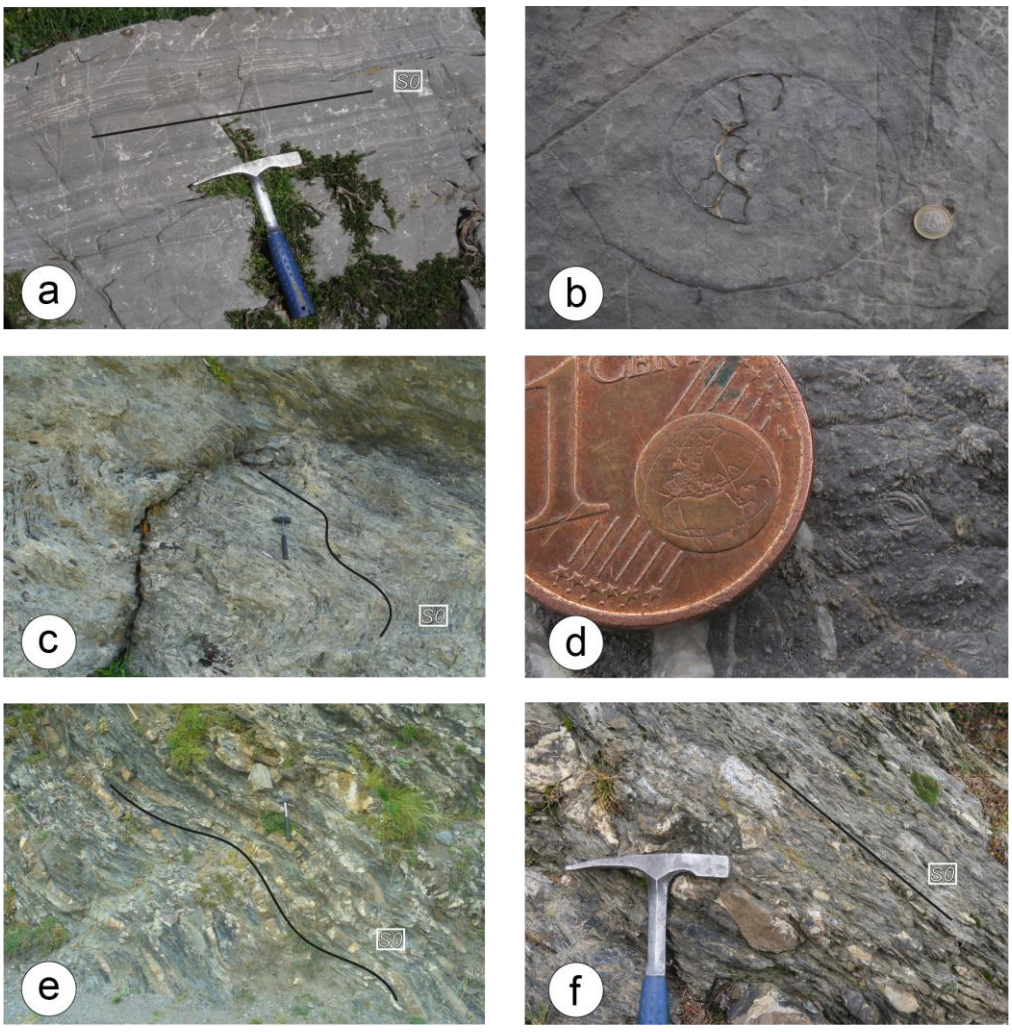

Figure 7. The Marguareis Unit formations. a) San Pietro dei Monti Dolostone. b) Ammonite in Rio di Nava Limestone. c) Outcrop of marly limestone (Upega Formation). d) Madonna dei Cancelli Limestone with fragments of Nummulite. e) middle Eocene turbidite deposits (Boaria Formation) with breccia levels (f). S0: bedding.

Decarlis *et al*., 2008). These deposits are referred to a low-energy platform to lagoon environment of Anisian-Ladinian age (Vanossi, 1969).

The Rio di Nava Limestone (RNL, Boni et al., 1971) lies at the top of the SPDM with about 70-100 m of thickness (Figure 7b). This formation consists of massive dark grey limestones that pass upward to cm-thick laminated fossils-free beds. At the top dm-thick levels of cherty-limestones are also present. Based on the micro- and macrofauna, Lualdi (1994) and Bertok *et al*. (2011) referred these deposits to Bajocian-Bathonian-Callovian-Oxfordian age sedimented in a lagoon environment, with slow circulation and oxygenation, episodically connected to the open shelf.

The Rio di Nava Limestones pass upward to the Val Tanarello Limestone (VTL, Boni *et al*., 1971, cf. *Marbres de Guillestre* of Fallot and Fauret-Muret, 1954) showing a thickness ranging from 25 to 70m (Plate 1). It consists of light grey limestones grade upward to well-bedded pink to violet nodular limestones (cf. *Marbres de Guillestre* Fallot and Faure-Muret, 1954). The upper part of these deposits is characterized by blue-grey Belemnite- and Ammonite-rich limestones. According to Bertok *et al*. (2011) these deposits can be referred to a current-swept pelagic plateau of Kimmerdgian(?)-Berriasian age.

The Val Tanarello Limestone are separated, with an Early Cretaceous hardground, from the overlying Upega Formation (cf. *Calcshistes Planctoniques* of Fallot and Faure-Muret, 1954). The Upega Formation shows about 150-200 m of thickness, and it is composed by grey hemipelagic marly-limestones (Figure 7c). Despite the disagreement between the authors about the age of this deposits (for more details see Lanteaume, 1968; Vanossi, 1963; Guillaume, 1969) a Late Cretaceous age was recentely proposed by Rendinella (2006) accordingly with Lanteaume *et al*. (1990). According with Fallot and Faure-Muret (1954) these deposits are referred to an hemipelagic environment.

The topmost deposits are represented by fossil-rich limestones (Madonna dei Cancelli Limestone, MCL - Vanossi, 1972) and siliciclastic turbidites deposits (Boaria Formation, BOF - cf. *Flysch Noir* of Lanteaume, 1968). The Madonna dei Cancelli Limestone shows a thickness not exciding 40 m. It is characterized by dark grey apparently massive *Nummulite*-rich limestones strongly affected by veins network (Figure 7d). According with Decarlis *et al*. (2013) they can be referred to middle Eocene age and sedimented in an inner to lower shoreface depositional environment (Campredon, 1972; Sinclair *et al*., 1998; Decarlis *et al*., 2013).

The Boaria Formation, uncoformably lies above both the MCL and the UPF (see stratigraphic log of Plate 1). The primary boundary between them appears to be sharp and probably erosive. The total thickness of

this formation is difficult to figure-out because of the tectonic events affecting the Marguareis Unit. However, about 100-150 m of thickness can be estimated (Plate 1). This formation consists of cm-thick beds of dark shales alternated to cm- to dm-thick beds of fine- to medium-grained arenites (Figure 7e) with the a/p ratio ≤1, showing stratigraphic features as lamination and ripples (F9 facies of Mutti, 1992). Upward, chaotic deposits like polymictic breccia levels with cm- to dm-sized clasts of Nummulite-rich limestones and medium-grained arenites are intercalated with the arenites (Figure 7f). These deposits are regarded as deep-sea fan turbidites of middle Eocene age (according with Barféty *et al.*, 1995; Decarlis *et al.*, 2013). The Cima del Becco (BS) and Chambeuil slices (CS) cover small areas (Plate 1, Figure 8). They are composed by the same lithotypes I have documented in the Marguareis Unit (Plate 1, Figures 8a-b-c-d-e). Despite the intense deformation in each tectonic slices the primary

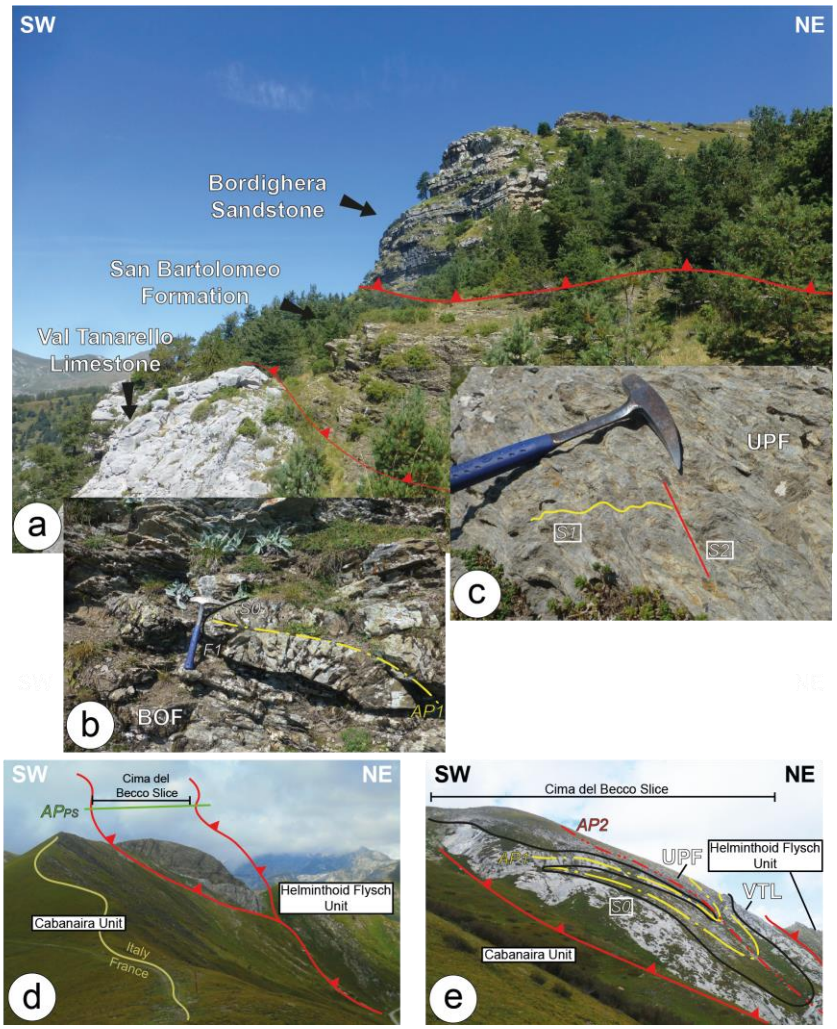

Figure 8. Panoramic view of the tectonic slices located at the bottom of the Helminthoid Flysch Unit. a) Landscape of Chambeuil Slices. b, c) Meso-scale deformations within the Chambeuil Slice. d, e) Cima del Becco Slice with two superposed folding events. BOF: Boaria Formation; UPF: Upega Formation; VTL: Val Tanarello Limestone; AP1: D1-related axial plane; AP2: D2-related axial plane; AP_{PS}: post-coupling-related axial plane; S1: D1-related foliation; S2: D2-related foliation.

stratigraphic relationships between different formations are still preserved (Figure 8e).

- The Cabanaira Unit

It is located in the SW sectors of the Marguareis Massif (Alta Valle Roja), and it is tectonically underlying the Helminthoid Flysch Unit and the continent-derived tectonic slices (*i.e.*, the Cima del Becco Slice, Plate 1). It extends for about 3 km^2 and consists of a Meso-Cenozoic sedimentary succession (see stratigraphic log of Plate 1).

From the bottom to the top, it is made up of Forte Pepin Limestone (Figure 9a, FPL - Gidon, 1972) represented by at least 70 m thick grey fossil-rich apparently massive limestones which, following Gidon (1972), are regarded as carbonate platform deposits of Middle Jurassic(?) age.

The unconformably(?) overlying Nummulitic Limestone (Figure 9b, NUM) shows a total thickness ranging from 30 to 50 m. It consists of dark grey *Nummulite*-rich limestones (Figure 9b) alternated to mm- to cm-thick beds of shales. According to Gidon (1972) and Decarlis *et al*. (2013) these deposits can be referred to middle Eocene (Luthetian?) and sedimented in a lower shoreface depositional environment. Nummulitic Limestone grading upward to the topmost deposits represented by

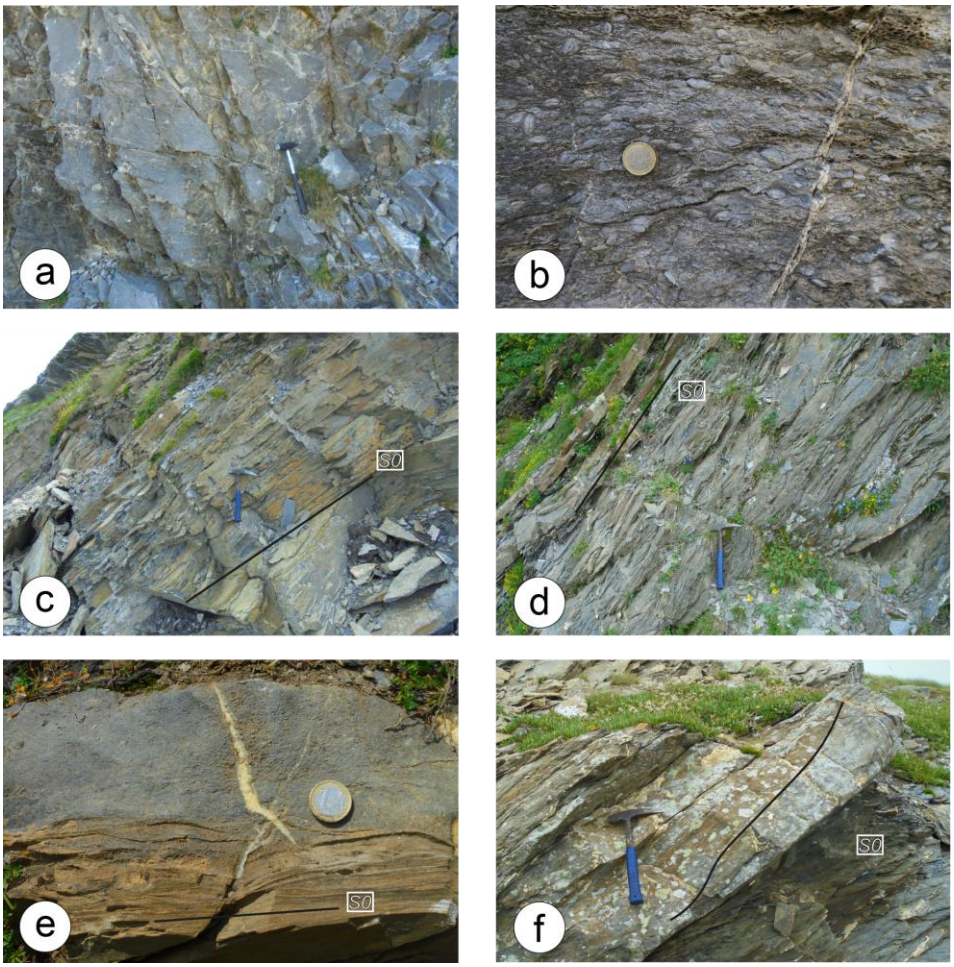

Figure 9. The Cabanaira Unit formation. a) outcrop of Forte Pepin Limestone. b) Outcrop of Nummulitic Limestone formation. c) Marly limestone at the top of Nummulitic Limestone formation. Cima Aurusi Formation (d) with evidence of (e) fossil-rich (Nummulites) layers and cross-stratification (f). S0: bedding.

the Cima Aurusi Formation (CAF, Plate 1). The boundary between each other is marked by cm-thick beds of marly limestones (Figure 9c, cf. *Marbres en plaquettes* of Gidon, 1972). The latter was not mapped because of their limited thickness (<5 m). The Cima Aurusi Formation shows about 150 m of thickness, and it is characterized by cm-thick beds of dark shales alternated to the cm- to dm-thick beds of fine- to medium-grained arenites (Figure 9d) with an a/p ratio ≥1 (F9 Facies of Mutti, 1992). Stratigraphic features as normal grading, Nummulite-rich beds (Figure 9e) and cross-stratification are well preserved (Figure 9f). Upward m-sized block of limestones and Nummulite-rich limestones are present. These deposits are referred to deep-sea fan depositional environments and their close primary relationships with the underlying Nummulitic Limestone formation strongly suggests a middle Eocene age according with Gidon (1972).

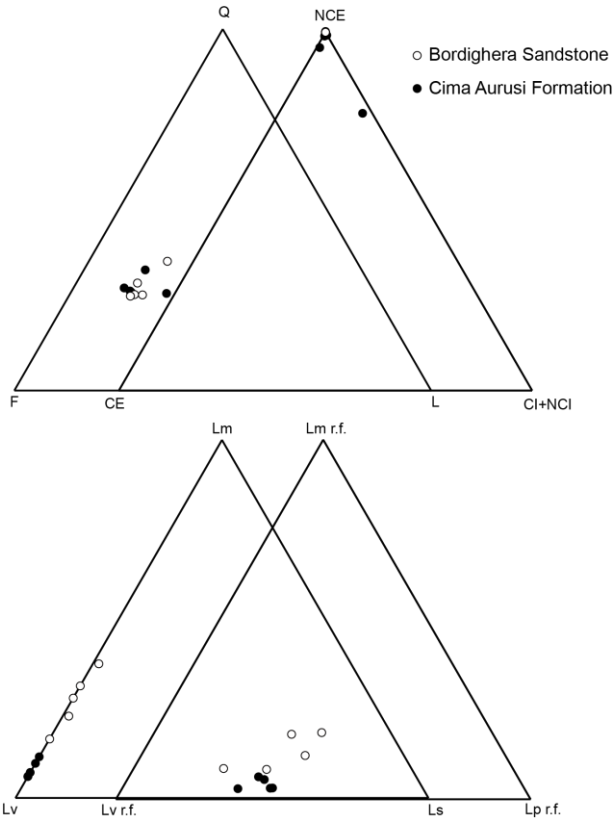

Figure 10. Ternary plot showing the framework modes of arenites from the Bordighera Sandstone and Cima Aurusi Formation.

5.2 Petrographic analysis of arenites

Modal analysis was performed on unaltered medium- to coarse grained arenites of the Helminthoid Flysch and Briançonnais Units deposits (Bordighera Sandstone and Cima Aurusi Formation, respectively) aimed to characterize their source area. The Moglio-Testico and the Marguareis units deposits are affected by intense deformation and metamorphic re-crystallization. These characteristics joined with lack of medium- to coarse-grained arenitic beds prevented any quantitative modal analysis. For these reasons, they are not included in this provenance study. 20 samples were collected to have 10 samples for each unit. For the modal analysis, an early qualitative analysis was carried out to avoid samples showing high-grade of alteration, slightly metamorphic re-crystallization and bad sorting. At the end, 5 samples for each tectonic unit were chosen (the location and the stratigraphic position of the samples are reported in the Plate 1; the geographic coordinates are reported in the S4 supplementary materials). The results are exposed in two separates sub-sections, and they are reported in the table S1 (see S1

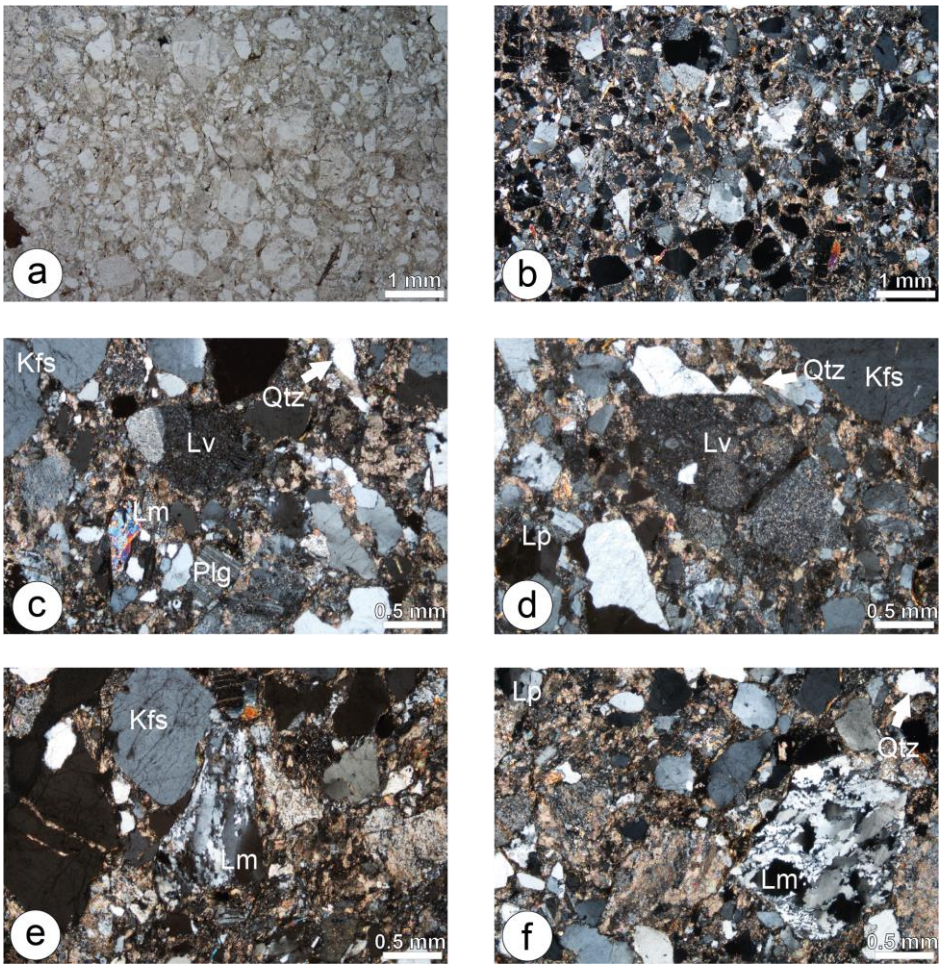

Figure 11. Microphotographs of the typical petrofacies of the Bordighera Sandstone (a, b, c). d) Coarse-grained felsic volcanic clast. e, f) High grade metamorphic rock fragments (Lm). Kfs: K-feldspar; Plg: Plagioclase; Qtz: Quartz; Lp: granitoid lithic fragments.

supplementary). Each modal analysis was plotted in ternary diagrams (Figure 10). The latter correspond to those proposed by Zuffa (1980) and (1985) (first order diagrams, NCE-CE-NCI+CI, Figure 10), which allows us to define the extra- vs intra-basinal contribute respect to carbonate vs siliciclastic. Besides, second (Q-F-L, Figure 10) and third (Lm-Lv-Ls for lithic fragments, Figure 10) order diagrams were also plotted. A further third order diagrams concerning the rock fragments (Lm r.f.-Lv r.f.-Lp r.f.) is also showed to highlights the differences between the Bordighera Sandstone and Cima Aurusi Formation deposits (Figure 10).

- The Helminthoid Flysch Unit

Arenites from Bordighera Sandstone are arkoses or sub-arkoses (Q_{27}-$F_{55}L_{18}$) characterized by siliciclastic dominant (Figure 11a-b) framework (NCE_{100}-CE_0-$NCI+CI_0$) showing a volcanic-dominated composition of fine-grained lithic fragment (Lm_{27}-Lv_{72}-Ls_1). The extra-basinal arenites framework is characterized by mono-crystalline fragments of quartz, K-feldspar and plagioclase (Figures 11c-d). Quartz is present also as polycrystalline clasts. Coarse-grained lithic fragments of felsic volcanic and metamorphic rocks are common (Figures 11d-e-f). Minor

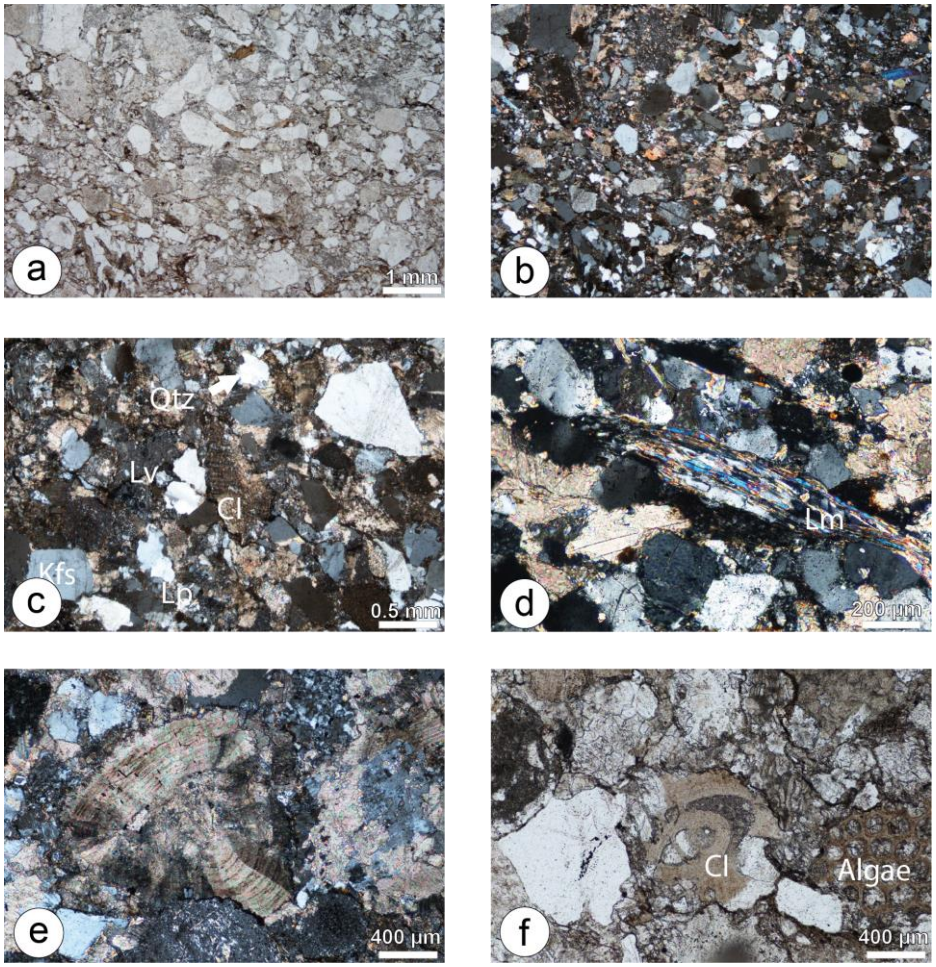

Figure 12. Microphotographs of the typical petrofacies of the Cima Aurusi Formation (a, b, c). d) Close-up of a low-grade metamorphic rock fragment (Lm, i.e., schists). Close-up of the Carbonate intra-basinal fragments (CI) as Nummulites (e) and Algae (f). Kfs: K-feldspar; Qtz: Quartz; Lp: granitoid lithic fragments; Lv: Volcanic lithic fragment.

granitoids rock fragments are also present. Volcanic rock fragments are mainly represented by rhyolites and porphyritic rhyolites (Figure 11d). Metamorphic rock fragments include low- to high-grade clasts (Figures 11e-f). Carbonate rock fragments are scare or lacking at all. Lack of ophiolite-derived rock fragments and the occurrence of high-grade metamorphic clasts are the most striking features of the Bordighera Sandstone.

- The Cabanaira Unit

Arenites from Cima Aurusi Formation are arkoses or sub-arkoses characterized by siliciclastic predominant framework (Figures 12a-b-c) and subordinate carbonate contribution (NCE_{94}-CE_{1}-NCI+CI_{5}) showing a volcanic-dominated composition of fine-grained lithic fragments (Lm_{8}-Lv_{92}-Ls_{0}). The extra-basinal siliciclastic framework is represented by mono-crystalline fragments of K-feldspar, quartz and plagioclase (Figures 12b-c). Mono- and polycrystalline quartz clasts are also present. Coarse-grained lithic

fragments mainly include felsic volcanic fragments and low-grade metamorphic rock fragments (Figures 12c-d). Minor amount of granitoids rock fragments is also present (Figure 12c) Medium- to high-grade metamorphic rock fragments are lacking at all. The extra-basinal carbonate framework (here grouped under "limeclast", see Table S1 in the supplementary materials) consists of carbonate clasts with textural features partially affected by diagenetic transformations, so indicating their extra-basinal origin. Carbonate intra-basinal clasts are represented by Nummulites and Algae bioclasts (Figures 12e-f). Ophiolite-derived rock fragments are lacking at all. Lack of high-grade metamorphic rock fragments and ophiolite-derived clasts are the most striking features of the Cima Aurusi Formation deposits.

The highlights of the chapter are summarized below:

- The Helminthoid Flysch Unit show a Late Cretaceous fining-upward turbidite succession with a fining-upward trend and detached from its original basement. The modal analysis performed on the arenites indicates that the framework is characterized by felsic volcanic and granitoids rock fragments as well as medium- to high-grade metamorphic clasts;
- The Moglio-Testico Unit consists of a Creatceous-Paleocene(?) succession detached from its oceanic basement. It shows a transition from hemipelagic to basin plain deposits. Chaotic deposits also occur and they are located at the top of the succession;
- The Briançonnais Units show a typical succession of Briançonnais Domain with a transition from Triassic platform carbonate to middle Eocene turbidite deposits. Modal analysis indicate that the framework is characterized by granitoids, acid volcanic and low-grade metamorphic rock fragments and extra and intra-basinal carbonate clasts.

6. The deformation strain patterns of the studied units

Fieldwork combined with the structural analysis allowed me to reconstruct the strain pattern recorded by each tectonic unit exposed in the investigated area. The deformation history of each unit is characterized by the overprinting of different folding and thrusting events developed during the oceanic subduction until the continental collision, so experiencing underthrusting, accretion and exhumation into the Alpine wedge up to the shallower crustal levels. To avoid confusion to the readers, the different deformation events recognized in this work will be grouped in three types: (i) The Pre-coupling events (6.1 section) in which will be described different superposed folding systems confined to each unit and related to the their involvement into the alpine wedge; (ii) The Syn-coupling events (6.2 section) which are represented by the unit-bounded shear zone systems, which cut the axial planes of the previous structures, and map-scale folding; (iii) The Post-coupling events which produced folding and faulting systems developed after the coupling of the units and shared by the whole tectonic stack. Owing that each deformation event related to the Pre-coupling structures was recorded at different crustal levels and timespan by the units, to avoid confusion to the readers, each folding event was labelled with different subscripts, *i.e.*, $D1_{MU}$, $D1_{MT}$, $D1_{CU}$, $D1_{FH}$ (MU: Marguareis Unit; MT, Moglio-Testico Unit; CU: Cabanaira Unit; FH: Helminthoid Flysch Unit).

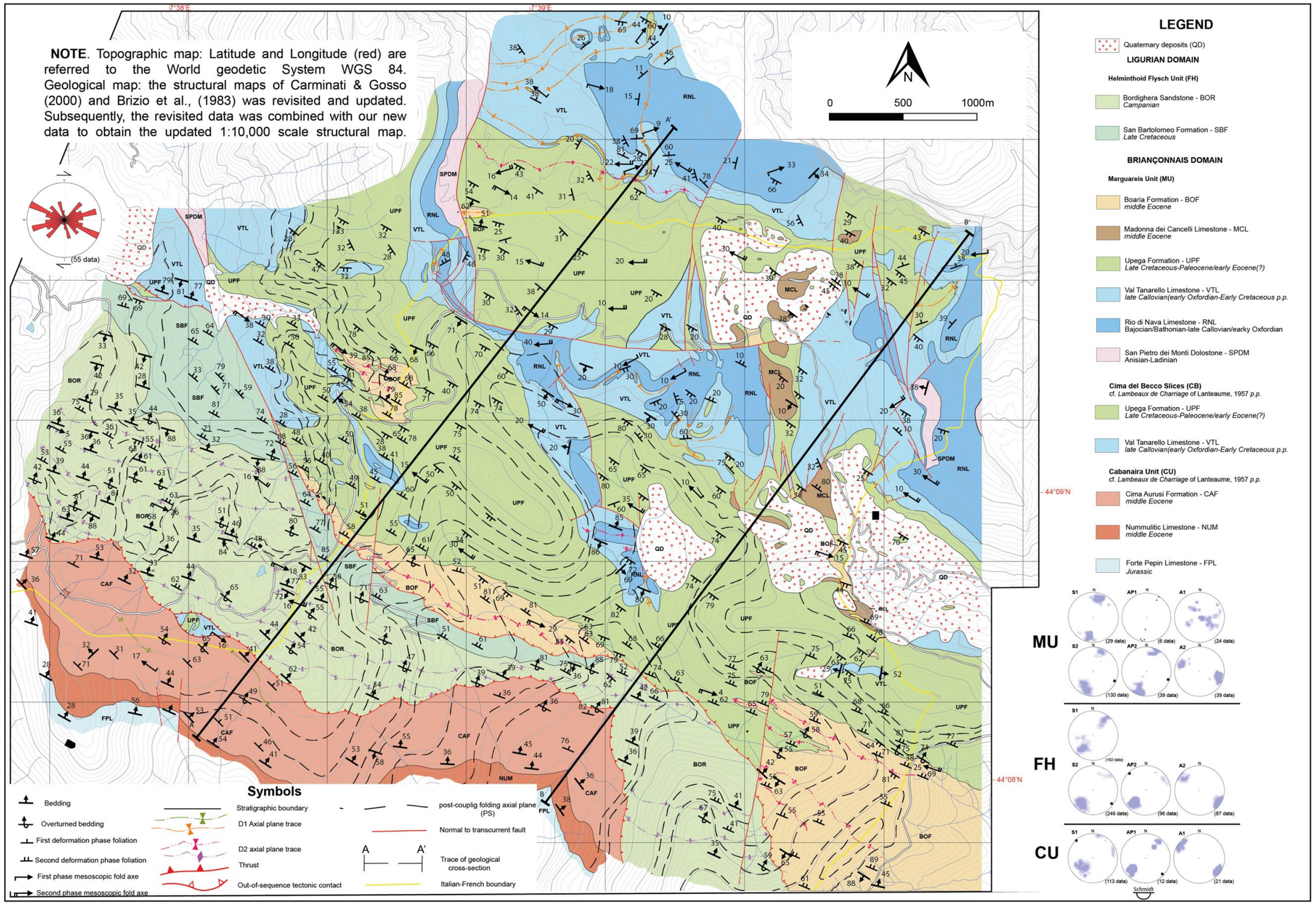

Plate 2. 1:10.000 scale geological map of the southwestern sector of the Marguareis Massif area (white box "a" of Plate1, field data from Sanità et al., 2021).

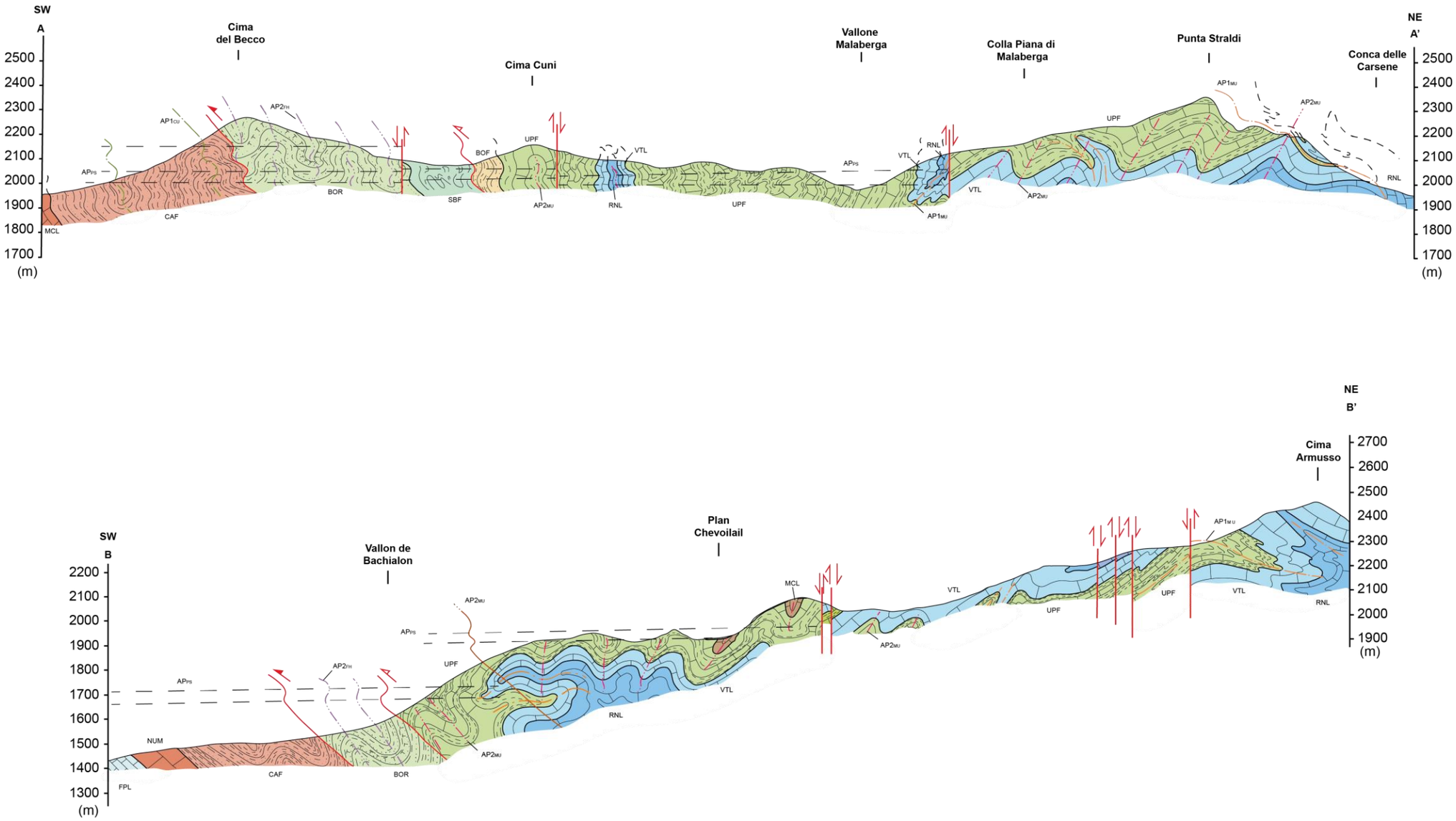

Plate 3. A-A' and B-B' geological cross-sections whose traces are reported in the geological map of Plate 2.

6.1 Pre-coupling deformation events

- The Helminthoid Flysch Unit

Two pre-coupling deformation phases ($D1_{FH}$ and $D2_{FH}$) have been documented in the Helminthoid Flysch Unit (Plates 2, 3, 4, 5 and Figure 13). They are well-developed in the finer-grained rocks (*i.e.*, marly-limestones and shales). The $D1_{FH}$ produced a pervasive $S1_{FH}$ foliation (Figures 13a-b) parallel or at low angles to the bedding (S0). The $S1_{FH}$ foliation shows a NW-SE strike with dips both towards SW and NE at various angles (stereonet of Plate 2). At the meso-scale, the $S1_{FH}$ is well preserved in the hinge zone of $F2_{FH}$ folds, and it is also present in the slices at the bottom of the FH (Monte Bertrand area, Figure 13c) where it is associated with tight $F1_{FH}$ folds with rounded hinges and characterized by a NE-SW trending fold axes plunging NE and SW and axial planes with NE-SW direction and dips toward SE (stereonet of Plate 4). At the

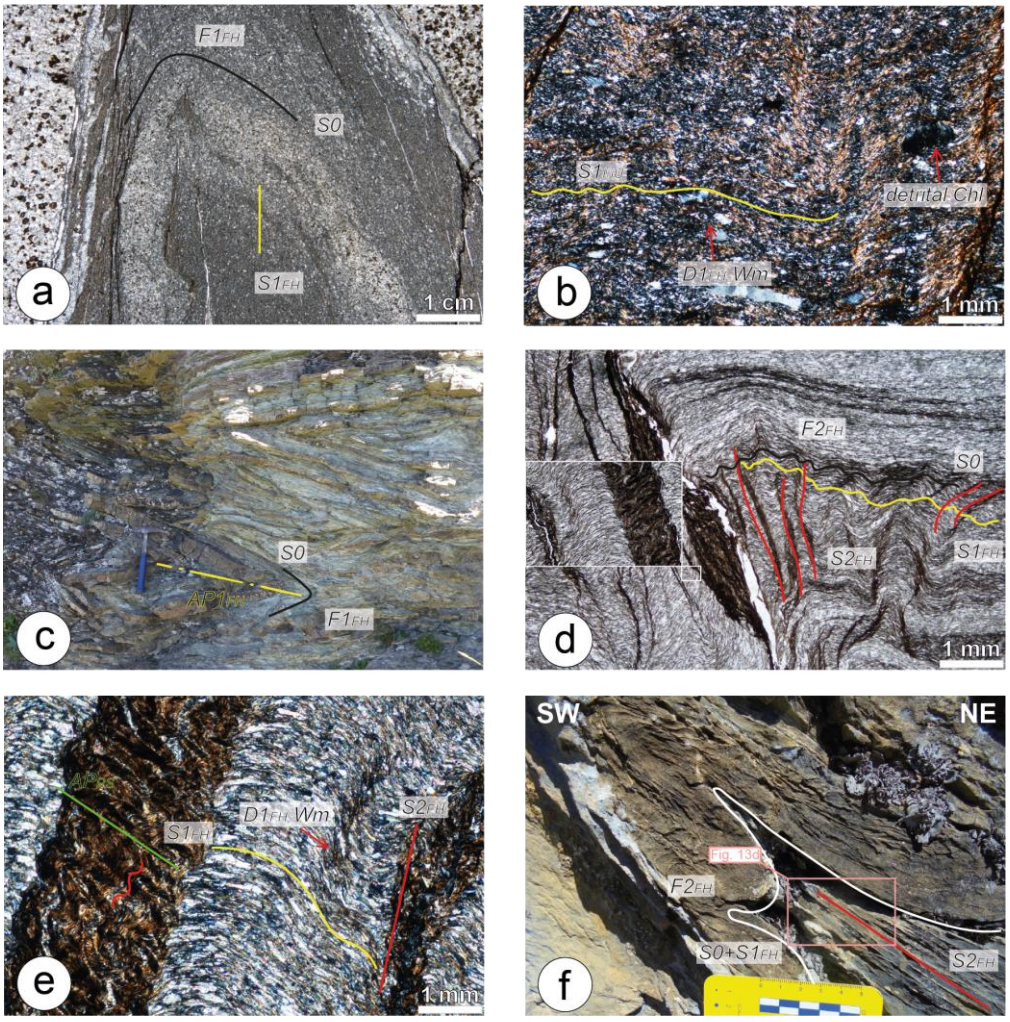

Figure 13. Structural features of The Helminthoid Flysch Unit. a) Micro-scale $S1_{FH}$ foliation in $F1_{FH}$ fold hinge zone. b) Details of the $S1_{FH}$ foliation. c) Meso-scale tight $F1_{FH}$ folds (San Bartolomeo Formation). d) Micro-scale $F2_{FH}$ fold hinge zone showing the cross-cutting relationships between $S1_{FH}$-$S2_{FH}$. In the white box on the left a close-up of this interference is shown. e) Details of $S1_{FH}$ and $S2_{FH}$ foliation at the micro-scale. f) $F2_{FH}$ tight fold with the related $S2_{FH}$ foliation (Bordighera Sandstone). The pink box indicates the close-up of "d". S0: bedding; Chl: chlorite; Wm: white mica; $AP1_{FH}$: D1FH-related axial plane; AP_{PS}: post-coupling- related axial plane.

microscale (Figures 13d-e), $S1_{FH}$ is a slaty cleavage outlined by stylolitic surfaces, elongated grains of Cc, Qz, never exceeding 20 μm, fine-grained (1-10 μm) of Ill and Chl, and detrital Ab and phyllosilicates, *i.e.*, white mica and chlorite with grain-size up to 60 μm, (mineral abbreviations of Warr, 2021 was used in the whole text, S5 supplementary materials.) with strong preferred orientations (Figures 13d-e). The main grain-scale deformation mechanism appears to have been assisted by pressure solution; passive rotation is also evident in phyllosilicates.

The $D2_{FH}$ phase is mainly marked by $S2_{FH}$ foliation that at the meso-scale is well-visible in the only finer-grained rocks (marls and shales, Figures 13d-e-f). At the micro-scale, $S2_{FH}$ is a crenulation cleavage marked by stylolitic surfaces and re-oriented grains of calcite and quartz without evidence of metamorphic re-crystallization (Figure 13d-e). The main foliation-forming mechanism appears to be the pressure solution. The $S2_{FH}$ shows a NW-SE trend and dips both toward SW and NE (stereonet of Plates 2, 4). The $S2_{FH}$ is associated with SW-verging F2 fold system (Figure 13f) developed from micro- to map-scale and showing parallel geometry generally with low interlimb angles and rounded hinge zones (Figure 13f), NW-SE trending fold axes plunging toward NW and SE and axial planes with NW-SE strike and dips toward SW and NE (Plates 2, 4). At the map-scale, the $F2_{FH}$ folding system is the prominent deformation feature extending for several km in the whole unit as appreciable in the map of Plates 2 and 4. Amazing map-scale $F2_{FH}$ folding structures can be observed along the southern wall (French side) of the Monte Bertrand and along southeast wall of the Bric Campanin ridge.

- The Moglio-Testico Unit

Pre-coupling $D1_{MT}$ and $D2_{MT}$ deformation phases have been recognized in the Moglio-Testico Unit (Figures 14a-f, Plates 6, 7). The oldest $D1_{MT}$ phase produced the most pervasive tectonic foliation ($S1_{MT}$) well preserved in the fine-grained rocks (marls and shales, Figures 14a-b-c). In the more competent layers (arenites or calcareous rocks), instead, this foliation is less pervasive (sometimes absent) and appears as a spaced cleavage. $S1_{MT}$ foliation shows NW-SE strike and dips both toward SW and toward NE with various angles (Plate 6). At the microscale, the $S1_{MT}$ is a slaty cleavage marked by the preferred orientation of Chl1 + Phg1 + Cc ± K-Fsp ± Ox mineral assemblages and anastomosed stylolitic surfaces (Figure 14b). Along the $S1_{MT}$ foliation, rigid objects like pyrites grains showing asymmetric quartz-rich re-crystallized tails occur, and these suggest shearing during the $D1_{MT}$ phase. Chl1 grains growth along the $S1_{MT}$ reach 30-40μm in size showing a stocky shape, undulose extinction, sometimes recrystallization tails and sharp edges (Figure 14b). As for the Chl1, the Phg1

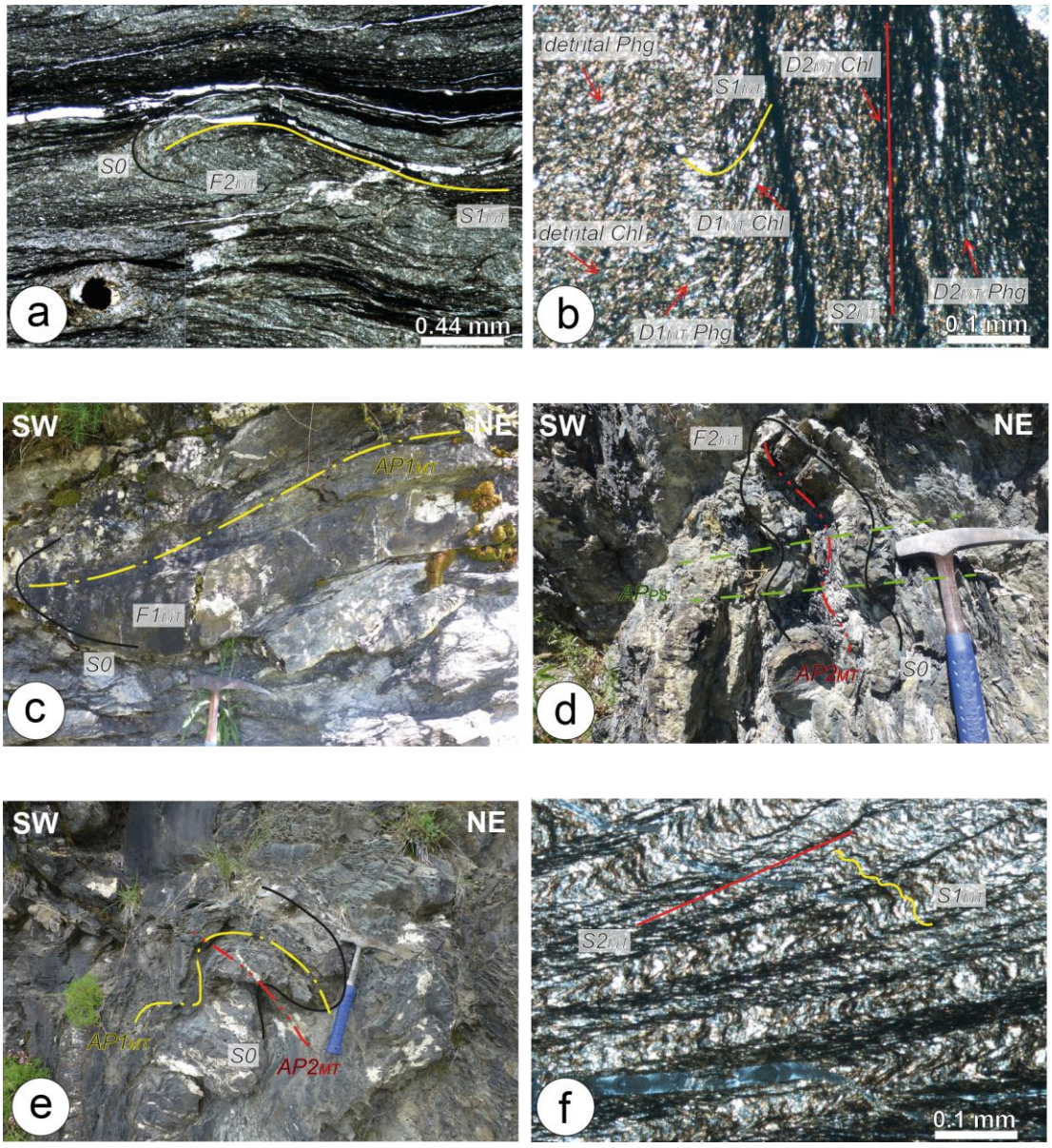

Figure 14. Structural features of the Moglio-Testico Unit. a, b) Microphotographs of $S1_{MT}$ and $S2_{MT}$ foliations. The close-up on the bottom left of "a" shows a piryte grain with quartz-rich re-crystallization tails. c) $F1_{MT}$ isoclinal fold (Palombini Shale). d) $F2_{MT}$ fold re-worked by flat-lying post-coupling folding system (Palombini Shale). Meso-scale (e) interference pattern between $D1_{MT}$ and $D2_{MT}$ folding systems (Palombini Shale). f) Micro-scale cross-cutting relationships between $S1_{MT}$ and $S2_{MT}$. S0: bedding; $AP1_{MT}$: $D1_{MT}$-related axial plane; $AP2_{MT}$: $D2_{MT}$-related axial plane; AP_{PS}: post-coupling folding-related axial plane.

growth along the $S1_{MT}$ show undulose extinction and sharp edges but they show more elongated shape with lengths ranging from 20 to 30 μm (Figure 14b). Detrital altered grains of Chl and Phg are also present and they show coarser size (from 50 to 100 μm), frayed edges, chemical zoning, and re-crystallization tails (Figure 14b).

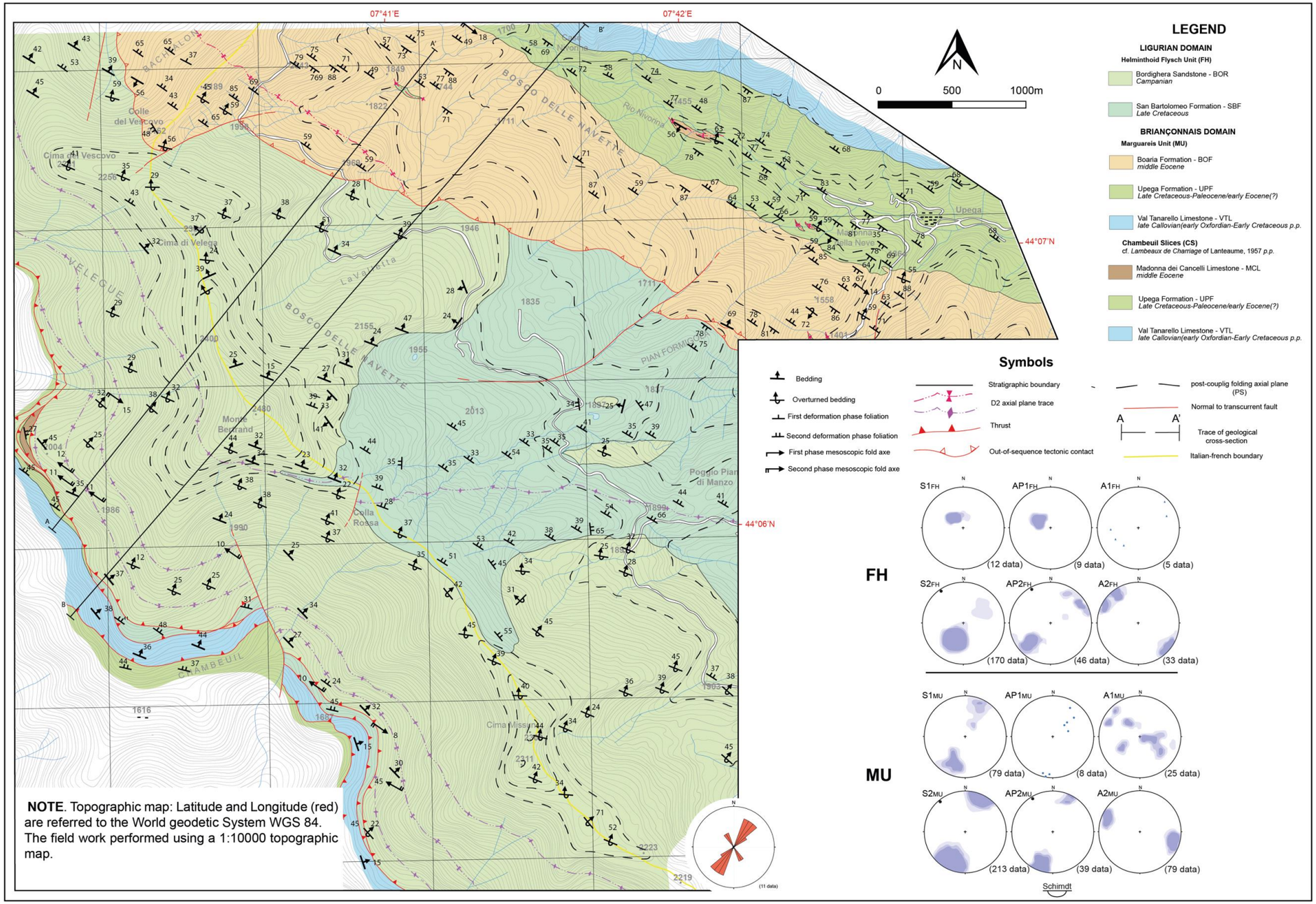

Plate 4. 1:10.000 scale geological map of the Upega-Mt.Bertrand area (white box "b" of Plate 1).

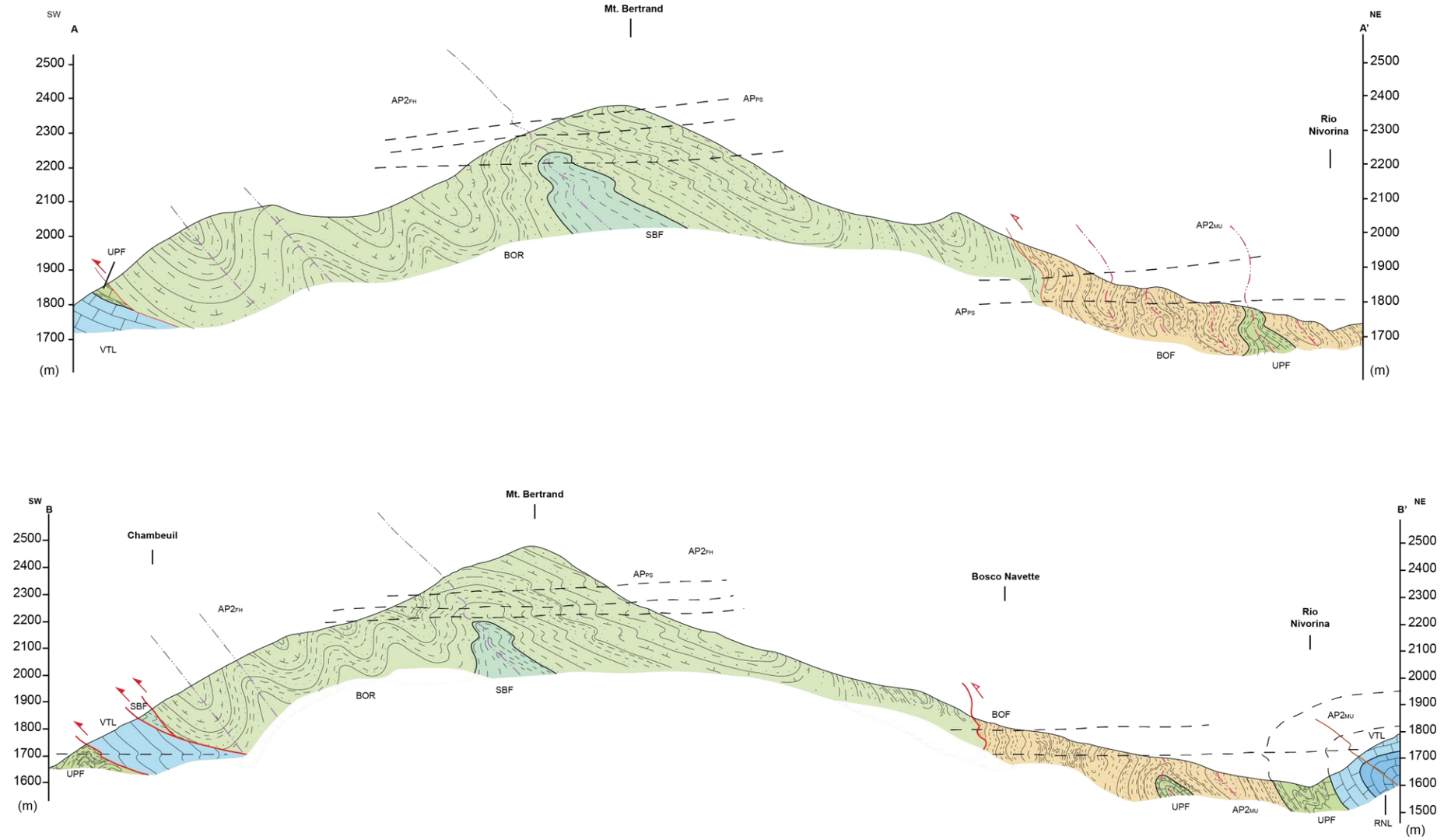

Plate 5. A-A' and B-B' geological cross-sections whose traces are reported in the map of Plate 4.

At the outcrop-scale, along the $S1_{MT}$ foliation NE-SW trending $L1_{MT}$ mineral lineations represented by quartz and calcite occur and they plunge toward SW and NE (stereonet of Plate 6). $S1_{MT}$ is associated to SW-verging isoclinal to sub-isoclinal $F1_{MT}$ fold system showing similar geometry (Figure 14c), thickness hinges and attenuated limbs, and scattered fold axes ($A1_{MT}$, see stereonet of Plate 6). The axial planes ($AP1_{MT}$) show a NW-SE strike and dips toward SW and NE with ranging angles (see stereonet of Plate 6). The $D2_{MT}$ phase produced the most prominent folding event in the Moglio-Testico Unit (Figures 14d-e, Plate 7). During this event, the $S2_{MT}$ foliation developed (Figure 14b). It is well-recognizable in the fine-grained rocks and it appears as a crenulation cleavage (Figure 14f) show a NW-SE strike and dips toward SW and NE with various angles (see stereonet of Plate 6). At the micro-scale, $S2_{MT}$ foliation is a crenulation cleavage marked by Phg2 + Chl2 ± Qz syn-metamorphic mineral assemblage and stylolitic surfaces (Figure 14b). Along the $S2_{MT}$ micro-domains, Phg2 and Chl2 grains are small, thin never exceeding 10-15 µm in size with sharp edges without evidence of chemical zoning (Figure 14b). The $S2_{MT}$ is associated to the D2 folding system which produced similar to parallel SW-verging F2 folds with rounded hinges and tight interlimb angles (Figures 17d-e) showing NW-SE trending fold axes ($A2_{MT}$) plunging toward NW and SE with ranging angles, axial planes ($AP2_{MT}$) showing NW-SE strikes and dips toward SW and NE (see stereonets of Plate 6). At the map-scale, $D1_{MT}$- and $D2_{MT}$-related interference patterns can be observed along the road located in the southern wall of the Bric Scravaglion ridge (Plate 7).

- The Marguareis Unit

Two pre-coupling deformation phases ($D1_{MU}$, $D2_{MU}$, Figures 15a-h, Plates 2, 4, 6) well-developed at any scale can be observed (according with Brizio *et al.*, 1983).

$D1_{MU}$ phase produced a pervasive $S1_{MU}$ foliation well-developed in the finer-grained rocks like marly limestones and shales (Figures 15a-b-c-d). The $S1_{MU}$ foliation shows a NW-SE to WNW-ESE strike with both SW and NE dips (see stereonet of Plates 2, 4, 6). At the microscope, the $S1_{MU}$ is, in the fine-grained rocks, a slaty cleavage marked by thin lenticular aggregates of oriented Cc + Ab + Qz

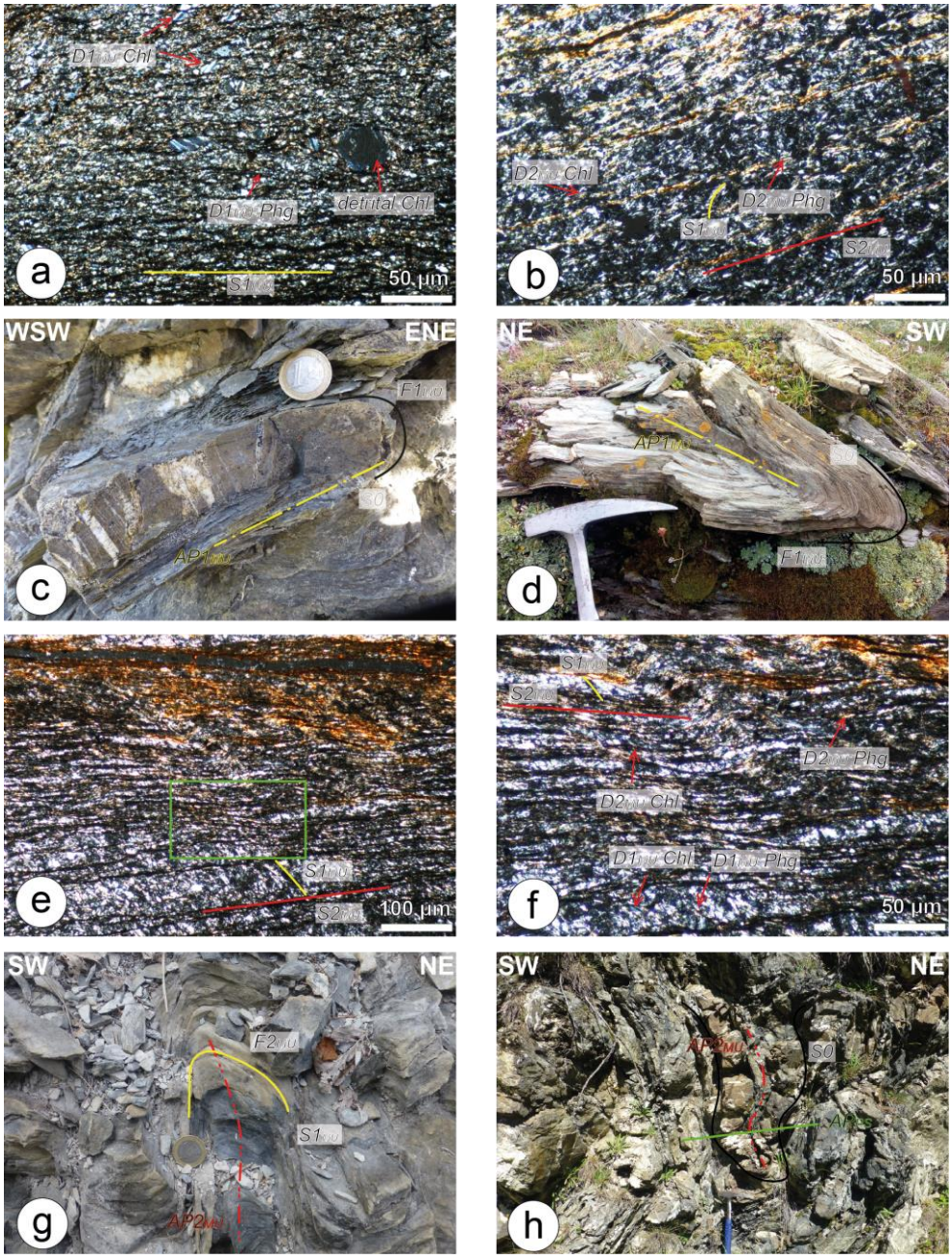

Figure 15. Structural features of the Marguareis Unit. a, b) Microphotographs of $S1_{MU}$ and $S2_{MU}$ foliation. Meso-scale of isoclinal $F1_{MU}$ folds in Boaria Foration (c) and Upega Limestone (d). e) $S1_{MU}$-$S2_{MU}$ cross-cutting relationships. f) Details of S1MU-$S2_{MU}$ relationships (close-up of green box of "e"). Meso-scale tight $F2_{MU}$ folds in Upega Limestone (g) and Boaria Formation (h). The relationships between $F2_{MU}$ folds and the post-coupling fold system is outlined. S0: bedding; $AP1_{MU}$: $D1_{MU}$-related axial plane; $AP2_{MU}$: $D2_{MU}$-related axial plane; AP_{PS}: post-coupling-related axial plane.

grains, detrital and syn-metamorphic white micas (Phg1), chlorite (Chl1) and stylolitic surfaces (Figures 15a-b). So, the $S1_{MU}$ is marked by Chl1 + Phg1 + Qz ± Ab ± K-Fsp ± Cc mineral assemblage. Within the $S1_{MU}$, Chl1 are stocky, sometimes with re-crystallization tails, and reach 30 µm in size (Figures 15a-b). Pgh1, instead, are more elongated and range in length between 20 and 30 µm (Figures 15a-b). The grain-scale deformation mechanisms include thus re-crystallization, pressure solution and passive rotation of phyllosilicates. Big altered grains of detrital chlorites (about 80 µm) and white micas (about 40 µm in length) of clear sedimentary origin are also present and both characterized by frayed edges, chemical zoning and re-crystallization tails (Figures 15a-b). $S1_{MU}$ is parallel to axial planes ($AP1_{MU}$) of SW-verging $F1_{MU}$ folds developed from micro- to map-scale (Plates 2, 3, 4, 5, 6, 7, Figures 15c-d). The latter show a similar geometry with thickened and rounded hinges, attenuated limbs sometimes with boudinaged layers and scattered $A1_{MU}$ fold axes with a main trend-oriented NW-SE and plunge with different angles. The $AP1_{MU}$ shows a strike ranging from NW-SE to WNW-ESE with both NE and SW dip (see stereonet of Plates 2, 4, 6). At the map-scale $F1_{MU}$ folds are testified by flat-lying to SW-verging synclines and anticlines developed in the Jurassic and Late Cretaceous deposits, with the latter at the core, in the Vallon de Malabergue area and along the Cima Armusso-Punta Straldi ridge (Plates 2, 3), respectively. The latter probably continues in the Pian Ambrogi area involving the youngest formation of this unit (*i.e.*, the Boaria Formation).

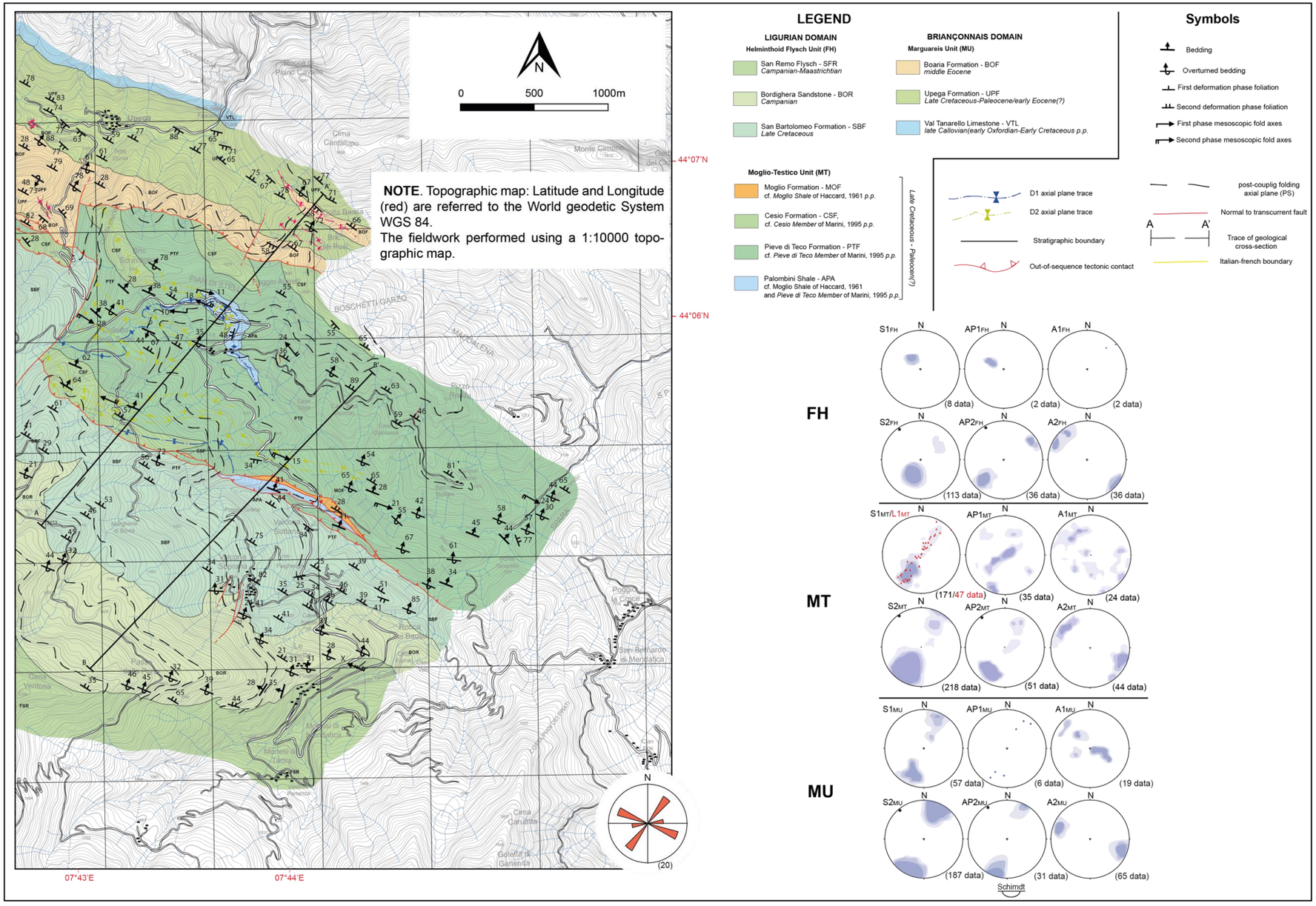

Plate 6. 1:10.000 geological map of the Upega-Piaggia area, High Arroscia Valley (white box "c" of Plate 1).

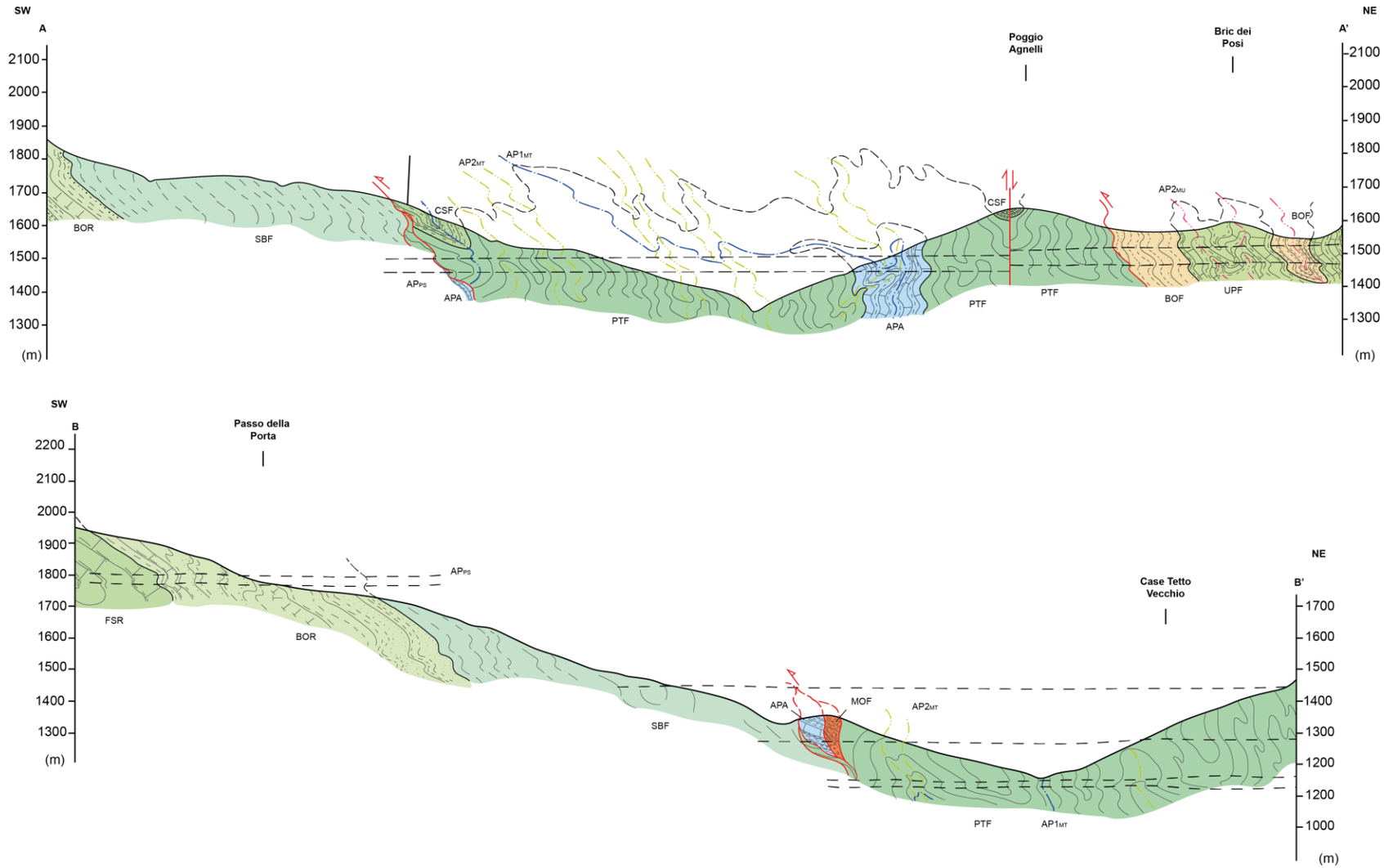

Plate 7. A-A' and B-B' geological cross-sections whose traces are reported in the map of Plate 6.

However, the low degree of exposition of the outcrops did not allow a good reconstruction of this structure.

It must be underlined that, moving from NE to SW in the Marguareis Unit, the $S1_{MU}$ and $AP1_{MU}$ attitudes show a change in dip from gently dipping toward NE (this is well evident along the southwestern side of Punta Marguareis, Plates 2, 3), in Cima Armusso-Punta Straldi ridge, to sub-horizontal attitude in the Vallon de Malabergue area (Plates 2, 3, Figure 16).

The $D2_{MU}$ phase is defined by the $S2_{MU}$ foliation, showing NW-SE strikes and dips toward SW or NE (see stereonet of Plates 2, 4, 6). It is well preserved in fine-grained rocks (*i.e.*, shales of Boaria Formation) and it appears as a penetrative crenulation cleavage marked by syn-metamorphic Phg2 + Chl2 + Qz ± Cc mineral assemblage (Figures 15g-h). Both Phg2 and Chl2 grains along the S2 are thin, not exceeding 10 µm in length and show sharp edges. In the more competent layers (*i.e.*, marly calcareous rocks), instead, $S2_{MU}$ corresponds to a disjunctive cleavage marked by dissolution surfaces with rare syn-metamorphic white micas. The main deformation mechanisms appear to have been the pressure solution and metamorphic re-crystallization.

The $S2_{MU}$ foliation is associated to the NE verging $F2_{MU}$ fold system developed from micro- to map-scale. $F2_{MU}$ folds show parallel geometry ($F2_{MU}$ folds with similar geometry are locally present) with thickened and rounded hinges. They show $A2_{MU}$ fold axes with NW-SE trend and plunge toward NW and SE (see stereonet of Plates 2, 4, 6). The related axial planes ($AP2_{MU}$) show a NW-SE strike with a dip toward SW or NE (see stereonet of Plates 2, 4, 6) with ranging angles.

The $F2_{MU}$ folds are very common, from micro- to map-scale, in the Boaria and Upega formations whereas in the Val Tanarello Limestone, Rio di Nava Limestone and San Pietro dei Monti Dolostone have been recognized at the decametric to map-scale only. Map-scale $F2_{MU}$ folds are represented by the Col de La Boaria and Colle delle Selle Vecchie Synform and Cime de Pertega Antiform (Plates 2, 3). The Boaria Formation occurs at the core of the synforms, whereas the core of the antiform is made of Val Tanarello Limestone (Plates 2, 3). The synform structure at the Colle de La Boaria is probably prosecuted in the Colle dei Signori area (Plate 2) where the Boaria Formation crops out at the core of a folding structure mostly made of Jurassic-Cretaceous carbonate rocks (*i.e.*, Val Tanarello Limestone and Upega Fm.). As for $D1_{MU}$-related planar structural features, also the $S2_{MU}$ and $AP2_{MU}$ dip changes moving from NE to SW (Plates 2, 3, Figure 16) into the Marguareis Unit. In fact, from Cima Armusso-Punta Straldi ridge toward Cime de Malabergue areas, the $S2_{MU}$ and $AP2_{MU}$ dip

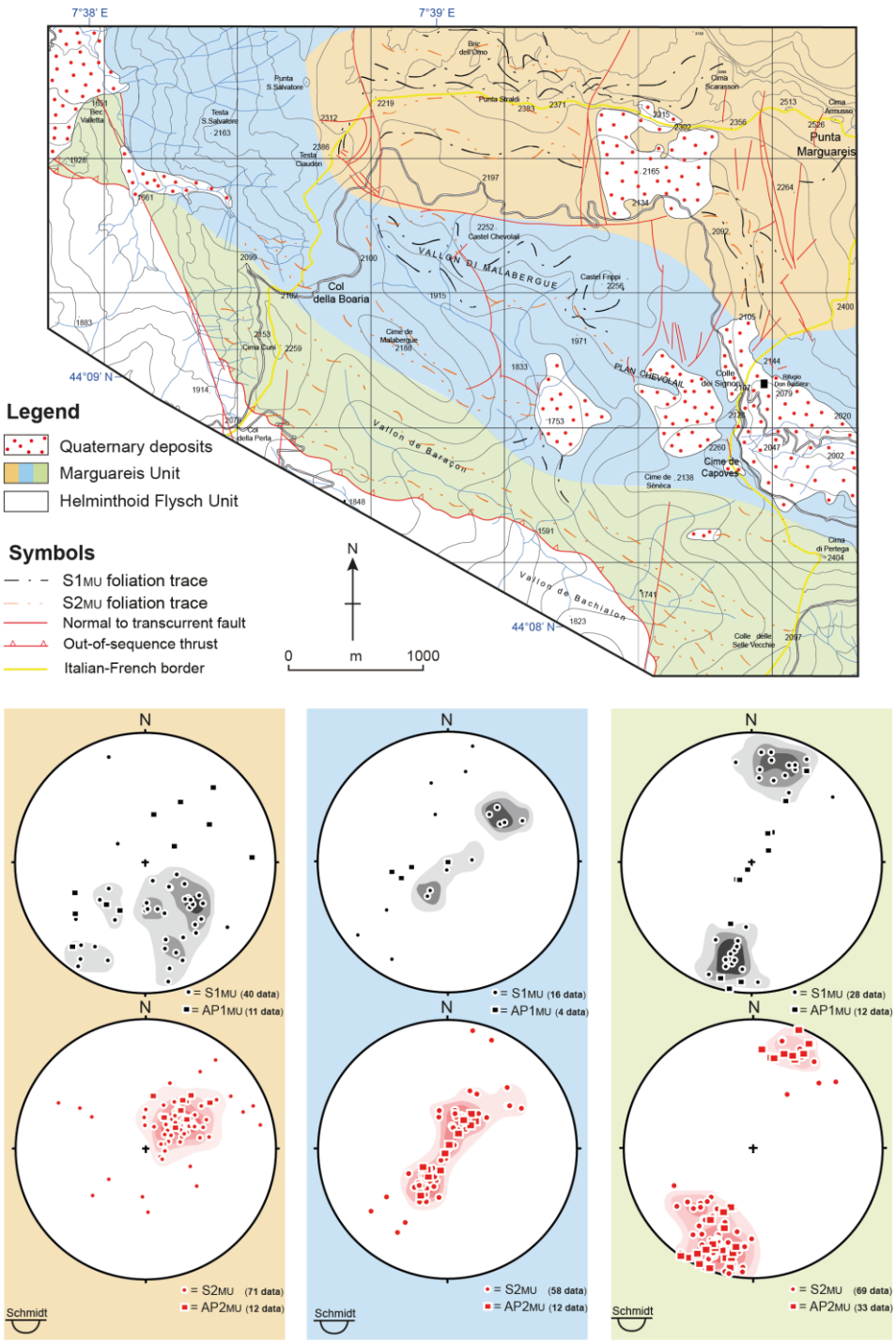

Figure 16. Structural Sketch of the Marguareis Unit cropping out along the southwestern sector of the Punta Marguareis area. The different colors indicate structural domains with different attitudes of F1 and F2 folds. The stereoplots of their planar structural features are also reported.

progressively change from gently dipping toward SW up to sub-vertical in the Col de La Boaria area, and dipping to NE in the Vallon de Malabergue area. As for the D1MU planar structural features, clear evidences of this architecture are appreciable in the southwestern sector of Punta Marguareis area (Plates 2, 3, Figure 16).

Note that the overprinting relationships between $F2_{MU}$ and $F1_{MU}$ folding systems produces a type 3 interference pattern from meso- to map-scale (Plates 2, 3), deriving from

the superposition of two fold systems with axial planes at high angles and roughly co-axial fold axes. The best examples of this interference are provided by Cima Armusso-Punta Straldi ridge and Vallon de Malaberga areas (Plates 2, 3). The same deformation phases, as well as the interference patterns, were recognized in the Cima del Becco and Chambeuil tectonic slices (Figures 8, Plate 4).

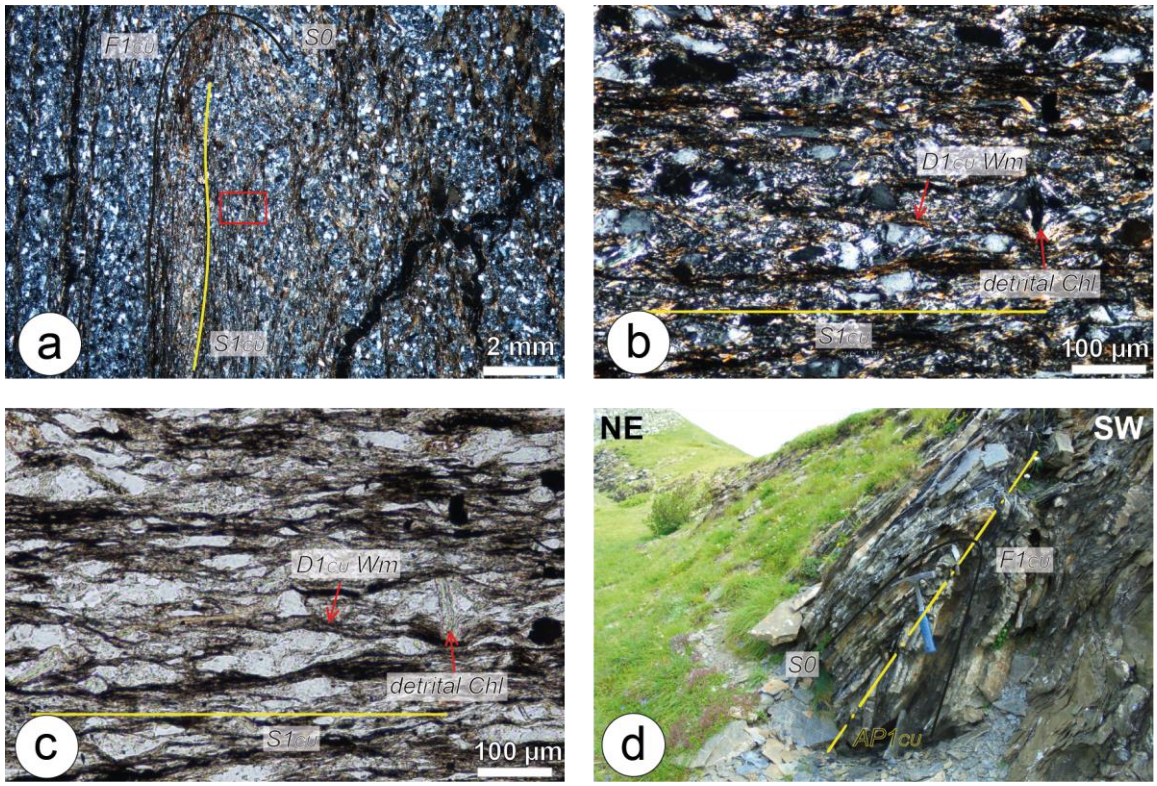

Figure 17. Structural Features of the Cabanaira Unit. a) Microphotographs of $S1_{CU}$ foliation (Cima Aurusi Formation). b, c) Details (red box of "a") of $S1_{CU}$ foliation. d) Meso-scale isoclinal $F1_{CU}$ fold (Cima Aurusi Formation). S0: bedding; AP1: $D1_{CU}$-related axial plane.

- The Cabanaira Unit

Only one pre-coupling deformation phase ($D1_{CU}$) has been recognized in Cabanaira Unit (Plates 2, 3, Figure 17a, d). In the more competent rocks (*i.e.*, arenites and limestones), the $D1_{CU}$ phase is marked by a $S1_{CU}$ spaced foliation roughly parallel to the S0 bedding. In the fine-grained layers (shales), it is outlined by a pervasive $S1_{CU}$ slaty cleavage showing a NW-SE strikes and dips toward SW or NE with various angles. At the micro-scale. it is composed by elongated Qz, (detrital?) feldspar grains (*i.e.*, albite) and fine-grained Phg1 and Chl1 never exceeding 30 µm in size. Lenticular domains of Qz and Cc grains and stylolitic surfaces are also present (Figures 17a-b-c). The mineral assemblage is thus represented by Phg1 + Chl1 + Qz ± Cc ± Ox. The $S1_{CU}$ is associated to SW-verging $F1_{CU}$ fold system showing rounded hinges, tight interlimb angles and fairly similar geometry (Figure 17d). The $A1_{CU}$ fold axis show a NW-SE trend and

plunge both toward SE and toward NW with angles between 20° and 30° (see stereonet of Plate 2), whereas the axial planes ($AP1_{CU}$) have a NW-SE strike and dips toward SW or NE. The $F1_{CU}$ folds develop from micro- to map-scale but they are more appreciable in the fine-grained rocks *i.e.*, the Cima Aurusi Formation. In fact, antiforms and synforms within this formation were documented (Plates 2, 3, Figure 17d).

6.2 Syn-coupling history: Thrusting and folding events

The syn-coupling deformation events were largely documented in the whole study area (Plates 2, 3, 4, 5, 6, 7) and they are represented by thrusting and folding events.

The thrusting event, responsible for the coupling of the units, produced the unit-bounding shear zone systems showing a NW-SE strike with a complex geometry (Figures 18a-d, 19a-b). In the southwestern sector of the Marguareis Massif, the uppermost shear zone system separates the Marguareis Unit from the underlying Helminthoid Flysch Unit. It is well exposed in the Monte Alpetta and La Perla Mt. areas (Figure 18a-b). Southeastward, this uppermost shear zone system prosecuted along the Vallone di Upega (High Valle Tanaro, Plates 6, 7) until the Piaggia Village and Val Tanarello Stream. In this area, this upper shear zone system separates the topmost Marguareis Unit from the underlying Moglio-Testico Unit,

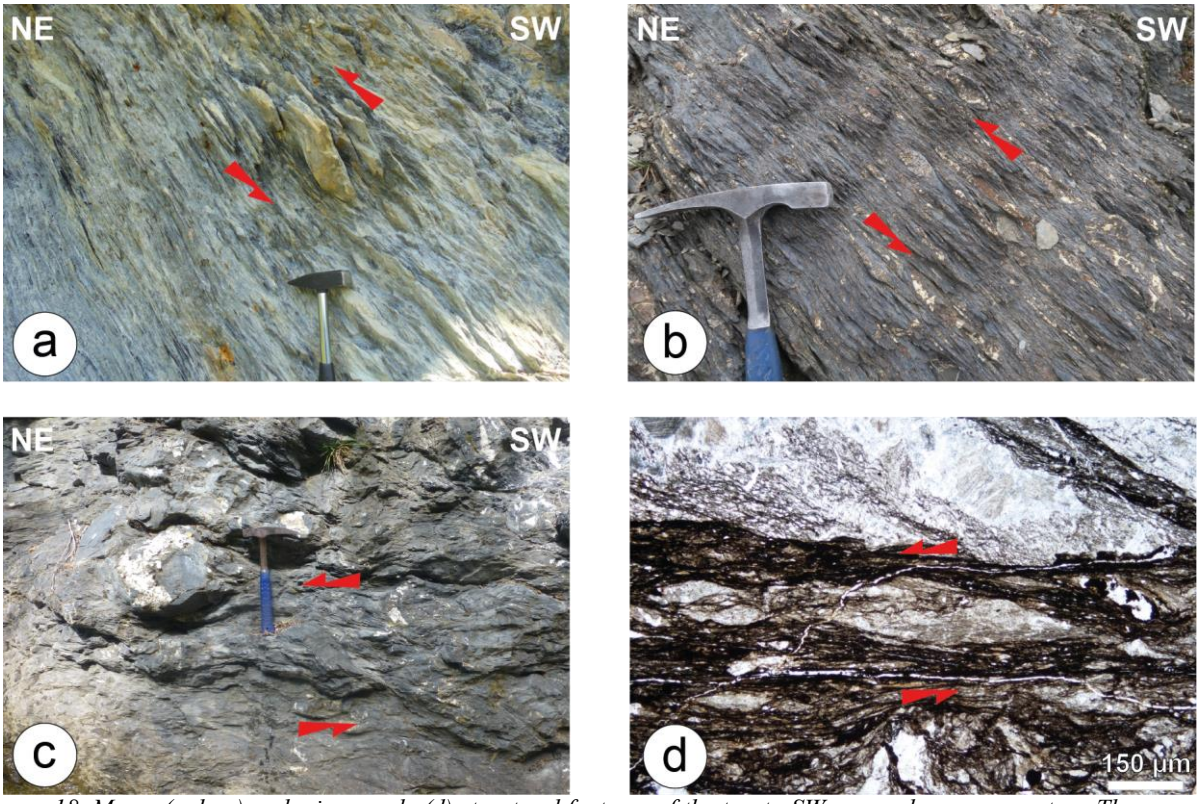

Figure 18. Meso- (a, b, c) and micro-scale (d) structural features of the top-to-SW upper shear zone system. The sense of shear (red arrows) is indicated.

and the latter in turn from the Helminthoid

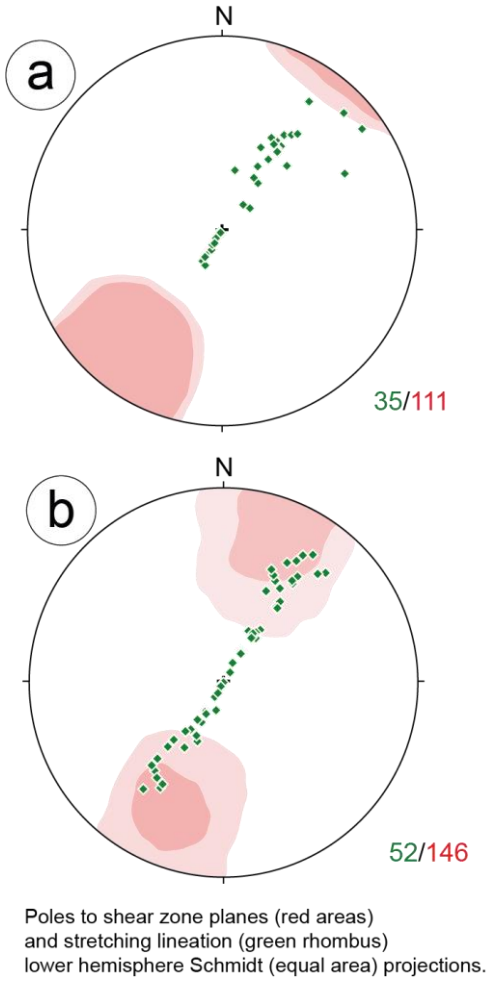

Figure 19. a, b) Stereographic plots of the main cataclastic foliation planes (red areas) related to lower and upper shear zone systems. The spatial orientation of the stretching lineations (green rhombus) is also reported.

Flysch Unit (Plates 6, 7). At the meso-scale, the uppermost shear zone is represented by m-thick high-strain zone characterized by a foliated cataclasite (Figures 18a-b-c-d). Kinematic indicators pointing out to top-to-SW sense of movement. These are represented by cm-sized sigma-shaped carbonate and siliciclastic clasts (Figures 18a-b-c-d). Along the shear planes, evidence of metamorphic re-crystallization of small calcite and quartz grains occur (Figure 18d). The stretching lineations show a NE-SW trend and plunges both toward NE and toward SW (Figure 19a), whereas the stereoplots of the poles to shear plane foliation clearly indicate dips toward SW and NE. The lowermost shear zone system, instead, is located at the bottom of the Helminthoid Flysch Unit (Plates 2, 3, 4, 5) and separates it from the underlying Cabanaira Unit and the Cima del Becco and Chambeuil tectonic slices. This shear zone system is well exposed in the Colletto Campanin area (Figure 20a) and prosecutes southeastward throughout the High Roja Valley (Plates 2, 3) and along the southwest wall (France side) of the Monte Bertrand-Cima Missun ridge (Plates 4, 5). This shear zone system consists of intensively foliated dm- to m-thick high-strain cataclastic zone (Figures 20b-c-d). Top-to-SW kinematic indicators are represented by sigma-shaped dm- to cm-sized siliciclastic and carbonates clasts (Figures 20b-d) observed in various lithologies (*i.e.*, Bordighera Sandstone, Boaria Formation and Upega Formation). Evidence of metamorphic re-crystallization of small calcite and quartz grains are present (Figure 20d). The stretching lineations on the shear planes show a NE-SW trend and plunges both toward NE and toward SW (Figure 19b), whereas the stereoplots about the poles to shear planes indicate dips toward NE and SW with medium- to high-angles.

The folding event was recognized in the topmost Margaureis Unit only (hereafter called $D3_{MU}$). It is testified by a kilometric-scale (its

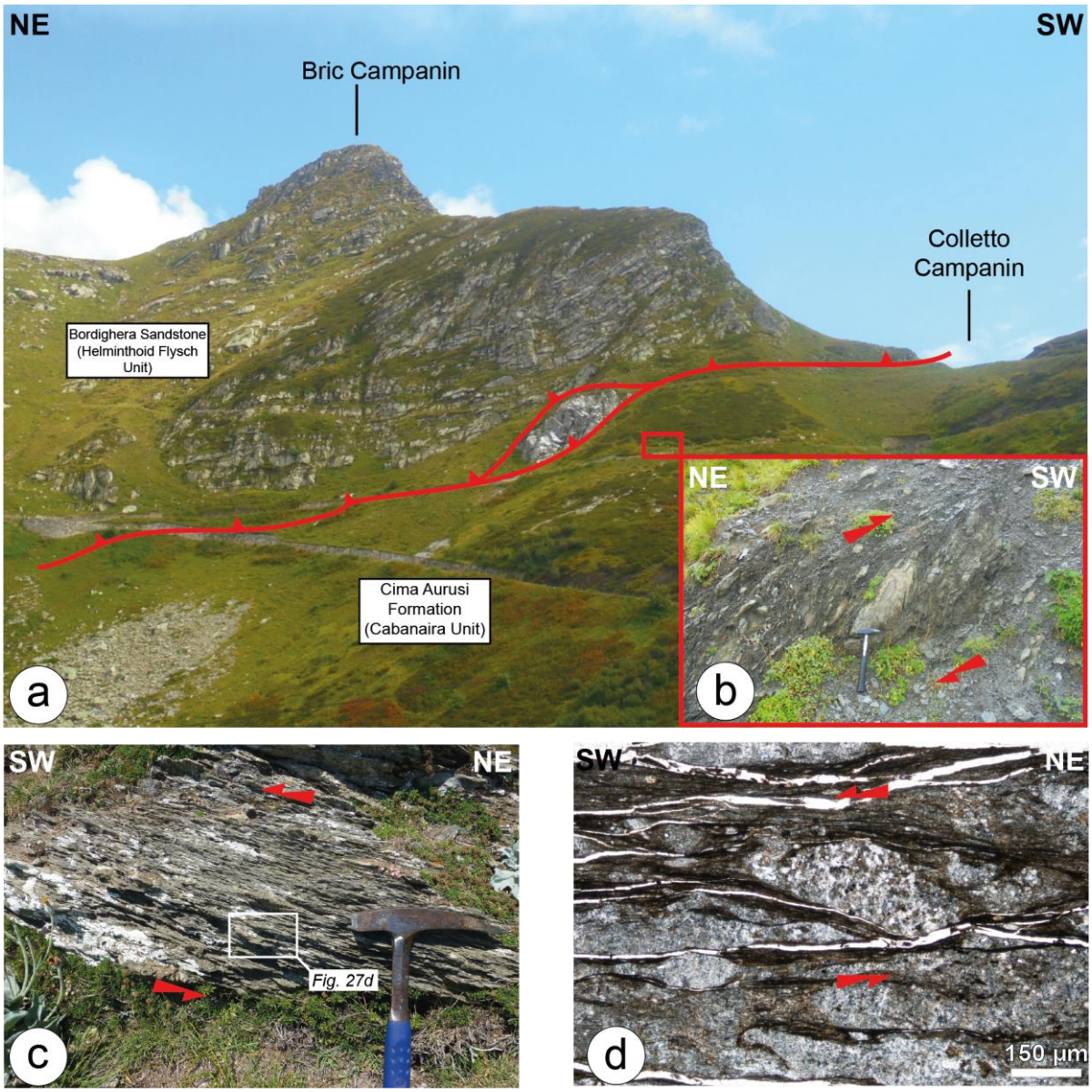

Figure 20. Structural features of lower shear zone system. a) Panoramic view of lower shear zone system cropping out along the western wall of Bric Campanin ridge (see the geological map of Figure 4 and 14 for the geographic location). b, c) Meso-scale evidence of shearing related to the lower shear zone system. the sense of shear is indicated (red arrows). Micro-scale details of cataclastic shear zone (white box of "c") with clear kinematic indicators.

extension is more than 80 km) knee-shaped $F3_{MU}$ fold with NW-SE trending $A3_{MU}$ fold axes plunging both toward NW and toward SE and an eastward-dipping axial plane ($AP3_{MU}$, Plates 2, 3, 4, 5, 6, 7 and Figure 16). The $F3_{MU}$ is testified by the folding of the $D1_{MU}$ and $D2_{MU}$- related structural features as appreciable in the map of Plates 2 and 3. The associated $S3_{MU}$ tectonic foliation is rarely observed and it is represented by stylolitic surfaces without evidences of metamorphic re-crystallization suggesting its development at shallow crustal levels. Note that the trend of $A3_{MU}$ axis, the strike of the $AP3_{MU}$ and the attitude of the uppermost unit-bounding thrust surfaces are sub-parallel suggesting their coeval development. In map view, the sub-vertical limb of the $F3_{MU}$ fold is developed

along the uppermost thrust system separating the Marguareis Unit from the other units (*i.e.*, Moglio-Testico Unit and Helminthoid Flysch Unit), whereas the normal sub-horizontal limb can be observed in its more internal sector (*i.e.*, toward NE). This is well-evident along the southwestern sector of Punta Margaureis Plates 2, 3, Figure 21).

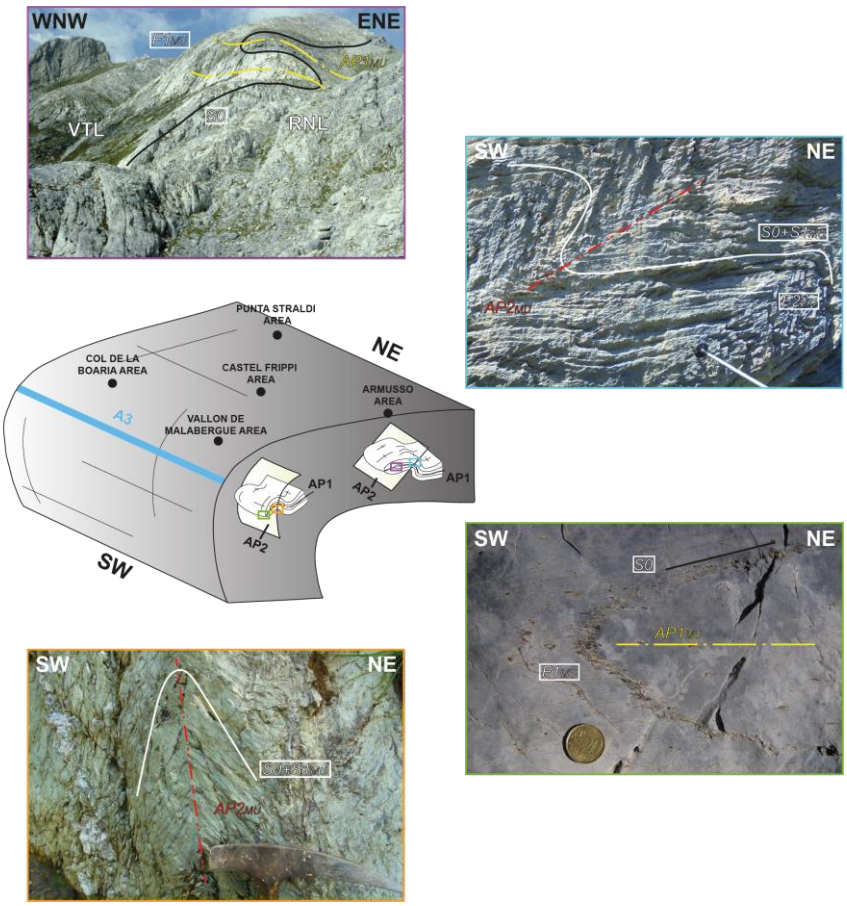

Figure 21. 3D simplified sketch showing the D3 fold developed during the syn-coupling tectonics and affecting the previous D1MU and D2MU structures observed in the Marguareis Unit. S0: bedding; F1MU: D1MU-related fold; S1MU: D1MU-related foliation; AP1MU: D1MU-related axial plane; AP2MU: D2MU-related axial plane; RNL: Rio di Nava Limestone; VTL: Val Tanarello Limestone.

6.3 Post-coupling history of the tectonic stack

The whole tectonic stack, including the syn-coupling structures, share the same deformation history represented by the post-coupling fold system (PS fold) and later high-angles faults (Plates 2, 3, 4, 5, 6, 7). The PS fold show parallel geometry (Figures 22a-b-c), open interlimb angles and rounded hinges. A tectonic foliation (S_{PS}) is associated to PS folds, and it is rarely observed in the less competent layers only (*i.e.*, shales – Figure 22d). At the micro-scale, S_{PS} is marked by stylolitic surfaces without evidence of metamorphic re-crystallization. S_{PS} foliation as the axial planes (AP_{PS}) of the PS fold show a sub-horizontal to gently southwestward-dipping attitude, whereas the A_{PS} fold axes have a NW-SE direction (Figure 22e). Micro- to map-scale type-3 interference pattern due to the superposition of these PS fold system onto the previous folding can be observed in the

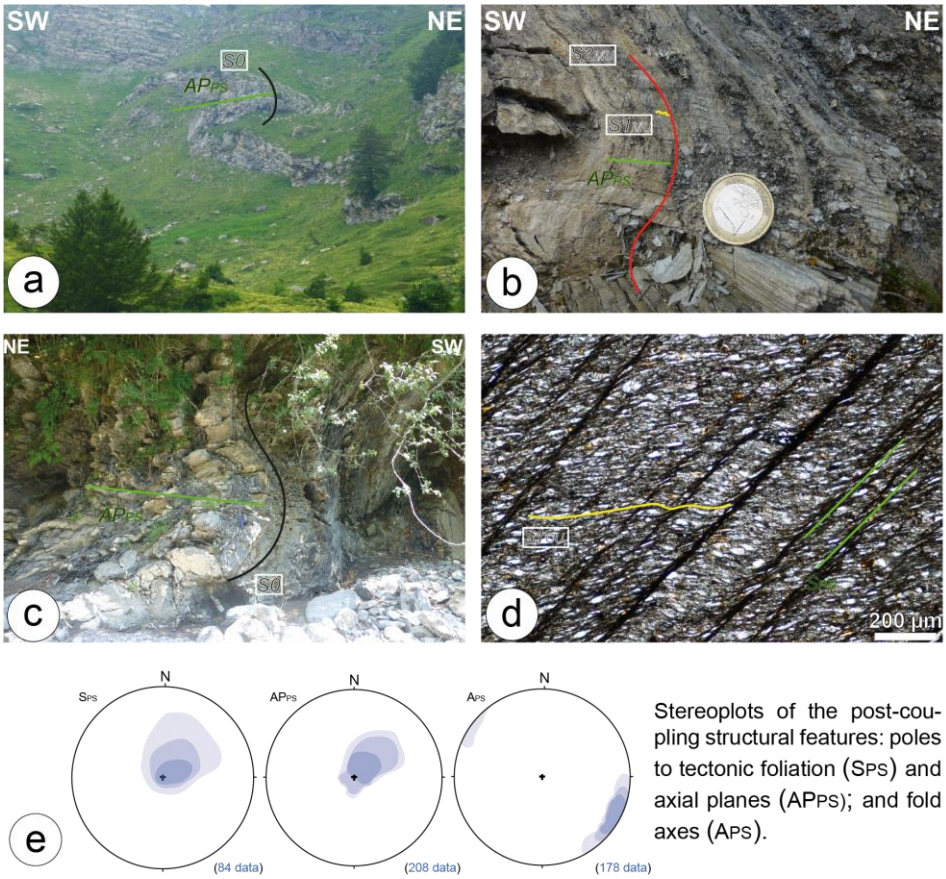

Figure 22. Meso- (a, b, c) and micro- (d) scale structural features of post-coupling folding events (PS). e) Stereographic plots of linear and planar structural features of post-coupling folds.

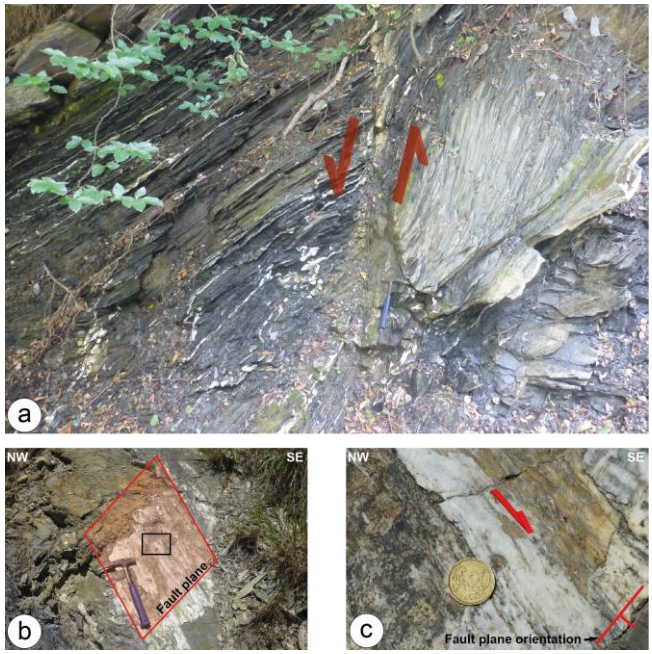

Figure 23. a) Fault plane trace. The sense of displacement is indicated (red arrows). c) Fault plane with calcite-rich striae. f) Close-up (black box of "b") with clear kinematic indicators.

areas where sub-vertical layering is present (*i.e.*, Bric Campanin ridge, Vallon de Malabergue, Le Salse Village and Cima Aurusi areas, Plates 2, 3, 4, 5, 6, 7).

Subsequently, sub-vertical to vertical transcurrent to normal fault network cut at high angle all the previously described structures (Figure 23a), including the post-stacking fold system and the unit-bounding shear zones (Plates 2, 3, 4, 5, 6, 7).

Locally the faults juxtapose different tectonic units without profoundly modify the structural architecture previously achieved by the stack. Kinematic indicators are rarely observed and indicate both oblique and down dip movement (Figures 23b-c). The statistical analysis of fault distribution (see the rose diagrams of Plates 2, 4, 6) highlights a well-developed Riedel system characterized by two major fault systems showing a N050-N70 directions and N110-120. Minor fault systems showing various directions and associated with the previous major systems occur. A third fault system shows N160-N170 direction and forms a high-angle with the previously systems.

The main points of the chapter are summarized below:

- Each tectonic unit show evidence of a polyphase deformation history dealing with pre-, syn- and post-coupling structures;
- Pre-coupling structures are represented by folding system whose associated tectonic foliation is mainly supported by syn-metamorphic Chl, Phg and Qz crystals. The related axial planes are confined to each unit;
- Syn-coupling tectonics is represented by thrusting and folding which cut the axial planes of the previous structures. The thrust surfaces are responsible for the coupling of the units and show *top-to-SW* sense of movement. The folding event produced a map-scale structures affected only the Marguareis Unit;
- The whole tectonic pile shared the same deformation history, the latter represented by open folding system with sub-horizontal axial plane and faulting. These cut at high-angle all the previously described structures without profoundly modify the architecture of the study area.

7. Metamorphism

The deformation history of each tectonic units, including the tectonic slices showing Briançonnais affinity, is accompanied by metamorphic re-crystallization developed under different *P* and *T* conditions. However, not all of units show evidence of significant metamorphic re-crystallization. Therefore, different techniques were applied to the tectonics units to estimate their *P*–*T* conditions experienced during their tectonic evolution. For the Helminthoid Flysch Unit and the Cabanaira Unit, showing lower degree of metamorphic re-crystallization, the Illite crystallinity index distribution (Ill_{IC}) and the b_0 cell parameter were calculated; while for the Marguareis Unit and the Moglio-Testico Unit showing mineral assemblages showing more significant metamorphic re-crystallization coherent with higher *P* and *T* conditions, the Chl-Phg multi-equilibrium thermobarometry was carried out. In the next paragraphs will be showed only the result obtained for each tectonic unit. The detailed explanations of the employed methods are reported in the supplementary section.

To calculate the Ill_{IC} distribution and the b_0 cell parameter values of carbonate-free pelites, sampling were performed along a transect (Plate 1) in which the Helminthoid Flysch Unit and the Cabanaira Unit are well exposed. For each unit 10 samples have been collected. For the thermobarometric estimations, samples collected in F2 and F1 fold hinge zones were used in order to have microstructures as constraints (see *Part V: The deformation strain patterns of the studied units*) and to quantify the *P* and *T* ranges recorded during the deformation phases showing evidence of metamorphic re-crystallization (*i.e.*, $D1_{MU}$, $D2_{MU}$, $D1_{MT}$ and $D2_{MT}$). In other words, using the Chl-Phg thermodynamic multi-equilibrium approach the reconstruction of the *P*–*T* paths of the units was performed. The chlorite-quartz-water (Chl-Qz-wt) method (Vidal *et al.*, 2006) was employed to calculate the *T* range for the chlorite formation. For the *P* range the phengite-quartz-water (Phg-Qz-wt) method (Dubacq *et al.*, 2010) was applied on phengite grains grown during the different deformation phases. The chlorite-Phengite-quartz-water (Chl-Phg-Qz-wt) method (Vidal and Parra, 2000) was used to calculate the *P* and *T* equilibrium conditions using the Chl-Phg couples, located in the same microstructures, and thought thus to have formed in chemical equilibrium (see the supplementary for more details).

7.1. The Ill_{IC} and the b_0 cell parameter

The Ill_{IC} distribution measured along the investigated transect (Plate 1) shows values progressively lower moving from the highest to the lowest structural levels, *i.e.*, from the Helminthoid Flysch Unit to the Cabanaira Unit. The results are showed in the histograms of Figure 24 with the relative standard

deviations for each tectonic unit. The dashed lines indicate the lower and upper limit of very

the distribution of the Ill_{IC} values into the Cabanaira Unit is in good agreement with the

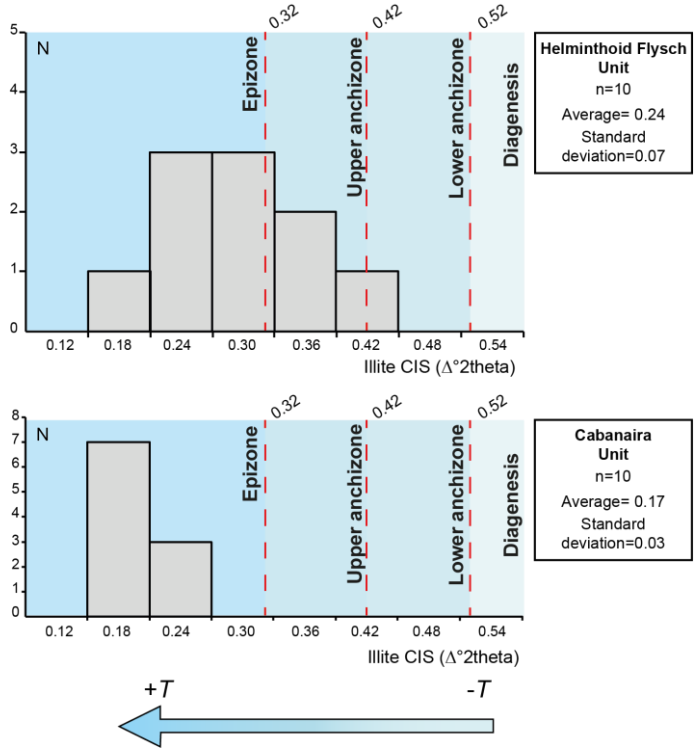

Figure 24. Illite crystallinity index distribution in the Helminthoid Flysch Unit and the Cabanaira Unit. The boundaries of very-low-grade metamorphic zone proposed by Warr and Ferreiro Mählmann (2015) are reported. N: number of examined samples.

low-grade metamorphic conditions proposed by Warr and Ferreiro Mahlmann (2015).

For the Helminthoid Flysch Unit the Ill_{IC} ranges from 0.20 to 0.42 $\Delta°2\theta$ with a peak at 0.30-0.36 $\Delta°2\theta$ indicating clearly upper anchizone/epizone metamorphism related temperature conditions. Mixed-layers are not present. The Cabanara Unit shows fewer variable Ill_{IC} distribution the latter represented by clearly lower values than those calculated for the Helminthoid Flysch Unit (from 0.13 to 0.22 $\Delta°2\theta$, Figure 24). Mixed-layers are not present. These data strongly indicate that the Cabanaira Unit recorded temperature conditions (Figure 24) typical of the epizone region, during its deformation history. Overall, microstructural observations and the observed paragenesis (see the paragraphs *Part V: The deformation strain patterns of the studied units*).

The b_0 value distribution is represented in the histograms of Figure 25 in which the barometric limit values suggested by Franceschelli et al. (1989) are also shown (blue dashed lines). Overall, an increase of the b_0 values moving from Helminthoid Flysch Unit to the Cabanaira Unit is observed. For the Helminthoid Flysch Unit the b_0 distribution measurement show high variability from 9.000 to 9.042 Å (Figure 25) with a peak between 9.002 and 9.007 indicating medium to lower pressure conditions (about 0.2-0.6 GPa). The Cabanaira Unit shows, again, fewer variability

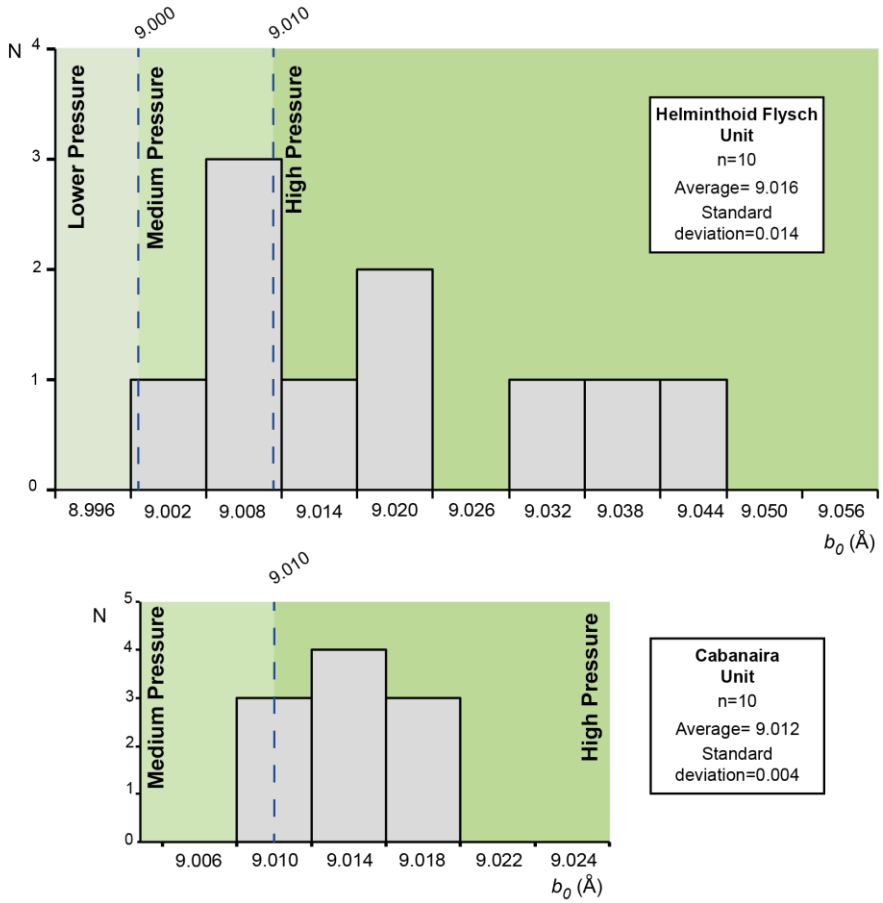

Figure 25. Illite b_0 cell parameter distribution in the Helminthoid Flysch Unit and the Cabanaira Unit. The boundaries of baric fields proposed by Franceschelli et al. (1989) are reported.

about the distribution values of the b_0 cell parameter, which ranges between 9.006 and 9.018 Å (Figure 25) with a peak at 9.011-9.013 Å (Figure 25). The b_0 values measured on the Cabanaira Unit clearly indicate higher pressure metamorphic conditions than Helminthoid Flysch (about 0.4-0.6 GPa).

7.2. Estimation of P–T metamorphic conditions of the Moglio-Testico Unit and the Marguareis Unit

- The Moglio-Testico Unit

The sample ED18 and ED91 collected in the Palombini Shale and Pieve di Teco Fm. were analyzed (see Plate 1 for the location of the samples). In ED18, two different generations of Chl and Phg grains growth along the $S1_{MT}$ and $S2_{MT}$ foliation (Chl1-Phg1 and Chl2-Phg2, respectively) have been treated to perform thermobarometric estimations. In the sample ED91 only the Chl-Phg couple grown along the $S1_{MT}$ foliation (Chl1-Phg1) have been found and considered for *P–T* calculations. In all of samples, chlorite and phengite structural formula were calculated assuming 14 and 11 oxygens, respectively.

In ED18 sample, the Chl1 grains show, on average, higher XMg content than Chl2 (Figure 26a). The Chl2 has more homogeneous

Si a.p.f.u. (atoms per formula unit) content than those of Chl1 (Figure 26a) as well as the Altot ranges (2.31 and 2.85 a.p.f.u. in Chl1 and 2.89 and 3.22 a.p.f.u. in Chl2, Figure 26b).

The Chl1 grains are also characterized by an end-members composition intermediate between Clc+Dph and Sud (about 40% of Sud content, Figure 26c). The Chl2 grains are instead characterized by Clc+Dph and Sud end-member proportions of 1:1. Am content is for all the Chl types always less than 30% and the vacancies less than 0.5 a.p.f.u. in almost all the grains (Figure 26c).

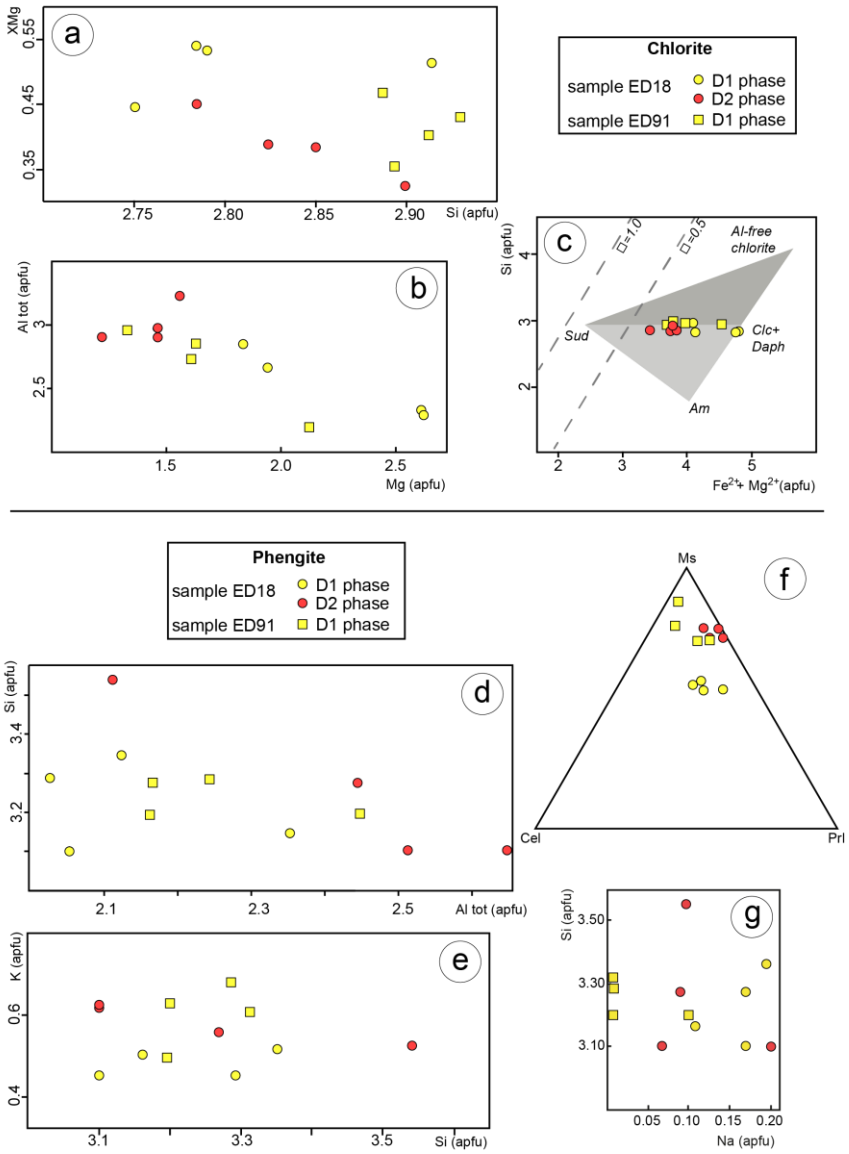

Figure 26. Geochemistry of chlorite (a, b, c) and phengite (d, e, f, g) selected on X-ray calibrated maps of ED18 and ED91 samples using XMapTools software (Lanari et al., 2014c). Chlorite and phengite structural formula are calculated assuming 14 and 11 oxygen, respectively.

The Phg1 and Phg2 grains have Si content of 3.10-3.35 and 3.10-3.54 a.p.f.u., respectively (see the S2 supplementary and Figure 33d). The Al content is higher in Phg2 (2.11-2.66 a.p.f.u., Figure 26d) than Phg1 (2.03-2.36 a.p.f.u.), which has instead variable K content (0.46-0.56 a.p.f.u., Figure 26e). White mica

end-member proportion is intermediate between Ms, Prl and Cel in both Phg1 and Phg2, with the latter tending to Cel-free solid solution than the former. The Cel- content is however less than 40% in both Phg1 and Phg2 (Figure 26f).

In the ED91 sample, the Chl1 grains grown along the $S1_{MT}$ foliation show XMg values ranging between 0.35 and 0.47, while the Si-content from 2.89 and 2.93 a.p.f.u. (Figure 26a). The Al- and Mg- contents range between 2.43 and 2.96 a.p.f.u. and between 1.33 and 2.12 a.p.f.u., respectively (Figure 26b). The composition of Chl1 is close to those of Clc+Dph, with minor Sud, whereas Am end-member is almost absent (Figure 26c) and the vacancy are less of 0.5.

The Phg1 grains have values of Si- content ranging between 3.20 and 3.32 a.p.f.u. and Al content slightly variable (2.16-2.45 a.p.f.u., Figure 26d). The K content in Phg1 varies between 0.50 and 0.69 a.p.f.u (Figure 26e). The Phg1 grains show end-member compositions close to pure Ms (always higher than 70%) with a slightly content of Prl (less than 30%, Fig. 26f).

Overall, in both of samples, a slightly trend between Si-rich Na-poor Phg1 to Si-poor Na-rich Phg2 can be observed (Figure 26g).

- *P–T* estimation for the Moglio-Testico Unit

The Chl-Qz-wt (Vidal et al., 2006) and Phg-Qz-wt (Dubacq et al., 2010) methods based on the activity of chlorite and phengite end-members and the water activity were applied on the samples ED18 and ED91. The Chl-Qz-wt method was used on the chlorites grown on $S1_{MT}$ and $S2_{MT}$ foliations. *T* range was calculated setting 30 °C of equilibrium tolerance and the percentage of Fe^{3+} for each chlorite analysis setting two different pressure values (1.2, 1.0 GPa in this case) following the procedure of Lanari and Duesterhoeft (2019). Among them, the *P* value chosen is those for which the corresponding *T* range included a large number of analysis and are characterized by a homogeneous Fe^{3+} content. The water activity was set to 0.8 in both samples to account for the presence of calcite (*i.e.*, Di Rosa et al., 2020; Frassi et al., 2022). The chlorite grains crystallized along the $S1_{MT}$ foliation (samples ED18 and ED91) and the $S2_{MT}$ foliation (sample ED18) show different *T* ranges (Figure 27). In both samples, Chl1 temperature ranges between 200-330 °C, whereas *T* of Chl2 of the sample ED18 ranges between 120-300 °C (Figure 27).

The Phg-Qz-wt method was used to calculate the *P* conditions basing on the Phg analysis included into the *T* range obtained with the Chl-Qz-wt method. The optimizes water content obtained is 0.96% for all the Phg groups processed (*i.e.*, Phg1 of ED18 and ED91 and Phg2 of ED18). The resulting P ranges are 0.7 and 1.4 GPa for $D1_{MT}$ phase in ED18 and ED91, and 0.2-1.0 GPa for the $D2_{MT}$ phase estimated with Phg_2 of ED18 (Figure 27).

The Chl-Phg-Qz-wt method (Vidal & Parra, 2000) allowed to find the Chl-Phg pairs related to $S1_{MT}$ and $S2_{MT}$ foliations which are in equilibrium under conditions of low free energy of Gibbs (small circles and squares of Figure 27). The equilibrium tolerance that we have set above which the energy is considered too high to represent a convergence between the selected equilibria (<15000 J).

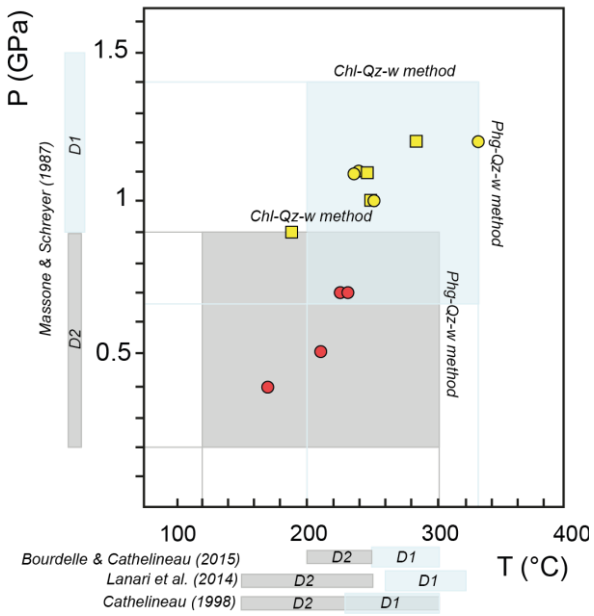

Figure 27. P/T diagram showing the results of the thermobarometric estimation performed on the samples ED18 and ED91. The light blue and grey pale squares in the P/T space indicate the areas constrained with Chl-qz-Wt (Vidal et al., 2006) and Phg-qz-Wt (Dubacq et al., 2010) methods; the yellow and red small circles and squares indicate the P–T equilibrium conditions of single Chl-Phg couples obtained with the Chl-Phg-qz-Wt method (Vidal and Parra, 2000). Along the Y and X axes the used geothermobarometers are reported with the range values related to $D1_{MT}$ and $D2_{MT}$ phases.

In the Figure 27 is showed the matching between the *P–T* estimates calculated by means the Chl-Phg-Qz-wt compared with the *T* and *P* ranges defined with the previous methods. Only the couples included between the *P*- and *T*-ranges obtained through the Chl-Qz-wt and Phg-Qz-wt have been considered.

The estimates suggest that the two different deformation events ($D1_{MT}$ and $D2_{MT}$) were accompanied by multistage metamorphic history (*i.e.*, two metamorphic events). Two clusters of data were observed in the samples collected from the Moglio-Testico Unit (ED18 and ED91). The first set of data is related to first Chl1-Phg1 generation grown along the S1 foliation and it is associated to metamorphic peak condition (*P* peak= 1.0-1.2 GPa and *T* peak= 330-260 °C); the second data set, still related to the $S1_{MT}$ foliation, and the second set related to Chl2-Phg2 couples grown along the $S2_{MT}$ foliation and stable at *LP–LT* metamorphic conditions (*P*= 0.7-0.4 GPa and *T*= 230-170 °C).

The different *P–T* ranges obtained in this work have been compared with the classic geothermometers and geobarometers. For the chlorite grains grown along the $S1_{MT}$ foliation, the semi-empirical calibration of Cathelineau (1988) yielded a temperature ranging from 320-230 °C and 300-150 °C for those grown along the $S2_{MT}$ foliation. The calibration for low-temperature conditions (*T*< 400 °C), even if the amount of Fe^{3+} in chlorites is unknown (for details see Lanari *et al.*, 2014), yielded a more restricted range (Figure 34). Using this calibration, we obtained a *T* range of 300-250 °C for chlorites in $S1_{MT}$ and 230-200°C for chlorites in $S2_{MT}$ foliation. Using the geothermometer of Bourdelle and Cathelineau (2015) which is specifically thought for chlorites recrystallized in a *T* interval between

100 and 400 °C, 300-250 °C is the *T* resulting from Chl1 and 230-200 °C those related to the Chl2. *P* was instead calculated with the geobarometer of Massonne and Schreyer (1987) despite the absence of the buffering assemblage. The pressure range of the phengites grown along the $S1_{MT}$ and $S2_{MT}$ foliations are 1.5-0.9 GPa and of 0.9-0.2 GPa, respectively.

- The Marguareis Unit

The samples ED1 and TSE236 collected in the Eocene meta-pelites (Boaria Formation, see Plate 1 for the location of the samples) were analyzed. In these samples, two different generartions of Chl and Phg growth along the $S1_{MU}$ and $S2_{MU}$ foliation (Chl1-Phg1 and Chl2-Phg2, respectively) have been sampled and they were considered to calculate the *P* and *T* conditions. In all of samples, Chl and Phg structural formula was calculated assuming 14 and 11 oxygens, respectively.

In the ED1 sample, the Chl1 is characterized by low Si content (2.65-2.80 a.p.f.u.) and Al content ranging from 2.60 to 3.00 a.p.f.u. (Figure 28a-b). Chl2 grains grown along the $S2_{MU}$ foliation and show Altot content slightly lower (2.40-2.90 a.p.f.u.), whereas the Si content is higher (2.75-3.00 a.p.f.u.) than those of Chl1 (Figures 28a-b). The Mg content like the XMg value (Figure 28a-b) tend to be higher and less variable in the Chl1 (1.6-1.8 and 0.40-0.42 a.p.f.u., respectively), than those of Chl2 (1.4-1.8 and 0.37-0.43 a.p.f.u., respectively). Chl1 grains show higher clinochlore+daphinite content (more than 50%) than those of Chl2 which ranging between 40-50% (Figure 28c). Small differences between Chl1 and Chl2 exist about the Amesite content which is higher and lower than 20% respectively. The Sudoite content is lower in Chl1 (lower than 20%) than those in Chl2 (more than 20%). All the Chl types always show the vacancies less than 0.5 a.p.f.u. (Figure 28c). Similarly, also the phengite compositions various according to the different microstructural site (*i.e.*, $S1_{MU}$ and $S2_{MU}$ foliation). The Phg1 grains show higher Si- and K contents (2.90-3.40 and 0.75-0.84 a.p.f.u, respectively) and slightly low Al content (2.40-2.55 a.p.f.u.) than those of Phg_2 (Si: 2.95-3.10; K: 0.77-0.64 and Al: 2.30-2.60 a.p.f.u., Figures 28d-e). A clear trend from Si-rich-Na-poor Phg1 (Na content: 0.03-0.05 a.p.f.u.) to Si-poor-Na-rich Phg2 (Na content: 0.05-0.10 a.p.f.u.) is appreciable (Figure 28f). The Phg1 and Phg2 are characterized by a celadonite content always lower than 20% (Figure 28g) and a dominant muscovite component. Both Phg1 and Phg2 can be classified as impure muscovite with the pyrophyllite content slightly higher for the first one.

In the TSE236 sample (Figure 28a-b) Chl1 are characterized by Si content ranging between 2.70-3.1 a.p.f.u. and Al content fewer variable (2.70-2.90 a.p.f.u.). Chl2, instead show fewer variable of Si content (2.8-2.9 a.p.f.u.) and Al

content (2.7-2.9 a.p.f.u.) than those of Chl1. The Mg content (Figure 28a) is more variable

The Amesite content ranging between 35%-55% in Chl1, whereas it is always lower than

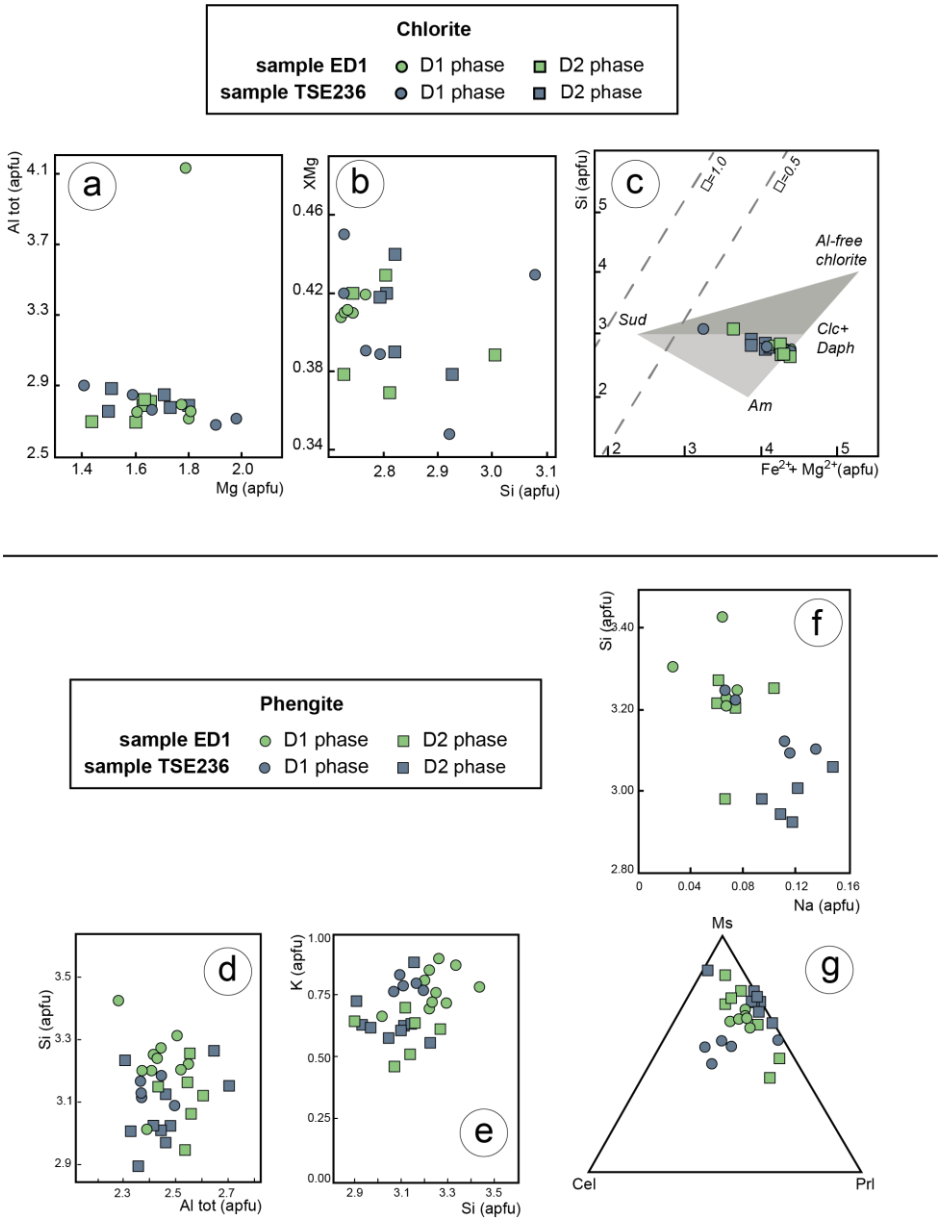

Figure 28. Geochemistry of (a) chlorite and (b) phengite sampled into ED1 and TSE236. Chlorite and phengite structural formula are calculated assuming 14 and 11 oxigen, respectively (modified from Sanità et al., 2022b).

in the Chl_1 (1.4-2.0 apfu) than in Chl2 (1.5-1.8 a.p.f.u.). The XMg (Figure 28b) tends to be higher in the Chl1 (0.39-0.45) than that in Chl2 (0.38-0.44). The Chl1 show clinochlore+daphnite content lower than 40% and range between 50% and 40% in Chl2 (Figure 28c).

40% in the Chl2 (Figure 35c). As for the ED1 sample, all the Chl types in the TSE236 sample always show the vacancies less than 0.5 a.p.f.u. (Figure 28c).

Phg1 show higher Si content and quite homogeneous Al content (Si: 3.10-3.20 a.p.f.u.; Al content: 2.40-2.50 a.p.f.u.) than those of Phg2 (Si: 2.90-3.10 a.p.f.u.; Al

content: 2.35-2.50 a.p.f.u.); whereas show higher K content (Figures 28d-e) than Phg2 (0.83-0.57 and 0.73-0.58 a.p.f.u., respectively). A Si-rich-Na-poor Phg1 (Na: 0.06-0.14 a.p.f.u.) to Si-poor-Na-rich Phg2 (Na: 0.09-0.15 a.p.f.u.) trend can be observed also in the sample TSE236 (Figure 28f). Phg_1 are characterized by a celadonite content always lower than 40% while it is basically absent in Phg2. The pyrophyllite content is variable but never exceeding the 25-30% (Figure 28g). Both Phg1 and Phg2 show muscovite content lower and higher, respectively, but never below 40% (Figure 28g) and therefore classifiable as impure muscovite.

- *P–T* estimation for the Marguareis Unit

P–T estimates based on the activity of chlorite and phengite end-members and the water activity were obtained through the Chl-Qz-wt, Phg-Qz-wt and Chl-Phg-Qz-wt methods. These methods were applied on chlorites and phengites related to the $D1_{MU}$ phase in the sample ED1 and those of the $D2_{MU}$ phase in the sample TSE236. With the Chl-Qz-wt (Vidal *et al.*, 2005), *T* ranges were calculated setting the equilibrium tolerance to 30 °C and the percentage of Fe^{3+} for each Chl analysis fixing a starting pressure value (in this case 0.6 GPa) following the procedure of Lanari and Duesterhoeft (2019). The water activity was set to 1 in the sample ED1 and to 0.8 in the sample TSE236, based on the presence/lack of calcite (see Frassi *et al.*, 2022). Temperature ranges related to the $D1_{MU}$ and $D2_{MU}$ phases are 230-330 °C and 160-330 °C, respectively.

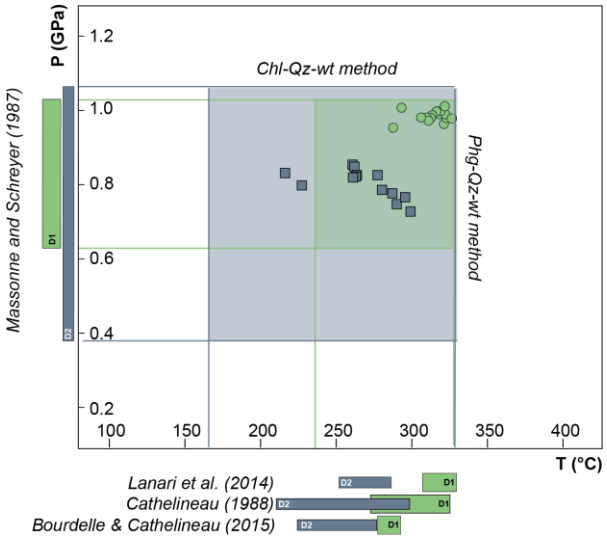

Figure 29. P/T diagram showing the results of the thermobaric methods applied to samples ED1 and TSE236. In the P/T space, the pale squares indicate the areas constrained by the Chl-qz-wt (Vidal et al., 2006) and Phg-qz-wt (Dubacq et al., 2010) methods; the position of data (small circles and squares) indicate the P-T equilibrium conditions of single Chl-Phg couples obtained with Chl-Phg-qz-wt method (Vidal and Parra, 2000). Along the Y and X axes the comparison between our results and the classic geothermobarometers is reported.

The Phg-Qz-wt (Dubacq *et al.*, 2010) was applied in order to quantify the *P* conditions of the Marguareis Unit during the $D1_{MU}$ and the $D2_{MU}$ phases. The *P* range related to the $D1_{MU}$ phase was estimated with Phg1 of the sample ED1 grown along the $S1_{MU}$, setting an average temperature of 300 °C and assuming 0.95 % of water as optimized value (see Supplementary material 4, Frassi *et al.*, 2022). Pressure range for the $D1_{MU}$ phase is between 1.05 and 0.65 GPa (Figure 29). Pressure values related to the $D2_{MU}$ phase were calculated using Phg_2 of the sample TSE236, assuming an average *T* of 300°C and the water optimized values of 0.95

% (see Frassi *et al.*, 2022). Pressure range of the $D2_{MU}$ phase is 0.38-1.10 GPa (Figure 29).

The Chl-Phg-Qz-wt (Vidal and Parra, 2000) method allowed to find the chlorite-phengite couples related to the $D1_{MU}$ (sample ED1) and $D2_{MU}$ (sample TSE236) phases (see supplementary material). Only the couples equilibrated with a tolerance <1000 J and included between the *T*- and *P*- ranges of the Chl-Qz-wt and Phg-Qz-wt method were considered. The *P*–*T* conditions for the $D1_{MU}$ phase are 1.00-0.90 GPa and 280-330 °C and those related to the D2 phase are 0.85-0.7 GPa and 230-300 °C (Figure 29).

The results obtained were compared with *T* and *P* values estimated with classical geothermobarometers (Figure 29). We first used the semi-empirical calibration proposed by Cathelineau (1988) and this thermometer yields a temperature range of 275-327 °C for chlorites in $S1_{MU}$ and of 215-300 °C for chlorites in $S2_{MU}$. However, Lanari *et al.* (2014) proposed a calibration for low temperature conditions (*i.e.*, T< 400 °C) even when the amount of Fe^{3+} in chlorite is unknown. Using this calibration, we obtained a temperature range of 310-330 °C for chlorites in $S1_{MU}$ and a *T* range of 250-280 °C for chlorites in $S2_{MU}$. Moreover, we used also the calibration established by Bourdelle and Cathelineau (2015), which is also an efficient tool for chlorite thermometry between 100 and 400 °C, even if the non-ideal contribution of site mixing is not considered. This thermometer yields temperatures of 275-285 °C for chlorite in S1 and of 225-275 °C for chlorites in S2. Altogether, chlorite solid-solution thermometry indicates *T* conditions of 300 ±30°C for the $D1_{MU}$ phase and *T* conditions of 250 ± 40 °C for the $D2_{MU}$ phase.

The geobarometer of Massonne and Schreyer (1987) were applied on the samples ED1 and TSE236 (XMapTools, Lanari *et al.*, 2014) to obtain the pressure range related to the $D1_{MU}$ and the $D2_{MU}$ phases, respectively (Figure 29). The pressure range calculated on phengite of the sample ED1 grown along the $S1_{MU}$ is 1.03-0.63 GPa, while that of the sample TSE236 related to the $S2_{MU}$ is 1.07-0.38 GPa.

The results obtained from quantitative and semi-quantitative *P*–*T* estimates are summarized in the Figure 30.

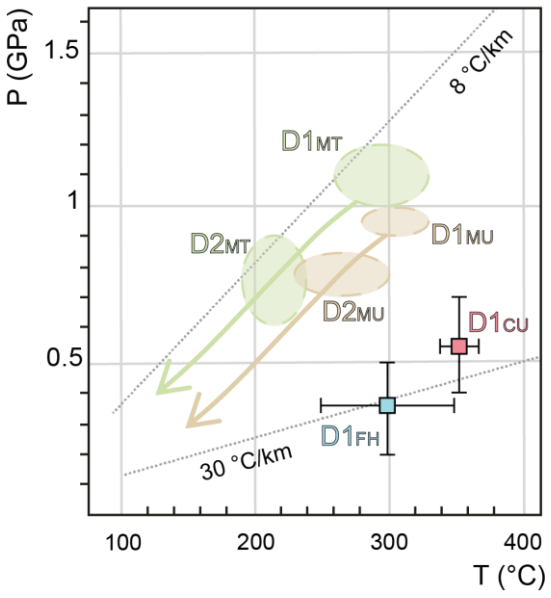

Figure 30. Simplified diagram summarizing the quantitative (green and orange ellipses) and semi-quantitative (light blue and red squares) P–T conditions, with the relative errors (long and short axes of ellipses and black segments), estimated for each tectonic unit.

8. Discussion and Conclusion

The convergent history proposed for the Western Alps (*i.e*, Rosenbaum and Lister, 2002; Oberhansli *et al*., 2004; Rosembaum *et al*., 2005; Lardeaux *et al*., 2006; Handy *et al*., 2010; Beltrando *et al*., 2010; Lardeaux, 2014; Schmid *et al*., 2017) requires before the involvement of the oceanic lithosphere into the subduction zone until the onset of the continental subduction of the Europe margin and the subsequently collision during Eocene-Oligocene timespan. The continental and oceanic tectonic units were thus affected by underthrusting, accretion and subsequent exhumation processes, into the Alpine accretionary/orogenic wedge, recording different deformation histories and *P*–*T* paths (i.e., Schmid *et al*., 2004; Oberhansli *et al*., 2004; Goffé *et al*., 2004; Handy *et al*., 2010; Lardeaux, 2014; Agard *et al*., 2018; Agard, 2021; Hervioue *et al*., 2022).

In this Thesis, the multi-scale analysis performed on the tectonic units (oceanic and continental) cropping out in the investigated area allow to unravel their tectonic evolution, developed during the convergence between Europe and Adria Plates, as well as their pre-deformation setting. Previous authors considered that these tectonic units have recorded a deformation history associated to the alpine accretionary and orogenic wedge at shallower crustal levels (*i.e*., Lanteaume, 1968; Brizio *et al*., 1983; Vanossi *et al*., 1984; Vanossi *et al*., 1986; Di Giulio, 1992; Carminati, 2001; Seno *et al*., 2003; Seno *et al*., 2005; Piana *et al*., 2009; Bonini *et al*., 2010; Piana *et al*., 2014; d'Atri *et al*., 2016; Bertok *et al*., 2018; Mueller *et al*., 2020; Piana *et al*., 2021). Besides, the same authors agree about the current map-scale tectonic stacking order, characterized by the oceanic-derived Helminthoid Flysch and Moglio-Testico units tectonically overlying onto the Europe-derived units (Briançonnais Units), thus reflecting the original pre-convergent paleogeographic setting (Figure 3a-b, i.e., Lanteaume and Haccard, 1961; Sagri, 1984; Vanossi *et al*., 1984; Marini and Terranova, 1984; Vanossi *et al*., 1986; Di Giulio, 1992; Seno *et al*., 2003; DeCarlis *et al*., 2013; d'Atri *et al*., 2016; Piana *et al*., 2021). However, the new lithostratigraphic, structural and metamorphic dataset obtained in this Thesis point out to a different pre-deformation setting, with different paleogeographic origin for each tectonic unit, as well as their structural evolution. In the next paragraphs, basing on the new data previously described, some of these issues will be taken up and new arguments will be discussed to propose a new tectonic scenario.

8.1 Paleogeographic origin of the tectonic unit: Insights from stratigraphy and arenites petrography

Field mapping performed on the investigated area allowed us to reconstruct the sedimentary succession of each tectonic unit (Figure 31).

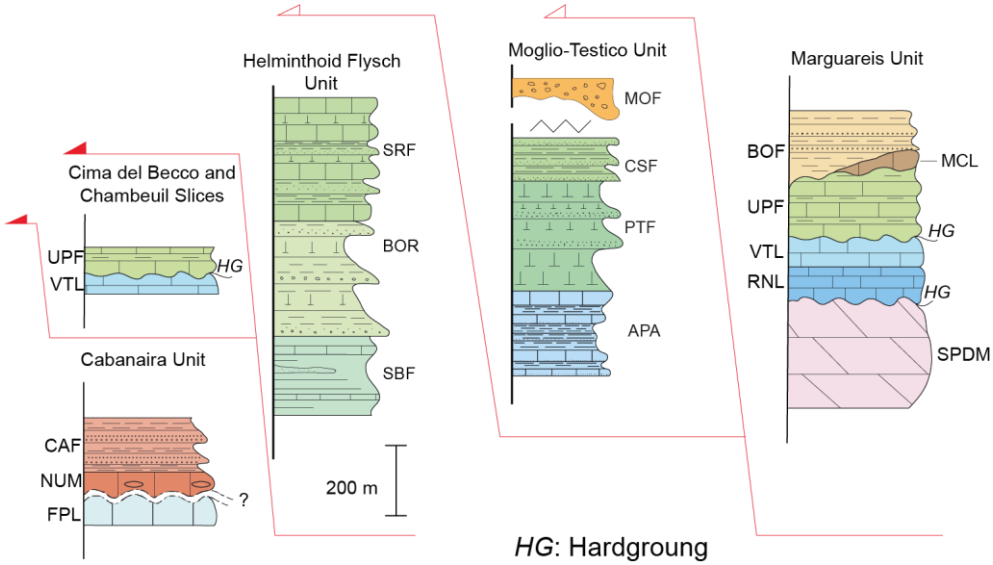

Figure 31. Stratigraphic logs of the tectonic units cropping out in the study area. The thickness is indicated.

The Marguareis Unit, including the tectonic slices (BS and CS, see stratigraphic logs of Figure 31), and the Cabanaira Unit consist of Meso-Cenozoic sedimentary sequences showing a coarsening upward trend. The successions are characterized by a transition from carbonate peritidal deposits, spanning from Triassic to middle Eocene (San Pietro dei Monti Dolostone, Rio di Nava Limestone, Val Tanarello Limestone, Upega Formation and Madonna dei Cancelli Limestone for the Marguareis Unit and Cima del Becco Slice; Forte Pepin Limestone for the Cabanaira Unit), to middle Eocene foredeep turbidites (Boaria Formation for Marguareis Unit; Nummulitic Limestone and Cima Aurusi Formation for Cabanaira Unit), as outlined by several authors (Decarlis *et al.*, 2013 and quoted references). The facies association recognized in the Boaria and Cima Aurusi formations suggests a slope environment characterized by gravitational instability. Besides, the modal analysis (Figure 10, 12) performed on the Cima Aurusi deposits indicates that the source area was characterized by granitoids, low-grade metamorphic rocks, felsic to intermediate volcanic and carbonate rocks. The lacking of ophiolite and High-grade metamorphic rocks, which formed the Alpine wedge at middle Eocene, seems in contrast with a source area located along it. The Cima Aurusi deposits, thus, were supply by a source area characterized by upper continental crust including its sedimentary cover. This dataset calls for the Europe continental margin as source area of the Briançonnais Units exposed in this sector of the Alps, accordingly with Decarlis *et al.* (2013) which proposed the same

paleogeographic location for analogue units located in neighboring areas. The sedimentary evolution of these Briançonnais Units thus suggests a foredeep-ward motion of a portion of the Europe continental lithosphere approaching toward the subduction zone, before to be underthrusted and subsequently accreted and then exhumed into the Alpine wedge.

In contrast, the Helminthoid Flysch and the Moglio-Testico units reveal a different sedimentary evolution and both are classically regarded as oceanic-derived unit (*i.e.*, Sagri, 1984; Vanossi *et al.*, 1984; Lanteaume, 1962; Vanossi *et al.*, 1986; Marini and Terranova, 1985; Marini, 1995; Seno *et al.*, 2003; Seno *et al.*, 2005; Di Giulio, 1992; Mueller *et al.*, 2018; Mueller *et al.*, 2020). However, the succession of the Moglio-Testico Unit described in this Thesis is quite different from that proposed by the previous authors (i.e., Lanteaume and Haccard, 1962; Di Giulio, 1987; Marini, 1995 - Figures 5, 6). In fact, the described sedimentary and stratigraphic features indicate a transition from pelagic/hemipelagic (here represented by the Palombini Shale, cf. Moglio Shale *p.p.* of Haccard, 1961, and Pieve di Teco Member *p.p.* of Marini, 1995) to fine-grained turbidite deposits related to basin plain environment (Pieve di Teco and Cesio Formation, cf. Pieve di Teco Member *p.p.* and Cesio Member *p.p.*, respectively, of Marini, 1995) with an upward increasing siliciclastic component (Figures 5, 31). The chaotic deposits (Moglio Formation, see Figure 5), that occur within a tectonic slice at the base of the Moglio-Testico Unit (Plates 6, 7) are made up by cm- to dm-sized blocks embedded into a shaly matrix. The lithologies from the blocks, that derive from the youngest formations (*i.e.,* Cesio Formation and/or Pieve di Teco Formation) documented in the mapped area, suggest that these deposits represent the top of the succession of the Moglio-Testico Unit (Figure 31). These observations seem suggest a different evolution of the Moglio-Testico Unit respect those proposed until now. A similar sedimentary sequence evolution was described for the Internal Ligurian Units exposed in the Northern Apennine (see Marroni *et al.*, 2010; 2017 for details). In fact, these units are composed by a Jurassic oceanic basement including radiolarites (Diaspri Formation), an Early Cretaceous oceanic cover (*i.e.,* Calpionella Limestone and Palombini Shale), a Late Cretaceous turbidite sequence (Manganesiferi Shale, Monte Verzi Marl, Zonati Shale, Gottero Sandstone; Marroni and Perilli, 1990, Marroni and Pandolfi, 1996; Marroni *et al.*, 2017) topped by a Late Cretaceous-Paleocene trench/slope chaotic deposits (Bocco Shale, see Marroni and Pandolfi, 2001 and Meneghini *et al.*, 2020 for further details). The Internal Ligurian Units sequence is classically regarded as reflect the sedimentary evolution of an area of the Ligure-Piemontese Ocean approaching the subduction zone before to be underthrust, accreted and

subsequent exhumed into the alpine accretionary wedge (Marroni *et al.*, 2010; Marroni *et al.*, 2017). The Internal Ligurian Units succession was recently used as proxy to unravel the pre-deformation setting evolution of others oceanic-derived units cropping out in the Western Alps (*i.e.,* Ellero and Loprieno, 2017; Festa *et al.*, 2021) where primary features (*i.e.,* stratigraphic and sedimentary features) are partially or completely deleted because of the strongly deformation recorded by all of them. For these reasons, the Internal Ligurian Units succession can be a powerful tool to decipher the sedimentary evolution of the Moglio-Testico Unit. The sedimentary evolution of the Moglio-Testico Unit reconstructed in this work seems correspond, at least partially, with that largely described for the Internal Ligurian Units in Eastern Liguria. This interpretation allowed me to re-assess the stratigraphic meaning of the chaotic deposits of the Moglio Shale classically located at the bottom of the Moglio-Testico Unit sequence. The stratigraphic observations indicate that the

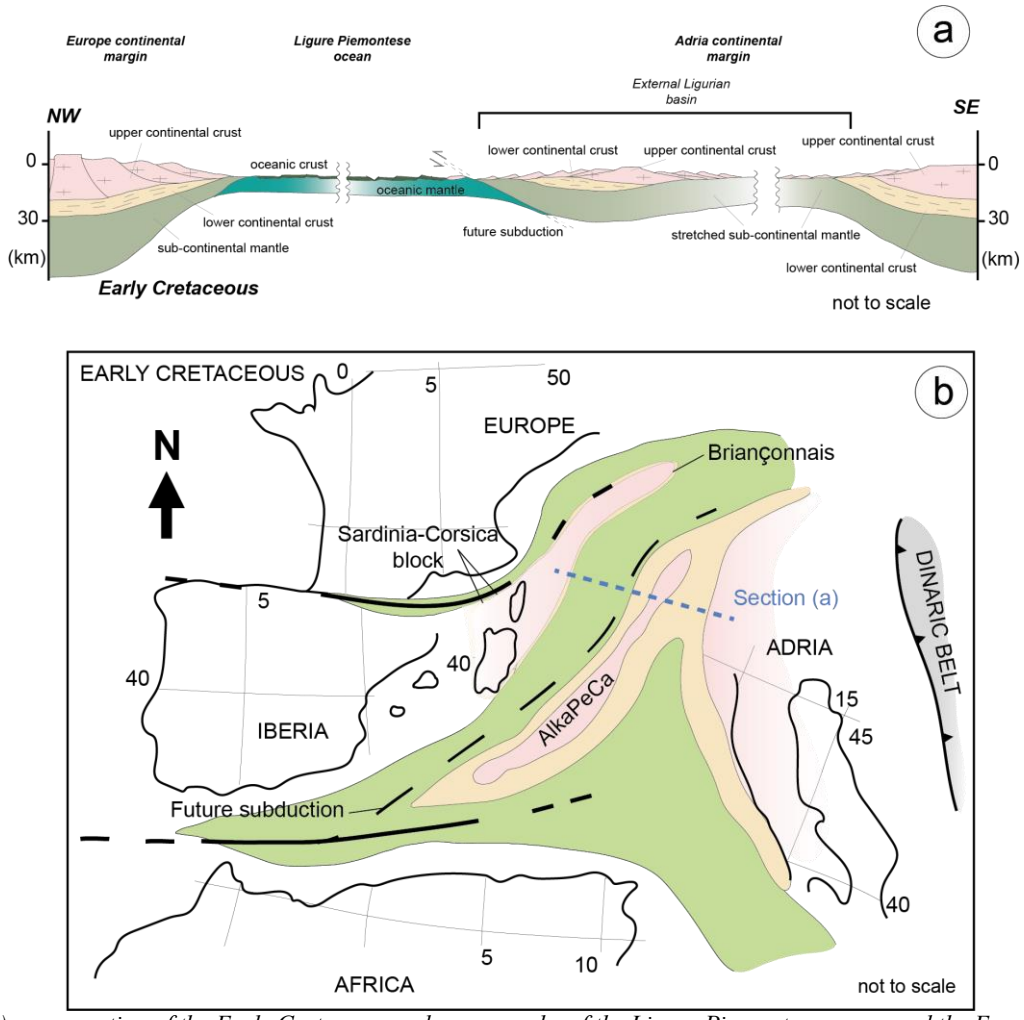

Figure 32. a) cross-section of the Early Cretaceous paleogeography of the Ligure Piemontese ocean and the Europe and Adria continental margins (modified from Marroni et al., 2017). The source-area of the Helminthoid Flysch and the External Ligurian units is reported. b) Snapshot of the Early Cretaceous paleogeography of the Mediterranean area with the location of the cross-section of (a). Coordinates and displacements (black arrows) of Africa Iberia Adria versus Europe and position of the Corsica-Sardinia Block versus Iberia based on Michard et al., 2002. Simirarly to (a), green areas area is the oceanic crust, the yellow areas are the thinned continental crust, and the pink area are the upper continental crust. The Dinaric belt (grey area) is also reported.

Moglio Shale chaotic deposits show characteristics like those described for the trench/slope deposits largely documented at the top of the Internal Ligurian Unit sedimentary sequence exposed in Northern Apennine (cf. with Bocco Shale, Marroni and Pandolfi, 2001). Therefore, in this frame, the sequence of the Moglio-Testico Unit can be considered as reflecting the sedimentary evolution of an oceanic cover approaching the subduction zone. Evidence of these large-scale chaotic bodies are documented in other active subduction systems (*i.e.,* Nankai Trough, Moore and Strasser, 2016).

The Helminthoid Flysch Unit consists of a Late Cretaceous turbidites showing a fining upward trend and detached from its original basement along the weak horizon corresponding to the varicoloured shales of the San Bartolomeo Formation (Figure 31). The upper part of the succession shows stratigraphic features indicating a depositional environmental dominated by turbidite reworking of carbonate oozes (San Remo Flysch) with a deep sea turbidite deposits (Bordighera Sandstone) arranged as a lobe system characterized by medium- to coarse-grained deposits (Figure 31).

The lack of syn-sedimentary deformation as slumps, intraformational breccias and the absence of chaotic deposits at the top of succession clearly indicate the absence of gravitational instability of the depositional interface. The modal analysis performed on the Bordighera Sandstone deposits (Figures 10, 11) indicate that the source area was characterized by granitoids, low- to high-grade metamorphic rocks, felsic to intermediate volcanites with relative carbonate cover rocks. This suggest that the Bordighera Sandstone deposits were supply by lower to upper continental crust.

The collected data suggest a different evolution for the succession of the Helminthoid Flysch Unit respect to those of the Moglio-Testico Unit. Marroni *et al*. (2010) regarded the Helminthoid Flysch Units of the Northern Apennines (*i.e.,* the External Ligurian Units) as sedimentary cover of an ocean–continent transition located near the Adria Plate (Figure 32, for a discussion see Marroni *et al*., 2010; Marroni *et al*., 2017). Differently, Mueller et al. (2018), accordingly to Sagri (1979) and Vanossi *et al*., (1984), regarded the San Remo-Monte Saccarello Unit of Western Ligurian Alps (cf. Helminthoid Flysch Unit in this work) as an oceanic-derived unit. These authors proposed a Late Cretaceous paleogeography where the succession of the Helminthoid Flysch Unit was located onto the oceanic lithosphere, close to the Europe margin, that is the paleogeographic location proposed for the Internal Ligurian Units (see Marroni *et al*., 2010; Marroni *et al*., 2017 and quoted references). Taking in mind the previously described stratigraphy of all these tectonic units, the comparison between San Remo-Monte Saccarello Unit (cf. Helminthoid

Flysch Unit this work) and the Internal Ligurian Units seems to be weak mainly due to the absence of the Jurassic oceanic sequence and a Late Jurassic-Early Cretaceous oceanic sedimentary cover (cf. Chert Fm. and Calpionella Limestone) and also for the lack of the Late Cretaceous-Early Paleocene trench-slope deposits.

On the contrary, the Helminthoid Flysch Unit shows a stratigraphic sequence corresponding to those well known in the tectonic units interpreted as External Ligurian Units that were deposited in the ocean-continent transition between the Ligure Piemontese ocean and the Adria Plate margin (Figure 38a-b, Marroni *et al.*, 2010, cf. Cassio and Antola units). A comparison between the modal analysis performed on the Helminthoid Flysch Unit (this work) and those available on the Internal Ligurian Units and External Ligurian Units deposits of the Northern Apennine was attempted (Figure 33a-b). It is evident that Bordighera Sandstone composition do not match with those described for the Internal Ligurian Unit deposits (*i.e.,* the Gottero Sandstone, Figure 33a). On the contrary, there is a good fit between the Helminthoid Flysch (this work) and the External Ligurian Units deposits (*i.e.,* Cassio Flysch and Valmozzola Flysch, Figure 33b, see Bianchi and Daniele, 1995; Daniele and Plesi, 2000; Marroni *et al.*, 2010 and quoted references for more details). In this frame, for the Helminthoid Flysch Unit of the Western Ligurian Alps area a

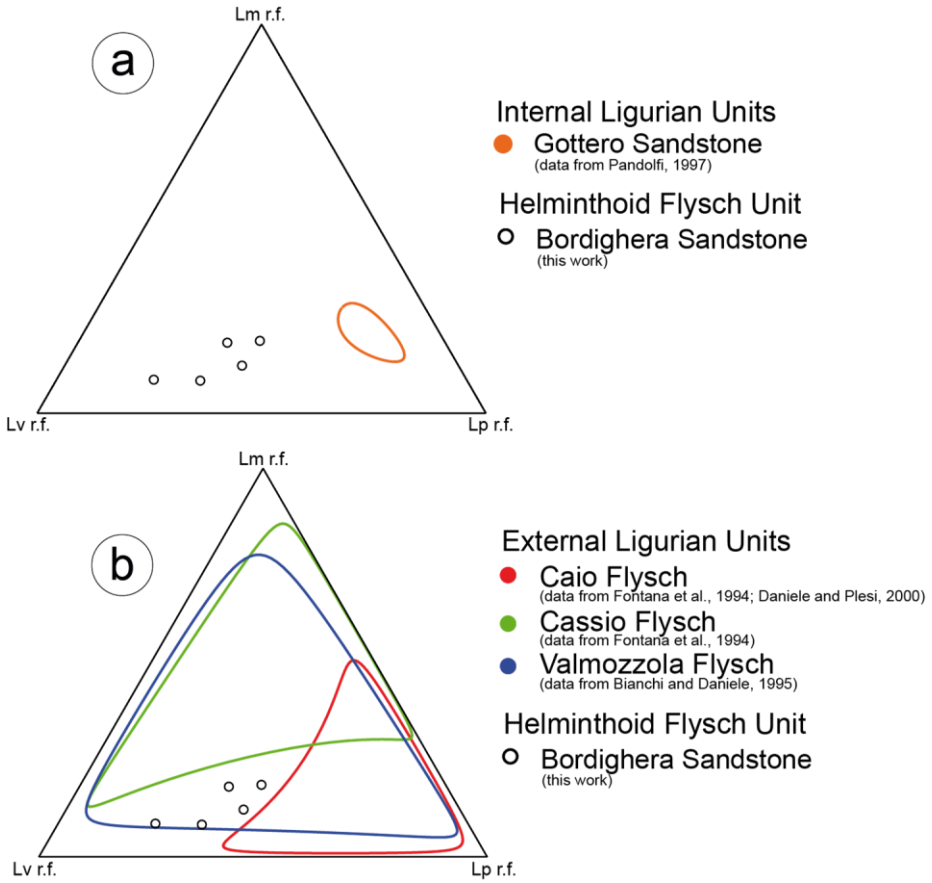

Figure 33. Comparison between Third order diagrams (rock fragments) of the Bordighera Sandstone and Internal and External Ligurian turbidite deposits. The colored line indicates the compositional ranges for the arenitic deposits of the External Ligurian units.

paleogeographic location similar to External Ligurian Units is thus proposed (Figure 32a-b).

8.2 Tectonic evolution of the units: Deep vs shallow structural levels deformations during convergence

- Tectonic meaning of the pre-coupling structures

The tectonic units exposed in the study area recorded different pre-coupling deformation events. In the Marguareis Unit, including the tectonic slices (Cima del Becco and Chambeuil Slices), these events are represented by the first two folding events, $D1_{MU}$ and $D2_{MU}$ (cf. Brizio *et al*., 1983). Based on results of their structural analysis, which are confirmed by this Thesis, several authors (*i.e.,* Seno, 1992; Vanossi et al., 1984; Carminati, 2001) proposed that $D1_{MU}$ folding developed in ductile shear zones during overall southwestward motion of the Marguareis Unit. The $D2_{MU}$ folding event is instead associated with the regional NE-direct backthrusting event. Carminati (2001) proposed that the metamorphic peak conditions were reached during the $D1_{MU}$ phase according with the recrystallizations supported by the $S1_{MU}$ foliation. In other sectors of the Briançonnais Domain corresponding deformation phases have been documented by Menardi-Noguera (1988), Michard et al. (2004), Strzerzynski et al. (2011), and Bonini et al. (2010).

In the Cabanaira Unit, only one pre-coupling deformation event ($D1_{CU}$) has been documented. The $F1_{CU}$ fold system suggests, however, a southwestward tectonic transport as that detected in the Marguareis Unit. The lack of the polyphase deformation history as reconstructed in the Marguareis Unit is probably due to the prevalence of lithologies without competence contrast that, in association with the low-grade metamorphic conditions (see chapter *Metamorphism*), hampered the development of the weaker deformations. According with these observations, a pre-coupling structural evolution as recognized in the Marguareis Unit, including the tectonic slices, can be supposed also for the Cabanaira Unit. According with Menardi-Noguera (1988), Michard *et al*. (2004), and Strzerzynski *et al*. (2011), the pre-coupling deformation history recognized in Marguareis Unit, including the tectonic slices, and the Cabanaira Units can be interpreted as the result of the involvement into the subduction zone of the thinned Europe continental margin that experienced underthrusting, accretion and later exhumation into the Alpine wedge. The result of this pre-coupling geodynamic history is not only the deformation and metamorphism of these units but also the thrusting of the Marguareis Unit, including the tectonic slices, onto the Cabanaira Unit. It must be underlined that the pre-coupling deformation history of the Marguareis Unit, including the tectonic slices,

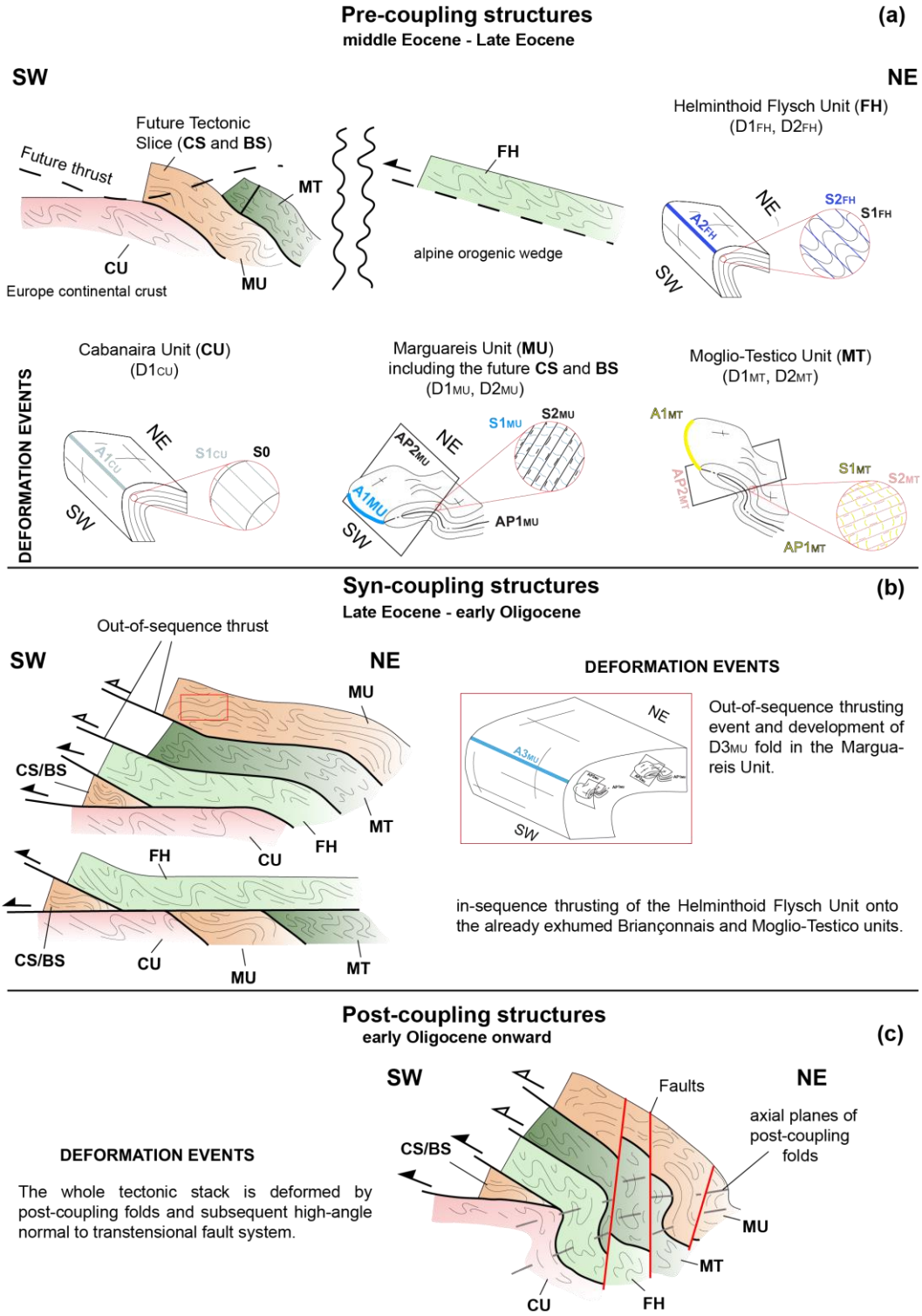

Figure 34. Sketch illustrating the tectonic evolution of the units cropping out in the study area starting from middle to late Eocene. a) Pre-coupling folding events developed in the Moglio-Testico and Briançonnais units, after their underthrusting, accretion and subsequently exhumation into the alpine accretionary and orogenic wedge, respectively; and in the Helminthoid Flysch Unit. b) Syn-coupling structures: In- and out-of-sequence thrusting and $D3_{MU}$ folding affecting the Margaureis Unit (Briançonnais Domain). c) Post-coupling deformation history represented by open folding system and later high-angle normal to transcurrent fault system. Black full arrows indicate the kinematics of the thrust surfaces at the base of the Helminthoid Flysch Unit; black empty arrows indicate the kinematics of the out-of-sequence thrust surfaces.

and the Cabanaira Unit and including their exhumation toward shallow structural level, pre-dates the coupling with the Helminthoid Flysch Unit (Plates 2, 3, 4, 5 and Figure 34a, see chapter *the deformation strain patterns of the studied units*). The ages of these

deformations are unfortunately poorly constrained. The middle Eocene age of the *Flysch Noir* (Lanteaume, 1968 – cf. Boaria Formation in this article) places a lower boundary for the age of metamorphism and related deformations (Figure 34a). In fact, Michard *et al.* (2004) proposed a post-Bartonian age (38 Ma, similar timespan was proposed by Lanari *et al.*, 2012) for the syn-metamorphic main deformation phase. Strzerzynski *et al.* (2011) estimated 45–37 Ma for the metamorphic peak pressure achieved during continental subduction of units from Briançonnais Domain. This age is coherent with geochronological data obtained by Monié (1990) from the metamorphic white micas (37 Ma). The exhumation of the Briançonnais units is regarded as accomplished between 37 and 31 Ma (Michard *et al.*, 2004; Strzerzynski *et al.*, 2011). A similar age-range for the tectonic evolution of the Marguareis Unit can be supposed (Figure 34a). Based on the middle Eocene age of the Cima Aurusi Formation (Gidon, 1972), we also propose a post middle Eocene age for $D1_{CU}$ phase (Figure 34a).

The structural analysis performed on the Moglio-Testico Unit highlighted a much more complex deformation history respect that proposed by previous authors (*i.e.,* Marini & Terranova, 1985; Vanossi *et al.*, 1986; Di Giulio, 1987; Galbiati and Rodi, 1989) dealing with the superposition of two pre-coupling folding events ($D1_{MT}$ and $D2_{MT}$) which can be observed in the whole tectonic unit (Plates 6, 7). $D1_{MT}$ phase produced the $S1_{MT}$ tectonic foliation associated with a SW-vergence similar $F1_{MT}$ fold system (Figure 34a) and characterized by the oldest metamorphic assemblage recognized in this unit (see chapter *Metamorphism*). The structural features associated with the $D1_{MT}$ phase suggest its development during high-strain conditions, *i.e.,* in a ductile shear zone characterized by a top-to-SW sense of movement. The $D2_{MT}$ phase is instead associated with a $F2_{MT}$ folding event associated to the $S2_{MT}$ crenulation cleavage characterized by a different metamorphic assemblage than that observed along the $S1_{MT}$ foliation (see chapert *Metamorphism*). After retrodeformation from the subsequent syn- and post-coupling events The D2 fold system show a gently NE-vergence to flat-lying attitude (Figure 34a). Di Giulio (1988), accordingly with Vanossi *et al.* (1986), proposed a structural model in which the different vergence of the folding systems recognized in different areas, *i.e.,* in the external (toward West) and in the internal (toward East) sectors of the unit, is due to a regional-scale folding event affecting the whole unit including the unit-bounding thrust surfaces. However, in this work no evidence of this regional-scale folding event affecting the whole Moglio-Testico Unit were observed. Thus, it can be assumed that both the present-day geometry of the $D1_{MT}$ and $D2_{MT}$ folding events and vergence of this folding event not correspond to that now detected. Its current

attitudes (*i.e.,* geometry and vergence) are, therefore, the results of the subsequent deformation events, including thrusting (syn-coupling events), folding and, lately, faulting (post-coupling events). Geochronological ages about the pre-coupling deformation phases recorded by the Moglio-Testico Unit are poorly constrained. However, taking in mind the paleontological time ranges proposed by Galbiati (1985), the Paleocene is assumed to be a minimum age for the development of the pre-coupling folding systems confined to the Moglio-Testico Unit (Figure 34a).

The Helminthoid Flysch Unit is characterized by a different tectonic history. The recrystallizations along the related foliations $S1_{FH}$, and $S2_{FH}$ (see chapters *The deformation strain patterns of the studied units* and *Metamorphism*) suggest that the entire structural evolution of this unit developed at the shallow structural levels. The oldest deformation event ($D1_{FH}$) is testified by $S1_{FH}$ foliation, mostly preserved as relict in hinge zone of $D2_{FH}$-related microlithons. It is also present in the slices at the bottom of the Helminthoid Flysch where it is associated with $F1_{FH}$ folds (Figure 13c). The $D2_{FH}$ phase is the most prominent deformation event recorded by the Helminthoid Flysch Unit. It is testified by $S2_{FH}$ foliation associated with SW-verging F2 fold system (Plates 2, 3, 4, 5 and Figures 13f, 34a). These folding events indicate a northwestward and, subsequently, a southwestward tectonic transport, respectively. A similar deformation strain pattern was reconstructed by Merle and Brun, (1984) in the Embrunais-Ubaye sector (Figure 2a). Unfortunately, geochronological ages about the pre-coupling deformation history of the Helminthoid Flysch Unit are poorly constrained. However, the structural evolution described in this work, for the Helminthoid Flysch Unit, pre-dates the coupling with the Cabanaira and the Marguareis units (Plates 2, 3, 4, 5, Figures 34a) as suggested by the cross-cutting relationships between the unit-bounding shear zones and the $D1_{FH}$, and $D2_{FH}$ fold systems (Figure 34a).

- The role of the syn-coupling structures: Kinematics and timing

The deformation developed during the syn-coupling tectonics are mainly represented by the unit-bounding shear zones, all characterized by southwestward sense of shear. These shear zones are interpreted as thrusts responsible for the coupling of the units recognized in the study area. During this event, the present-day geometry of the unit stack was achieved immediately before the development of the post-coupling deformations. This stack includes the Cabanaira Unit that is thrust by the Cima del Becco/Chambeuil slices and the Helminthoid Flysch Unit, that in turn is thrust by the Moglio-Testico Unit and by the topmost Marguareis Unit (Plate 1). According to the correlation between the Cima del Becco and

the Chambeuil slices with the Marguareis Unit, both derived from Briançonnais Domain (see stratigraphic logs of Figure 31), it is possible to propose a chronology for the development of the unit-bounding thrusts. This chronology includes first the development of the shear zone corresponding to thrusting of the Helminthoid Flysch Unit over the units derived from the Europe continental margin, *i.e.*, the Cabanaira Unit, the Cima del Becco-Cambeuil slices and the Marguareis Unit and the oceanic-derived Moglio-Testico Unit (Figure 34b); and then the development of a later shear zone corresponding to an out-of-sequence thrust system today recognized between the Marguareis Unit and the Helminthoid Flysch Unit, in the southwestern sectors of the Margaureis Massif. The same thrust system, to southeast, separates the topmost Marguareis Unit from the Moglio-Testico Unit and the underlying Helminthoid Flysch (Figure 34b). In this reconstruction, the out-of-sequence thrust is thought to be responsible for the $F3_{MU}$ knee-shaped mega-fold development recognized in the Marguareis Unit (Figures 16, 21), whose tectonic foliation is rarely observed and generally not associated with metamorphic re-crystallization. This suggests that this folding event took place at very shallow structural levels. Taking in account the youngest ages proposed for the pre-coupling deformation history affecting the tectonic units exposed in the investigated area (middle Eocene, Figure 34a), the syn-coupling tectonics is thought developed in the late Eocene-early Oligocene age (Figure 34b) according with the timespan proposed by Maino *et al*. (2015) for the thrusting of the Helminthoid Flysch Unit onto the Europe-derived continental units in the Monte Saccarello area (South of the investigated area). This age range thus supports that the pre-coupling structures recorded by each unit developed before the Oligocene time (Figure 34a-b; a paper about this topic was published on the international Journal *Comptes Rendus of Geoscience*, see Sanità *et al*., 2022a).

In the Embrunais-Ubaye transect (central sector of the Western Alps), Merle (1982) and Merle and Brun (1984) described similar geometrical relationships between the Helminthoid Flysch (cf. *nappe du Flysch à Helminthoïdes*, Kerckhove, 1969) and the Briançonnais Units. In addition, also the order of stacking of the different tectonic units is similar to what we documented in the Marguareis Massif. In fact, in the Embrunais-Ubaye area the Helminthoid Flysch unit of this area are first thrust onto the already exhumed Briançonnais Units and, then, thrust by the latter by an out-of-sequence thrust. In the geological section provided by Merle (1982) and Merle and Brun (1984), the Helminthoid-type Flysch unit occurs at the base and at the top of the Briançonnais Units. This picture is coherent with an uppermost position of Helminthoid Flysch Unit in the tectonic pile, as recognized in the external sector of the

Western Alps (cf. Escher *et al.*, 1997; Merle and Brun, 1984). Also in this sector, the uppermost position of the Helminthoid Flysch Unit is only later modified by an out-of-sequence thrust. So, in this emblematic key target for studying the lithology and the structure of the Helminthoid Units (see Kerckhove, 1963, 1969, and quoted references), a tectonic evolution entirely consistent with the one proposed in this Thesis was reconstructed (cf. Figures 8 and 7 of Merle and Brun, 1984 with Figure 34 of this work).

- Post-coupling history of the tectonic stack

The whole stack is affected by the same deformation history testified by the overprinting of the post-stacking fold system and subsequent brittle faults on the pre- and syn-coupling structures (Plates 2, 3, 4, 5, 6, 7 and Figure 34c). The post-coupling fold system, which is characterized by horizontal fold axes and flat-lying to southwestward-dipping axial planes associated with a tectonic foliation without evidence of metamorphic re-crystallization, is mostly observed in zones where vertical or sub-vertical layering is present; therefore, it can be interpreted as having originated from vertical shortening and folding of pre-existing inclined layers. These observations indicate that this folding event occurred at very shallow level represents the last stage of the exhumation for the studied stack of tectonic units. This type of deformation is typical of extensional tectonics, as recognized in some areas of the Alpine belt (Froitzheim, 1992; Ratschbacher *et al.*, 1989; Wheeler and Butler, 1994).

The last tectonic event is represented by a high-angle normal to transcurrent fault system that cut at high angle all the previous structures and only locally juxtapose different tectonic units. Referring to theoretical models of transtensional tectonics (Dooley and Schreurs, 2012; Naylor *et al.*, 1986), the geometrical pattern of the faults belonging to three systems depicts a map-scale Riedel system coherent with a roughly E-W-direct dextral shear deformation. In contrast with recent interpretations (Bertok *et al.*, 2018; d'Atri *et al.*, 2016), these brittle deformations are not able to deeply modify the pre-existing structural setting of the study area, as detectable in the structural maps and the related geological cross-sections, shown in this work (Plates 2, 3, 4, 5, 6, 7), thus played not significant role during the structural evolution of the tectonic units exposed in the investigated area. The age of the post-coupling history is scarcely constrained. Taking into account, the geochronological data provided by Michard *et al.* (2004), Strzerzynski *et al.* (2011) and Maino et al. (2015) combined with the field constraints largely described in this Thesis, a post early Oligocene age for the post-coupling structures can be proposed (Figure 34c).

8.3 Metamorphic imprint of the tectonic units

Each tectonic unit exposed in the investigated area recorded their deformation history under different *P–T* conditions.

- Insights from Ill_{IC} and the b_0 parameter

The Ill_{IC} and the b_0 cell parameter distributions measured on the Cabanaira Unit and the Helminthoid Flysch Unit, indicate different *P* and *T* recorded during their deformation history (Figure 35). It must be underlined that these methods do not provide constraints about the metamorphic peak conditions reached by the units (especially the b_0), but they are rather sensitives to temperature and pressure variations. These tectonic units are both characterized by, at least, one tectonic foliation ($S1_{CU}$ and $S1_{FH}$) showing evidence of metamorphic re-crystallization (*i.e.*, Illite).

As consequence, the metamorphic conditions recorded by the structural transformation of Illite grains constrained the development of the $S1_{CU}$ and $S1_{FH}$ portraying thus the metamorphic peak conditions of the Cabanaira Unit and the Helminthoid Flysch Unit, respectively. A comparison between the *P* and *T* conditions recorded by these two units is shown in Figure 35.

The Ill_{IC} distribution calculated on the Cabanaira Unit indicate low-grade metamorphic condition (epizone) with temperature higher than 300 °C according to Kisch (1987), or ranging between 300-360 °C according to Niedermayr *et al.* (1984) and Weaver and Boekstra (1984) and medium to higher metamorphic pressure conditions as suggested by the b_0 distribution values (Franceschelli *et al.*, 1989). Contrary, for the Helminthoid Flysch Unit the Ill_{IC} measurement

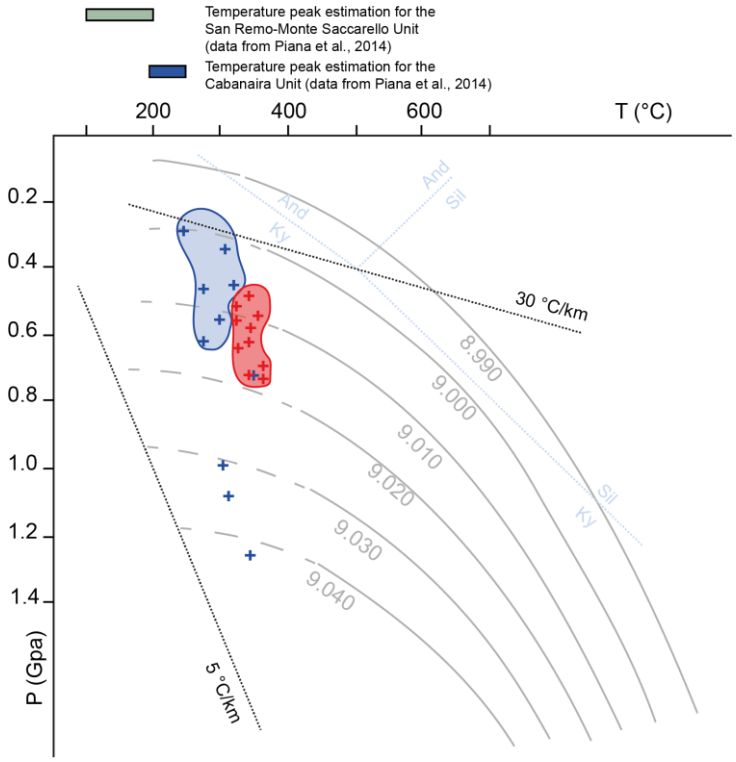

Figure 35. P–T diagram showing the variation of b_0 parameter of Illite grains with T and P (modified from Guidotti and Sassi, 1986) for the Helminthoid Flysch Unit (blue cross) and the Cabanaira Unit (red cross). The different T range for each sample is based on the Illite crystallinity Index accordingly with Kisch (1987); Niedermayr et al. (1984); Weaver and Boekstra (1984). Along the X axis the metamorphic peak conditions (T-peak) obtained from Piana et al. (2014) are reported.

suggest low- to very low metamorphic conditions with *T* values lower than 300 °C (according with Kisch, 1987; Niedermayr *et al*., 1984; Weaver and Boekstra, 1984), and medium to lower metamorphic pressure conditions (Figure 35, based on the barometric limits of Franceschelli *et al*., 1989). It must be underlined that only three samples (outliers, Figure 35) fall outside of the main cluster (blue cloud of Figure 35) and they are characterized by the highest b0 values suggesting High pressure condition for the Helminthoid Flysch Unit. Contrary to the main cluster (blue cloud of Figure 35), these data seem to be strongly in contrast with the described mineral assemblage along the $S1_{FH}$ foliation and the deformation history (see chapter *The deformation strain pattern of the studied units*) recorded by the Helminthoid Flysch Unit. Taking that in mind, the three outliers can be considered as unreliable.

The estimated *P* and *T* conditions are coherent with the microstructural and microtextural observation (see chapter *The deformation strain pattern of the studied units*) performed on the Cabanaira Unit and Helminthoid Flysch Unit. However, the *P* and *T* conditions estimated in this Thesis for the Helminthoid Flysch and the Cabanaira Unit are in contrast with those proposed by Piana *et al*. (2014). These authors through the Illite crystallinity index distribution measurement performed on the San Remo-Monte Saccarello Unit and the Roja Unit (cf., Helminthoid Flysch Unit and the Cabanaira Unit of this work, respectively) estimated metamorphic temperature conditions related to diagenesis and anchizone fields, respectively, thus never exceeding 250 °C. Taking in mind that the same methodologies (see Piana *et al*., 2014 for more details) were used, the differences between their data and the results obtained in this work could be due to the location of the sampling. In this work the sampling was performed along a transect on which structural features, like the unit-bounding thrust systems (see Plate 1), occur. The lower crystallinity values (=higher metamorphic temperature conditions, this work) could be related to the thrust activity largely described in the whole investigated area. On the contrary, the higher crystallinity values (=lower metamorphic conditions) estimated by Piana *et al*. (2014) were obtained on samples collected in areas where tectonic structures like thrusts or fault systems are lacking at all. So, having seen the impact of this, the metamorphic temperature conditions calculated in this work by means the Illite crystallinity index measurement could be overestimated due to the effect of the thrust activity as already largely demonstrated by several authors (*i.e.,* Fernandez-Caliani and Galan., 1992; Ducci *et al*., 1995; Giorgetti *et al*., 2000; Brogi, 2006). In this frame the illite crystallinity index distribution calculated in the investigated transect could be thus the witnesses of the syn-coupling tectonics events largely documented in the mapped area.

However, this topic needed more dataset obtained with a quantitative method in order to better constraint the metamorphic history of these units (this topic is a work in progress job).

- *P–T* path of the Moglio-Testico Unit

Contrary to the previous authors (Bonazzi *et al.*, 1987; Cabella *et al.*, 1988), which considered the Moglio-Testico Unit as characterized by a very low-grade metamorphic imprint based on the distribution of the illite crystallinity, thermobarmometric estimates obtained in this work performed on Chl-Phg couples grown during the $D1_{MT}$ and $D2_{MT}$ events portrayed a *P–T* path typical of the oceanic subduction setting (Goffé *et al.*, 2004; Lardeaux, 2014; Agard *et al.*, 2001; Handy *et al.*, 2010 - see Figure 36), with a geothermal gradient of 8 °C/km similar to that reconstructed for the Schistes Lustrés complex by other authors (5-10 °C/km *i.e.*, Agard *et al.*, 2001; Agard *et al.*, 2018; Agard, 2021; Hervioue *et al.*, 2022 and quoted references). The thermobarometric estimation indicates that prograde path is no recorded and that the chlorite and phengite grains growth along the $S1_{MT}$ and $S2_{MT}$ foliations portrayed the retrograde one. The metamorphic peak conditions of 1.2-1.0 GPa and 330-260 °C were recorded by the chlorite-phengite pairs grown during the $D1_{MT}$ phase (Figure 36), testifying thus the underthrusting, accretion and exhumation of the Moglio-Testico Unit into the Alpine wedge. The $D2_{MT}$ phase is instead characterized by chlorite-phengite couples re-equilibrated at 0.7-0.4 GPa and 230-170 °C (Figure 36) without heating events. Therefore, thermobarometric estimates performed on chlorite-phengite pairs grown during the $D2_{MT}$ phase constrain the retrograde path of the Moglio-Testico Unit, indicating that the exhumation toward shallower crustal

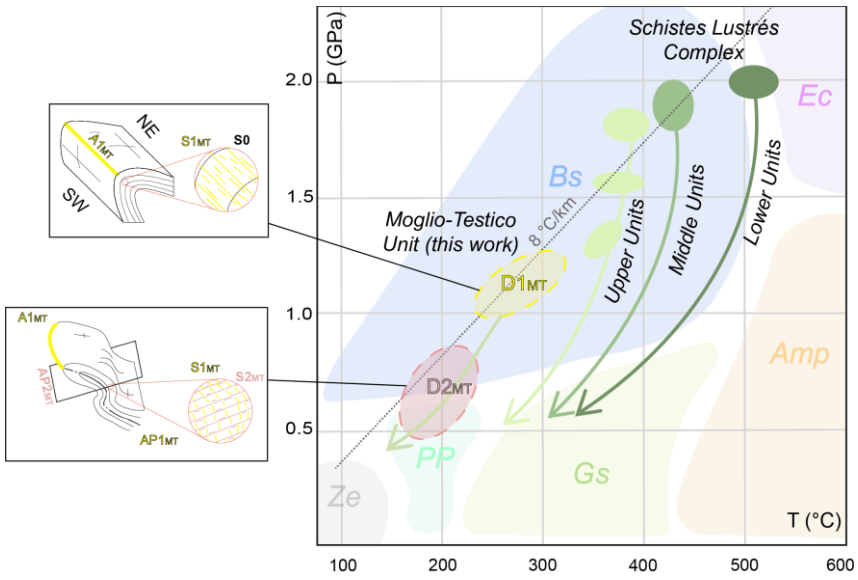

Figure 36. P–T path of the Moglio-Testico Unit (yellow and red ellipses). The elliptic areas indicated the point clouds reported in the P/T diagram of Figure 34. On the left a simplified sketch of the pre-coupling folding events developed during the $D1_{MT}$ and $D2_{MT}$ phases are reported. The P–T paths of the oceanic-derived units (i.e., Schistes Lustrés Complex – data from Agard et al., 2001; Agard et al., 2018; Agard, 2021; Hervioue et al., 2022) are also reported.

levels into the Alpine wedge continue during this deformation phase. The different *P* values recorded by the $D1_{MT}$ and $D2_{MT}$ Phg grains are of paramount importance because they are the witnesses of vertical movement of this unit into the Alpine accretionary wedge, *i.e.,* from the deeper up to shallower structural levels as already documented for others oceanic units cropping out in in the Western Alps (*i.e.,* Schistes Lustrés complex, Figure 36). In this scenario, the distribution of the illite crystallinity performed by Bonazzi *et al.* (1987), indicating *T* peak metamorphic conditions corresponding to the anchizone (200-250 °C) for the Moglio-Testico Unit, could seem apparently in contrast with those obtained in this work. However, the illite crystallinity distribution was measured on small grain of phyllosilicates (<2 µm, see Bonazzi *et al.*, 1987 for technical details), which were observed mostly to grow along the $S2_{MT}$ foliation (See chapter *The deformation strain patterns of the studied units*). In fact, the *T* values estimated by Bonazzi *et al.* (1987) are coherent with those proposed in this work for the $D2_{MT}$ deformation event (probably recorded by white micas grains during the final stage of the $D2_{MT}$ phase) and, therefore, they do not represent the *T* peak recorded by the Moglio-Testico Unit during its metamorphic history (these results were published on international Journal *Minerals*, see Sanità *et al.* 2022c).

The exhumation strain pattern continues up to very shallower structural levels with the subsequent deformation events, including the thrusting (syn-coupling tectonics) and post-coupling structures. This kind of HP-LT path was already described also for analogue oceanic units, made up of cover rocks, exposed in other sectors of the Western Alps (*i.e.,* Ellero and Loprieno, 2017; Schwartz *et al.*, 2007; Agard *et al.*, 2001; 2018; Agard and Handy, 2021).

- *P–T* path of the Marguareis Unit

The thermobarometric estimation was performed on the $D1_{MU}$ and $D2_{MU}$ phases, during which metamorphic re-crystallization of chlorite and phengite grains occurred. The thermobarometric quantification performed in this study show that the prograde path is not recorded, and the chlorite–phengite pairs grown along the $S1_{MU}$ and $S2_{MU}$ foliations depict the retrograde path of the Marguareis Unit (Figure 37). The exhumation already started during the $D1_{MU}$ phase and it continues during the $D2_{MU}$ phase up to shallower crustal levels into the Alpine wedge. P-peak conditions of 1.00–0.90 GPa and 280–330 °C were registered by phengite–chlorite couples related to $D1_{MU}$ phase (Figure 37). The retrograde path of the Marguareis Unit is constrained by the re-crystallization of chlorite and phengite during the $D2_{MU}$ phase at 0.85–0.7 GPa and 230–300 °C (Figure 37). No

significative heating events during the $D2_{MU}$ exhumation phases were identified from the thermobarometry for the Margureis Unit. The metamorphic conditions estimated by Piana *et al*. (2014), which suggest *T* peak conditions typical of the lower anchizone region (≈ 250-200 °C), seem apparently in contrast with the data described in this Thesis and, therefore, they need of further clarifications. The illite crystallinity index calculated by these authors was measured on the fine-grained white micas (<2 μm, see Piana *et al*., 2014 for details), which were clearly observed to grow along the $S2_{MU}$ foliation (see chapter *Metamorphism*). This suggest that the *T* values estimated by Piana *et al*. (2014) do not reflect the *T* peak conditions recorded by the Margureis Unit. On the contrary, they are coherent with the temperature conditions estimated for the $D2_{MU}$ phase in this work (Figure 37).

The different *P* values constrained on $D1_{MU}$ and $D2_{MU}$ phengites are considered as the witnesses of the vertical movement of the Margureis Unit inside the Alpine wedge. Thus, the reconstructed pathway strongly indicate that the metamorphic imprint of the Margureis Unit was recorded in a continental subduction setting, the latter already documented in other similar sectors of the Alpine belt (*i.e.,* Michard *et al*., 2004; Lanari et al., 2012; Sterzynsky et al., 2011; Di Rosa *et al.,* 2019). These results allow to re-interpret the Margureis Unit, till now regarded as a very low-grade unit (Messiga *et al*., 1981; Piana *et al*., 2014), as a HP-LT unit. In the South-Western Alps, HP-LT continent-derived units were documented by others authors (Goffé *et al*., 2004; Lardeaux, 2014), and similar HP–LT paths were reconstructed for the Briançonnais Units in more internal sector of the belt (Sterzynsky *et al*., 2011; Lanari *et al*., 2014). Michard et al. (2004) reconstructed the *P–T* path for the Briançonnais Units outcropping in the Embrunais–Ubaye area. The authors

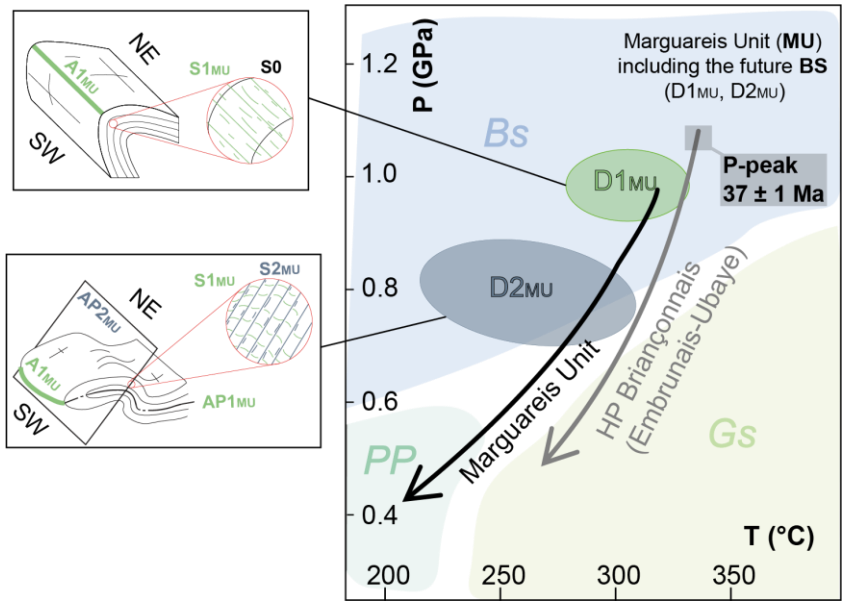

Figure 37. P–T path of the Margureis Unit (green and grey ellipses). The elliptic areas indicated the point clouds reported in the P/T diagram of Figure 36. On the left a simplified sketch of the pre-coupling folding events developed during the $D1_{MU}$ and $D2_{MU}$ phases are reported. The P–T paths of the Briançonnais units exposed along the Embrunais-Ubaye sector is also reported as the dating of the metamorphic peak conditions (data from Michard et al., 2004).

proposed that the Briançonnais Units recorded their metamorphic peak during the D1 phase (HP Briançonnais path in Figure 37) immediately followed by the onset of the exhumation which begins at the end of D1 phase. The *P–T* path proposed for the HP Briançonnais Units by Michard *et al.* (2004) shows clear similarities with those proposed for the Marguareis Unit (Figure 37) in this work (these results were published on the international Journal *TerraNova*, see Sanità *et al.*, 2022b). The exhumation of the Marguareis Unit continues and it clearly developed at shallower structural levels as suggested by the lack of metamorphic re-crystallization during the syn- and post-coupling events (see chapter *The deformation strain patterns of the studied units*).

8.4 Toward a new model for the tectonic evolution of the southwestern Alps

Accordingly to the geodynamic evolution proposed for the Western Alps (i.e, Rosenbaum and Lister, 2002; Oberhansli *et al.*, 2004; Rosembaum *et al.*, 2005; Lardeaux *et al.*, 2006; Handy *et al.*, 2010; Beltrando *et al.*, 2010; Lardeaux, 2014; Schmid *et al.*, 2017), also the geological survey carried out on the junction area between Maritime and Ligurian Alps firstly confirms that the relationships between the major Alpine tectonics units of interest can only be interpreted in the framework of a polyphase tectonic evolution (as already proposed by Vanossi *et al.*, 1984; Seno *et al.*, 2003; Seno *et al.*, 2005; Lardeaux *et al.*, 2006; Bonini *et al.*, 2010) and not as a result of a single transpressive brittle tectonic event as proposed by Piana *et al.* (2021) and quoted references. Secondly, it demonstrates that the very low-grade Helminthoid Flysch Unit (Ligurian Domain) is tectonically located in between tectonic units stemming from continental (Europe continental margin, here represented by the Briançonnais Units) and oceanic (Moglio-Testico Unit) paleogeographic domains, which show higher metamorphic conditions (HP-LT) recorded during their underthrusting, accretion and subsequent exhumation into the Alpine accretionary and orogenic wedge, during different timespan and under *P* and *T* conditions reflecting several depths. The geological cross-sections reported on the plates 3, 5 and 7, showing the whole architecture of the investigated area, clearly highlight amazing structural analogies. In all of them the Marguareis Unit forms the topmost portion of the tectonic pile and it is thrusted, with an out-of-sequence thrust, onto the Helminthoid Flysch Unit and its basal complex, to northwest, and onto the Moglio-Testico Unit, to southeast (Plate 7). The Helminthoid Flysch Unit is thrust onto the Briançonnais units both represented by tectonic slices (*i.e.,* Cima del Becco and Chambeuil Slices) and units (*i.e.,* the Cabanaira Unit). Each unit recorded

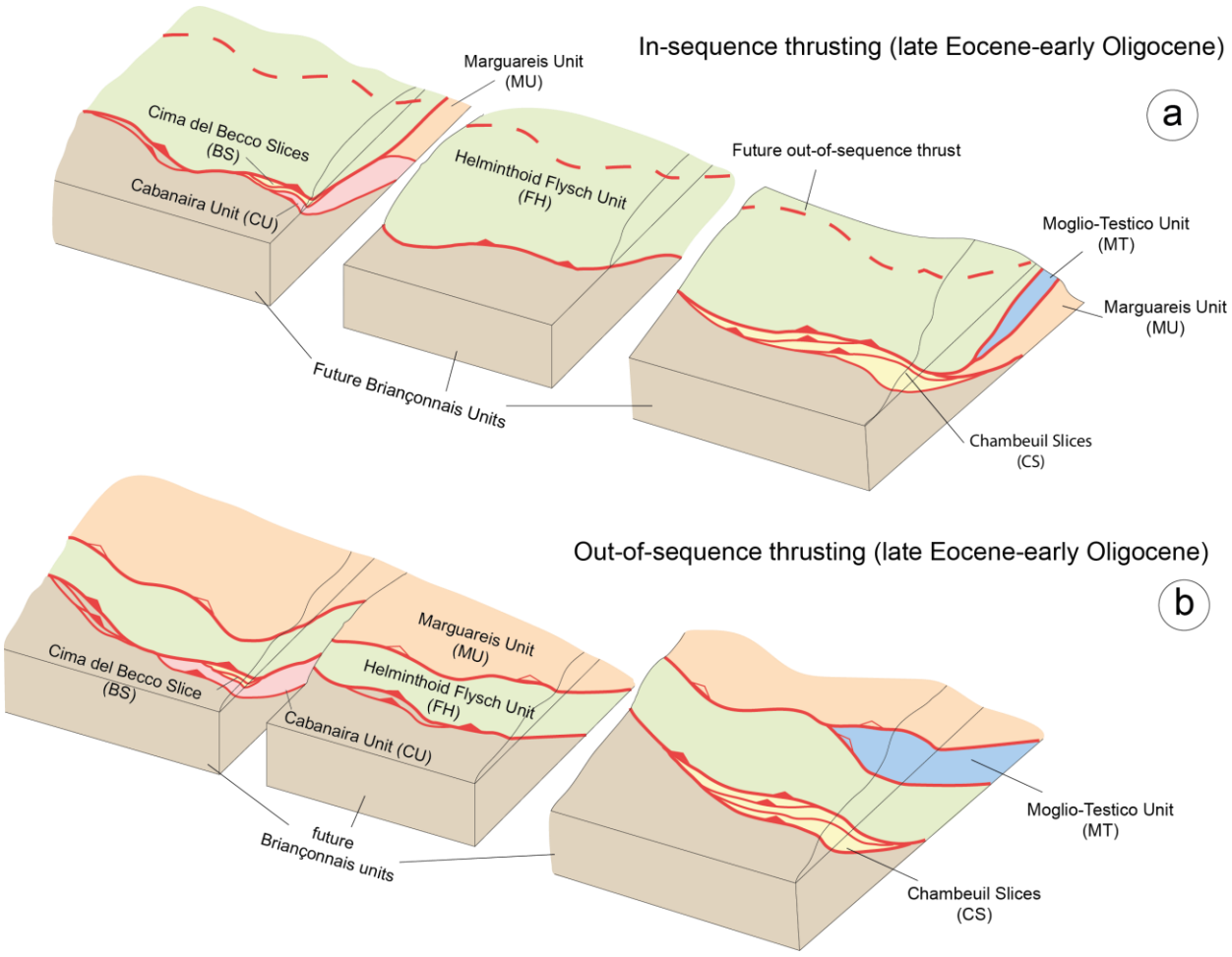

Figure 38. a, b) Simplified 3D sketch showing the structural architecture developed during the syn-coupling tectonics.

different pre-coupling deformation histories dealing with the superposition of different generations of fold systems developed at different structural levels ranging from 4-5 up to 30-35 km. The related axial planes are cut by the unit-bounding thrust systems, thus indicating a clear relative chronology. The thrust systems (in-sequence and out-of-sequence thrusts, Figure 38a-b) show a *top-to-SW* sense of shear, and are responsible for the coupling of the units (Figure 38a-b). So, the thrusting events are thought to have occurred during the syn-coupling tectonics. As recognizable in the geological cross-sections, the out-of-sequence thrusting and the associated knee-shaped folding affecting the Marguareis Unit can be observed from the Upega village to Col di Perla area (Plates 2, 3, 4 and 6), thus on more than 80 km. In contrast with the previous authors (Di Giulio, 1988, Merizzi and Seno, 1991, Mueller *et al.*, 2020, Piana *et al.*, 2021), I hold that the reconstructed thrust surfaces and the associated knee-shaped folding must be considered as first-order structural features in this area and, consequently, that the syn-coupling tectonics played a significant role in the finite structural architecture of the units exposed at the junction area between Maritime and Ligurian Alps (Plate 1, Figures 38a-b). This hypothesis is

corroborated by the fact that the inverted structural relationships between the Helminthoid Flysch, Briançonnais Units and the Moglio-Testico Unit (Plate 1, Figures 38a-b) can be appreciated at the regional scale and not just locally. The dataset described in this Thesis strongly indicate that during late Eocene-early Oligocene, *i.e.,* after the consumption of the Ligure Piemontese ocean and the subsequently involvement of the Europe continental crust into the subduction zone (Plate 8a-b), the Helminthoid Flysch Unit (this work) and the External Ligurian Units formed the uppermost and leading edge of the Alpine orogenic wedge (Plate 8c); which is composed by oceanic (*i.e.,* Moglio-Testico Unit) and continental (*i.e.,* Briançonnais Units) already exhumed from different depths (as already proposed by Elter, 1997; Molli, 2008). The ongoing SW-NE-direct convergence led to the progressive SW-ward motion of the whole stack, which is formed by the Europe-derived units (Briançonnais Units, here the Margaureis Unit, including the tectonic slices, and the Cabanaira Unit), the oceanic-derived unit, here the Moglio-testico Unit) and the Helminthoid Flysch Unit, onto the ancient Europe continental margin (Plate 8c); this, currently represented by the Dauphinois/Helvetic Units, is partially or poorly involved in the Alpine collision. This first-order tectonic boundary is known as Penninic Front (*i.e.,* Vanossi *et al.*, 1984; Vanossi *et al.*, 1986; Seno *et al.*, 2003: Seno *et al.*, 2005; Lardeaux *et al.*, 2006) whose activity in this sector is constrained at late Eocene-early Oligocene age (Maino *et al.*, 2015; and toward southern sectors by Perotti *et al.*, 2012). According with the classic tectonic frame proposed by the previous authors (*i.e.,* Vanossi *et al.*, 1984; Vanossi *et al.*, 1986; Seno *et al.*, 2003; Seno *et al.*, 2005) for the Southwestern Alps, the Penninic Front is "physically located" at the bottom of the Helminthoid Flysch Unit (Figures 2b, 3a-b), which correspond to the in-sequence thrust system in this work (Figure 38a). This "physical location" seems to be in contrast with the results obtained in this Thesis, and it needed to be revisited owing the occurrence of continent-derived units and/or slices tectonically underlying to the Helminthoid Flysch and profoundly involved into the alpine orogenic wedge and showing clear evidence of continental subduction-related strain patterns (see chapter *The deformation strain pattern of the studied units*).

The out-of-sequence thrusting events needed also of further clarifications. This event is responsible for the current "inverted" stacking of the units in this sector of the southwestern Alps, *i.e.,* the Briançonnais Units onto the Moglio-Testico Unit onto the Helminthoid Flysch. Its development can be thought as the result of Penninic front activity. This assumption calls for a tectonic scenario in which the Penninic Front is a complex thrust zone (as already proposed for other sectors of the Penninic Front, *i.e.,* Ceriani *et al.*, 2001;

Trulluque *et al*., 2003; Schmid *et al*., 2004) active in several times and spaces, and where oceanic- and continent-derived tectonic units showing different tectono-metamorphic history were progressively piled-up without an apparent logic. However, the hypothesis of a "multistage" activity of the Penninic Front needed more investigations to be supported.

Finally, the results obtained in this work outline how fundamental is the multidisciplinary approach to unveil the tectonic evolution of very low- and low-grade units cropping out in the collisional orogens. The combination between classic field mapping, stratigraphic analysis, semi-quantitative and quantitative *P*–*T* estimates can provide useful constraints about the tectonic evolution recorded by units, deformed and metamorphosed at shallow crustal levels (*i.e*., 4-5 to 30-35 km), during the convergence between plates. In particular, this combination allows to distinguish the deeper (here represented by the pre-coupling history of each unit during which metamorphic peak conditions were achieved) and shallower processes (here represented by syn- and post coupling deformation history) recorded by each unit, as well as their interaction, into a convergence setting. Such as discrimination made possible to perform thus a detailed reconstruction of the long-lived geodynamic history of units deformed and metamorphosed at different crustal levels.

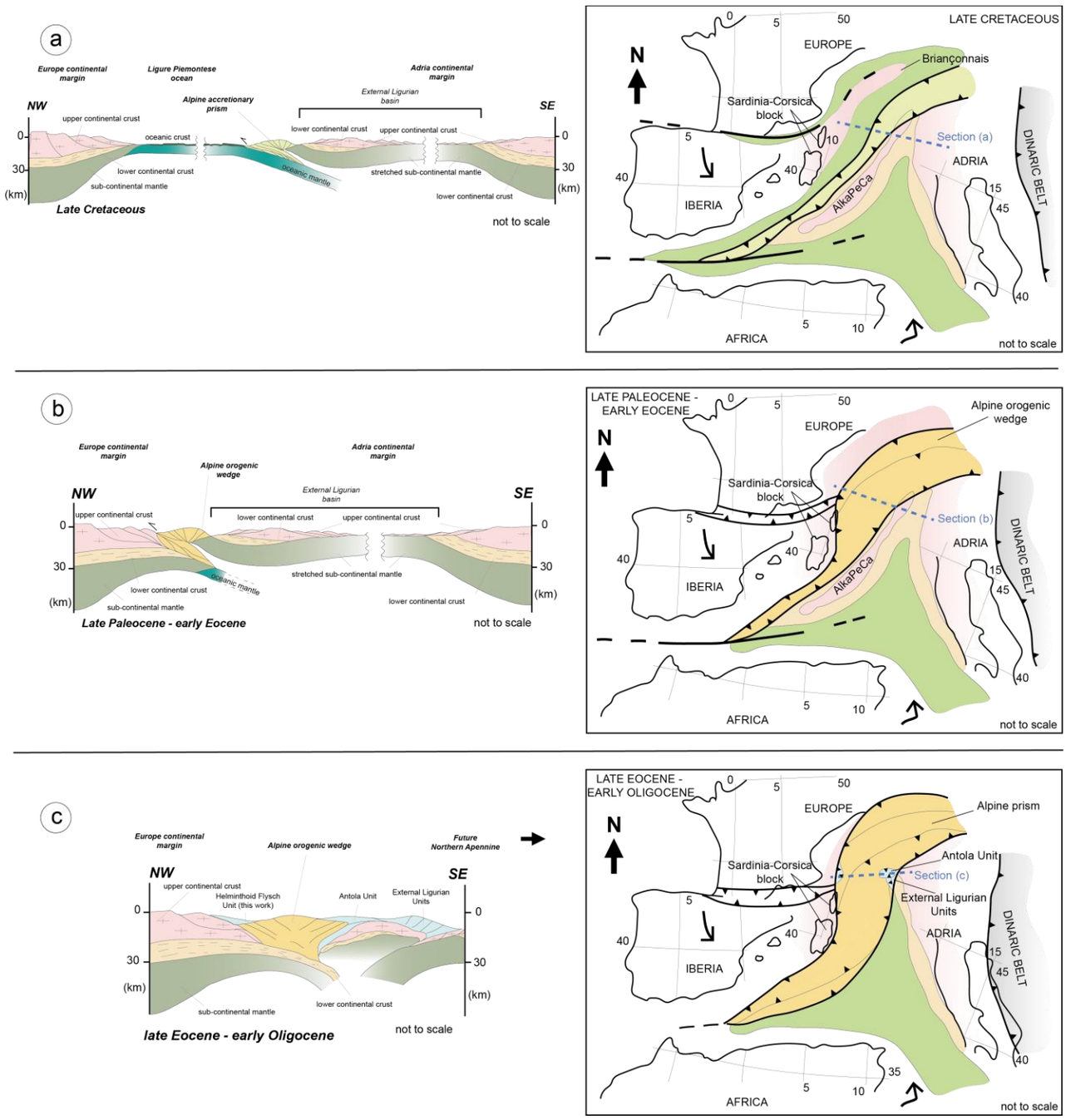

Plate 8. Evolutionary model of the Alps-Apennines orogenic system (modified by Marroni et al., 2017) comprising: a) The Alpine subduction (Late Cretaceous) with consumption of the Ligure Piemontese ocean; b) the Late Paleocene-early Eocene inception of the of continental subduction with the involvement of the Europe continental margin; c) the late Eocene-early Oligocene continental collision toward West, and the flip of subduction and onset of the Appenines history to East. The map view paleogeography for each time span with the location of the related geological cross-section and the displacements (black arrows) of Africa, Iberia Adria versus Europe and position of Corsica Sardinia Block versus Iberia, based on the study of Michard et al. (2002) is also reported. The Dinaric Belt (grey area) is also reported. Similarly to the related geological cross-sections, dark green areas are represent the Ligure Piemontese ocean, pink and light yellow areas represent the upper and lower continental crust, respectively, light green and dark yellow areas represent the Alpine accretionary and orogenic wedge respectively. The External Ligurian Units and the Helminthoid Flysch Unit (this work) are also reported (light blue areas).

References

Agard, P., Monié, P., Jolivet, L., Goffé, B. 2002. In situ laser probe 40Ar/39Ar dating of the Schistes Lustrés complex: implications for the exhumation of the Western Alps. J. Metamorph. Geol. 20, 599-618.

Agard, P., Jolivet, L., Goffé, B. 2001. Tectonometamorphic evolution of the Schistes Lustrés Complex: implications for the exhumation of HP and UHP rocks in the western Alps. Bull. Soc. Geol. Fr. 172, 617-636.

Agard, P., Yamato, P., Jolivet, L., Burov, E. 2009. Exhumation of ocean blueschists and eclogites in subduction zones: timing and mechanisms. Earth-Science Reviews. 92, 53-79

Agard, P., Plunder, A., Angiboust, S., Bonnet, G., Ruh, J. 2018. The subduction plate interface: Rock record and mechanical coupling (from long to short time scales). Lithos. 320-321, 537-566.

Agard, P., Handy, M. 2021. Ocean subduction dynamics in the Alps. Elements. 17, 9-16.

Agard, P. 2021. Subduction of oceanic lithosphere in the Alps: Selective and archetypal from (slow-spreading) oceans. Earth-Sciences Reviews. 214.

Alvarez, W., Cocozza, T., Wezel, F. C. 1974. Fragmentation of the Alpine orogenic belt by microplate dispersal. Nature, 248(5446), 309-314.

Angrand, P., Mouthereau, F. 2021. Evolution of the Alpine orogenic belts in the Western Mediterranean region as resolved by the kinematics of the Europe-Africa diffuse plate boundary. BSGF-Earth Sciences Bulletin, 192, 42.

Balestro, G., Festa, A., Dilek, Y., Tartarotti, P. 2015. Pre-Alpine extensional tectonics of a peridotitelocalized oceanic core complex in the late Jurassic, high-pressure Monviso ophiolite (Western Alps). Episodes Journal of International Geoscience, 38, 266-282.

Balestro, G., Festa, A., Borghi, A., Castelli, D., Gattiglio, M., Tartarotti, P. 2017. Role of Late Jurassic intra-oceanic structural inheritance in the Alpine tectonic evolution of the Monviso meta-ophiolite Complex (Western Alps). Geol. Mag. 155, 233-249.

Barbero, E., Festa, A., Saccani, E., Catanzariti, R., & D'Onofrio, R. 2020. Redefinition of the Ligurian Units at the Alps–Apennines junction (NW Italy) and their role in the evolution of the Ligurian accretionary wedge: constraints from mélanges and broken formations. Journal of the Geological Society, 177, 562-574.

Barfety, J. C., Lemoine, M, Mercier, D, Polino, R., Nievergelt, P., Bertrand, J., Dumont, T., Amaudric du Chaffaut, S., Pecher, A., Monjuvent, G. 1996. Carte Geologique de France (1/50.000), Feuille Briançon (823). Bur. de Rech. Geol. et Min., 180 p.

Bearth, P. 1967.Die Ophiolithe der Zone von Zermatt–Saas-Fee, Stämpfli and Cie, Bern.

Beltrando, M., Lister, G.S., Hermann, J., Forster, M., Compagnoni, R., 2008. Deformation mode switches in the Penninic Units of the Western Alps. J. Struct. Geol., 30, 194-219.

Beltrando, M., Compagnoni, R., Lombardo, B., 2010b. (Ultra-)high-pressure metamorphism and orogenesis: an Alpine perspective. Gondwana Research 18, 147-166.

Bertok, C., Musso, A., d'Atri, A., Martire, L., Piana, F. 2018. Geology of the Colle di Tenda–Monte Marguareis area (Ligurian Alps, NW Italy). Journal of Maps, 14, 542-551.

Bertotti, G., Picotti, V., Bernoulli, D., Castellarin, A. 1993. From rifting to drifting: Tectonic evolution of the South-Alpine upper crust from the Triassic to the Early Cretaceous. Sedimentary Geology, 86, 53-76.

Bertrand, J.-M., Paquette, J.L., Guillot, F., 2005. Permian zircon U–Pb ages in the Gran Paradiso massif: revisiting post-Variscan events in the Western Alps. Schweiz. Mineral. Petrogr. Mitt., 85, 15–29.

Bersezio, R., Barbieri, P., & Mozzi, R., 2002. Redeposited limestones in the Upper Cretaceous succession of the Helvetic Argentera Massif at the Italy–France border. Eclogae Geologicae Helvetiae, 95, 15–30.

Bertok, C., Martire, L., Perotti, E., d'Atri, A., Piana, F. 2011. Middle-Late Jurassic syndepostional tectonicsrecorded in the Ligurian Brian.onnais succession (Marguareis-Mongioie area, Ligurian Alps, NW Italy). Swiss Journal of Geosciences, 104, 237-255.

Béthoux, N., Tric, E., Chery, J., & Beslier, M. O. 2008. Why is the Ligurian basin (Mediterranean sea) seismogenic? Thermomechanical modeling of a reactivated passive margin. Tectonics, 27.

Bigot-Cormier, F., Sosson, M., Poupeau, G., Stephan, J.F., Labrin, E. 2006. The denudation history of the Argentera Alpine External Crystalline Massif (Western Alps, France– Italy): an overview from the analysis of fission tracks in apatites and zircons. Geodinamica Acta 19, 455-473.

Bloch, J. P., 1958. Une coupe du Trias des Alpes ligures italiennes [A section of the Trias of the italian Ligurian Alps]. C. R. Sommaire des Seances de la Societ. geologique de France, 10, 204.

Boccaletti, M., Elter, P., Guazzone, G. 1971. Plate tectonic models for the development of the Western Alps and Northern Apennines. Nature Physical Science, 234, 108-111.

Bonazzi, A., Cobianchi, M., Galbiati, B. 1987. Primi dati sulla cristallinità dell'illite nelle unità tettoniche più esterne e strutturalmente più elevate delle Alpi Liguri. At. Tic.i Sc. Ter., 31, 63-77.

Boni, A., Cerro, A., Gianotti, R., Vanossi, M. 1971. Note illustrative della Carta Geologica d'Italia alla scala 1:100.000, foglio Albenga-Savona (92-93). Roma.

Bonini, L., Dallagiovanna, G., Seno, S. 2010. The role of pre-existing faults in the structural evolution of thrust systems: Insights from the Ligurian Alps (Italy). Tectonophysics, 480, 73–87.

Bourdelle, F., Cathelineau, M. 2015. Low-temperature chlorite geothermometry: A graphical representation based on a T-R2+-Si diagram. Eu. J. Min., 27, 617-626.

Bousquet, R., Engi, M., Gosso, G., Oberhänsli, R., Berger, A., Spalla, M. I., Goffé, B. 2004. Explanatory notes to the map: metamorphic structure of the Alps transition from the Western to the Central Alps.

Brizio, F. D., Deregibus, C., Eusebio, A., Gallo, M., Gosso, G., Rattalino, E., Oxilia, M., 1983. Guida all'escursione: i rapporti tra la zona Brianzonese Ligure e il Flysch a Elmintoidi, Massiccio del Marguareis. (Limone Piemonte-Certosa di Pesio, 468 Cuneo, 14/15 Settembre 1983) [Field trip guide: Relationships between the Ligurian Brian.onnais Zone and the Helminthoides Flysch, Marguareis Massif (Limone Piemonte-Certosa di Pesio, Cuneo, September 14/15th, 1983)]. Memorie della Societ. Geologica Italiana, 26, 579–595.

Brogi, A. 2006. Evolution, formation mechanism and kinematics of a contractional shallow shear zone within sedimentary rocks of the Northern Apennines (Italy). Eclogae Geologicae Helvetiae, 99, 29-47.

Bucher, S., Bousquet, R., 2007. Metamorphic evolution of the Briançonnais units along the ECORS-CROP profile (Western Alps): new data on metasedimentary rocks. Swiss Journal of Geosciences, 100, 227–242.

Burov, E., Francois, T., Yamato, P., Wolf, S. 2014. Mechanisms of continental subduction and exhumation of HP and UHP rocks. Gondw. Res. 25, 464-493.

Butler, R. W. H. 1986. Thrust tectonics, deep structure and crustal subduction in the Alps and Himalayas. Journal of the Geological Society, 143, 857-873.

Cabella, R., Cortesogno, L., Dallagiovanna, G., Vannucci, R., Vanossi, M. 1988. Vulcanismo, sedimentazione e tettonica nel Brianzonese ligure esterno durante il Permo-Carbonifero. At. Tic. Sc. Ter. 1988, 31, 269-326.

Campredon, R. 1972. Les formations paléogènes des Alpes maritimes franco-italiennes (Doctoral dissertation, Université Nice Sophia Antipolis).

Campredon, R. 1977. Les deformations de conglomerats pliocens de l'arc de Nice.

Capponi, G., Crispini, L. 2002. Structural and metamorphic signature of alpine tectonics in the Voltri Massif (Ligurian Alps, North-Western Italy). Eclogae Geologicae Helvetiae, 95, 31-42.

Capponi, G., Crispini, L., Federico, L., Piazza, M., Fabbri, B. 2009. Late Alpine tectonics in the Ligurian Alps: constraints from the Tertiary Piedmont Basin conglomerates. Geological Journal, 44, 211-224.

Cardello, G. L., Di Vincenzo, G., Giorgetti, G., Zwingmann, H., Mancktelow, N. 2019. Initiation and development of the Pennine Basal Thrust (Swiss Alps): a structural and geochronological study of an exhumed megathrust. Journal of Structural Geology, 126, 338-356.

Carminati, E. 2001. Incremental strain analysis using two generations of syntectonic coaxial fibres: An example from the Monte Marguareis Briançonnais cover nappe (Ligurian Alps, Italy). Journal of Structural Geology, 23, 1441–1456.

Caron, J.M., Delcey, R., Scius, H., Eissen, J.P., De Fraipont, P., Mawhin, B., Reuber, I. 1979. Répartition cartographique des principaux types de séries dans les Schistes lustrés de Corse. C. R. Acad. Sci. Paris 288, 1363-1366.

Cathelineau, M. 1988. Cation site occupancy in chlorites and illites as a function of temperature. Clay Min. 23, 471-485.

Ceriani, S., Fugenschuh, B., Schmid, S.M. 2001. Multi-stage thrusting at the "Penninic Front" in the Western Alps between Mont Blanc and Pelvoux massifs. Int. J. Earth Sci. 90, 685-702.

Chemenda, A.I., Mattauer, M., Malavieille, J., Bokun, A.N. 1995. A mechanism for syn-collisional deep rock exhumation and associated normal faulting: Results from physical modeling. Earth Plan. Sci. Lett. 132, 225-232.

Chemenda, A.I., Mattauer, M., Bokun, A.N. 1996. Continental subduction and a mechanism for exhumation of high-pressure metamorphic rocks: new modeling and field data from Oman. Earth Plan. Sci. Lett. 143, 173-182.

Chopin, C. 1984. Coesite and pure pyrope in high-grade blueschists of the Western Alps: a first record and some consequences. Contrib. Mineral. Petrol. 86, 107-118.

Choukroune, P., Ballèvre, M., Cobbold, P., Gautier, Y., Merle, O., Vuichard, J. P. 1986. Deformation and motion in the western Alpine Arc. Tectonics, 5, 215-226.

Chiesa, S.; Cortesogno, L.; Forcella, F.; Galli, M.; Messiga, B., Pasquar, G.; Pedemonte, G.M.; Piccardo, G.B.; Rossi, P.M. 1975. Assetto strutturale ed interpretazione geodinamica del Gruppo di Voltri. Bol. Soc. Geol. It., 94, 555-581.

Claudel, M.E., Dumont, T., 1999. A record of multistage continental break-up on the Briançonnais marginal plateau (Western Alps): early and middle−late jurassic rifting. Eclogae Geolicae Helvetie, 92, 45-61.

Cloos, M. 1982. Flow melanges: Numerical modeling and geological constraints on their origin in the Franciscan subduction complex. Geol. Soc. Am. Bull. 93, 330-345.

Cobianchi, M., Di Giulio, A., Galbiati, B., Mosna, S. 1991. Il "Complesso di base" del Flysch di San Remo nell'area di San Bartolomeo, Liguria occidentale (nota preliminare). Atti Ticinesi di Scienze della Terra, 34, 45-154.

Compagnoni, R., Elter, G., Lombardo, B., 1974. Eterogeneit. stratigrafica del Complesso degli "Gneiss Minuti" nel massiccio cristallino del Gran Paradiso. Memorie della Societ. Geologica Italiana, 13, 227-239.

Corsini M, Ruffet G, Caby R. 2004. Alpine and late Hercynian geochronological constraints in the Argentera Massif (Western Alps). Eclogae Geolicae Helvetie, 97, 3-15.

Coward, M.P. and Dietrich, D., 1989. Alpine tectonics-and overview, in Coward M.P., Dietrich D., Park R.G., (Eds.), Alpine tectonics, Geological Society, 45, London, Special Publications, 1-29.

Culshaw, N. G., Beaumont, C., Jamieson, R. A. 2006. The orogenic superstructure-infrastructure concept: Revisited, quantified, and revived. Geology, 34, 733-736.

Dal Piaz, G.V., Bistacchi, A., Massironi, M., 2003. Geological outline of the Alps. Episodes, 26, 175–180.

Dal Piaz, G. V. 2010. The Italian Alps: a journey across two centuries of Alpine geology. J. Virt. Explorer, 2010, 36, 77-106.

Daniele, G., Bianchi, L., 1995. Studio petrografico sulle Arenarie di Ostia della media Val di Taro e loroconfronto con arenarie di altre successioni: Memorie dell'Accademia Lunigianense delle Scienze "G Cappellini", 64-65, 131-138.

Daniele, G. and Plesi, G., 2000. The Helminthoid flysch units of the Emilian Apennines: stratigraphic and petrographic features, paleogeographic restoration and structural evolution. Geodinamica Acta, 13, 313-333.

d'Atri, A., Piana, F., Barale, L., Bertok, C., & Martire, L. 2016. Geological setting of the southern termination of Western Alps. International Journal of Earth Sciences, 105, 1831-1858.

De Andrade, V., Vidal, O., Lewin, E., O'Brien, P., Agard, P. 2006. Quantification of electron microprobe compositional maps of rock thin sections: an optimized method and examples. Journal of metamorphic Geology 24, 655-668.

Debelmas, J. 1989. One some key features of the evolution of the western Alps. In Tectonic Evolution of the Tethyan Region(pp. 23-42). Springer, Dordrecht.

Decarlis, A., and Lualdi, L., 2008. Late Triassic-Early Jurassic paleokarst from the Ligurian Alps and its geological significance (Siderolitico Auct., Ligurian Brian.onnais domain). Swiss Journal of Geosciences, 101, 579–593.

Decarlis, A., Dallagiovanna, G., Lualdi, A., Maino, M., Seno, S. 2013. Stratigraphic evolution in the Ligurian Alps between Variscan heritagesand the Alpine Tethys opening: A review. Earth-Sciences Reviews, 125, 43–68.

Dewey, J. F., Helman, M. L., Knott, S. D., Turco, E., Hutton, D. H. W. 1989. Kinematics of the western Mediterranean. Geological Society, London, Special Publications, 45, 265-283.

Di Giulio, A. 1988. Evoluzione strutturale delle Unità di Moglio-Testico e di S. Remo-M. Saccarello (Piemontese-Ligure delle Alpi Marittime): nuovi dati. At. Tic. Sc. Ter., 31, 54-62.

Di Giulio, A., 1992. The evolution of the Western Ligurian Flysch Units and the role of mud diapirism in ancient accretionary prisms (Maritime Alps, Northwestern Italy). Geologische Rundschau, 81, 655-668.

Dooley, T. P., Schreurs, G. 2012. Analogue modelling of intraplate strike-slip tectonics: A review and new experimental results. Tectonophysics, 71, 574–575.

Dubacq, B., Vidal, O., De Andrade, V. 2010. Dehydration of dioctahedral aluminous phyllosilicates: thermodynamic modelling and implications for thermobarometric estimates. Contrib. Mineral. Petrol. 159, 159-174.

Duchene, S., Blichert-Toft, J., Luais, B., T.louk, P., Lardeaux, J.M., Albar.de, F. 1997. The Lu–Hf dating of garnets and the ages of the Alpine high-pressure metamorphism. Nature, 387, 586-589.

Dickinson, W.R., 1970. Interpreting detrital modes of greywacke and arkose. J. Sediment. Petrol., 40, 695-707.

Di Rosa, M., Frassi, C., Meneghini, F., Marroni, M., Pandolfi, L., De Giorgi, A. 2019. Tectono-metamorphic evolution in the European continental margin involved in the alpine subduction: New insights from the alpine Corsica, France. C. R. Geoscience, 351, 384-394.

Di Rosa, M., Frassi, C., Malasoma, A., Marroni, M., Meneghini, F., Pandolfi, L. 2020. Syn-exhumation coupling of oceanic and continental units along the western edge of the Alpine Corsica: A review. Ofioliti, 45, 71-102.

Di Rosa, M. (2021). Tectono-metamorphic evolution of the continental units along the edge between Alpine and Hercynian Corsica: Constraints for the exhumation models in the continental collision setting. pp 222.

Doglioni, C., Gueguen, E., Sàbat, F., Fernandez, M. 1997. The Western Mediterranean extensional basins and the Alpine orogen. Terra Nova, 9, 109-112.

Ducci, M., Leoni, L., Marroni, M., Tamponi, M. 1995. Determinazione del grado metamorfico delle Argille a Palombini dell'Alta Val Lavagna (UnitaGottero, Appennino Settentrionale. Atti Societa Toscana Scienze Naturali, Memorie, Serie A, 102.
Dumont, T., Schwartz, S., Guillot, S., Malusa, M., Jouvent, M., Monié, P., Verly, A. 2022. Cross-propagation of the western Alpine orogen from early to late deformation stages: Evidence from the Internal Zones and implications for restoration. Earth-Science Reviews, 104106.

Durand-Delga M. 1984. Principaux traits de la Corse Alpine et correlations avec les Alpes Ligures. Mem. Soc. Geol. It. 28, 285-329.

Ellero, A., Leoni, L., Marroni, M., Sartori, F. 2001. Internal Liguride Units from Central Liguria, Italy: new constraints to the tectonic setting from white mica and chlorite studies.

Ellero, A., Loprieno, A. 2017. Nappe stack of Piemonte-Ligurian units south of Aosta Valley: New evidence from Urtier Valley (Western Alps). Geol. J., 53, 1665-1684.

Ellero, A., Frassi, C., Göncüoğlu, M. C., Lezzerini, M., Marroni, M., Ottria, G., Tamponi, M. 2021. Geological, Structural and Mineralogical Approach to Investigate the Evolution of Low-and very Low-Grade Metamorphic Units from the Intra-Pontide Suture Zone, Central Pontides, Turkey. Journal of Earth Science, 32, 1512-1527.

Elter, P., Haccard, D., Lanteaume, M.,Raggi, G. 1961. Osservazioni sui rapporti tra flysch ad Elmintoidi ed Arenaria superiore nell'Appennino ligure e nelle Alpi Marittime. Bollettino della Società Geologica Italiana, 80, 115-120.

Elter, G., Elter, P., Sturani, C., & Weidmann, M. 1966. Sur la prolongation du domaine ligure de l'Apennin dans le Monferrat et les Alpes et sur l'origine de la Nappe de la Simme sl des Préalpes romandes et chablaisiennes. éditeur non identifié.

Elter, P., and Pertusati, P.C., 1973. Considerazioni sul limite Alpi-Appennino e sulle relazioni con l'arco delle Alpi Occidentali: Memorie della Societ. Geologica Italiana, 12, 359–375.

Elter, P., 1975. L'ensemble ligure: Bullettin d. la Soci.t. G.ologique de France, 17, 984-997.

Elter, P. 1997. Detritismo ofioltico e subduzione: riflessioni sui rappporti Alpi e Appennino. Memorie della Società Geologica Italiana, 49, 205–215.

Escher, A., Hunziker, J.C., Marthaler, M., Masson, H., Sartori, M., Steck, A., 1997. Geologic framework and structural evolution of the Western Swiss–Italian Alps. In: Pfiffner, O.A., Lehner, P., Heitzmann, P.Z., Mueller, S., Steck, A. (Eds.), Deep Structure of the Swiss Alps: Results from NRP 20. Birkh.user, Basel, 205-221.

Falletti P, Gelati R, Rogledi S. 1995. Oligo-Miocene evolution of Monferrato and Langhe, related to deep structures. In Polino R, Sacchi R (eds) Atti del convegno "Rapporti Alpi-Appennino". Acc Naz Sci detta dei XL, 14, 1-20.

Fellin, M.G., Picotti, V., Zattin, M. 2005. Neogene to Quaternary rifting and inversion in Corsica: Retreat and collision in the western Mediterranean. Tectonics 24. TC1011, doi:10.1029/2003TC001613.

Fallot, P., and Faure-Muret, A., 1954. Sur le Secondaire et le Tertiaire 491 aux abords sudorientaux du Massifde l'Argentera-Mercantour (feuille de Saint Martin V.subie, Tende et Vi.ve au 50.000) [On the Secondary andTertiary in the southern edge of the Argentera-Mercantour Massif (Saint Martin V.subie, Tende et Vi.ve sheetat 1:50000 scale)]. Bulletin de la Carte g.ologique de la France, 52, 283-319.

Fernández-Caliani, J. C., Galán, E. 1992. Influence of tectonic factors on illite crystallinity: a case study in the Iberian pyrite belt. Clay Minerals, 27, 385-388.

Festa, A., Meneghini, F., Balestro, G., Pandolfi, L., Tartarotti, P., Dilek, Y., Marroni, M. 2021. Comparative analysis of the sedimentary cover units of the Jurassic Western Tethys ophiolites in the Northern Apennines and Western Alps (Italy): processes of the formation of mass-transport and chaotic deposits during seafloor

spreading and subduction zone tectonics. The Journal of Geology, 129, 533-561.

Fontana, D., Spadafora, E., Stefani, C., Stocchi, S., Tateo, F., Villa, G., Zuffa, GG., 1994. The Upper Cretaceous Helminthoid Flysch of the Northern Apennines; provenance and sedimentation. Memorie della Societ. Geologica Italiana, 48, 237-250.

Ford, M., Lickorish, W.H. 2004. Foreland basin evolution around the western Alpine Arc. Geol Soc London Spec Publ, 221, 39-63.

Ford, M., Duchêne, S., Gasquet, D., Vanderhaeghe, O. 2006. Two-phase orogenic convergence in the external and internal SW Alps. Journal of the Geological Society, 163, 815-826.

Franceschelli, M., Leoni, L., Memmi, I., 1989. b0 of Muscovite in Low and High Variance Assemblages from Low Grade Verrucano Rocks, Northern Apennines, Italy. Schweizerische Mineralogische und Petrographische Mitteilungen, 69, 107–115

Frassi, C., Di Rosa, M., Farina, F., Pandolfi, L., Marroni, M. Anatomy of a deformed upper crust fragment from western alpine Corsica (France): Insights into continental subduction processes. Int. Geol. Review 2022, 64, 1-21.

Frisch, W., 1979. Tectonic progradation and plate tectonic evolution of the Alps. Tectonophysics, 60, 121-139.

Frey, M., Robinson, D. 1999. Low-grade metamorphism. Blackwell Science.

Froitzheim, N. 1992. Formation of recumbent folds during synorogenicrustal extension Austroalpine nappes, Switzerland. Geology, 20, 923–926.

Froitzheim, N., Manatschal, G. 1996. Kinematics of Jurassic rifting, mantle exhumation, and passive-margin formation in the Austroalpine and Penninic nappes (eastern Switzerland). Geological Society of America Bulletin, 10, 1120–1133.

Galbiati, B. 1985. L'unità di Borghetto ed i suoi legami con quella di Moglio-Testico (Alpi Liguri): conseguenze paleogeografiche. Riv. It. Paleont. Strat., 90, 205-226.

Galbiati, B., Rodi, E. 1989. Caratteri strutturali dell'Unità di Moglio-Testico tra Alassio e Laigueglia (Liguria occidentale). Bol. Soc. Geol. It., 108, 491-502.

Galbiati, B., Cobianchi, M. 1997. L'indipendenza tettonica dell'unità di Sanremo rispetto all'unità di Moglio-Testico. Boll. Soc. Geol. It., 116, 453-472.

Goffé, B..Schwartz, S., Lardeaux, J. M., & Bousquet, R. 2004. Metamorphic structure of the western and Ligurian Alps. In R. Oberhansli (Ed.), Explanatory note to the map "metamorphic structure of the Alps" (pp. 125–144). Mitt. Österr. Mineral. Gesell.

Gasco, I., Gattiglio, M., Borghi, A. 2013. Review of metamorphic and kinematic data from Internal Crystalline Massifs (Western Alps): PTt paths and exhumation history. Journal of Geodynamics, 63, 1-19.

Gazzi, P., 1966. Le arenarie del flysch sopracretaceo dell'Appennino modenese: correlazioni con il flysch di Monghidoro. Mineral. Petrogr. Acta, 12, 69-97.

Gidon, M. 1972. Les chainons brian.onnais et subbrian.onnais de la rive gauche de la Stura entre le Val de l'Arma (province de Cuneo Italie). Geologie Alpine, 48, 87-120.

Giglia, G., Capponi, G., Crispini, L., Piazza, M. 1996. Dynamics and seismotectonics of the western-Alpine arc. Tectonophysics, 267, 143-175.

Giorgetti, G., Memmi, I., Peacor, D. R. 2000. Retarded illite crystallinity caused by stressinduced sub-grain boundaries in illite. Clay Minerals, 35, 693-708.

Gosso, G., Lardeaux, J. M., Zanoni, D., Volante, S., Corsini, M., Bersezio, R., Camera, L. 2019. Mapping the progressive geologic history at the junction of the Alpine mountain belt and the western Mediterranean ocean. Ofioliti, 44, 97–110.

Grandjacquet, C., Haccard, D. 1977. Position structural et ro^le pale`oge´ographique de l'unite´ du Bracco au sein du contexte ophiolitique ligure-pie´montais (Apennin-Italie). Bulletin de la Socie´te Ge´ologique de France, 19, 901–908.

Gratier, J. P., Ménard, G., Arpin, R. 1989. Strain-displacement compatibility and restoration of the Chaînes Subalpines of the western Alps. Geological Society, London, Special Publications, 45, 65-81.

Graveleau, F., Malavieille, J., Dominguez, S. 2012. Experimental modelling of orogenic wedges: A review. Tectonophysics, 538, 1-66.

Gueguen, E., Doglioni, C., Fernandez, M., 1998. On the post-25 Ma geodynamic evolution of the western Mediterranean. Tectonophysics 298, 259–269.

Guillaume, A. 1969. Contribution à l'étude géologique des Alpes liguro-piémontaises. 2e fascicule. Travaux et Documents des Laboratoires de Géologie de Lyon, 30(2)

Guillaume, A. 1980. Tectonophysics of the western Alps.

Guillot S., Hattori K., Agard P., Schwartz S., Vidal O. 2009. Exhumation Processes in Oceanic and Continental Subduction Contexts: A Review. In: Lallemand S. and Funiciello F. (eds.), Subduction Zone Geodynamics, Springer-Verlag Berlin, 175-205.

Haccard, D. 1961. La série du Flysch de Moglio-Testico de la nappe du Flysch à Helminthoides des Alps maritimes franco-italiennes. C. R. Ac. Sc. Fr., 252, 3609-3611.

Herviou, C., Agard, P., Plunder, A., Mendes, K., Verlaguet, A.. Deldicque, D., Cubas, N. 2022. Subducted fragments of the Liguro-Piemont ocean, Western Alps: Spatial correlations and offscraping mechanisms during subduction. Tectonophysics 2022, 10.1016/j.tecto.2022.229267

Handy, M.R., Schmid, S.M., Bousquet, R., Kissling, E., Bernoulli, D. 2010. Reconciling plate–tectonic reconstructions of Alpine Tethys with the geological–geophysical record of spreading and subduction in the Alps. Earth Sci. Rev. 102, 121–158.

Inger, S., Ramsbotham, W., Cliff, R.A., Rex, D.C., 1996. Metamorphic evolution of the Sesia-Lanzo Zone, Western Alps: time constraints from multi-system geochronology. Contrib. Mineral. Petrol., 126, 152-168.

Jolivet, L., Daniel, J.M., Fournier, M. 1991. Geometry and Kinematics of ductile extension in Alpine Corsica. Earth Plan. Sci. Lett. 104, 278-291.

Jolivet, L., Faccenna, C., Goffé, B., Mattei, M., Rossetti, F., Brunet, C., Storti, F., Funiceiello, R., Cadet, J.-P., D'Agostino, N., Parra, T. 1998. Midcrustal shear zones in post-orogenic extension: Example from the Tyrrhenian Sea. J. Geoph. Res. 103, 12-123.

Kerckhove, C. 1963. Schema structural de la nappe du Flysch a Helminthoides de l'Embrunais-Ubaye. Trav. Lab. Geol. Fac. Sci. Grenoble, 39, 7-24.

Kerckhove, C., 1969. La ''zone du Flysch'' dans les nappes de l'Embrunais (Alpes Occidentales). GeÅLol, Alpine, 45, 5-204.

Kisch, H. J., 1987. Correlation between Indicators of very Low-Grade Metamorphism. In: Frey, M., ed., Low-Temperature Metamorphism. Blackie and Son Ltd., Glasgow. 227–300

Kisch, H. J. 1980a. Incipient metamorphism of Cambro-Silurian clastic rocks from the JHmtland Supergroup, central Scand- inavian Caledonidcs, western Sweden: illite crystallinity and 'vitrinitc' reflectance. Journal of Geological Society, London, 137,271-288.

Kisch, H. J., 1980b. Illite crystallinity and coal rank assodated with lowest-grade metamorphism of the Taveyanne greywadre in the Helvetic zone of the Swiss Alps. W g a e geologicochelvetie Hdueticu, 73,753-777.

Kisch, H. J., Sassi, R., Sassi, F. P., 2006. The b0 Lattice Parameter and Chemistry of Phengites from HP/LT Metapelites. European Journal of Mineralogy, 18, 207–222. https://doi.org/10.1127/0935-1221/2006/0018-0207

Kubler, B., 1967a. La cristallinitt de I'illitc et la zones tout B fait suptricures du mCtamorphisme. In: Eraga Tectonique – Colloque de Neuchael, 18-21 auvril 1966, pp 105-122, A la Baconnierè, Neuchatel (Suisse)

Kubler,B..1967b.Anchimetamorphisme et schistosité. Bulletin du Centre de Recherches de Pau- SNPA,1,259-278.

Kubler, B., 1968. Evaluation quantitative du metamorphisme par cristallinité de I'illite. Bulletin du Centre de Recherches de Pau SNPA, 2.385-397.

Lagabrielle, Y., Brovarone, A.V., Ildefonse, B. 2015. Fossil oceanic core complexes recognized in the blueschist metaophiolites of Western Alps and Corsica. Earth-Sciences Reviews, 141, 1-26.

Lanari, P. 2012. Micro-cartgraphie P-T dans les roches métamorphiques. Applications aux Alpes et à l'Himalaya. Thèse de doctorat Sciences de la Terre, Université de Grenoble.

Lanari, P., Guillot, S., Schwartz, S., Vidal, O., Tricart, P., Riel, N., Beyssac, O. 2012. Diachronous evolution of the alpine continental subduction wedge: evidence from P–T estimates in brianconnaise zone houllière (France-Western Alps). J. Geodyn. 56-57, 39–54.

Lanari, P., Wagner, T., Vidal, O. 2014a. A thermodynamic model for di-trioctahedral chlorite from experimental and natural data in the system MgO-FeO-Al2O3-SiO2-H2O: applications to P-T sections and geothermometry. Contrib. Mineral. Petrol. 167. doi:10.1007/s00410-014-0968-8.

Lanari, P., Rolland, Y., Schwartz, S., Vidal, O., Guillot, S., Tricart, P., Dumont, T. 2014b. P-T-t estimation of deformation in lowgrade quartz-feldspar-bearing rocks using thermodynamic modelling and 40Ar/39Ar dating techniques: example of the Plan-de-Phasy shear zone unit (Briançonnais Zone, Western Alps). Terra Nova 26, 130-138.

Lanari, P., Vidal, O., De Andrade, V., Dubacq, B., Lewin, E., Grosch, E., Schwartz, S. 2014c. XMAPTOOLS: a MATLAB c -based program for electron microprobe X-ray image processing and geothermobarometry. Computers and Geosci. 62, 227-240.

Lanari, P.; Engi, M. 2017. Local bulk composition effects on metamorphic mineral assemblages. Rev. Min. Geochem., 53, 83, 55-102.

Lanari, P.; Duesterhoeft, E. 2019. Modeling metamorphic rocks using equilibrium thermodynamics and internally consistent databases: Past achievements, problems and perspectives. J. Petrol., 60, 19-56.

Lanteaume, M., 1957. Nouvelles donnes sur le Flysch a helminthoides de la Ligurie occidentale (Italie). Bull. Soc. G.ol. Fr., 7, 115-123.

Lanteaume, M., 1962. Consid.rations pal.og.ographiques sur la patrie suppos.e des nappes de Flysch Helminthoides des Alpes et des Apennins. Bull. Soc. g.ol. France, 4, 627-643.

Lanteaume, M., Haccard, D. 1962. Stratigraphie et variation de facies de formations constitutives de la nappe du Flysch à Helminthoides des Alpes Maritimes franco-italiennes. Bol. Soc. Geol. It., 80, 101-113.

Lanteaume M., Haccrd D., Labesse B., and Lorenz Cl. 1963. L'origine de la nappe du flysch à Helminthoiides et la liaison alps -Appennins. Livre à la mémoire du Professor Paul Fallo, Mèm. Hors. Sér. Soc. Géol. Fr., pp 257

Lanteaume, M., 1968. Contribution l'etude g.ologique des Alpes Maritimes franco-italiennes. Mem Carte Geol France, 405.

Lanteaume, M., et al., 1991. Carte geÅLologique France (1/50 000), feuille Vie`ve-Tende (948), Bur. de Rech,GeÅLol. et. Min., Orleans, France.

Lardeaux, J.M., Spalla, M.I. 1991. From granulites to eclogites in the Sesia Zone (Italian Western Alps): a record of the opening and closure of the Piemont Ocean. J. Metam. Geol., 9, 35-59.

Lardeaux, J. M., Schwartz, S., Tricart, P., Paul, A., Guillot, S., Béthoux, N., Masson, F. 2006. A crustal-scale cross-section of the south-western Alps combining geophysical and geological imagery. Terra Nova, 18, 412-422.

Lardeaux, J. M. 2014. Deciphering orogeny: a metamorphic perspective Examples from European Alpine and Variscan belts: Part II: Variscan metamorphism in the French Massif Central–A review. Bulletin de la Société géologique de France, 185, 281-310.

Laubscher, H. P. 1971. The large-scale kinematics of the western Alps and the northern Apennines and its palinspastic implications. American Journal of Science, 271, 193-226.

Laubscher, H. 1988. Material balance in Alpine orogeny. Geological Society of America Bulletin, 100(9), 1313-1328.

Lavier, L. L., Manatschal, G. 2006. A mechanism to thin the continental lithosphere at magma-poor margins. Nature, 440, 324–328.

Lefèvre, R. 1983. La cicatrice de Preit: une discontinuité structurale majeure au sein de la zone briançonnaise entre Acceglio et l'Argentera (Alpes Cottiennes méridionales). C.R. Acad. Sci. Paris 296, 1551-1554.

Le Bayon, B., Ball.vre, M., 2004. Field and petrological evidence for a Late Palaeozoic (Upper Carboniferous–Permian) age of the Erfaulet orthogneiss (Gran Paradiso, western Alps). Comptes rendus G.oscience, 336, 1079-1089.

Leoni, L., Marroni, M., Sartori, F., & Tamponi, M. 1996. Metamorphic grade in metapelites of the internal liguride units (Northern Apennines, Italy). European Journal of Mineralogy-Ohne Beihefte, 8, 35-50.

Levi, N., Ellero, A., Ottria, G., and Pandolfi, L., 2006. Polyorogenic deformation history at very shallow structural levels: The case of the Antola Unit (Northern Apennine, Italy): Journal of Structural Geology, 28, 694-1709.

Levi, N., Malasoma, A., Marroni, M., Pandolfi, L., Paperini, M. 2007. Tectono- metamorphic history of the ophiolitic Lento unit (northern Corsica): evidences for the complexity of accrection-exhumation processes in a fossil subduction system. Geod. Acta 20, 99-118.

Lezzerini, M., Sartori, F., Tamponi, M. 1995. Effect of Amount of Material Used on Sedimentation Slides in the Control of Illite "Crystallinity" Measurements. European Journal of Mineralogy, 7, 819–824. https://doi.org/10.1127/ejm/7/4/0819

Lorenz C. 1986. Tectonique cassante à l'Oligocène supérieur dans le Briançonnais de la bordure septentrionale des Alpes Ligures. Mem. Soc. Geol. It., 28, 487-491.

Lualdi, A., 1994a. I Calcari di Rio di Nava (Dogger, Brianzonese ligure): Inquadramento stratigrafico e sedimentologico. Bollettino della Societa` Geologica Italiana, 113, 501-520.

Luoni, P., Rebay, G., Roda, M., Zanoni, D., Spalla, M. I. 2021. Tectono-metamorphic evolution of UHP Zermatt-Saas serpentinites: a tool for vertical palaeogeographic restoration. International Geology Review, 63, 1236-1261.

Maino, M., Casini, L., Ceriani, A., Decarlis, A., Di Giulio, A., Seno, S., Stuart, F. M. 2015. Dating shallow

thrusts with zircon (U-Th)/He thermochronometry: The shear heating connection. Geology, 43, 495–498.

Maino, M., & Seno, S. 2016. The thrust zone of the Ligurian Penninic basal contact (Monte Fronté, Ligurian Alps, Italy). Journal of Maps, 12, 341–351.

Malatesta, C., Crispini, L., Federico, L., Capponi, G., Scambelluri, M. 2012. The exhumation of high pressure ophiolites (Voltri Massif, Western Alps): Insights from structural and petrologic data on metagabbro bodies. Tectonophysics, 568, 102-123.

Malavieille, J. 1983. Etude tectonique de la nappe de socle Centuri (zone de Schistes Lustrés de la Corse); Consequence pour la géométrie de la chaine alpine. Bull. Soc. Géol. France 25, 195-204.

Malusa., M.G., Mosca, P., Borghi, A., Dela Pierre, F., Polino, R. 2002. Approccio multidisciplinare per la ricostruzione dell'assetto tettono-stratigrafico e dell'evoluzione metamorfico-strutturale di un settore di catena orogenica: l'esempio dell'Alta Valle di Susa (Alpi occidentali). Memorie della Societ. Geologica Italiana, 57, 249-257.

Manatschal, G., Müntener, O. 2009. A type sequence across an ancient magma-poor ocean–continent transition: the example of the western Alpine Tethys ophiolites. Tectonophysics, 473, 4-19.

Manivit, H., Prud'Homme, A. 1990. Biostratigraphiedu Flysch à Helminthoïdes des Alpes maritimes franco-italiennes. Nannofossiles de l'unité de San Remo-Monte Saccarello. Comparaison avecles Flyschs à Helminthoïdesdes Apennins. Bulletin Société Géologique de France, 8, 95–104.

Marini, M.; Terranova, R. 1985. Nuovi dati sulla litostratigrafia dei flysch della Liguria occidentale e sui loro rapporti strutturali. At. 805 Soc. Tos. Sc. Nat., 92, 95-163.

Marini M. 1995. Litologia, stratimetria e sedimentologia della Formazione di Testico (Alpi Marittime Liguri). Boll. Soc. Geol. It., 114, 497-516.

Marroni, M., Perilli, N. 1990. The age of the ophiolite sedimentary cover from the Mt. Gottero Unit (Internal Liguride Units, Northern Apennines): new data from calcareous nannofossils. Ofioliti, 15, 232-251.

Marroni, M., Pandolfi, L. 1996. The deformation history of an accreted ophiolite sequence: The internal Liguride units (northern Apennines, Italy). Geodinamica Acta, 9, 13-29.

Marroni, M., Molli, G., Montanini, A., Tribuzio, R. 1998. The association of continental crust rocks with ophiolites in the Northern Apennines (Italy): implications for the continent-ocean transition in the Western Tethys. Tectonophysics, 292, 43-66.

Marroni, M., Pandolfi, L. 2001. Debris flow and slide deposits at the top of the internal liguride ophiolitic sequence, Northern Apennines, Italy: A record of frontal tectonic erosion in a fossil accretionary wedge. Island Arc, 10, 9-21.

Marroni, M., Molli, G., Montanini, A., Ottria, G., Pandolfi, L., Tribuzio, R. 2002. The External Ligurian units (Northern Apennine, Italy): from rifting to convergence of a fossil ocean-continent transition zone. Ofioliti, 27, 119-131.

Marroni, M., Pandolfi, L., Meneghini, F. 2004. From accretion to exhumation in a fossil accretionary wedge: a case history from Gottero Unit (Northern Apennines, Italy). Geod. Acta 17, 41-53.

Marroni, M., Pandolfi, L. 2007. The architecture of the Jurassic Ligure-Piemontese oceanic basin: Tentative reconstruction along the Northern Apennines—Alpine Corsica transect. International Journal of Earth Sciences, 96, 1059–1078.

Marroni, M., Meneghini, F., Pandolfi, L. 2010. Anatomy of the Ligure-Piemontese subduction system: Evidence from Late Cretaceous-Middle Eocene convergent margin deposits in the Northern Apennines, Italy. Int. Geol. Rev., 52, 1160-1192.

Marroni, M., Meneghini, F., Pandolfi, L. 2017. A revised subduction inception model to explain the Late Cretaceous, double-vergent orogen in the precollisional western Tethys: Evidence from the Northern Apennines. Tectonics, 36, 2227-2249.

Massonne, H.J., Schreyer, W. 1987. Phengite geobarometry based on the limiting assemblage with K-feldspar, phlogopite, and quartz. Contrib. Mineral. Petr., 96, 212–224.

Mattauer, M., Faure, M., Malavieille, J. 1981. Transverse lineation and large-scale structures related to Alpine obduction in Corsica. J. Struct. Geol. 3, 401-409.

Menardi-Noguera, A. 1988. Structural evolution of a briançonnais cover nappe, the Caprauna–Armetta unit (Ligurian Alps, Italy). Journal of Structural Geology, 10, 625–637.

Meneghini, F., Pandolfi, L., Marroni, M. 2020. Recycling of heterogeneous material in the subduction factory: evidence from the sedimentary mélange of the Internal Ligurian Units, Italy. J. Geol. Soc., 177, 587-599.

Merizzi, G., Seno, S. 1991. Deformations and gravity-driven translation of the S. Remo-M. Saccarello nappe (Helminthoid Flysch, Ligurian Alps). Bollettino della Società geologica italiana, 110, 757-770.

Merle., O., 1982a. Mise en place s.quentielle de la Nappe de Parpallion (Flysch . Helmintoides, Alpes Occidentales). C. R. hebd. S.anc. Acad. Sci., Paris 294, 603-606.

Merle, O., Brun, J. P., 1984. The curved translation path of the Parpaillon nappe (French Alps). Journal of Structural Geology, 6, 711-719.

Messiga, B., Oxilia, M., Piccardo, G.B., Vanossi, M., 1982. Fasi metamorfiche e deformative alpine nel Brianzonese e nel pre-piemontese-piemontese esterno delle Alpi Liguri: un possibile modello evolutivo. Rend. Soc. Ital. Mineral. Petrol., 38, 261-280.

Michard, A., Chaloun, A., Feinberg, H., Goff., B., Montigny, R., 2002. How does the Alpine belt end between Spain and Morocco? Bulletin de la SocieÅLte GeÅLologique de France, 173, 3-15.

Michard, A., Avigad, D., Goff., B., Chopin, C., 2004. The high-pressure metamorphic front of the south Western Alps (Ubaye–Maira transect, France, Italy). Schweiz. Mineral. Petrogr. Mitt., 84, 215-235.

Mohn, G., Manatschal, G., Müntener, O., Beltrando, M., Masini, E. 2010. Unravelling the interaction between tectonic and sedimentary processes during lithospheric thinning in the Alpine Tethys margins. International Journal of Earth Sciences, 99, 75–101.

Molli, G., 2008. Northern Apennine–Corsica orogenic system: an updated overview. In S. Siegesmund et al. (Eds.) Tectonic aspects of the Alpine-Dinaride-Carpathian system (pp. 413-442). Geological Society London Special Publications, 298.

Molli, G., Crispini, L., Malusà, M., Mosca, P., Piana, F., Federico, L. 2010. Geology of the Western Alps-Northern Apennine junction area: a regional review. Eds Marco Beltrando, Angelo Peccerillo, Massimo Mattei, Sandro Conticelli, and Carlo Doglioni Journal of the Virtual Explorer, 36(3).

Molli, G., Malavieille J. 2011. Orogenic processes and the Corsica/Apennines geodynamic evolution: insights from Taiwan. Int. J. Earth Sci. 100, 1207–1224.

Moore, G. F., Strasser, M. 2016. Large mass transport deposits in kumano basin, Nankai trough, Japan. In Submarine mass movements and their consequences (pp. 371-379). Springer, Cham.

Monié, P. 1990. Preservation of Hercynian 40Ar/39Ar ages through high-pressure low-temperature alpine metamorphism in the western alps. European Journal of Mineralogy, 2, 343–361.

Mosca, P., Polino, R., Rogledi, S., Rossi, M. 2010. New data for the kinematic interpretation of the Alps–Apennines junction (Northwestern Italy). International Journal of Earth Sciences, 99, 833-849.

Mosna S., Seno S., Vanossi M. 1990 - Depositi post-orogeni del- l'Oligocene inferiore interposti tra il Brianzonese e la «Pietra di Finale» (Alpi liguri): conseguenze paleotettoniche e paleogeogra- fiche. Atti Tic. Sc. Terra, 33, 11-21.

Michard, A., Chalouan, A., Feinberg, H., Goffé, B. Montigny, R. 2002. How does the Alpine belt end between Spain and Morocco? Bulletin de la Societe Geologique de France, 173, 3-15.

Mueller, P., Langone, A., Patacci, M., Di Giulio, A. 2018. Detrital signatures of impending collision: The deep-water record of the Upper Cretaceous Bordighera Sandstone and its basal complex (Ligurian Alps, Italy). Sedimentary Geology, 377, 147-161.

Mueller, P., Maino, M., Seno, S. 2020. Progressive deformation patterns from an accretionary prism (Helminthoid Flysch, Ligurian Alps, Italy). Geosciences, 10, 26.

Mutti, E., 1992. Turbidite Sandstones. Agip, San Donato Milanese.

Naylor, M. A., Mandl, G., Sijpesteijn, C. H. K. 1986. Fault geometries in basement-induced wrench faulting under different initial stress states. Journal of Structural Geology, 8, 737–752.

Niedermayr, G., Mullis, J., Niedermayr, E. 1984. Zur Anchimetamorphose Permo-Skythischer Sedimentgesteine Im Westlichen Drauzug, Kärnten—Osttirol (Österreich). Geologische Rundschau, 73, 207–221. https://doi.org/10.1007/bf01820367

Oberhänsli, R., Bousquet, R., Engi, M., Goffé, B., Gosso, G., Handy, M.R., Höck, V., Koller, F., Lardeaux, J.M., Polino, R., Rossi, Ph., Schuster, R., Schwartz, S., Spalla, I., 2004. Metamorphic structure of the Alps. Commission for the Geological Map of the World, Paris, scale 1:1.000.000.

Pandolfi, L., 1997. Stratigrafia ed evoluzione strutturale delle successioni torbiditiche cretacee della Liguria orientale (Appennino Settentrionale). Tesi di Dottorato, Universià. di Pisa, 175 p.

Passchier, C. W., Trouw, R. A. 2005. Microtectonics. Springer Science & Business Media.

Paul, A., Cattaneo, M., Thouvenot, F., Spallarossa, D., Béthoux, N., Fréchet, J. 2001. A three-dimensional crustal velocity model of the southwestern Alps from local earthquake tomography. Journal of Geophysical Research: Solid Earth, 106, 19367-19389.

Perotti, E., Bertok, C., d'Atri, S., Martire, L., Piana, F., Catanzariti, R., 2012. A tectonically-induced Eocene sedimentary melange in the West Ligurian Alps, Italy Tectonophysics, 568-569, 200-214

Pfiffner, O. A., Lehner, P., Heitzmann, P., Mueller, S., Steck, A. 1997. Deep structure of the Swiss Alps: results of NRP 20. Birkhäuser.

Piana, F., Musso, A., Bertok, C., 2009. New data on post-Eocene tectonic evolution of the External Ligurian Brianconnais (Western Ligurian Alps). Bollettino della Societ. Geologica Italiana 128:353–366. doi:10.3301/IJG.2009.128.2.353

Piana, F., Battaglia, S., Bertok, C., 2014. Illite (KI) and chlorite (AI) "crystallinity" indices as a constraint forthe evolution of the External Brian.onnais Front in Western Ligurian Alps (NW Italy). Ital J Geosci, 133, 445-454.

Piana, F., Barale, L., Bertok, C., d'Atri, A., Irace, A., Mosca, P. 2021. The Alps-Apennines Interference Zone: A Perspective from the Maritime and Western Ligurian Alps. Geosciences, 11, 185.

Platt, J.P. 1987. The uplift of high pressure/low temperature metamorphic rocks. Phylosophical Transaction of the Royal Society of London, 321, 87 – 103.

Pleuger, J., Roller, S., Walter, J. M., Jansen, E., Froitzheim, N. 2007. Structural evolution of the contact between two Penninic nappes (Zermatt-Saas zone and Combin zone, Western Alps) and implications for the exhumation mechanism and palaeogeography. International Journal of Earth Sciences, 96(2), 229-252.

Powell, R., Guiraud, M., White, R. W. 2005. Truth and beauty in metamorphic phase-equilibria: conjugate variables and phase diagrams. The Canadian Mineralogist, 43, 21-33.

Ramsay, J. G. 1967. Folding and fracturing of rocks. Mc Graw Hill Book Company, 568.

Ratschbacher, L., Frisch, W., Neubauer, F., Schmid, S. M., Neugebauer, J. 1989. Extension in compressional orogenic belts: The eastern Alps. Geology, 17, 404–407.

Rebay, G., Zanoni, D., Langone, A., Luoni, P., Tiepolo, M., Spalla, M.I. 2018. Dating of ultramafic rocks from the Western Alps ophiolites discloses Late Cretaceous subduction ages in the Zermatt-Saas Zone. Geological Magazine, 155, 298-315

Reddy, S.M., Wheeler, J., Butler, R.H.W., Cliff, R.A., Freeman, S., Inger, S., Pickles, C., Kelley, S.P. 2003. Kinematic reworking and exhumation within the convergent Alpine Orogen. Tectonophys., 365, 77-102.

Rehault, J.P., Boillot, G., Mauffred, A. 1984. The western Mediterranean Basin Geological Evolution. Mar. Geol. 55, 447-477.

Regorda, A., Spalla, M. I., Roda, M., Lardeaux, J. M., Marotta, A. M. 2021 Metamorphic facies and deformation fabrics diagnostic of subduction: Insights from 2D numerical models. Geochemistry, Geophysics, Geosystems, 22, e2021GC009899.

Rendinella, P. (2006). Rilevamento geologico e studio strati- grafico della successione cretacico-paleogenica di Pian Ambrogi – Massiccio del Marguareis (Alpi Marittime) [Geological mapping and stratigraphic study of the Cretaceous- Paleogene succession of Pian Ambrogi – Marguareis Massif (Maritime Alps)]. (Unpublished mas- ter's thesis). Università degli Studi di Torino, Torino.

Ricou, L. E. 1981. Glissement senestre des nappes penniques le long de la bordure nord de l'Argentera: Son role dans le jeu de l'arc alpin. Compte Rendu Académie Science Paris 292, 1305-1308.

Ricou, L. E., Siddans, A. W. B. 1986. Collision tectonics in the Western Alps. Geological Society, London, Special Publications, 19, 229-244.

Roda, M., Spalla, M. I., Marotta, A. M. 2012. Integration of natural data within a numerical model of ablative subduction: a possible interpretation for the Alpine dynamics of the Austroalpine crust. J. Metam. Geol., 30, 973-996.

Roda, M., Regorda, A., Spalla, M. I., Marotta, A. M. 2019. What drives A lpine T ethys opening? Clues from the review of geological data and model predictions. Geol. J., 54, 2646-2664.

Rubatto, D., Gebauer, D., Compagnoni, R., 1999. Dating of eclogite-facies zircons: the age of Alpine metamorphism in the Sesia-Lanzo Zone (Western Alps). Earth Planet. Sci. Lett., 167, 141-158.

Rolland, Y., Perincek, D., Kaymakci, N., Sosson, M., Barrier, E., Avagyan, A. 2012. Evidence for ~ 80–75 Ma subduction jump during Anatolide–Tauride–Armenian block accretion and ~ 48 Ma Arabia–Eurasia collision in Lesser Caucasus–East Anatolia. Journal of Geodynamics, 56, 76-85.

Rosenbaum, G., Lister, G.S., Duboz, C. 2002. Relative motions of Africa, Iberia and Europe during Alpine orogeny. Tectonophysics, 359, 117-129.

Rosenbaum, G., Lister, G.S. 2005. The Western Alps from the Jurassic to Oligocene: spatio-temporal

constraints and evolutionary reconstructions. Earth-Sci. Rev., 69, 281-306.

Roure, F., R. Polino, and R. Nicolich. 1990. Early Neogene deformation beneath the Po plain, constraints on the post-collisional Alpine evolution, in Deep Structure of the Alps, edited by F. Roure et al., Mere. Soc. Geol. Fr., 156, 309-322.

Rubatto, D., Hermann, J. 2001. Exhumation as fast as subduction? Geology, 29, 3-6.

Sanità, E., Lardeaux, J. M., Marroni, M., Gosso, G., Pandolfi, L. 2020. Structural relationships between Helminthoid Flysch and Briançonnais Units in the MarguareisMassif: A key for deciphering the finite strain pattern in the external southwestern Alps. Geol. J., 56, 2024-2040.

Sanità, E., Lardeaux, J. M., Marroni, M., Gosso, G., Pandolfi, L. 2021. Deciphering large-scale superposed fold systems at shallow crustal levels in collision zones: insights from the Marguareis Massif (southwestern Alps). Journal of Maps, 17, 571-580.

Sanità, E., Lardeaux, J. M., Marroni, M., Padolfi, L. 2022a. Kinematics of the Helminthoid Flysch-Marguareis Unit tectonic coupling: consequences for the tectonic evolution of the Western Alps. C. R. Géoscience, 354, 141-157.

Sanità, E., DI Rosa, M., Lardeaux, J. M., Marroni, M., Pandolfi, L. 2022b. Metamorphic peak estimates of the Marguareis Unit (Briançonnais Domain): New constrains for the tectonic evolution of the south-western Alps. Terra Nova, 00, 1-9.

Sanità, E., Di Rosa, M., Lardeaux, J. M., Marroni, M., & Pandolfi, L. (2022). The Moglio-Testico Unit (Ligurian Alps, Italy) as Subducted Metamorphic Oceanic Fragment: Stratigraphic, Structural and Metamorphic Constraints. Minerals, 12, 1343.

Sagri, M. 1979. Upper Cretaceous carbonate turbidites of the Alps and Apennines deposited below the calcite compensation level. Journal of Sedimentary Research, 49, 23-28.

Sagri, M. 1984. Litologia, stratimetria e sedimentologia delle torbiditi di piana di bacino del Flysch di San Remo (Cretaceo superiore, Liguria occidentale). Mem. Soc. Geol. lt., 28, 577-586.

Sanchez, G., Rolland, Y., Jolivet. M., Brichau, S. 2010. Exhumation controlled by transcurrent tectonics: the Argentera-Mercantour massif (SW Alps). Terra Nova, 23,116-126.

Sanchez, G., Rolland, Y., Schneider, J. 2011. Dating low-temperature deformation by 40Ar/39Ar on white mica, insights from the Argentera-Mercantour Massif (SW Alps). Lithos, 125, 521-536

Sassi, F. P., Scolari, A., 1974. The b0 Value of the Potassic White Micas as a Barometric Indicator in Low-Grade Metamorphism of Pelitic Schists. Contributions to Mineralogy and Petrology, 45, 143–152. https://doi.org/10.1007/bf00371166

Scaillet, S., Féraud, G., Lagabrielle, Y., Ballevre, M., Ruffet, G. 1990. 40Ar/39Ar laser-probe dating by step heating and spot fusion of phengites from the Dora Maira nappe of the western Alps, Italy. Geology, 18, 741-744.

Schmid, S.M., Pfiffner, O.A., Froitzheim, N., Schönborn, G., Kissling, E. 1996. Geophysical–geological transect and tectonic evolution of the Swiss–Italian Alps. Tectonics 15, 1036–1064.

Schmid, S. M., Fügenschuh, B., Kissling, E., Schuster, R. 2004. Tectonic map and overall architecture of the Alpine orogen. Eclogae Geologicae Helvetiae, 97, 93-117.

Schmid, S.M., Kissling, E., Diehl, T., Douwe, J.J., van Hinsemberg, J.J., Molli, G. 2017. Ivrea mantle wedge, arc of the Western Alps and kinematic evolution of the Alps-Apennines orogenic system. Swiss J. Geosci. 110, 581-612.

Schreiber, D., Lardeaux, J. M., Martelet, G., Courrioux, G., Guillen, A. 2010. 3-D modelling of Alpine Mohos in Southwestern Alps. Geophys. J. Int., 180, 961–975.

Schwartz, S., 2002. La zone pi.montaise des Alpes occidentales: un paleo-complexe de subduction. Arguments metamorpiques, geochronologiques et structuraux, Doc. B. R.G.M. 302.

Schwartz, S., Lardeaux, J.M., Tricart, P., Guillot, S., Labrin, E. 2007. Diachronous exhumation of HP–LT metamorphic rocks from south-western Alps: evidence from fission-track analysis. TerraNova, 19, 133-140.

Schwartz, S. Guillot, S. Reynard, B., Lafay, R., Nicollet, C., Debret, B., Auzende, A.L. 2013. Pressure–temperature estimates of the lizardite/antigorite transition in high pressure serpentinites. Lithos, 178, 197-210.

Seno, S. 1992. Finite strain and deformation within the Briançonnais Castelvecchio-Cerisola nappe of the Ligurian Alps, Italy. Journal of structural geology, 14, 825-838.

Seno, S., Dallagiovanna, G., Vanossi, M., 2005. A kinematic evolutionary model for the Penninic sector of the central Ligurian Alps. International Journal of Earth Sciences 94, 114-129.

Seno, S., Dallagiovanna, G., Vanossi, M. 2003. Palaeogeography and thrust development in the Penninic domain of the Western Alpine chain: examples

from the Ligurian Alps. Bollettino Società Geologica Italiana, 122, 223-232.

Simon-Labric, T., Rolland, Y., Dumont, T., Heymes, T., Authermayou, C., Corsini, M., Fornari, M. 2009. 40Ar/ 39Ar dating of Penninic Front tectonic displacement (W Alps) during the Lower Oligocene (31–34 Ma). Terra Nova, 21, 127-136.

Sinclair, H.D. 1997. Tectono–stratigraphic model for underfilled peripheral foreland basins: an Alpine perspective. GSA Bull, 109, 324-346.

Sissingh, W. 2001. Tectonostratigraphy of the west Alpine Foreland: correlation of Tertiary sedimentary sequences, changes in eustatic sea-level and stress regimes. Tectonophysics, 333, 361-400.

Spalla, M. I., Zanoni, D., Marotta, A. M., Rebay, G., Roda, M., Zucali, M., Gosso, G. 2014. The transition from Variscan collision to continental break-up in the Alps: insights from the comparison between natural data and numerical model predictions. Special Publications: Geol. Soc. London, London, 405, 363-400.

Speranza, F., Villa, I.M., Sagnotti, L., Florindo, F., Cosentino, D., Cipollari, P., Mattei, M. 2002. Age of the Corsica-Sardinia rotation and Liguro- Provençal Basin spreading: new paleomagnetic and Ar/Ar evidence. Tectonophys. 347, 231-251.

Stampfli, G. M. 1993. The Brianconnais, exotic terrane in the Alps? Eclogae Geologicae Helvetiae, 86, 1-45.

Stampfli, G., Mosar, J., Favre, PH., Pillevuit A., Vannay, J.-C. 2001a. Permo-Mesozoic evolution of the western Tethys realm: the Neo-Tethys East Mediterranean Basin connection. In: ZIEGLER P.A. et al. (Eds.): Peri-Tethys Memoir 6: Peri-Tethyan Rift/Wrench Basins and Passive Margins. M.m. Mus. Natn. Hist. Nat. Paris 186, 51–108.

Storti, F., Salvini, F., McClay, K. 2000. Synchronous and velocity-partitioned thrusting and thrust polarity reversal in experimentally produced, doubly-vergent thrust wedges: Implications for natural orogens. Tectonics, 19, 378-396.

Strzerzynski, P., Guillot, S., Leloup, P.H., Arnaud, N., Vidal, O., Ledru, P., Corrioux, G., Darmendrail, X. 2012. Tectono-metamorphic evolution of Brianconnains zone (Modane-Aussois and Southern Vanoise units, Lyon Turin transect, Western Alps). J. Geodyn. 56-57, 55-75.

Thöni, M., Miller, C., Zanetti, A., Habler, G., Goessler, W. 2008. Sm–Nd isotope systematics of high-REE accessory minerals and major phases: ID-TIMS, LA-ICP-MS and EPMA data

Trullenque, G., Ceriani, S., Fügenschuh, B., Schmid, S. M. 2003. Polyphase tectonic activity on the penninic front: implications for the evolution of the western Alps. In EGS-AGU-EUG Joint Assembly (p. 8861).

Vanossi, M. 1963. Segnalazione di una microfauna di età titonica nei calcari a facies di" Guillestre" della val Tanarello (Alpi marittime). Stabilimento tipografico Ferri.

Vanossi, M. 1965. Studio sedimentologico del flysch ad Elmintoidi della Valle Argentina (Liguria occidentale). Atti Ist. Geo. Univ. Pavia, 16, 36-70.

Vanossi, M. 1969. La serie Brianzonese del Salto del Lupo (Liguria Occidentale): osservazione sedimentologico-stratigrafiche [The Brian.onnais succession of Salto del Lupo (western Liguria): sedimentologic-stratigraphic observations]. Atti Istituto Geologico Universitario di Pavia, 20, 3-16.

Vanossi, M. 1972. Rilevamento geologico ed analisi strutturale delle dorsali del M. Mongioie e del M. Cimone (Brianzonese ligure).

Vanossi M., Cortesogno L., Galbiati B., Messiga B., Piccardo G. B., Vanucci R. 1984. Geologia delle Alpi Liguri: dati, prohlemi, ipotesi. Mem. Soc. Geol. It. 28, 5-57.

Vanossi, M., Cortesogno, L., Galbiati, B., Messiga, B., Piccardo, G.B., Vannucci, R. 1986. Geologia delle Alpi liguri: dati, problemi, ipotesi. Mem. Soc. Geol. Ital. 28, 5-75.

Vanossi, M., Perotti, C. R., Seno, S. 1994. The Maritime Alps arc in the Ligurian and Tyrrhenian systems. Tectonophysics, 230, 75-89.

Vidal, O., Parra, T. 2000. Exhumation paths of high-pressure metapelites obtained from local equilibria for chlorite-phengite assemblage. Geol. J. 2000, 35, 139-161

Vidal, O., De Andrade, V., Lewin, E., Munoz, M., Parra, T., Pascarelli, S. 2006. P-T deformation Fe2+/Fe3+ mapping at the thin section scale and comparison with XANES mapping: Application to a garnet-bearing metapelite from the Sambagawa metamorphic belt (Japan). J. Metam. Geol., 24, 669-683.

Vitale Brovarone, A., Beyssac, O., Malavieille, J., Molli, G., Beltrando, M., Compagnoni, R. 2012. Stacking and metamorphism of continuous segments of subducted lithosphere in a high-pressure wedge: The example of Alpine Corsica (France). Earth Sci. Rev. 116, 35-56

Warr, L. N., Ferreiro Mählmann, R., 2015. Recommendations for Kübler Index Standardization. Clay Minerals, 50(3): 283–286.

https://doi.org/10.1180/claymin.2015.050.3.02

Warr, L. N. IMA-CNMNC approved minerals symbols. Mineral. Mag., 85, 291-320.

Wheeler, J., Butler, R. W. H. 1994. Criteria for identifying structures related to true crustal extension in orogens. Journal of Structural Geology, 16, 1023–1027.

Weaver, C. E. 1961. Clay mineralogy of the late Cretaceous rocks of the Washakie Basin.

Weaver, C. E., Boekstra, B. R. 1984. Illite-Mica. In: Weaver, C. E., ed., Shale-Slate Metamorphism in Southern Appalachians (USA). Development in Sedimentology 10. Elsevier Science, Amsterdam. 67–97

Wortmann, U. G., Weissert, H., Funk, H., Hauck, J. 2001. Alpine platekinematics revisited: The adria problem. Tectonics, 20, 134–147.

Zaccagna, D., Franchi, S., & Novarese, S. 1934. Carta geologica d'Italia. Foglio 90, 597 Demonte [Geological Map of Italy, sheet 90, Demonte]. Servizio Geologico Italiano, Roma.

Zuffa, G.G.. 1980. Hybrid arenites: their composition and classification. J. Sediment. Petrol., 49, 21-29.

Zuffa, G.G. 1985. Optical analyses of arenites: influence of methodology on compositional results. In: Zuffa, G.G. (Ed.), Provenance of Arenites, NATO Advanced Study Institute, vol. 148. D. Reidel, Dordrecht,165-189.

- **International and National congresses (O: oral; P: poster)**

TSK 18 International congress, virtual conference, June 2021. **O;** "*The complexity of tectonics in external sectors of Western Alps: evidence from the boundary between Maritime and Ligurian Alps*". Authors: Sanità, E. Pandolfi, L., Lardeaux, J.M., Marroni, M., Gosso, G.
Waiting for Yorsget 2022, virtual conference, June 2021. **P;** "*Evidence of intricate finite strain pattern in the external sector of collisional belts: The case of Marguareis Massif (southwestern Alps)*". Authors: Sanità, E., Lardeaux, J.M. Marroni, M., Gosso, G., Pandolfi, L.
BeGeo Scientist 2021, live conference, October 2021. **O;** "*Record of shallow level tectonics in Low-grade continental units: Insights from the Marguareis Massif (southwestern Alps)*". Authors: Sanità, E., Lardeaux, J.M., Marroni, M., Gosso, G., Pandolfi, L.
27th Reunion de le sciences de la Terre (RST) 2021, live conference, November 2021; **O**; "*A key for deciphering the finite strain pattern in southwestern Alps: Insight from structural relationships between Helminthoid Flysch and Briançonnais Units (Marguareis Massif)*". Authors: Sanità, E., Lardeaux, J.M., Marroni, M., Gosso, G., Pandolfi, L.
27th Reunion de le sciences de la Terre (RST) 2021, live conference, November 2021; **P**; "*The Marguareis Massif: A natural lab to unravel large-scale superposed fold systems at shallow structural levels in collisional setting*". Sanità, E., Lardeaux, J.M., Marroni, M., Gosso, G., Pandolfi, L.
DRT conference 2022, live conference, July 2022; **O**; *"Tectono-metamorphic evolution of the Briançonnais Units along the southwestern edge of the Alps: Constraints from the Marguareis Massif (Western Ligurian Alps)".* Authors: Sanità, E., Di Rosa, M., Lardeaux, J.M., Marroni, M., Pandolfi, L.
DRT conference 2022, live conference, July 2022; **P**; *"Structural architecture and kinematics of the Helminthoid Flysch-Briançonnais Units coupling: A key for deciphering the tectonic evolution of the southwestern Alps".* Authors: Sanità, E., Lardeaux, J.M., Marroni, M., Pandolfi, L.
Congresso SGI-SIMP, live conference, September 2022; **O**; *"Structural evolution and Pressure-Temperature path (P-T path) of the Moglio-Testico Unit (Western Ligurian Alps): A re-appraisal".*Authors: Sanità, E., Di Rosa, M., Lardeaux, J.M., Marroni, M., Pandolfi, L.
Congresso SGI-SIMP, live conference, September 2022; **P**; *"Tectono-metamorphic evolution of the Briançonnais Units along the southwestern sectors of the Alps: Insights from the Marguareis Massif (Western Ligurian Alps".* Authors: Sanità, E., Di Rosa, M., Lardeaux, J.M., Marroni, M., Pandolfi, L.
The abstracts are in the attached file titled "*Certificates_Sanità_second_year*".

- **Awards**

Waiting for Yorsget 2022 - Best Poster Award for the contribute titled "*Evidence of intricate finite strain pattern in the external sector of collisional belts: The case of Marguareis Massif (southwestern Alps)*".

- **Published Papers**

Sanità, E., Lardeaux, J.M., Marroni, M., Gosso, G., Pandolfi, L. 2020. *Structural relationships between Helminthoid Flysch and Briançonnais Units in the Marguareis Massif: a key for deciphering the finite strain pattern in the external southwestern Alps.* Geological Journal, 56, 2024-2040.
Sanità, E., Lardeaux, J.M., Marroni, M., Gosso, G., Pandolfi, L. 2021. *Deciphering large-scale superposed*

fold systems at shallow crustal levels in collision zones: Insight from the Marguareis Massif (southwestern Alps). Journal of Maps, 17, 559-568.

Sanità, E., Lardeaux, J. M., Marroni, M., Pandolfi, L. 2022a. *Kinematics of the Helminthoid Flysch-Marguareis Unit tectonic coupling: conseguences for the tectonic evolution of Western Ligurian Alps. Comptes Rendus of Geoscience*. 354, 141-157.

Sanità, E., Di Rosa, M., Lardeaux, J. M., Marroni, M., Pandolfi, L. 2022b. *Metamorphic peak estimates of the Marguareis Unit (Briançonnais Domain): New constrains for the tectonic evolution of the south-western Alps*. Terra Nova, 00, 1-9.

Sanità, E., Lardeaux, J.M., Marroni, M., Gosso, G., Pandolfi, L. (2022c). *The Moglio-testico Unit as subducted metamorphic oceanic fragment: stratigraphic structural and metamorphic constraints.* Minerals, 12, 1343.

Supplementary

S1. Provenance

Table S1. List of the counting classes and the results of the modal analysis performed on Bordighera Sandstone (Helminthoid Flysch Unit, Ligurian Domain) and Cima Aurusi Formation (Cabanaira Unit, Briançonnais Domain).

	SAMPLE	*TSE 138*	*TSE 146*	*TSE 147*	*TSE 152 B*	*TSE 152 T*	*TSE139*	*TSE 136*	*TSE 199*	*TSE 233*	*TSE 140*
	sampled unit	FH	FH	FH	FH	FH	CU	CU	CU	CU	CU
	Formation	BOR	BOR	BOR	BOR	BOR	CAF	CAF	CAF	CAF	CAF
	grainsize	mgA	mgA	mg/gA	mgA	mgA	m/gA	m/gA	m/gA	m/gA	m/gA
	sorting	G	G	G/B	G	G	G	G	G	G	G
	counted point	500	500	500	500	500	500	500	500	500	500
Q	**medium quartz single crystal**	9,85	9,05	3,31	6,2	11,16	5,3	11,64	12,58	16,73	9,75
	coarse quartz single crystal	7,49	8,19	11,4	8,76	9,66	5,7	5,22	6,5	3,31	5,39
	fine quartz polycrystalline	2,57	1,72	1,45	2,56	1,07	4,28	2,3	4,4	2,06	4,15
	medium quartz polycrystalline	2,36	2,59	4,54	2,78	4,29	2,24	1,04	2,1	1,65	2,49
	Quartz in granitoid r.f.	1,28	3,88	4,13	3,42	4,51	1,63	3,64	4,82	2,69	3,53
	Quartz in metamorphic r.f.	0	0,22	0	0	1,72	0	0	0	0	0
	Quartz in vulcanic r.f.	2,36	0,86	4,47	1,92	3	1,63	2,51	1,68	1,24	2,07
K	**medium K-feldspar single crystal**	14,13	13,36	9,5	10,47	9,44	9,78	11,9	20,94	21,9	15,77
	coarse K-feldspar single crystal	12,85	13,14	15,91	17,95	16,74	7,94	12,67	7,55	4,75	9,13
	K-feldspar in granitoids r.f.	2,57	5,39	4,75	6,41	5,15	3,26	3,79	1,47	1,24	2,49
P	**medium plagioclase single crystal**	8,99	9,27	3,93	6,84	2,79	4,07	12,73	8,81	14,88	14,32
	coarse plagioclase single crystal	6,42	9,27	8,06	5,13	5,36	5,09	8,98	6,29	6,4	8,3
	Plagioclase in granitoids r.f.	3,21	3,86	3,93	4,7	3	5,3	0,94	3,35	3,51	3,53
F	**Feldspar (s.l.) in volcanic r.f.**	6,21	3,02	8,26	5,98	2,15	3,06	4,48	1,26	1,03	3,53
NCE											
Lv	**Acid volcanic r.f.**	11,13	8,41	9,3	8,55	10,52	12,22	12,32	13,21	11,57	10,58
	Medium volcanic r.f.	3	1,08	1,65	1,28	2,79	3,46	0,63	0	0	0,21
Lm	**low to high grade metamorphic r.f.**	2,79	5,82	3,31	4,48	5,15	2,04	0,85	0,84	1,24	0,83
Ls	**Siltstone siliciclastic r.f.**	0	0,22	0,21	0	0	0	0	0	0	0
L											
Phyl.	**Phyllosilicate single crystal**	1,93	0,43	0,42	1,07	0,86	0	2,71	2,1	3,31	2,28
	Phyllosilicate in granitoids r.f.	0,86	0	0,63	0,43	0,64	0	1,23	0,84	0,83	0,62
	Phyllosilicate in volcanic r.f.	0	0	0,42	0,64	0	0	0,21	0	0,21	0
Lc	**Grainstone r.f.**	0	0	0	0	0	0	0	0	0	0
	Wackestone r.f.	0	0	0	0	0	0	0	0	0	0
	Mudstone r.f.	0	0	0	0	0	0	0	0	0	0
	Limeclast	0	0	0	0	0	2,44	0	0,84	0,21	0,21
CE											
NCI	**Siliciclastic rip-up (clay chips) r.f.**	0	0	0	0,43	0	0	0	0,42	0,21	0,41
CI	**Bioclast**	0	0	0	0	0	20,36	0	0	0,62	0,41
	Carbonatic rip-up (clay chips) r.f.	0	0	0	0	0	0	0	0	0	0
U	**Alterite**	0	0,22	0,42	0	0	0,2	0,21	0	0,41	0
	Total framework %	100	100	100	100	100	100	100	100	100	100
	Framework	93,4	92,8	96,8	93,6	93,2	98,2	95,8	95,4	96,76	96,4
	Siliciclastic matrix	3,8	4,2	1,8	4,6	4,2	0,6	3,6	4,4	2,64	3,6
	Calcite patchy	0,6	1,2	0,4	1,4	2	1,2	0,6	0,2	0,6	
	metamorphic re-crystallization	2,2	1,8	1	0,4	0,6					
	Total %	100	100	100	100	100	100	100	100	100	100

S2. Thermobarometry

1.1 Marguareis Unit

Chemical analysis, bulk composition and micromapping: the electron probe micro analysis (EPMA) data have been acquired using a JEOL 8800 electron microprobe apparatus of the Dipartimento di Scienze della Terra "A. Desio" (Milano, Italia), equipped with five wavelength-dispersive spectrometers and calibrated with the following standards: wollastonite (Ca, Si), orthoclase (K), albite (Al), periclase (Mg), rhodonite (Mn), TiO2 (Ti), Al2O3 (Al), Fe2O3 (Fe) and Cr2O3 (Cr). The operating conditions were 15 keV accelerating voltage, 17 µA sample current and 5 ms per grid point counting time. Two compositional maps and a total of 80 spot analysis was acquired; the X-ray maps resolution and the analytical spot size were set at 0,7 µm, as recommended by Lanari et al., (2014c), to detect any zoning in phengite and chlorite. The compositional map was calibrated with the spot analyses (De Andrade et al., 2006) using XMapTools 2.1.3 software (Lanari et al., 2014c), in order to obtain quantitative maps of oxide (wt %).

Chl-Qz-wt method: this method is based on the convergence of the reactions involving the Chl end-members (Mg- and Fe-Amesite, Clinochlore, Daphnite and Sudoite) in presence of quartz and water (Vidal et al., 2006). This thermometer is based on the equilibria 4 Clc + 5 Fe-Ame = 4 Dph + 5 Mg-Ame and 4 Dph + + 6 Sud = 5 Fe-Ame + 3 Mg-Ame + 14 Qz + 8 H2O. The *T* range in which the chlorite is in equilibrium is represented by histogram. Computations were made using the software ChlMicaEqui (Lanari, 2012). Using this matlab-based script we are able to plot the T resulting from the Chl-Qz-wt method of Vidal et al. (2006) into histograms by setting pressure, Fe3+ content and water activity. All the calculations were performed considering an equilibrium tolerance of 200 (J) and the uncertainty associated with each temperature range is ± 30 °C.

Phg-Qz-wt method: this method is based on the convergence of the reactions involving the Phg end-members (Celadonite, Muscovite, Pyrophyllite) in presence of quartz and water (Dubacq et al., 2010). This is a geobarometer based on the relative proportions of Phg end-members that are mainly controlled by Tschermak and Pyrophyllite substitutions (i.e., Guidotti and Sassi, 1998) reactions: Prl(H) = Prl + H_2O and 3Mg-Cel + 2Prl = 2Ms + Phl + 11Qtz + $2H_2O$ where Prl(H) is hydrated Prl. The estimations were performed for fixed temperature ranges and approximating the Fe^{3+} following Vidal et al. (2006), The equilibrium conditions of Phg are represented by a divariant line in the *P*–*T* space along which the amount of water (i.e., XH_2O %) in the interlayer site content varies (Dubacq et al., 2010). Pressure and XH_2O have been simultaneously estimated at a given temperature for selected water activity values (see main text). Computations were made using the

software ChlMicaEqui (Lanari, 2012). Using this matlab-based script we are able to plot the P resulting from the Phg-Qz-wt method of Dubacq et al. (2010) for specific water content into the P-T space by setting temperature, Fe3+ content and water activity. The operation is calculated for each single Phg analysis selected into the microdomains. All the calculations were performed considering an equilibrium tolerance of 200 (J) and the uncertainty associated with each P range is ± 0.2 GPa.

Chl-Phg-Qz-wt method: this is a semi-empirical approach based on the thermodynamic database proposed by Breman (1988) and implemented by Vidal and Parra (2000). This method consists in the determination of the points in the *P–T* diagram where all the independent reactions are intersected; such condition is satisfied whenever the Chl-Phg pairs are in equilibrium within the microstructure. For each sample, several Chl-Phg pairs have been selected within the S1 and S2 foliations, in order to test the *P–T* conditions related to the D1 an D2 phases. In the system K2O–Al2O3–MgO–SiO2–H2O, the assemblage Chl+Phg+Qtz+H2O has two degrees of freedom. The number of independent equilibria (IR) that can be calculated from this assemblage depends on the number of end-members (EM) used to describe the composition of Chl and Phg:

IR=(EM+2) -C

where "+2" correspond to the presence of water and quartz. The *P–T* conditions have been calculated using 64 equilibria involving the five Chl (Clin, Fe- and Mg-Am, Daph and Mg-Sud) and four dioctahedral Phg (Mg- and Fe-Cel, Ms and Prl) end-members (Vidal *et al.*, 2006 and references therein). To test the accuracy of the Chl-Phg-Qtz-H2O multiequilibrium approach, other thermodynamic methods were applied on the Phg (Massonne and Schreyer, 1987) and the Chl (Cathelineau, 1988). Equilibrium was considered to be achieved if the intersections between all equilibria present a scatter lower than 25 °C and 0.08 GPa; these values have been calculated with the Monte Carlo technique, as recommended by Vidal and Parra (2000). The Chl-Phg couples processed with the Chl-Phg-Qtz-H2O multi-equilibrium are the same studied with the Chl-Qtz-H2O and Phg-Qtz-H2O methods and the results have been compared with the previous one. Computations were made using the software ChlMicaEqui (Lanari, 2012). Using this matlab-based script we are able to plot the P-T results related to selected couples of Chl and Phg growing into the same microstructure, following the methodology modelled by Vidal and Parra (2000). The operation is calculated for each Chl-Phg couple into the P-T space by setting the Fe3+ content and water activity. Only the values which require low free Gibbs energy (this value is specified into the text) are considered in this work.

Figure S1**.** Fe in D1 and D2 phase-related chlorites in the micromap of sample ED1 (intensity map: Fe Kα).

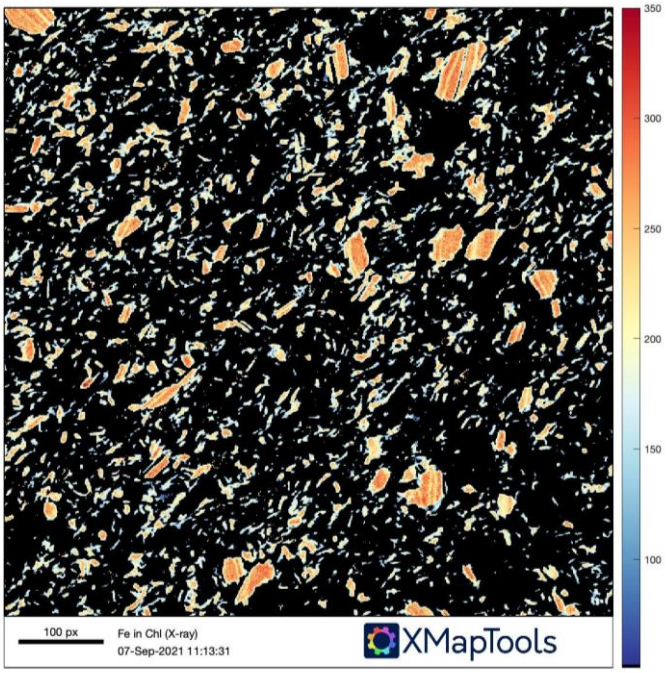

Figure S2. K in D1 and D2 phase-related phengites in the micromap of sample TSE236 (intensity map: K Kα).

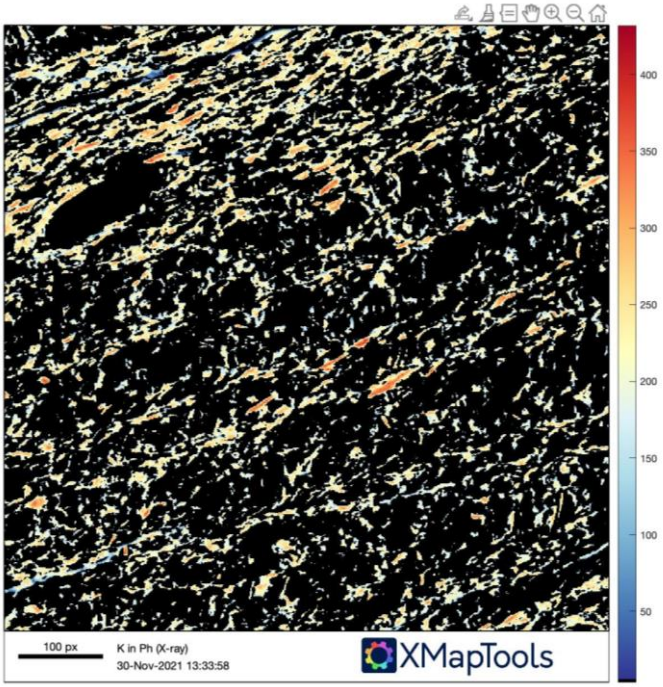

Figure S3. Distribution of temperature based on Cathelineau (1988) geothermometer on D1 and D2 phase-related chlorites in sample TSE236.

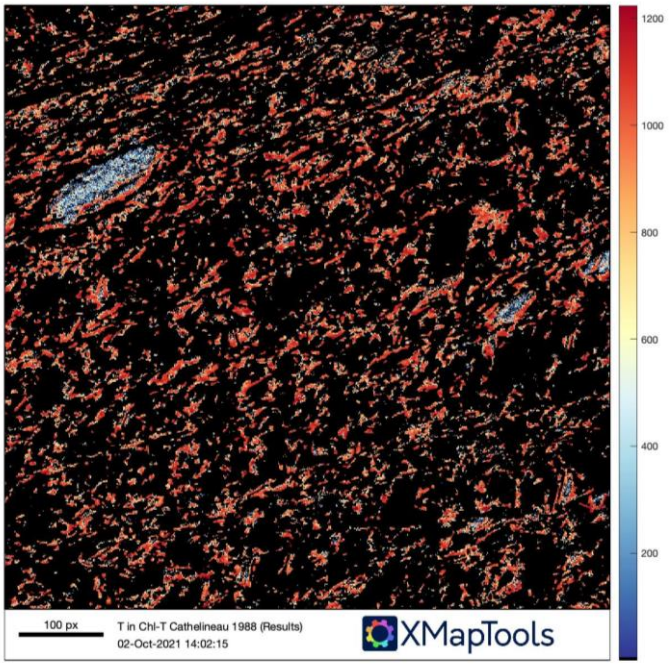

Table S1. Representative chlorite EPMA analysis.

Sample ED1

	Chl D1					*Chl D2*				
Chl analysis	*31*	*32*	*33*	*34*	*35*	*36*	*37*	*38*	*39*	*40*
Wt%										
SiO_2	26.47	25.55	25.08	25.36	25.03	26.28	28.96	25.94	25.47	25.39
TiO_2	0.02	0.05	0.00	0.04	0.03	0.06	0.05	0.01	0.00	0.08
Al_2O_3	21.81	21.38	21.64	21.92	21.19	21.65	21.38	21.24	21.99	21.96
FeO	28.67	28.03	28.94	29.00	28.38	27.37	25.03	29.76	29.76	28.84
MnO	0.13	0.10	0.09	0.13	0.14	0.07	0.08	0.14	0.12	0.13
MgO	10.10	11.33	11.09	11.13	11.09	11.65	9.09	9.82	10.22	11.54
CaO	0.04	0.03	0.06	0.02	0.05	0.04	0.05	0.03	0.02	0.02
Na_2O	0.05	0.04	0.06	0.01	0.00	0.05	0.09	0.00	0.05	0.06
K_2O	0.93	0.22	0.13	0.18	0.05	0.32	1.42	0.12	0.58	0.11
tot.	88.25	86.80	87.10	87.86	86.06	87.53	87.16	88.10	88.23	88.16
Cations										
Si	2.82	2.76	2.73	2.72	2.74	2.80	3.01	2.81	2.73	2.74
Ti	0.00	0.00	0.00	0.00	0.00	0.01	0.00	0.00	0.00	0.01
Al	2.74	2.72	4.14	2.77	2.73	2.72	2.69	2.71	2.78	2.80
Fe^{2+}	2.56	2.53	2.62	2.60	2.60	2.44	2.23	2.70	2.67	2.61
Mn	0.01	0.01	0.01	0.01	0.01	0.01	0.01	0.01	0.01	0.01
Mg	1.61	1.83	1.79	1.78	1.81	1.85	1.44	1.59	1.64	1.65
Ca	0.01	0.00	0.01	0.00	0.01	0.01	0.01	0.00	0.00	0.00
Na	0.01	0.01	0.01	0.00	0.00	0.01	0.02	0.00	0.01	0.01
K	0.13	0.03	0.02	0.03	0.01	0.04	0.19	0.02	0.08	0.08
sum ox	14	14	14	14	14	14	14	14	14	14
XMg	0.39	0.42	0.41	0.41	0.41	0.43	0.39	0.37	0.38	0.42
vacancy	0.19	0.12	0.09	0.10	0.10	0.16	0.43	0.17	0.12	0.09

Sample TSE236

	Chl D1					*Chl D2*				
Chl analysis	*58*	*60*	*61*	*64*	*69*	*70*	*71*	*72*	*73*	*74*
Wt%										
SiO_2	25.25	26.17	25.22	25.34	29.52	26.46	26.13	26.38	25.34	27.24
TiO_2	0.03	-	-	0.01	0.11	0.11	0.10	0.01	0.04	0.03
Al_2O_3	21.02	22.62	21.48	21.42	23.70	22.75	22.10	22.09	21.94	21.7
FeO	28.89	28.22	26.88	28.64	21.44	26.88	27.00	25.37	25.60	26.90
MnO	0.31	0.16	0.42	0.23	0.23	0.30	0.41	0.30	0.26	0.31
MgO	11.84	10.03	12.39	10.18	9.03	10.88	10.91	11.37	9.15	9.32
CaO	0.03	0.13	0.05	0.14	0.10	0.09	0.02	0.03	0.09	0.22
Na_2O	0.14	0.11	0.07	0.32	0.55	0.06	0.04	0.24	0.29	0.29
K_2O	0.03	0.26	0.05	0.40	1.58	0.06	0.56	0.69	0.81	0.49
tot.	87.58	87.73	86.56	86.72	86.25	87.64	87.30	86.53	83.55	86.50
Cations										
Si	2.72	2.79	2.72	2.76	3.08	2.80	2.79	2.82	2.82	2.93
Ti	0.00	0.00	0.00	0.00	0.01	0.01	0.01	0.00	0.00	0.00
Al	2.67	2.84	2.73	2.75	2.91	2.83	2.78	2.78	2.88	2.75
Fe^{2+}	2.60	2.51	2.42	2.61	1.87	2.38	2.41	2.27	2.38	2.42
Mn	0.03	0.01	0.04	0.02	0.02	0.03	0.04	0.03	0.02	0.03
Mg	1.90	1.59	1.99	1.65	1.40	1.71	1.74	1.81	1.52	1.49
Ca	0.00	0.01	0.01	0.02	0.01	0.01	0.00	0.00	0.01	0.03
Na	0.03	0.02	0.01	0.07	0.11	0.01	0.01	0.05	0.06	0.06
K	0.00	0.04	0.01	0.06	0.21	0.01	0.08	0.09	0.12	0.07
sum ox	14	14	14	14	14	14	14	14	14	14
XMg	0.42	0.39	0.45	0.39	0.43	0.42	0.42	0.44	0.39	0.38
vacancy	0.05	0,21	0,08	0,13	0,53	0,21	0,18	0,21	0,26	0,30

Table S2. Representative phengite EPMA analysis.

Sample ED1

	Phg D1					*Phg D2*				
Phg analysis	*56*	*57*	*25*	*26*	*45*	*46*	*41*	*42*	*43*	*44*
Wt%										
SiO_2	42.36	48.61	46.66	49.70	47.21	41.39	49.32	46.30	48.99	48.67
TiO_2	0.59	0.10	1.14	0.34	0.23	2.82	0.52	0.54	3.85	0.00
Al_2O_3	26.49	31.19	29.69	28.12	31.72	28.33	31.34	29.97	30.35	32.65
FeO	3.89	1.70	3.09	2.22	1.55	6.61	2.04	3.66	2.45	1.33
MnO	0.00	0.00	0.03	0.08	0.00	0.09	0.00	0.04	0.04	0.00
MgO	1.23	1.16	1.96	1.30	1.48	3.31	1.94	2.35	1.79	1.34
CaO	0.12	0.04	0.08	0.10	0.06	0.06	0.07	0.18	0.07	0.10
Na_2O	0.49	0.19	0.50	0.47	0.50	0.48	0.45	0.55	0.49	0.80
K_2O	8.54	9.55	8.84	8.52	8.76	6.99	8.79	7.91	8.02	8.56
tot.	83.74	92.60	92.02	90.89	91.51	90.15	94.50	91.53	96.06	93.49
Cations										
Si	3.25	3.30	3.22	3.43	3.24	2.98	3.28	3.20	3.21	3.26
Ti	0.03	0.01	0.06	0.02	0.01	0.15	0.03	0.03	0.19	0.00
Al	2.39	2.50	2.42	2.29	2.56	2.41	2.45	2.44	2.34	2.58
Fe^{2+}	0.25	0.10	0.18	0.13	0.09	0.40	0.11	0.21	0.13	0.08
Mn	0.00	0.00	0.00	0.01	0.00	0.01	0.00	0.00	0.00	0.00

Mg	0.14	0.12	0.20	0.13	0.15	0.36	0.19	0.24	0.18	0.13
Ca	0.01	0.00	0.01	0.01	0.00	0.01	0.01	0.01	0.01	0.01
Na	0.07	0.03	0.07	0.06	0.07	0.08	0.06	0.07	0.06	0.10
K	0.84	0.83	0.78	0.75	0.75	0.64	0.75	0.77	0.67	0.69
sum ox	11	11	11	11	11	11	11	11	11	11
vacancy	0.08	0.14	0.15	0.18	0.16	0.29	0.20	0.21	0.26	0.16

Sample TSE236

	Phg D1					*Phg D2*				
Phg analysis	*65*	*66*	*85*	*68*	*75*	*76*	*77*	*67*	*87*	*88*
Wt%										
SiO_2	41.63	45.78	43.90	43.65	50.82	39.84	40.86	39.64	41.04	39.93
TiO_2	0.20	0.50	1.51	0.69	0.26	3.48	0.44	0.13	0.19	1.98
Al_2O_3	28.27	33.93	26.50	29.44	34.57	27.57	27.76	28.31	27.42	26.45
FeO	5.61	1.46	4.08	6.04	2.37	7.79	8.06	8.72	7.81	8.86
MnO	1.72	0.13	0.00	0.35	0.03	0.00	1.93	1.95	0.07	0.13
MgO	2.09	0.63	2.30	2.16	1.04	3.38	3.11	2.76	3.25	3.18
CaO	0.31	0.10	0.11	0.27	0.12	0.13	0.36	0.54	0.13	1.02
Na_2O	0.80	0.84	0.51	0.98	0.53	0.82	0.84	0.76	1.02	0.65
K_2O	6.66	9.57	7.78	6.98	7.86	5.91	6.20	6.91	6.63	5.73
tot.	87.34	92.99	86.73	90.59	97.64	88.99	89.61	89.72	87.56	87.96
Cations										
Si	3.09	3.12	3.23	3.11	3.25	2.90	3.00	2.94	3.05	2.97
Ti	0.01	0.03	0.08	0.04	0.01	0.19	0.02	0.01	0.01	0.11
Al	2.47	2.72	2.30	2.47	2.61	2.37	2.41	2.48	2.41	2.32
Fe^{2+}	0.35	0.08	0.25	0.36	0.13	0.47	0.50	0.54	0.49	0.55
Mn	0.11	0.01	0.00	0.02	0.00	0.00	0.12	0.12	0.00	0.01
Mg	0.23	0.06	0.25	0.23	0.10	0.37	0.34	0.31	0.36	0.35
Ca	0.03	0.01	0.01	0.02	0.01	0.01	0.03	0.04	0.01	0.08
Na	0.12	0.11	0.07	0.14	0.07	0.12	0.12	0.11	0.15	0.09
K	0.63	0.83	0.73	0.63	0.57	0.73	0.58	0.65	0.63	0.63
sum ox	11	11	11	11	11	11	11	11	11	11
vacancy	0.23	0.05	0.19	0.21	0.29	0.32	0.27	0.19	0.21	0.28

1.2 Moglio-Testico Unit

Chemical analysis, bulk composition and micro-mapping: the electron probe micro analysis (EPMA) data have been acquired using a JEOL 8800 electron microprobe apparatus of the Dipartimento di Scienze della Terra "Ardito Desio" (Milano, Italy), equipped with five wavelength-dispersive spectrometers and calibrated with the following standards: wollastonite (Ca, Si), orthoclase (K), albite (Al), periclase (Mg), rhodonite (Mn), TiO2 (Ti), Al2O3 (Al), Fe2O3 (Fe) and Cr2O3 (Cr), The operating conditions were 15 keV accelerating voltage, 17 µA sample current and 20 ms per grid

point counting time. Two compositional maps and a total of 31 spot analysis was acquired; the X-ray maps resolution and the analytical spot size were set at 0,7 µm, as recommended by Lanari et al, (2014b), to detect any zoning in phengite and chlorite. The compositional map was calibrated with the spot analyses (De Andrade et al., 2006) using XMapTools 3.4.1 software (Lanari et al., 2014c), in order to obtain quantitative maps of oxide (wt %).

Chl-Qz-wt method: this method is based on the convergence of the reactions involving the Chl end-members (Mg- and Fe-Amesite, Clinochlore, Daphnite and Sudoite) in presence of quartz and water (Vidal et al., 2006), This thermometer is based on the equilibria 4 Clc + 5 Fe-Ame = 4 Dph + 5 Mg-Ame and 4 Dph + + 6 Sud = 5 Fe-Ame + 3 Mg-Ame + 14 Qz + 8 H2O, The *T* range in which the chlorite is in equilibrium is represented by histogram, Computations were made using the software ChlMicaEqui (Lanari, 2012), All the calculations were performed considering an equilibrium tolerance of 200 (J) and the uncertainty associated with each temperature range is ± 30 °C.

Phg-Qz-wt method: this method is based on the convergence of the reactions involving the Phg end-members (Celadonite, Muscovite, Pyrophyllite) in presence of quartz and water (Dubacq et al., 2010), This is a geobarometer based on the relative proportions of Phg end-members that are mainly controlled by Tschermak and Pyrophyllite substitutions (i.e., Guidotti and Sassi, 1998) reactions: Prl(H) = Prl + H_2O and 3Mg-Cel + 2Prl = 2Ms + Phl + 11Qtz + 2H_2O where Prl(H) is hydrated Prl. The estimations were performed for fixed temperature ranges and approximating the Fe^{3+} following Vidal et al. (2006) The equilibrium conditions of Phg are represented by a divariant line in the *P*–*T* space along which the amount of water (i,e,, *X*H_2O %) in the interlayer site content varies (Dubacq et al., 2010). Pressure and *X*H_2O have been simultaneously estimated at a given temperature for selected water activity values (see main text). Computations were made using the software ChlMicaEqui (Lanari, 2012). All the calculations were performed considering an equilibrium tolerance of 200 (J) and the uncertainty associated with each P range is ± 0,2 GPa.

Chl-Phg-Qz-wt method: this is a semi-empirical approach based on the thermodynamic database proposed by Breman (1988) and implemented by Vidal and Parra (2000). This method consists in the determination of the points in the *P*–*T* diagram where all the independent reactions are intersected; such condition is satisfied whenever the Chl-Phg pairs are in equilibrium within the microstructure, For each sample, several Chl-Phg pairs have been selected within the S1 and S2 foliations, in order to test the *P*–*T* conditions related to the D1 an D2 phases, In the system K2O–Al2O3–MgO–SiO2–H2O, the assemblage Chl+Phg+Qtz+H2O has two degrees of freedom, The number of independent equilibria (IR) that can be calculated from this assemblage depends on the number of end-members (EM) used to describe the composition of Chl and Phg:

IR=(EM+2) -C

where "+2" correspond to the presence of water and quartz, The *P–T* conditions have been calculated using 45 equilibria involving the five Chl (Clin, Fe- and Mg-Am, Daph and Mg-Sud) and four dioctahedral Phg (Mg- and Fe-Cel, Ms and Prl) end-members (Vidal *et al*,, 2006 and references therein). To test the accuracy of the Chl-Phg-Qtz-H2O multiequilibrium approach, other thermodynamic methods were applied on the Phg (Massonne & Schreyer, 1987) and the Chl (Cathelineau, 1988; Bourdelle & Cathelineau, 2015, see the main text), Equilibrium was considered to be achieved if the intersections between all equilibria present a scatter lower than 25 °C and 0,08 GPa; these values have been calculated with the Monte Carlo technique, as recommended by Vidal and Parra (2000). The Chl-Phg couples processed with the Chl-Phg-Qtz-H2O multi-equilibrium are the same studied with the Chl-Qtz-H2O and Phg-Qtz-H2O methods and the results have been compared with the previous one.

Figure S4. Fe in D1 and D2 phase-related chlorites in the micromap of sample ED18 (oxide weight percentage).

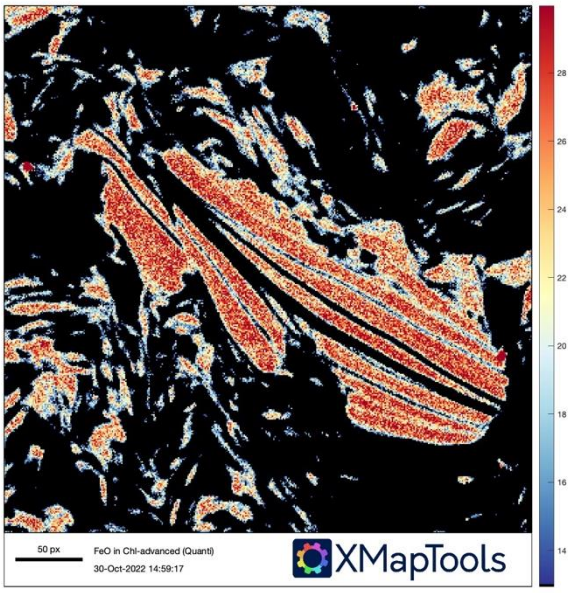

Figure S5. K in D1 phase-related phengites in the micromap of sample ED91 (oxide weight percentage).

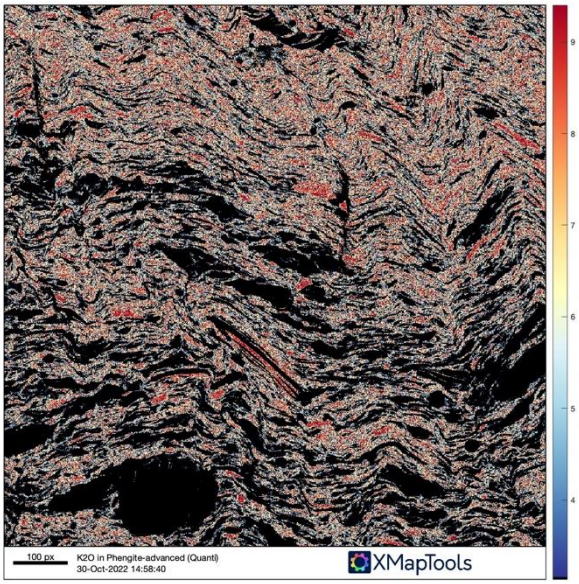

Figure S6. Distribution of pressure based on Massonne and Schreyer (1987) in D1 and D2 phase-related phengites in sample ED18.

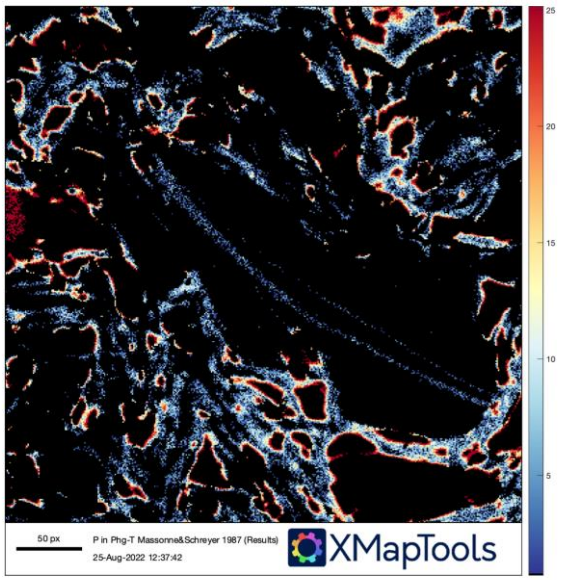

Table S3. Chlorite and Phengite analysis selected on X-ray calibrated map with XMapTools software and considered for the thermobarometric estimation.

Sample ED18

Wt%	Chl D1				Phg D1			
	Chl1	*Chl5*	*Chl7*	*Chl3*	*Phg1*	*Phg2*	*Phg7*	*Phg8*
SiO_2	30.34	25.14	27.3	27.3	46.28	43.06	45.88	46.28
TiO_2	0.15	0.15	0.15	0.15	2.21	3.54	0.00	0.00
Al_2O_3	23.72	22.11	19.5	19.5	24.24	24.24	29.03	24.76
FeO	26.99	24.99	25.99	25.99	8.79	11.86	8.79	8.35
MnO	0.04	0.03	0.02	0.02	0.01	0.00	0.01	0.01
MgO	13.63	11.26	17.19	17.19	2.85	3.29	3.07	2.2
CaO	0.02	0.02	0.01	0.01	0.01	0.01	0.01	0.01
Na_2O	0.09	0.04	0.12	0.12	1.20	1.20	0.93	1.33
K_2O	1.21	0.94	0.67	0.67	5.28	5.12	5.66	6.05
Total	96.19	84.68	90.95	90.95	90.87	92.32	93.38	88.99
Cations								
Si	2.90	2.75	2.79	2.79	3.28	3.10	3.16	3.35
Al	2.67	2.85	2.34	2.34	2.03	2.05	2.36	2.12
Ti	0.01	0.01	0.01	0.01	0.11	0.19	0.00	0.00
FeTOT	2.15	2.29	2.22	2.22	0.52	0.71	0.51	0.51
Mn	0.00	0.00	0.00	0.00	0.00	0.00	0.00	0.00
Mg	1.94	1.84	2.61	2.61	0.30	0.35	0.32	0.24
Ca	0.00	0.00	0.00	0.00	0.00	0.00	0.00	0.00
Na	0.02	0.01	0.02	0.02	0.17	0.17	0.12	0.19
K	0.15	0.13	0.09	0.09	0.48	0.46	0.50	0.56
sum ox	14	14	14	14	11	11	11	11
XMg	0.47	0.44	0.54	0.54	0.36	0.33	0.38	0.31
vacancy	0.23	0.18	0.04	0.08	0.35	0.36	0.37	0.25

Wt%	Chl D2				Phg D2			
	Chl4	*Chl14*	*Chl6*	*Chl31*	*Phg13*	*Phg20*	*Phg17*	*Phg7*
SiO2	26.87	27.3	28.17	28.6	51.11	45.08	46.68	51.51
TiO_2	0.15	0.29	0.44	0.00	0.88	3.09	1.77	0.44
Al_2O_3	26.33	23.11	24.72	25.32	25.78	31.07	34.15	32.44
FeO	21.66	28.66	27.32	27.99	3.08	3.51	2.64	3.95
MnO	0,02	0.02	0.03	0.01	0.00	0.00	0.01	0.00
MgO	10,08	7.71	9.78	9.78	1.54	1.10	1.98	1.98
CaO	0,01	0.02	0.02	0.01	0.01	0.01	0.01	0.01
Na_2O	0.22	0.17	0.16	0.12	0.80	1.47	0.53	0.80
K_2O	1.88	0.4	2.15	0.54	6.13	6.98	7.29	7.06
Total	87.22	87.68	92.79	92.37	89.33	92.31	95.05	98.19
Cations								
Si	2.78	2.90	2.82	2.85	3.54	3.10	3.10	3.28
Al	3.22	2.89	2.92	2.97	2.11	2.51	2.66	2.44
Ti	0.01	0.02	0.03	0.00	0.05	0.16	0.09	0.02
FeTOT	1.88	2.55	2.29	2.33	0.18	0.20	0.15	0.21
Mn	0.00	0.00	0.00	0.00	0.00	0.00	0.00	0.00

Mg	1.56	1.22	1.46	1.45	0.16	0.11	0.19	0.18
Ca	0.00	0.00	0.00	0.00	0.00	0.00	0.00	0.00
Na	0.04	0.04	0.03	0.02	0.12	0.20	0.07	0.09
K	0.25	0.05	0.27	0.07	0.50	0.61	0.61	0.57
sum ox	14	14	14	14	11	11	11	11
XMg	0.45	0.32	0.38	0.38	0.47	0.36	0.57	0.47
vacancy	0.39	0.35	0.28	0.34	0.35	0.19	0.32	0.33

Sample ED91

Wt%	Chl D1				Phg D1			
	Chl3	*Chl4*	*Chl6*	*Chl10*	*Phg8*	*Phg20*	*Phg12*	*Phg16*
SiO_2	20.64	25.8	25.8	28.9	43.36	38.15	43.36	38.15
TiO_2	0.08	0.00	0.16	0.08	1.27	0.64	0.64	0.64
Al_2O_3	17.11	22.37	18.42	24.31	24.81	24.81	24.81	21.42
FeO	18.09	25.84	25.84	24.74	9.45	2.7	5.4	6.75
MnO	0.1	0.00	0.1	0.07	0.00	0.01	0.00	0.01
MgO	7.69	7.96	12.73	10.81	2.86	2.86	2.54	1.91
CaO	0.04	0.14	0.02	0.0214	0.05	0.05	0.00	0.08
Na_2O	0.00	0.00	0.00	0.10	0.00	0.61	0.00	0.00
K_2O	0.39	0.1	0.00	1.64	6.79	4.7	6.27	6.27
Total	64.14	82.21	83.07	90.67	88.59	74.53	83.02	75.23
Cations								
Si	2.93	2.89	2.91	2.89	3.20	3.20	3.32	3.29
Al	2.86	2.96	2.89	2.43	2.16	2.45	2.24	2.17
Ti	0.01	0.00	0.01	0.01	0.07	0.04	0.04	0.04
FeTOT	2.15	2.42	2.08	2.42	0.58	0.19	0.35	0.49
Mn	0.01	0.00	0.01	0.01	0.00	0.00	0.00	0.00
Mg	1.63	1.33	1.62	2.12	0.31	0.36	0.29	0.25
Ca	0.01	0.02	0.00	0.00	0.00	0.00	0.00	0.01
Na	0.00	0.00	0.02	0.00	0.00	0.10	0.00	0.00
K	0.07	0.01	0.21	0.00	0.64	0.50	0.61	0.69
sum ox	14	14	14	14	11	11	11	11
XMg	0.43	0.35	0.44	0.47	0.35	0.65	0.46	0.34
vacancy	0.36	0.37	0.36	0.1	0.36	0.39	0.39	0.30

S.3 Illite Crystallinity Index (Ill_{IC}) and b0 cell parameter

1.1 Illite crystallinity

Fresh carbonate-poor sample of pelites were disaggregated in a jaw crusher for about 20 minutes to obtain the whole-rock powder following the procedure proposed by (Leoni et al., 1996) The obtained powder was subsequently treated to separate the <2 µm particles from the whole-rock powder via differential settling, with distillated water, for a time about of 4 hours. The particles <2 µm was treated with Mg^{++} and K^{++} aqueous solutions. These were, subsequently centrifugated to separate the aqueous solution from the particles. The particles were subsequently smeared on glass slides. In the latter, the Full Width at Half Maximum (FWHM) values expressed in Δ2theta CuKa unit of the Illite 10 Å peaks were measured using X-Ray Diffractometer (XRD) patterns of highly oriented (=glycolated) <2 µm grain-size fraction to account for the possible presence of mixed-layers (i.e., illite/smectite, Ferreiro Mählmann and Frey, 2012; Ferreiro Mählmann et al., 2012). The XRD patterns were obtained using a Philips PW1710 automatic diffractometer, equipped with a long fine-focus Cu tube with the following acquisition setting: CuKalfa Ni-filtered radiation, 40 kV; 20 mÅ; slits:1/2° divergence and scatter 0.2 mm receiving; continuous scanning; scan speed: 0.25 Δ2theta/minute; dwell time: 3s. For the identification of clay minerals, XRD patterns of glycolated <2 µm grain sizes were scanned in the air-dried and glycolated states from 2 to 18 Δ2theta in order to verify the presence of mixed-layer. The KI indexes were measured on the oriented glycolated samples using the DIFFRAC.EVA v4.1 software. The Ill_{IC} values were then converted for the CIS scale (Warr and Ferreiro Mahaltman, 2015).

1.2 b0 cell parameter measurement

The mica b0 cell parameter was calculated measuring the $d_{060,331}$ using the (211) quartz reflection as an internal standard (Padan et al., 1982; Sassi and Scolari, 1974; Kisch et al.., 2006); the positions of mica and quartz reflections were determinated on randomly oriented whole rock powder sample of carbonate-poor pelites run by step scanning from 59° to 63° with a scan speed of 0.25°/minute. The b0 value were calculated following the formula: $b_0 = d_{(060,331)} \times 6$. The measures were obtained using the DIFFRAC.EVA v4.1 software.

Table S4. Illite Crystallinity Index and Illite "b_0" cell parameter values with the related metamorphic grades.

Sample	Tectonic Unit	Thickness	Ill_{FWHM}	KI-CIS_{corr}	Metamorphic Zone (KI-CIS_{corr})	$2\theta_{qtz}$	$2\theta_{ill}$	$2\theta_{ill}$*	d	Ill "b_0"
203	CU	2,08	0,195	0,15	epizone	59,955	61,725	61,710	1,502	9,011
204	CU	1,13	0,208	0,17	epizone	59,920	61,730	61,750	1,501	9,006
205	CU	0,89	0,170	0,13	epizone	59,930	61,670	61,680	1,503	9,015
206	CU	1,26	0,204	0,17	epizone	59,920	61,650	61,670	1,503	9,017
207	CU	1,25	0,222	0,20	epizone	59,900	61,660	61,700	1,502	9,013
208	CU	0,71	0,168	0,13	epizone	59,920	61,650	61,670	1,503	9,017
217	CU	1,42	0,184	0,14	epizone	59,920	61,720	61,740	1,501	9,008
218	CU	0,93	0,240	0,22	epizone	59,925	61,705	61,720	1,502	9,010
219	CU	0,55	0,231	0,22	epizone	59,935	61,725	61,730	1,501	9,009
220	CU	1,14	0,194	0,15	epizone	59,915	61,675	61,700	1,502	9,013
198	FH	1,47	0,277	0,28	epizone	59,930	61,700	61,710	1,502	9,011
199	FH	1,53	0,248	0,23	epizone	59,930	61,750	61,760	1,501	9,005
201	FH	0,58	0,256	0,25	epizone	59,945	61,785	61,780	1,500	9,002
202	FH	1,76	0,321	0,33	upper anchizone	59,935	61,675	61,680	1,503	9,015
210	FH	2,19	0,380	0,42	upper anchizone	59,955	61,815	61,800	1,500	9,000
211	FH	1,47	0,300	0,31	epizone	59,940	61,745	61,745	1,501	9,007
213	FH	1,84	0,232	0,20	epizone	59,920	61,650	61,670	1,503	9,017
214	FH	1,28	0,264	0,26	epizone	59,905	61,535	61,570	1,505	9,030
215	FH	1,05	0,197	0,16	epizone	59,925	61,465	61,480	1,507	9,042
216	FH	2,14	0,254	0,23	epizone	59,935	61,535	61,540	1,506	9,034

S4. List of collected samples. The type of analysis and the related coordinates are reported.

Sample	Tectonic unit	Location (lat - long)	Analysis
ED5-14	Helminthoid Flysch Unit	44°06'06"N - 7°42'57"E	nannoplancton assemblage
ED22-34/53-58	Helminthoid Flysch Unit	44°42'17"N - 7°42'17"E	nannoplancton assemblage
ED94-98	Mooglio-Testico Unit	44°06'46''N - 7°43'37''E	nannoplancton assemblage
ED114-119	Mooglio-Testico Unit	44°06'49''N - 7°43'43''E	nannoplancton assemblage
ED127-138	Mooglio-Testico Unit	44°06'53''N - 7°43'53''E	nannoplancton assemblage
TSE138	Helminthoid Flysch Unit	44°09'33"N - 7°36'16"E	Provenance
TSE146	Helminthoid Flysch Unit	44°09'09"N - 7°36'53"E	Provenance
TSE147	Helminthoid Flysch Unit	44°09'09"N - 7°36'52"E	Provenance
TSE152b	Helminthoid Flysch Unit	44°09'33"N - 7°35'53"E	Provenance
TSE152t	Helminthoid Flysch Unit	44°09'32"N - 7°35'54"E	Provenance
TSE139	Cabanaira Unit	44°08'59"N - 7°36'32"E	Provenance
TSE136	Cabanaira Unit	44°09'18"N - 7°35'56"E	Provenance
TSE199	Cabanaira Unit	44°08'05"N - 7°36'55"E	Provenance
TSE233	Cabanaira Unit	44°09'19"N - 7°35'55"E	Provenance
TSE140	Cabanaira Unit	44°08'57"N - 7°36'8"E	Provenance
ED203	Cabanaira Unit	44°08'53"N - 7°37'06"E	$Ill_{IC} + b_0$
ED204	Cabanaira Unit	44°08'54"N - 7°37'02"E	$Ill_{IC} + b_0$
ED205	Cabanaira Unit	44°09'06"N - 7°37'03"E	$Ill_{IC} + b_0$
ED206	Cabanaira Unit	44°09'04"N - 7°37'04"E	$Ill_{IC} + b_0$
ED207	Cabanaira Unit	44°09'05"N - 7°37'03"E	$Ill_{IC} + b_0$
ED208	Cabanaira Unit	44°09'00'N - 7°36'57"E	$Ill_{IC} + b_0$
ED217	Cabanaira Unit	44°09'17"N - 7°35'52"E	$Ill_{IC} + b_0$
ED218	Cabanaira Unit	44°09'19"N - 7°35'51"E	$Ill_{IC} + b_0$
ED219	Cabanaira Unit	44°09'23"N - 7°35'47"E	$Ill_{IC} + b_0$
ED220	Cabanaira Unit	44°09'20"N - 7°35'46"E	$Ill_{IC} + b_0$
ED198	Helminthoid Flysch Unit	44°09'08"N - 7°37'24"E	$Ill_{IC} + b_0$
ED199	Helminthoid Flysch Unit	44°09'07"N - 7°37'24"E	$Ill_{IC} + b_0$
ED201	Helminthoid Flysch Unit	44°09'02"N - 7°37'24"E	$Ill_{IC} + b_0$
ED202	Helminthoid Flysch Unit	44°08'51"N - 7°37'10"E	$Ill_{IC} + b_0$
ED210	Helminthoid Flysch Unit	44°09'18"N - 7°37'26"E	$Ill_{IC} + b_0$
ED211	Helminthoid Flysch Unit	44°09'17"N - 7°37'25"E	$Ill_{IC} + b_0$
ED213	Helminthoid Flysch Unit	44°09'19"N - 7°37'18"E	$Ill_{IC} + b_0$
ED214	Helminthoid Flysch Unit	44°09'14"N - 7°36'45"E	$Ill_{IC} + b_0$
ED215	Helminthoid Flysch Unit	44°09'07"N - 7°36'39"E	$Ill_{IC} + b_0$
ED216	Helminthoid Flysch Unit	44°09'07"N - 7°36'38"E	$Ill_{IC} + b_0$
ED1	Marguareis Unit	44°07'25"N - 7°43'19"E	*P–T estimate*
TSE236	Marguareis Unit	44°08'32"N - 7°40'37"E	*P–T estimate*
ED18	Moglio-Testico Unit	44°06'52"N - 7°44'16"E	*P–T estimate*
ED91	Moglio-Testico Unit	44°06'37"N - 7°44'16"E	*P–T estimate*

S5. List of minerals with the adopted abbreviation.

Mineral	Mineral abbreviation (Warr, 2021)
chlorite	Chl
phengite	Phg
Illite	Ill
quartz	Qz
albite	Ab
K-feldspar	K-Fsp
calcite	Cc
oxide	Ox

References

Breman, R.G. 1998. Internally-consistent thermodynamic data for stoichiometric minerals in the system Na2O-K2O-CaO-MgO-Feo_Fe2O3-Al2O3-SiO2-TiO2-H2O-CO2, J,Petrol, 29, 445-522.

Cathelineau, M. 1988. Cation site occupancy in chlorites and illites as a function of temperature, Clay Min, 23, 471-485.

De Andrade, V, Vidal, O., Lewin, E., O'Brien, P., Agard, P. 2006. Quantification of electron microprobe compositional maps of rock thin sections: an optimized method and examples, Journal of metamorphic Geology, 24, 655-668.

Dubacq, B., Vidal, O., De Andrade, V. 2010. Dehydration of dioctahedral aluminous phyllosilicates: thermodynamic modelling and implications for thermobarometric estimates, Contributions to Mineralogy and Petrology, 159, 159–174.

Ferreiro Mählmann, R., Frey, M., 2012. Standardisation, Calibration and Correlation of the Kübler-Index and the Vitrinite/bituminite Reflectance: An Inter-Laboratory and Field Related Study. Swiss Journal of Geosciences, 105(2): 153–170. https://doi.org/10.1007/s00015-012-0110-8

Ferreiro Mählmann, R., Giger, M., 2012. The Arosa Zone in Eastern Switzerland: Oceanic, Sedimentary Burial, Accretional and Orogenic very Low- to Low Grade Patterns in a Tectono-Metamorphic Mélange. Swiss Journal of Geosciences, 105(2): 203–233. https://doi.org/10.1007/s00015-012-0103-7

Guidotti, C.V., Sassi, F.P. 1998. Miscellaneous isomorphous substitutions in Na-K white micas: a review, with special emphasis to metamorphic micas: Rendiconti Lincei, 9(9), p, 57-78.

Kisch, H. J., Sassi, R., Sassi, F. P., 2006. The b0 Lattice Parameter and Chemistry of Phengites from HP/LT Metapelites. European Journal of Mineralogy, 18(2): 207–222. https://doi.org/10.1127/0935-1221/2006/0018-0207

Lanari, P., Wagner, T., Vidal, O. 2014. A thermodynamic model for di-trioctahedral chlorite from experimental and natural data in the system MgO-FeO-Al_2O_3-SiO_2-H_2O: applications to P-T sections and geothermometry, Contributions to Mineralogy and Petrology, 167, doi:10,1007/s00410-014-0968-8.

Lanari, P. 2012. Micro-cartgraphie P-T-‘t’ dans les roches métamorphiques, Applications aux Alpes et à l’Himalaya (Ph,D, thesis), Grenoble, Université de Grenoble.

Leoni, L., Marroni, M., Sartori, F., et al., 1996. Metamorphic Grade in Metapelites of the Internal Liguride Units (Northern Apennines, Italy). European Journal of Mineralogy, 8(1): 35–50. https://doi.org/10.1127/ejm/8/1/0035

Massonne, H.J., Schreyer, W. 1987. Phengite geobarometry based on the limiting assemblage with K-feldspar, phlogopite and quartz, Contributions to Mineralogy and Petrology, 96, 212–224.

Vidal, O., Parra, T., 2000, Exhumation paths of high pressure metapelites obtained from local equilibria for chlorite-phengite assemblage, Geol, J, 35, 139-161.

Padan, A., Kisch, H. J., Shagam, R., 1982. Use of the Lattice Parameter b0 of Dioctahedral Illite/Muscovite for the Characterization of P/T Gradients of Incipient Metamorphism. Contributions to Mineralogy and Petrology, 79(1): 85–95. https://doi.org/10.1007/bf00376965

Sassi, F. P., Scolari, A., 1974. The b0 Value of the Potassic White Micas as a Barometric Indicator in Low-Grade Metamorphism of Pelitic Schists. Contributions to Mineralogy and Petrology, 45(2): 143–152. https://doi.org/10.1007/bf00371166

Vidal, O., De Andrade, V., Lewin, E., Munoz, M., Parra, T., Pascarelli, S. 2006. P–T-deformation-Fe^{2+}/Fe^{3+} mapping at the thin section scale and comparison with XANES mapping: application to a garnet-bearing metapelite from the Sambagawa metamorphic belt (Japan), Journal of Metamorphic Geology, 24, 669-683.

Warr, L. N. IMA-CNMNC approved minerals symbols. Mineral. Mag., 85, 291-320.